The Synthesis of Triangular Phosphido-Bridged Iridium Alkyne Clusters

by

Daniel Dönnecke

Diplomchemiker
Friedrich-Schiller-Universität Jena, Germany, 1996

A Dissertation Submitted in Partial Fulfilment of the Requirements for the Degree of

Doctor of Philosophy

in the Department of Chemistry

Research Director: Dr. K. R. Dixon

We accept this dissertation as conforming to the required standard

---

Dr. D. J. Berg (Department of Chemistry, Acting Supervisor)

Dr. T. M. Fyles (Department of Chemistry)

Dr. R. G. Hicks (Department of Chemistry)

Dr. D. A. Vandenberg (Department of Physics and Astronomy)

Dr. M. Cowie (Department of Chemistry, University of Alberta)

Abstract

Supervisor: Dr. K. R. Dixon

This thesis describes the synthesis and chemistry of triangular phosphido-bridged iridium clusters. The cluster $[Ir_3(\mu\text{-}PPh_2)_3(CO)_6]$ was obtained analytically pure for the first time. In the solid state this 48 electron cluster exhibits one short iridium-iridium bond of 2.6702(3) Å and two long iridium-iridium bonds, 2.9913(3) Å on average. Two phosphido bridges rest closely within the plane of the metal triangle while the unique phosphido group, bridging the short metal-metal bond, is almost orthogonal to this plane. NMR data suggest that this structure is also adopted in solution below 183 K. At higher temperature however the phosphido bridges give rise to an average signal which is presumably due to a rapid flip-flop motion of these groups.

Addition of one molar equivalent of dimethylacetylendicarboxylate to $[Ir_3(\mu\text{-}PPh_2)_3(CO)_6]$ results in formation of $[Ir_3(\mu\text{-}PPh_2)_3(CO)_6(\mu\text{-DMAD})]$ which contains a diiridacyclobutene. Addition of excess alkyne leads to the CO-inserted $[Ir_3(\mu\text{-}PPh_2)_3(CO)_5(\mu\text{-DMAD})\{\kappa_2\text{-}MeO_2C\underline{C}C(CO_2Me)\underline{C}(O)\}]$ which photochemically decarbonylates to give $[Ir_3(\mu\text{-}PPh_2)_3(CO)_5(\mu\text{-DMAD})_2]$.

The 50 electron cluster $[Ir_3(\mu\text{-}PPh_2)_3(CO)_5(t\text{-BuNC})_2]$ also reacts with dimethylacetylendicarboxylate to yield the CO-inserted $[Ir_3(\mu\text{-}PPh_2)_3(CO)_3(t\text{-BuNC})_2\{\kappa_2\text{-}MeO_2C\underline{C}C(CO_2Me)\underline{C}(O)\}_2]$ in two isomeric forms. The new CO-insertion products represent stable iridacyclobutenones which are reluctant to undergo further insertion reactions involving carbon monoxide, tert-butylisocyanide or dimethylacetylenedicarboxylate.

Addition of dimethylacetylendicarboxylate to cluster mixtures containing predominantly $[Ir_2Rh(\mu\text{-}PPh_2)_3(CO)_5]$ and $[Ir_3(\mu\text{-}PPh_2)_3(CO)_6]$ results in selective reaction at the triiridium cluster which allowed for the isolation of the heterometallic cluster by chromatography. In contrast to the tri-iridium parent, $[Ir_2Rh(\mu\text{-}PPh_2)_3(CO)_5]$ is much less reactive to dimethylacetylendicarboxylate and inert to CO. Similarly, the heterometallic $[Ir_2Rh(\mu\text{-}PPh_2)_3(CO)_4(RNC)_3]$ (R=*tert*-butyl; 1,1,3,3-tetramethylbutyl) are reluctant to undergo oxidative addition reactions with dimethylacetylendicarboxylate and iodomethane which readily afford addition products with the homometallic parent clusters. The kinetic difference is a consequence of electronic rather than steric factors in the clusters.

Dr. D. J. Berg (Department of Chemistry, Acting Supervisor)

Dr. T. M. Fyles (Department of Chemistry)

Dr. R. G. Hicks (Department of Chemistry)

Dr. D. A. Vandenberg (Department of Physics and Astronomy)

Dr. M. Cowie (Department of Chemistry, University of Alberta)

Table of Contents

List of Tables

List of Figures

List of Abbreviations

^{t}Bu	tertiary-butyl
^{t}BuNC	tertiary-butyl isocyanide
Bz	benzyl
COD	1,5-cyclooctadiene
COE	cyclooctene
Cp	cyclopentadienyl
cy	cyclohexyl
dba	dibenzylidene acetone
DMAD	dimethylacetylendicarboxylate
dppm	bis(diphenylphosphino)methane
Et	ethyl
FAB MS	Fast Atom Bombardment - Mass Spectrometry
IR	infrared spectroscopy
isopr	isopropyl
L	ligand
M	metal
Me	methyl
NMR	nuclear magnetic resonance
Ph	phenyl
R	alkyl
THF	tetrahydrofuran
tmBuNC	tetramethylbutylisocyanide
UV/Vis	ultraviolet/visible spectroscopy
Xy	m-xylyl

List of Compounds

1.1	$[Ir_3(\mu\text{-}PPh_2)_3(CO)_3(\mu\text{-dppm})]$
1.2	$[Ir_3(\mu\text{-}PPh_2)_3(CO)_4(\mu\text{-dppm})]$
1.3	$[Ir_3(\mu\text{-}PPh_2)_3(CO)_3(PPh_3)_2]$
1.4	$[Ir_3(\mu\text{-}PPh_2)_3(CO)_3\{P(OMe)_3\}_3]$
1.5	$[Ir_3(\mu\text{-}PPh_2)_3(CO)_5(t\text{-BuNC})_2]$
1.6	$[Ir_3(\mu\text{-}PPh_2)_3(CO)_4(t\text{-BuNC})_3]$
1.7	$[Ir_3(\mu\text{-}PPh_2)_3(CO)_4(t\text{-BuNC})_3(CH_3)][I]$
1.8	$[Ir_3(\mu\text{-}PPh_2)_3(CO)_3(\mu\text{-dppm})(OH)(I)]$
2.1	$[Ir_3(\mu\text{-}PPh_2)_3(CO)_6]$
2.2	$[Ir_3(\mu\text{-}PPh_2)_3(CO)_5]$
3.1	$[Ir_3(\mu\text{-}PPh_2)_3(CO)_5(\mu\text{-DMAD})\{\kappa_2\text{-}MeO_2C\underline{C}C(CO_2Me)\underline{C}(O)\}]$
3.2	$[Ir_3(\mu\text{-}PPh_2)_3(\mu\text{-CO})(CO)_4(\mu\text{-DMAD})]$
3.3	$[Ir_3(\mu\text{-}PPh_2)_3(CO)_6(\mu\text{-DMAD})]$
3.4a	C_2 - $[Ir_3(\mu\text{-}PPh_2)_3(CO)_3(t\text{-BuNC})_2\{\kappa_2\text{-}MeO_2C\underline{C}C(CO_2Me)\underline{C}(O)\}_2]$,
3.4b	C_s - $[Ir_3(\mu\text{-}PPh_2)_3(CO)_3(t\text{-BuNC})_2\{\kappa_2\text{-}MeO_2C\underline{C}C(CO_2Me)\underline{C}(O)\}_2]$,
3.5a	C_2 - $[Ir_3(\mu\text{-}PPh_2)_3(CO)_2(t\text{-BuNC})_3\{\kappa_2\text{-}MeO_2C\underline{C}C(CO_2Me)\underline{C}(O)\}_2]$
3.5b	C_s - $[Ir_3(\mu\text{-}PPh_2)_3(CO)_2(t\text{-BuNC})_3\{\kappa_2\text{-}MeO_2C\underline{C}C(CO_2Me)\underline{C}(O)\}_2]$
4.1	$[Ir_3(\mu\text{-}PPh_2)_3(CO)_5(\mu\text{-DMAD})_2]$
4.2	$[Ir_3(\mu\text{-}PPh_2)_3(CO)_6(\mu\text{-DMAD})_2(t\text{-BuNC})]$

5.1	$[Ir_2Rh(\mu\text{-}PPh_2)_3(CO)_5]$
5.1a	$[IrRh_2(\mu\text{-}PPh_2)_3(CO)_5]$
5.1b	$[Rh_3(\mu\text{-}PPh_2)_3(CO)_5]$
5.2	$[Ir_2Rh(\mu\text{-}PPh_2)_3(CO)_5(\mu\text{-DMAD})]$
5.3	$[Ir_2Rh(\mu\text{-}PPh_2)_3(CO)_4(\text{t-BuNC})_3]$
5.4	$[Ir_2Rh(\mu\text{-}PPh_2)_3(CO)_5(\text{t-BuNC})_2]$
5.5	$[Ir_2Rh(\mu\text{-}PPh_2)_3(CO)_4(1,1,3,3\text{-tmBuNC})_3]$
5.6	$[Ir_2Rh(\mu\text{-}PPh_2)_3(CO)_5(1,1,3,3\text{-tmBuNC})_2]$
5.7	$[Ir_2Rh(\mu\text{-}PPh_2)_3(CO)_3(\mu\text{-dppm})]$
5.8	$[Ir_2Rh(\mu\text{-}PPh_2)_3(CO)_3(\mu\text{-dppm})]$
5.9	$[Rh_3(\mu\text{-}PPh_2)_3(CO)_3(\mu\text{-dppm})]$
6.1	$[Ir_3(\mu\text{-}PPh_2)_3(CO)_4(1,1,3,3\text{-tmBuNC})_3]$
6.1a	C_2 - $[Ir_3(\mu\text{-}PPh_2)_3(CO)_4(1,1,3,3\text{-tmBuNC})_3(DMAD)_2]$
6.1b	C_s - $[Ir_3(\mu\text{-}PPh_2)_3(CO)_4(1,1,3,3\text{-tmBuNC})_3(DMAD)_2]$
6.2	$[Ir_3(\mu\text{-}PPh_2)_3(CO)_5(\text{isoprNC})_2]$
6.3	$[Ir_3(\mu\text{-}PPh_2)_3(CO)_4(\text{isoprNC})_3]$
6.4	$[Ir_3(\mu\text{-}PPh_2)_3(CO)_5(\text{cyNC})_2]$
6.5	$[Ir_3(\mu\text{-}PPh_2)_3(CO)_4(\text{cyNC})_3]$
6.6	$[Ir_3(\mu\text{-}PPh_2)_3(CO)_4(\text{XyNC})_3]$
7.1	$[Ir_3(\mu\text{-}PPh_2)_3(CO)_4(1,1,3,3\text{-tmBuNC})_3(CH_3)][I]$
7.2	$[Ir_3(\mu\text{-}PPh_2)_3(CO)_4(\text{isoprNC})_3(CH_3)][I]$
7.3	$[Ir_3(\mu\text{-}PPh_2)_3(CO)_4(\text{cyNC})_3(CH_3)][I]$

Acknowledgments

I would like to thank my supervisor, Professor K.R. Dixon for his guidance and support during the course of this work.

I also wish to express my deep appreciation to Drs. D. Berry, D.J. Berg, R.G. Hicks, T. M. Fyles, A.G. Briggs, A.D. Kirk, R. H. Mitchell, and A. McAuley of this department who have always been enthusiastic about offering advice in the many discussions throughout my time at Uvic.

I am very grateful to my mentor and Diplomvater Professor D. Walther at the Fridrich-Schiller-Universität Jena for stimulating and encouraging my interest in organometallic chemistry and to Dr. H. Schreer and Dr. Schmidt of the same institution for teaching my invaluable lessons about the preparation of extremely air sensitive compounds.

The author would like to deeply thank Dr. Bob McDonald, Crystallographer in the Department of Chemistry at the University of Alberta for the excellent work on all the crystal structures presented in this thesis.

Finally my thanks go to Mrs. C. Greenwood for recording many NMR spectra and patiently training me on the NMR spectrometers in this department and to Dr. D. McGillivray for invaluable service in acquiring FAB MS spectra of all the clusters.

Financial support from the University of Victoria is gratefully acknowledged.

To my dear wife and children

for their patience and love

1.Introduction

The field of cluster chemistry has advanced steadily over the past three decades with the number and nuclearity of the clusters synthesized increasing every year [1]. The scope of the following sections cannot be to summarize the development in this area as a whole. Comprehensive reviews of the field have appeared [2-7] and the literature is surveyed annually [8]. This introduction will seek to emphasize the reasons behind the rapid growth of cluster chemistry as a modern science and on the chemistry of a selected group of clusters: the triangular phosphido-bridged carbonyl clusters of the group 9 transition metals. Before analysing the reasons for the growth of this field, a definition a cluster is appropriate.

1.1.What is a cluster?

Several different definitions of clusters have appeared [3]. For the context of this thesis, a cluster is defined as a molecular array of at least three metal atoms in which the metals are bonded to each other or are within the van der Waals contact distance. The requirement of a metal-metal contact is introduced to exclude oligomeric compounds formed by many transition metals with chelating ligands which do not exhibit metal-metal bonding and in which the proximity of the metals is dictated solely by the chelating effect of the ligand. Using this definition, the linear compounds $[Os_3(CO)_{12}I_2]$ [9,10] and $[\{(C_6F_5)(PPh_3)Pt(\mu\text{-}PPh_2)(\mu\text{-}H)\}_2Pt]$ [11], which exhibit unsupported and supported metal-metal

bonds, respectively, are included in the family of clusters, while $[Ni(acac)_2]_3$ [12] is not a cluster. The notion of molecularity is considered in order to exclude inorganic polymers which might exhibit metal-metal bonding like the Krogmann salts [13].

1.2. Original interests in clusters and recent trends

About two decades ago the strong interest in this field of chemistry originated from the idea that clusters might bridge the reactivity gap between transition metal complexes and the bulk metal. Why is this so relevant? Some important industrial processes involve heterogenous catalysts. Product formation in such processes usually occurs when the substrate contacts the catalyst - typically a metal or metal oxide surface - at elevated temperature and pressure. Two examples include the Fischer-Tropsch process, in which carbon monoxide is reduced with hydrogen to give small hydrocarbons or alcohols depending on the conditions and the catalyst employed, or the Haber-Bosch process, in which ammonia is produced from the elements. In contrast, homogenous catalysis employs a soluble catalyst which reacts with the substrates in solution under much milder conditions. Important industrial processes of this type include the SHOP process, in which ethylene is oligomerized to give terminal alkenes of specific molecular weights, desired for the production of fatty acids and detergents on a multi-million ton scale, as well as the Monsanto process, which involves the carbonylation of methanol to give acetic acid. The advantages of

homogenous over heterogenous catalysis are significant and the most important of these are included under the following headings

1. Low pressure and low temperature

Besides the high energetic cost, it is not very desirable from an industrial point of view to operate plants at high pressure and temperature especially when the substrates involve extremely combustible compounds such as hydrogen, olefins, carbon monoxide, alkynes or hydrocarbons because it involves the design and manufacturing of expensive reactors which will guarantee the safety of the process.

2. Enhanced selectivity

The probably most important advantage of homogenous catalysis is the design of single site catalysts which, together with the mild conditions employed, usually lead to enhanced selectivity and uniform products which are very desirable qualities of a catalytic transformation. An important example includes the isotactic polymerization of propene [14].

3. Control over the process.

Many catalytic reactions are highly exothermic and control over the process becomes essential. Homogenous catalysis is stopped much more easily, often instantaneously by the addition of a quenching reagent (for example the addition of methanol to the very exothermic cyclooligomerization of propargyl alcohol leads to an immediate halt of the catalytic cycle due to the hydrolysis of the active nickel catalyst). It is much more difficult to shut down a plant that operates

at 300 bar and 500 K.

Disadvantages of homogenous catalysis are minor but deserve consideration. Because substrate and catalyst are in the same phase (in solution) separation of products is necessarily. This can cause problems, for example, when the product is a pharmaceutical and the catalyst contains a toxic metal (Cr, Ni). Furthermore, the design and synthesis of a specific single site catalyst is often expensive.

Initial interest in transition metal clusters strongly evolved from the idea that they could be viewed as small "chunks of metal" having their surface coordinated by a variety of ligands which allowed for properties such as solubility and stability. It seemed tempting to assume that clusters would combine properties of the bulk phase metal with that of transition metal complexes and could possibly bridge the gap between homogenous and heterogenous catalysis.

The advances that were subsequently made using clusters as model compounds for heterogenous catalysis greatly enhanced our understanding of the processes that might occur on the metal surface under catalytic conditions. An important example includes the formation of the carbido cluster anion $[Fe_4(\mu^4\text{-}C)(CO)_{12}(\mu\text{-}H)]^-$ from the carbonyl cluster dianion $[Fe_4(\mu^3\text{-}CO)(CO)_{12}]^{2-}$ upon protonation under reducing conditions [15]. The carbido cluster can be further protonated to the methylidyne species $[Fe_4(\mu^3\text{-}CH)(CO)_{12}(\mu\text{-}H)]$. Through this series of intermediates which are illustrated schematically in Figure 1.2.1, one could

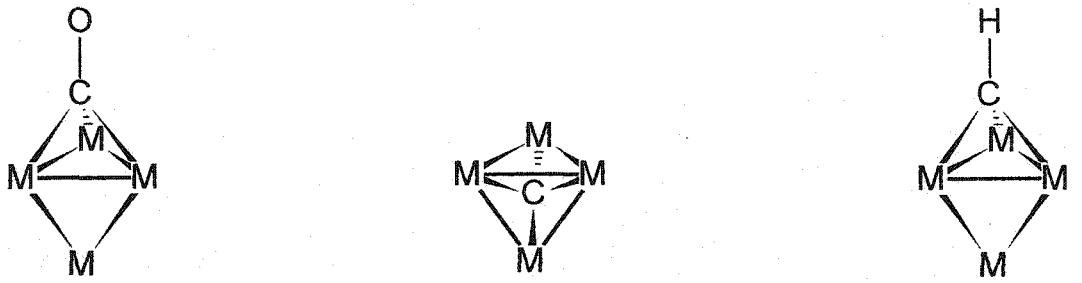

A **B** **C**

Figure 1.2.1 *Schematic representation of μ^3-carbonyl-, **A**, carbido-, **B**, and methylidene clusters, **C**.*

envision a mechanism that might be operating on an iron-iron oxide surface during the Fischer-Tropsch process. It is not difficult to imagine future sequential reduction of the methylidyne moiety via a methylidene and methyl species to methane or the coupling and elimination of such organic fragments yielding small hydrocarbons [16]. The important initial step that most likely involves the C-O bond dissociation can be understood in terms of a C-O bond activation due to the coordination of the μ^3-CO ligand which is unique to cluster chemistry. The degree to which the C-O bond in the μ^3-coordination mode is weakened might be estimated from IR data or bond distances.

Another remarkable example concerns the reversible addition of hydrogen to the ruthenium cluster $[Ru_3(\mu\text{-}P^tBu_2)_2(\mu\text{-}H)_2(CO)_8]$ initially discovered by Jones and co-workers [17] and reinvestigated by Safarowic *et al* [18]. The addition and

elimination of dihydrogen involves the reversible cleavage and formation of a metal-metal bond resulting in opening and closing of the triruthenium framework as illustrated in Figure 1.2.2.

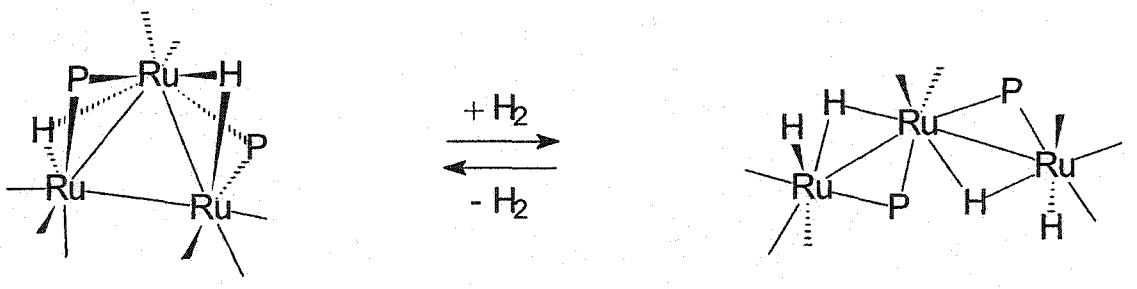

Figure 1.2.2 *Reversible metal-metal bond cleavage and cluster opening resulting from dihydrogen addition and elimination. For clarity CO ligands are represented as sticks (P=P^{t}Bu$_2$).*

Despite such remarkable findings, transition metal clusters have not replaced heterogenous catalysts today. The assumption that clusters represent small metal surfaces is an oversimplification. The very ligands at the periphery of the cluster that make it possible to handle the metal cluster "in a bottle", also alter the activity of the surface. It is now generally recognized that clusters possess a distinct and often unique chemistry that differs from that found at the surface or at mononuclear transition metal centres. Thus recent activity in cluster chemistry, although still strongly influenced by catalysis [19-20], is devoted to uncovering the rich and unique chemistry of this class of compounds.

The evolution of cluster chemistry as we know it today would not have been possible without two major achievements. The first achievement, although purely theoretical, was the development of the isolobal principle [21] which allowed a general strategy for building high nuclearity clusters from low nuclearity synthons. For the first time, chemists could design a route to a desired cluster by breaking it into fragments on paper, and combining the appropriate synthons which were capable of generating these fragments in the laboratory. With this new tool at hand, cluster synthesis evolved from an "accidental affair" to a science of its own. The second achievement, which cannot be understated, involves such advances in analytical techniques as the routine use of X-ray crystallography and multinuclear NMR spectroscopy which present the major methods of characterizing clusters.

1.3. Clusters, ligands and stability.

Metal atom clusters which do not contain any ligands are known and have been isolated in matrices. As one might expect, such clusters are not studied nor synthesized in a Schlenk-tube and their characterization rests mainly on spectroscopy and theoretical studies [22]. Metal atom clusters might be stabilized when absorbed on a supporting surface where they can exhibit interesting catalytic properties depending on the cluster size [23].

The stability of such metal atom clusters increases dramatically when the periphery is shielded by coordinating ligands. Many clusters known today contain terminal ligands only and are held together entirely through metal-metal-bonding. The majority of these clusters are homoleptic transition metal carbonyl clusters. Although much more stable than their bare metal atom counterparts, the chemistry of this class of clusters is still influenced to a high degree by fragmentation reactions. Thus, oxidation of $Ru_3(CO)_{12}$ with halides yields mainly *cis*-$Ru(CO)_4X_2$. Even simple substitution reactions, as with tertiary phosphines, often result in mononuclear fragments [24]. It must however be recognized, that this tendency for fragmentation decreases dramatically as one proceeds down the triads to the third row transition metal carbonyl clusters. Thus $[Os_3(CO)_{12}]$ is much more robust than $[Fe_3(CO)_{12}]$ or $[Ru_3(CO)_{12}]$.

The stability of clusters can be greatly enhanced by the introduction of multi-hapto ligands, capable of bridging the edge (μ-SR, μ-OH, μ-PR_2, μ-Cl, μ-CH_2) or capping the face (μ^3-CR, μ^3-CO,μ^3-S, μ^3-PR) of a cluster, as well as through the introduction of chelating ligands. One of the most interesting features of these clusters concerns the observation that their integrity is often preserved during a chemical transformation even if metal-metal bonds in the cluster are formally broken. It is thus not surprising that these clusters, which are by far the most numerous class of clusters today, have received a great deal of attention.

Tough and not-so-tough bridges

The implication of flexibility and stability of bridging ligands is illustrated in the following examples. The dinuclear complex $[Fe_2(\mu\text{-}PPh_2)_2(CO)_6]$ contains an iron-iron bond that is supported by two bridging diphenylphosphido groups. Upon oxidation to the dication $[Fe_2(\mu\text{-}PPh_2)_2(CO)_6]^{2+}$ metal-metal bond cleavage occurs with retention of the dinuclear structure. The increase in iron-iron distances from 2.62 Å to 3.63 Å during the oxidation is remarkable and clearly indicates that without the supporting diphenylphosphido bridges mononuclear products would have resulted [25].

In the solid state the somewhat related $Fe_2(CO)_9$, being bridged by three carbonyl groups, contains a supported iron-iron bond as well ($d_{Fe\text{-}Fe}$ = 2.46 Å). Although under reducing conditions the dinuclear structure is preserved, the bridging carbonyls cannot prevent fragmentation upon exposure to oxidizing reagents [26]. Similarly, the interesting triangular clusters $[(\eta^5\text{-}C_9H_7)_3M_3(\mu\text{-}CO)_3]$, (M=Ir, Rh) fragment into mononuclear species upon exposure to 1 atm of CO, clearly indicating the weak nature of the carbonyl bridge [27].

These examples clearly illustrate that not every bridging ligand is capable of preserving the integrity of the original framework during the course of a chemical reaction. The phosphido group, which has been used as the supporting bridging group throughout this thesis, fulfils this requirement and has several other advantages that will be discussed below.

Why phosphido bridges?

Besides the strong but flexible binding mode of the phosphido bridge, the second most important feature of this group concerns the phosphorus nucleus which is NMR active (100% ^{31}P, I=1/2) and provides an excellent tool for analyzing the clusters. In some cases the ^{31}P NMR spectrum provides the most convenient way to elucidate the outcome of a chemical reaction.

1. The number, shape and pattern of the resonances give a first insight into the overall symmetry of the cluster.

2. The magnitude of the coupling constants reveals important information on the relative orientation of the phosphido bridges with respect to one another. Typically, the observed two-bond coupling $^{2}J\{PP\}$ is small (10 - 30 Hz) for a mutually *cis* and much larger, (150-250 Hz) for a *trans* geometry of phosphido bridges [28]. If NMR active metals are involved (eg ^{103}Rh) additional coupling to the metal can disclose important information in analysing mixed-metal clusters (for example).

3. The value of the chemical shift is a strong indicator of the presence or absence of a metal-metal bond. It has been argued that the phosphorus nucleus is deshielded by the presence of a metal-metal bond and experiences a strong downfield shift (300ppm downfield from 85% H_3PO_4 is not uncommon). In contrast, when no metal-metal bond is present the signal of the phosphido bridge appears well upfield, usually between 0 and +250 ppm [29]. Although this argument holds for a surprisingly large number of di- and trinuclear phosphido-

bridged systems, it is not consistent for all cases. The deshielding effect of the electron pair in the metal-metal bond on the phosphorus nucleus is an oversimplification. To rationalize the chemical shift of the ^{31}P nucleus is much more complicated and involves, for example, the HOMO-LUMO gap and paramagnetic contributions [107]. Density-functional-theory (DFT) calculations have been carried out on ^{31}P NMR chemical shifts in mononuclear phosphine complexes and it was shown that these chemical shifts are sensitive to many different factors [108].

Another desirable feature of the phosphido bridge is its inertness to a wide variety of reagents. One example from the early work of our group illustrates why this is relevant. Attempts to protonate or alkylate the *triangulo* palladium cluster $[Pd_3(\mu\text{-}S)(\mu\text{-}PPh_2)_2(PR_3)_3]$, (R=Et, Ph) resulted cleanly in reactivity at the sulfide bridge but not at the metal centre [30].

From a synthetic point of view the phosphido group is chemically accessible from a broad variety of reagents (PR_2H, PR_2Cl, PR_2Li, R_2PPR_2 and PR_3) which not only allows for different synthetic approaches, as will be shown in the next section, but also introduces a convenient method of fine tuning steric and electronic parameters of the bridge itself by allowing the selection of a specific R group.

1.4. Synthesis of triangular phosphido-bridged transition metal carbonyls of group 9 metals

Strategies like the isolobal relationship and the synthon concept have been invaluable for the systematic synthesis of clusters using low nuclearity fragments, especially in the relatively new field of heteronuclear mixed-metal clusters [21]. However, the isolobal principle was much less successful in the preparation of homoleptic metal carbonyl clusters including the trinuclear phosphido-bridged carbonyl clusters of group 9 transition metals due to the lack of suitable starting materials as building blocks. As a consequence, the synthesis of such clusters could never be systematically developed and remains to this date an experimental task with cluster yields varying from excellent to poor depending on the metal and phosphine employed.

There are two major entries to trinuclear phosphido-bridged carbonyl clusters of group 9 transition metals. One route is via thermolysis and involves refluxing a metal carbonyl cluster of either higher or lower nuclearity with a secondary phosphine or biphosphine in a high boiling solvent. The pyrolysis of mononuclear tertiary phosphine complexes can also lead to phosphido-bridged clusters [31, 32] but this route usually yields highly substituted clusters and will not be discussed here in detail since the emphasis in this summary is on phosphido-bridged carbonyl clusters. The other major entry is via metathesis and commonly involves the reaction of a group 9 transition metal carbonyl chloride with either a

secondary phosphine or its lithium salt. Just how dramatically the synthetic approach can vary is illustrated by the lightest member of the cobalt triad. The cluster $[Co_3(\mu\text{-}PPh_2)_3(CO)_6]$, obtained originally from $[Co_2(CO)_8]$ and tetraphenylbiphosphine in a high boiling solvent (Equation I), has been known since 1973, when it was structurally characterized by Huntsman and Dahl [33].

$$3[Co_2(CO)_8] + 3Ph_2PPPh_2 \rightarrow 2[Co_3(\mu\text{-}PPh_2)_3(CO)_6] + 12CO \qquad (I)$$

If the same precursor $[Co_2(CO)_8]$ is treated with a secondary phosphine under similar conditions, the nuclearity of the product depends on the R-group of the phosphine. If dicyclohexylphosphine is used, a trinuclear cluster is formed [34] (Equation II) while with di-tert-butylphosphine a dinuclear Co=Co doubly bonded complex results [35] (Equation III).

$$3[Co_2(CO)_8] + 6HPCy_2 \rightarrow 2[Co_3(\mu\text{-}PCy_2)_3(CO)_6] + 12CO + 3H_2 \qquad (II)$$

$$[Co_2(CO)_8] + 2HP^tBu_2 \rightarrow [Co_2(\mu\text{-}P^tBu_2)_2(CO)_4] + 4CO + H_2 \qquad (III)$$

In 1978 Vahrenkamp employed the propene elimination method for the preparation of some higher nuclearity cobalt carbonyl clusters. Upon reacting η^3-allyl tricarbonylcobalt with dimethylphosphine, the cluster $[Co_3(\mu\text{-}PMe_2)_3(CO)_6]$ was obtained in moderate yield [36]. When the phosphine addition was carried

out at low temperature a thermolabile product was obtained that rapidly lost propene upon warming to ambient temperature. It was concluded that this intermediate (Equation IV) had both the η^3-allyl moiety as well as the secondary phosphine coordinated to the same metal centre. Elimination of propene led to the formation of the trinuclear cobalt cluster (Equation V).

$$\eta^3\text{-}C_3H_5Co(CO)_3 + PMe_2H \rightarrow \eta^3\text{-}C_3H_5Co(CO)_2(PMe_2H) + CO \qquad (IV)$$

$$3\ \eta^3\text{-}C_3H_5Co(CO)_2(PMe_2H) \rightarrow [Co_3(\mu\text{-}PMe_2)_3(CO)_6] + 3\ C_3H_6 \qquad (V)$$

Moving down the cobalt triad, Haines and co-workers reported in 1981 a convenient synthesis of the trinuclear rhodium cluster $[Rh_3(\mu\text{-}PPh_2)_3(CO)_5]$ under very mild conditions. Treatment of tetracarbonyl di-μ-chloro dirhodium with two molar equivalents of diphenylphosphine in the presence of base afforded the cluster in 60 % isolated yield [37] (Equation VI).

$$3[Rh_2(\mu\text{-}Cl)_2(CO)_4] + 6HPPh_2 + 6R_3N \rightarrow 2[Rh_3(\mu\text{-}PPh_2)_2(CO)_5] + 2CO + 6[HR_3N]Cl \qquad (VI)$$

Shortly after this Atwood *et al.* reported that carbonyl di-μ-chloro dirhodium reacts with di-tert-butylphosphido lithium in THF at -78 °C to afford a mixture of compounds from which the dinuclear $[Rh_2(\mu\text{-}^tBu_2P)_2(CO)_4]$ along with the

remarkable trinuclear cluster $[Rh_3(\mu\text{-}^tBu_2P)_3(CO)_3]$, were isolated in moderate yield [38]. The latter represents the only structurally characterized triangular phosphido-bridged cluster of a group 9 transition metal possessing 42 valence electrons.

Concerning the heaviest member of the cobalt triad, it was not until 1987 that Jones and co-workers reported that refluxing a suspension of $[Ir_4(CO)_{12}]$ in the presence of a small excess of di-tert-butylphosphine for 12 hours led to a dark red colored homogenous solution from which the cluster $[Ir_3(\mu\text{-}^tBu_2P)_3(CO)_5]$ along with a dinuclear iridium complex were isolated and characterized [39]. The cluster, obtained in 24 % yield, was the first example of a trinuclear phosphido-bridged carbonyl cluster of iridium which at the time seemed unusual because of the general tendency of iridium to form dinuclear species. It was for example known for some time that pyrolysis of the two mononuclear complexes $[M(CO)H(PPh_3)_3]$ (M=Ir, Rh) using the same experimental conditions proceeds quite differently depending on the metal. Upon heating the iridium complex the dinuclear Ir=Ir doubly bound complex *trans*-$[Ir_2(CO)_2(\mu\text{-}PPh)_2(PPh_3)_2]$ is obtained [40, 41], while the isoelectronic and presumably isostructural rhodium complex converts under similar treatment to the trinuclear cluster $[Rh_3(\mu\text{-}PPh_2)_3(PPh_3)_2]$ in high yield [32]. In this light the isolation of the trinuclear iridium cluster by Jones seemed reasonable because the starting material was a tetranuclear iridium carbonyl cluster and the trimer could be viewed as an arrested intermediate in

the formation of a dinuclear species which was formed primarily. Finally in 1991 our group showed that it is possible to synthesize a triangular phosphido-bridged carbonyl in a metathesis-like reaction employing essentially the conditions used by Haines to prepare his trirhodium cluster. Thus, treatment of *in situ*- prepared iridium carbonyl chloride with diphenylphosphine and base led to the isolation of $[Ir_3(\mu\text{-}PPh_2)_3(CO)_6]$ in low yield [28].

1.5. The chemistry of triangular phosphido bridged carbonyl clusters of the cobalt group.

By far the best studied clusters are those in which the metals are bridged by diphenyl-phosphido groups and on which this short review will focus. Several different types of reactions have been encountered and might be classified as follows:

1. Simple ligand substitution reactions that lead to no change in cluster valence electron count and little or no structural change of the cluster frame work.
2. Ligand additions accompanied by metal-metal bond cleavage.
3. Oxidative additions.
4. Ligand additions resulting in fragmentation of the cluster.

Before describing the chemistry of each cluster a remarkable trend in their

general reactivity and stability is worth mentioning. The clusters $[M_3(\mu\text{-}PPh_2)_3(CO)_n]$, (M=Co, n=6; M=Rh, n=5; M=Ir, n=6) are reactive towards CO which will be discussed in more detail later. For M=Co, the absence or presence of CO results in reversible interconversion of the di and trinuclear cobalt systems where cobalt-cobalt and cobalt-phosphido bridges are broken and reformed. In the rhodium case there have been at least three different trinuclear carbonyl clusters observed that readily interconvert depending on the presence or absence of CO and the solvent [43]. In contrast, the equilibrium between the penta- and the hexacarbonyl form of the iridium cluster lies well on the side of the hexacarbonyl. Only after extensive purging of solutions of $[Ir_3(\mu\text{-}PPh_2)_3(CO)_6]$ with dinitrogen for several days can pure pentacarbonyl be obtained. There are important structural consequences involving CO addition or elimination from the cluster which will be discussed in more detail in Chapter 2. For now all that shall be mentioned is that for each CO a cluster takes on, the valence electron count rises by two and the cluster core expands. Thus comparing the ease with which rhodium adds or eliminates CO reflects the ease with which rhodium-rhodium bonds are broken and formed. For iridium the interconversion between hexa- and pentacarbonyl clusters is slowed down and it is tempting to rationalize this trend in terms of the increasing metal-metal bond strength down the triad.

Only limited chemistry has been reported for the cobalt cluster series $[Co_3(\mu\text{-}PR_2)_3(CO)_6]$, (R=Ph, Me, Cy) even though clusters of this group were amongst

the first ones to be characterized. The cobalt cluster $[Co_3(\mu\text{-}PPh_2)_3(CO)_6]$ has been known since 1973 but is was not until Geoffroy and coworkers reexamined this cluster 10 years later that we learned about its remarkable chemistry [42]. The most impressive feature of this cluster concerns the ease with which dinuclear, trinuclear and oligomeric systems interconvert (Scheme 1.5.1) depending on the reaction conditions employed. It is not immediately obvious why the substitution products with diethylphenylphosphine that were sub-

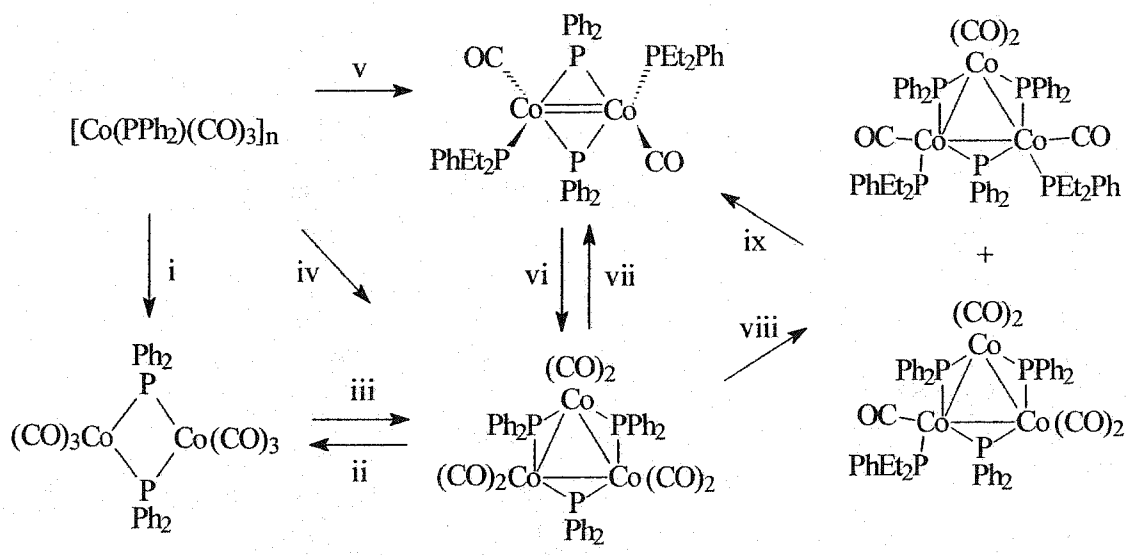

Scheme 1.5.1 *Interconversions between different diphenylphosphido bridged cobalt carbonyl species [42]: i) CO (1000 psi), 110 °C, 24 h; ii) CO (1000 psi), 110 °C, 24 h; iii) hv (360 nm); iv) 80 °C, 2-3 h, N_2 (1 atm); v) PEt_2Ph, 110 °C, 3 h; vi) CO (1 atm), 25 °C, 30 min; vii) PEt_2Ph, 110 °C, 3 h; viii) 2.4 equiv. PEt_2Ph, 80 °C, 3 h; ix) xs. PEt_2Ph, 140 °C, 3 h.*

sequently isolated and characterized spectroscopically only formed under forcing conditions. The fact that the leaving group (CO) was not allowed to exit the system (sealed Carius-tube) might be partially responsible for this observation. It has however been found that the cluster $[Co_3(\mu\text{-}PCy_2)_3(CO)_6]$ does not react with trimethylphosphine even at elevated temperatures [34] which might be interpreted as a result of greater steric crowding in this cluster or as a more general indication that clusters of the series $[Co_3(\mu\text{-}PR_2)_3(CO)_6]$ are more reluctant to undergo substitution reactions than their heavier counterparts. Reactivity studies on Vahrenkamp's less sterically crowded cluster $[Co_3(\mu\text{-}PMe_2)_3(CO)_6]$ would allow a more conclusive interpretation, but as yet such studies have not appeared in the literature.

Knowledge concerning the chemistry of the similar rhodium cluster $[Rh_3(\mu\text{-}PPh_2)_3(CO)_5]$, studied by Haines and co-workers and later by our group, is far more extensive. The cluster does not interconvert between di- and trinuclear complexes as found for the cobalt analog but easily and reversibly forms at least three different carbonyl species [43] as illustrated in Scheme 1.5.2. This Scheme also shows substitution chemistry which is far more extensive and more easily achievable than in the cobalt clusters mentioned previously. When the phosphine is added in the presence of CO the outcome of the reaction resembles that of a combination of ligand addition and substitution reactions. Our group has shown that in the absence of CO the outcome of phosphine

addition is quite different (viii, Scheme 1.5.2) and in fact resembles the chemistry of the iridium analog [28]. It was found that solutions of $[Rh_3(\mu\text{-}PPh_2)_3(CO)_5]$ react readily and irreversibly with phosphines such as PPh_3 or dppm to give simple substitution products analogous to the cluster $[Rh_3(\mu\text{-}PPh_2)_3(CO)_3(PPh_3)_2]$ reported first by Billig and Jamerson [32] from the pyrolysis of $[RhH(CO)(PPh_3)_3]$.

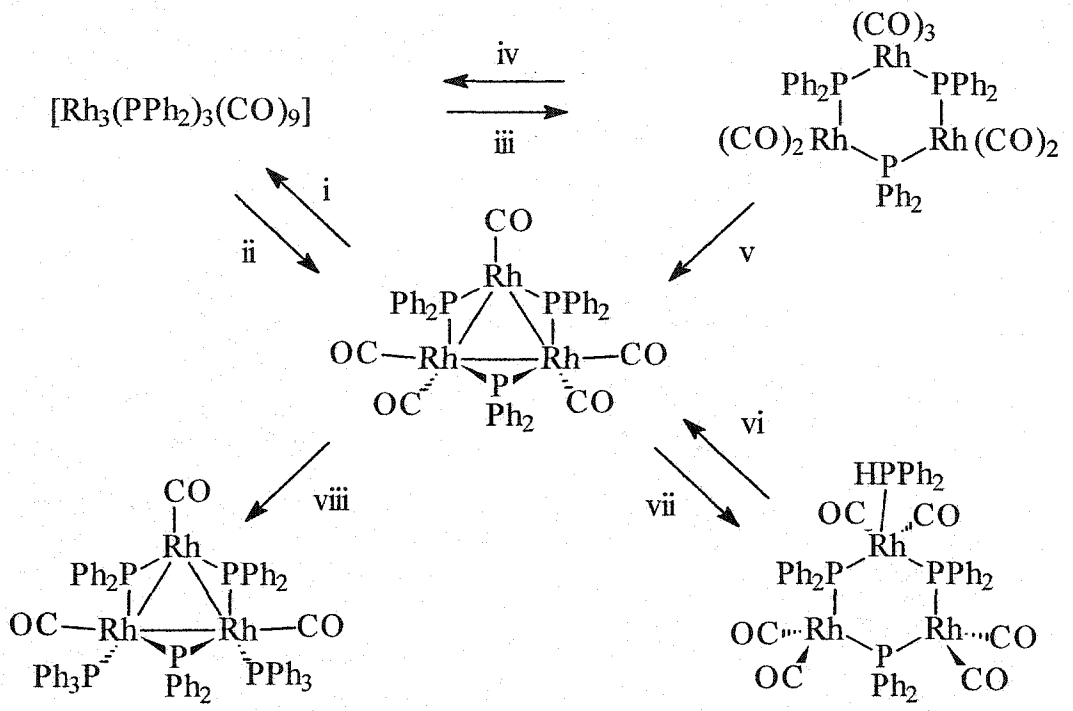

Scheme 1.5.2 *Some important reactions of $[Rh_3(\mu\text{-}PPh_2)_3(CO)_5]$: i), CO (1 atm); ii) N_2 (1 atm) or vacuum; iii) MeOH, CO (1 atm); iv) CO (1 atm); v) N_2 (1 atm); vi) N_2 (1 atm) or vacuum; vii) PPh_2H, CO, EtOH; viii) 2 equiv. PPh_3, N_2 (1 atm).*

Oxidative addition reactions are also observed. Upon reacting $[Rh_3(\mu\text{-}PPh_2)_3(CO)_3(PPh_3)_2]$ and iodine the cluster $[Rh_3(\mu\text{-}PPh_2)_3(\mu\text{-}I)_2(\mu\text{-}CO)(CO)_2(PPh_3)]$ was isolated and characterized by our group [44]. This cluster is structurally similar to $[Rh_3(\mu\text{-}PPh_2)_3(\mu\text{-}Cl)_2(\mu\text{-}CO)(CO)_3]$ obtained by Haines and coworkers through an alternative pathway [45]. These oxidative addition products are rare examples of 50-electron clusters containing a metal-metal bonded cluster core; a situation entirely different from dinuclear chemistry, where oxidative additions have dramatic effects on internuclear distances [46]

The cluster $[Ir_3(\mu\text{-}PPh_2)_3(CO)_6]$, prepared by our group in 1991 [28], exhibits an even more diverse chemistry. It reversibly decarbonylates in solution upon purging with nitrogen or as a solid under vacuum to give the reactive pentacarbonyl cluster $[Ir_3(\mu\text{-}PPh_2)_3(CO)_5]$ although this reaction occurs much more slowly than that of its rhodium counterpart. The outcome of substitution reactions, which are quantitative and often instantaneous, depend on the nature of the substrate. Di- or tri-substituted phosphine clusters can be obtained as illustrated in Scheme 1.5.3. The ligand addition chemistry of $[Ir_3(\mu\text{-}PPh_2)_3(CO)_5]$ (Scheme 1.5.3) was found to resemble that of $[Rh_3(\mu\text{-}PPh_2)_3(CO)_5]$ qualitatively with the most important feature being the expansion of the cluster core upon ligand addition. In recent years it has been a major goal of our group to study the relationship between the cluster valence electron count and the average metal-metal bond length using the framework of the $Ir_3(\mu\text{-}PPh_2)_3$-cluster core. Scheme

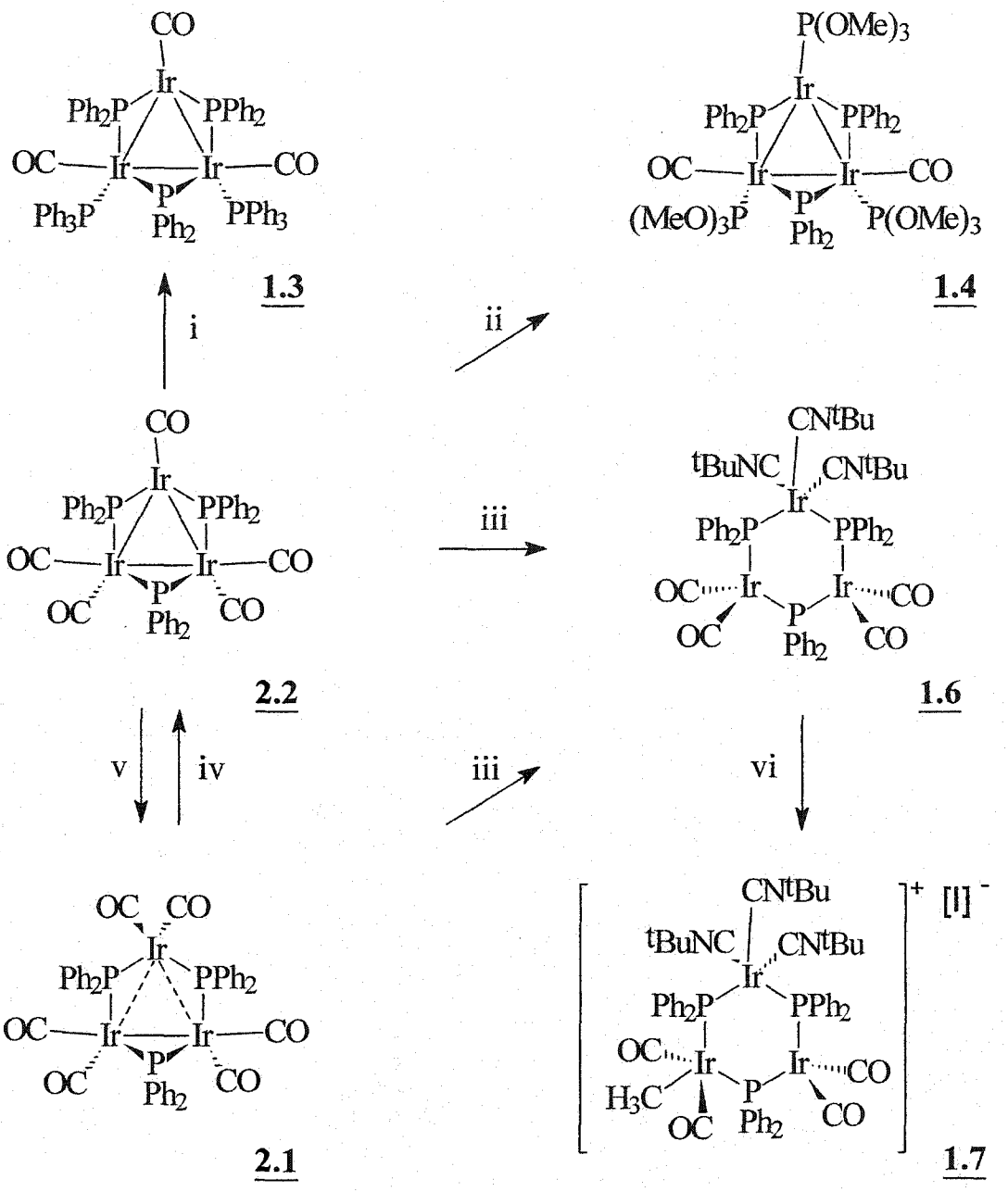

Scheme 1.5.3 *Important reactions of $[Ir_3(\mu\text{-}PPh_2)(CO)_5]$ (**2.2**):*

i) PPh_3, N_2 (1 atm);ii) xs. $P(OMe)_3$, N_2 (1 atm); iii) xs. ^tBuNC;

iv) vacuum (2 days); v) CO (1 atm) 30 sec. vi) xs. CH_3I.

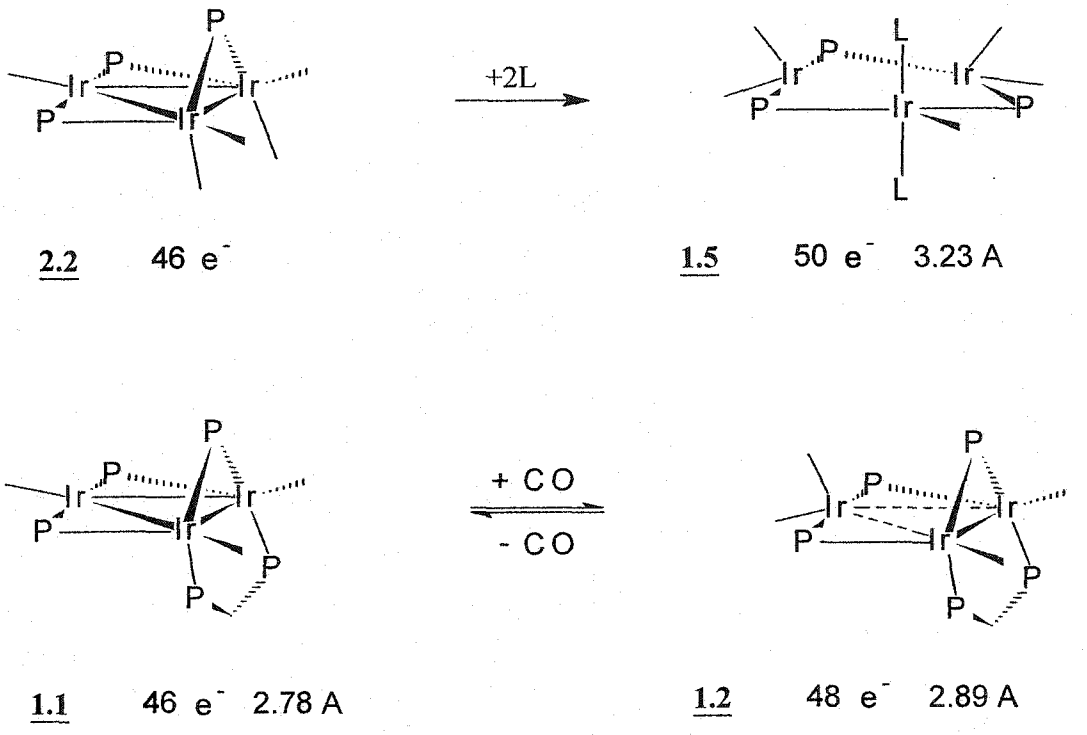

Scheme 1.5.4 *Geometry, cluster valence electron count and average metal-metal bond length (where available) for clusters $[Ir_3(\mu\text{-}PPh_2)_3(CO)_5]$, (**2.2**); $[Ir_3(\mu\text{-}PPh_2)_3(CO)_5(^tBuNC)_2]$, (**1.5**); $[Ir_3(\mu\text{-}PPh_2)_3(CO)_3(\mu\text{-}dppm)]$, (**1.1**) and $[Ir_3(\mu\text{-}PPh_2)_3(CO)_4(\mu\text{-}dppm)]$, (**1.1**). L=^{t}BuNC, P=PPh_2, For clarity carbonyls are represented as sticks, L=^{t}BuNC, P=PPh_2.*

1.5.4 illustrates the systematic expansion of the cluster core as the valence electron count rises from 46 to 48 to 50 as a result of ligand additions [47]. It is worth pointing out that this relationship, which will be discussed further in Chapter 2, seems unaffected by the nature of the terminal ligands, which have

clearly different electronic and steric parameters. Finally, oxidative addition reactions of substrates such as MeI, HCl or BzBr to the cluster $[Ir_3(\mu\text{-}PPh_2)_3(CO)_4(^tBuNC)_3]$ led to unexpected and unprecedented addition at a single iridium centre to give a 50-electron cluster having formally one cationic Ir(III)-centre [48] in which the halide remained uncoordinated (see **1.7** in Scheme 1.5.3).

1.6. Concluding remarks and goal of thesis.

The rich and diverse chemistry of the clusters $[M_3(\mu\text{-}PPh_2)_3(CO)_5]$ (M=Rh, Ir) with relatively simple molecules such as carbon monoxide, phosphines, isocyanides or halogens is remarkable. To our knowledge no studies on the phosphido-bridged carbonyl clusters have ever focused on more complex substrates, such as alkynes. Unfortunately, the iridium clusters $[Ir_3(\mu\text{-}PPh_2)_3(CO)_n]$ (n=5, 6) have never been obtained in an analytically pure state which presents a major problem for the further development of their chemistry, especially concerning multiple step procedures or reactions which led to more than one product. Thus before exploring the alkyne chemistry of $[Ir_3(\mu\text{-}PPh_2)_3(CO)_n]$ (n=5, **2.2**; n=6, **2.1**) a reliable strategy for the preparation of pure **2.2** was needed. In Chapter 2 of this thesis a route to analytically pure **2.1** and **2.2** is described including a full characterization of **2.1**. Chapters 3-5 deal with the synthesis and chemistry of novel diphenyl phosphido-bridged iridium alkyne clusters.

2. Synthesis and purification of $[Ir_3(\mu\text{-}PPh_2)_3(CO)_n]$, (n=5, 2.2; n=6, 2.1)

2.1 Isolation and full characterization of $[Ir_3(\mu\text{-}PPh_2)_3(CO)_6]$, (2.1)

In 1991 our laboratory reported [28] that treatment of polymeric iridium carbonyl chloride with diphenylphosphine in the presence of a base such as diethylamine affords *tris*-μ^2-diphenylphosphido-hexacarbonyl-*triangulo*-triiridium (**2.1**) in low yield. The cluster was found to be in equilibrium with a pentacarbonyl cluster (**2.2**) as shown in Equation 2.1.1.

$$[Ir_3(\mu\text{-}PPh_2)_3(CO)_5] + CO \rightleftharpoons [Ir_3(\mu\text{-}PPh_2)_3(CO)_6] \qquad (2.1.1)$$

Characterization was by ^{31}P NMR data alone. While the pentacarbonyl (**2.2**) exhibited a mutually coupled doublet and triplet as expected for an A_2X spin system, the more symmetrical hexacarbonyl (**2.1**), showed only a single resonance at room temperature. However, much more could be estimated from the NMR spectra. First, the ^{31}P resonances for both clusters appeared well downfield indicative of the presence of iridium-iridium bonds. Further, the small coupling constant, $^2J\{PP\}$, found for **2.2** suggested a *cis* relationship between the unique phosphido bridge and the two equivalent PPh_2 groups, similar to that found in the isoelectronic and presumably isostructural $[Rh_3(\mu\text{-}PPh_2)_3(CO)_5]$, by Haines and co-workers [37]. Support for these suggestions was provided by the crystal structure of $[Ir_3(\mu\text{-}PPh_2)_3(\mu\text{-}dppm)_2(CO)_3]$ (**1.1**) in which the unique

phosphido bridge is almost orthogonal to the plane of the metal triangle, while the other PPh_2 groups remain closely within this plane [28]. Modifications in the work-up procedure for $[Ir_3(\mu\text{-}PPh_2)_3(CO)_6]$ (**2.1**) (see experimental section for details) led to the purification and full characterization of **2.1**, which was previously available only as a red oil. It was found that **2.1** precipitates as a red brown powder when impure, but that very large crystals, suitable for crystallographic analysis, can be obtained when solutions of pure **2.1** in dichloromethane were saturated with CO and carefully layered with hexane. Unlike its rhodium counterpart, **2.1** is stable in the solid state without an accompanying atmosphere of carbon monoxide. It only decarbonylates after extensive periods *in vacuo*. Even solutions require several days of N_2 purging to generate the highly reactive **2.2** quantitatively. On the other hand, introducing a CO atmosphere to solutions of **2.2** results in immediate regeneration of **2.1**, suggesting that the equilibrium in equation 2.1.1 lies well on the product side.

Spectroscopic analysis

^{31}P NMR data have been reported previously [28], and these data suggested D_{3h} symmetry of $[Ir_3(\mu\text{-}PPh_2)_3(CO)_6]$ in solution. ^{13}C NMR studies are in agreement with this assumption. A pseudo quartet is observed at +182 ppm and assigned to the six carbonyl ligands which are equivalent on the NMR timescale.

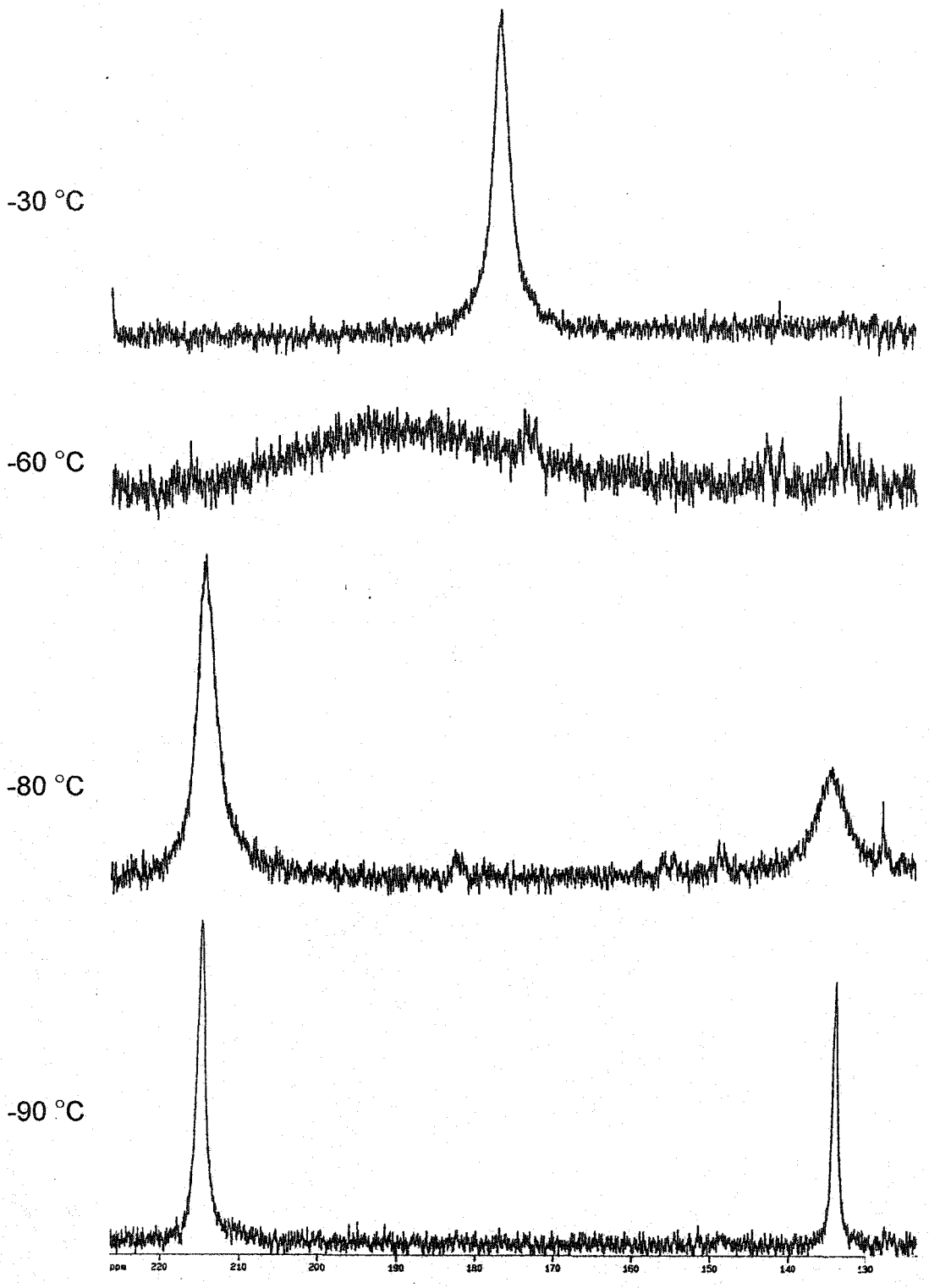

Figure 2.1.1

*^{31}P NMR spectrum of $[Ir_3(\mu\text{-}PPh_2)_3(CO)_6]$ (**2.1**) at selected temperatures (CD_2Cl_2).*

However, the broad appearance of the ^{31}P NMR singlet of **2.1** at ambient temperature and the reported fluxional behaviour for the closely related clusters $[Co_3(\mu\text{-}PR_2)_3(CO)_6]$ (R=Me, Cy), that show severe distortion from D_{3h} symmetry in the solid state [34, 36], justified a reinvestigation. The ^{31}P NMR of **2.1** is shown at selected temperatures in Figure 2.1.1. The singlet at 180 ppm, found at ambient temperature, broadens significantly upon cooling and disappears almost completely at -60 °C. Continued cooling of the sample results in the appearance of two new signals in a 2:1 ratio that are broad at -70 °C but sharpen considerably after lowering the probe temperature to -90 °C, when the two resonances appear at 215 and 134 ppm respectively. Unfortunately coupling constants cannot be extracted from the spectrum at -90 °C. Lowering the temperature even more, using toluene as a solvent, could possibly provide such information. The variable temperature ^{31}P NMR results are clearly at odds with D_{3h} symmetry but suggest instead that at least one of the phosphido bridges is bent out of the plane of the iridium triangle as found in $[Ir_3(\mu\text{-}PPh_2)_3(\mu\text{-}dppm)(CO)_3]$ [28], $[Rh_3(\mu\text{-}PPh_2)_3(CO)_5]$ [37], and especially in isoelectronic $[Ir_3(\mu\text{-}PPh_2)_3(\mu\text{-}dppm)(CO)_4]$ [47]. The ^{31}P NMR singlet of $[Ir_3(\mu\text{-}PPh_2)_3(CO)_6]$ observed at ambient temperature implies a highly fluxional behavior of the diphenylphosphido bridges which randomly undergo a "flip flop" motion, while passing through the plane defined by the three metal atoms. This process is fast on the NMR time scale, but very slow in comparison to a bond vibration. In other words, during the oscillation of a carbonyl ligand, the overall geometry of the

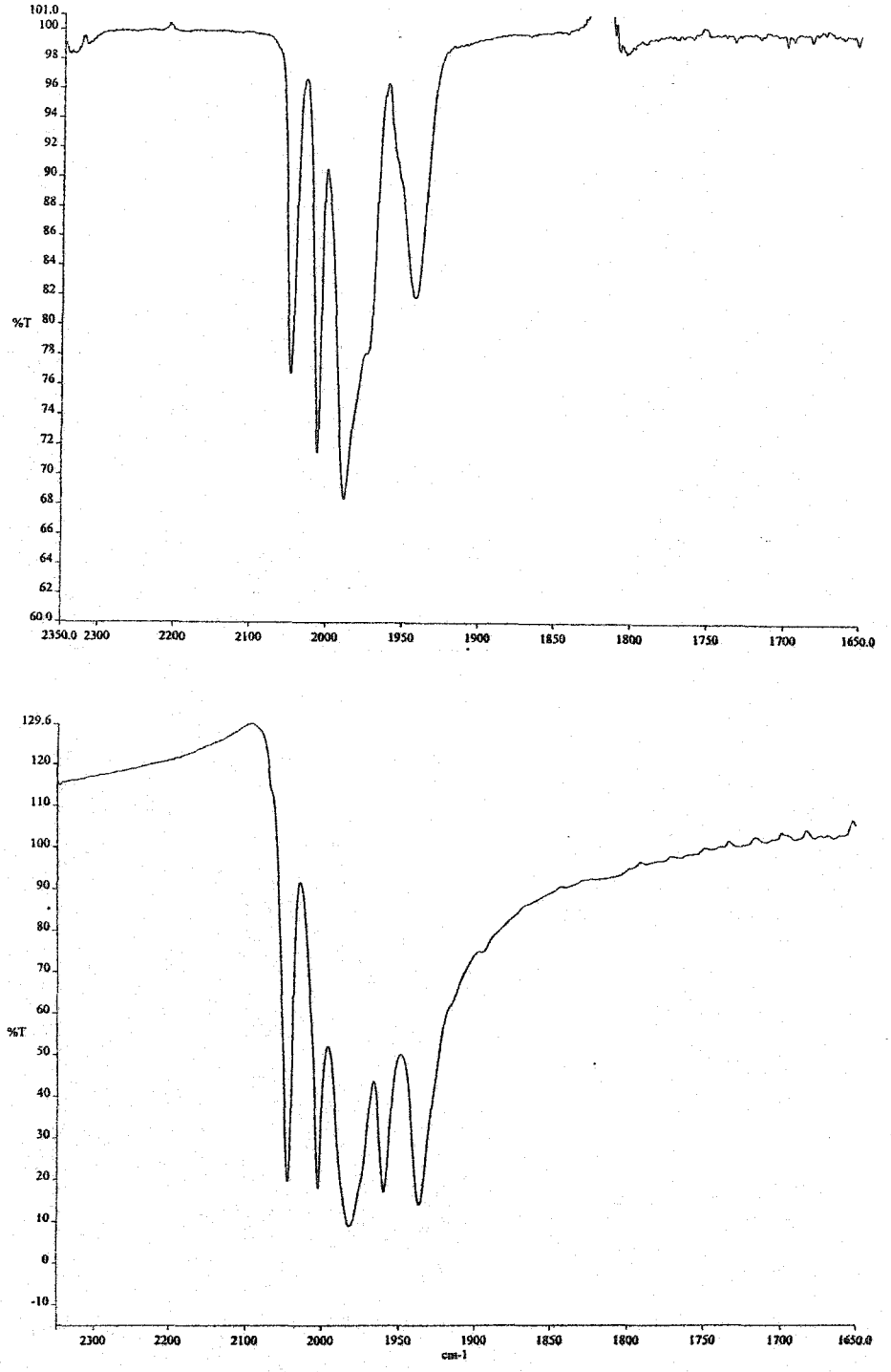

Figure 2.1.2. *Carbonyl region of the infrared spectrum of* $[Ir_3(\mu\text{-}PPh_2)_3(CO)_6]$ *(**2.1**) in benzene solution (top) and KBr (bottom)*

cluster frame remains approximately constant resulting in several inequivalent carbonyl environments. Thus, the vibrational spectrum of **2.1** exhibits six bands in the region of terminal carbonyl absorption, both in benzene solution and in the solid state, as shown in Figure 2.1.2. In D_{3h} symmetry some of the fundamental CO vibrations in **2.1** are related by symmetry, and a much simpler infrared spectrum would be expected. The appearance of six carbonyl bands is thus in good agreement with a less symmetric structure.

In general, Fast Atom Bombardment Mass Spectrometry (FAB MS) is a particularly diagnostic and helpful technique in analysing iridium cluster systems. The occurrence of two significant isotopes of iridium, ^{191}Ir and ^{193}Ir, causes a very characteristic pattern in the molecular ion and fragment peaks depending on the nuclearity of the system. Comparison of the observed with the theoretical isotopic distribution allows the unambiguous assignment of the molecular ion which may not necessarily be the most intense signal in the cluster of peaks. The FAB MS spectrum of **2.1** does not show the expected molecular ion either using dichloromethane solutions of the cluster or solid samples (both with *meta*-nitrobenzylalcohol as a matrix). The fragment peak with the highest mass/charge ratio (m/z) appears at 1272 amu and can readily be assigned to the fragment generated from **2.1** after the loss of a CO ligand. Sequential loss of three more carbonyl ligands is also apparent from the spectrum. The absence of a molecular ion is not surprising when considering that the pressure during the FAB MS

experiment is below 10^{-6} Torr and decarbonylation of **2.1** starts to occur at 1 Torr (ambient temperature).

Structural analysis

The crystal structure of **2.1** was determined by Dr. Bob McDonald, University of Alberta, and is shown in Figure 2.1.3. Relevant crystallographic parameters as well as selected internuclear distances and bond angles are listed in Tables 2.1.1 and 2.1.2, respectively. Most notable in the molecular structure of **2.1** is the almost perpendicular orientation of the unique phosphido bridge with respect to the plane defined by the three iridium atoms. The dihedral angle between the two planes defined by atoms Ir(1)-Ir(2)-Ir(3) and Ir(2)-Ir(3)-P(2), respectively is 80.62(3) ° (see atomic numbering scheme in ORTEP diagram , Figure 2.1.3). The other two phosphido bridges remain fairly closely within the Ir_3 plane having dihedral angles of 7.03(3) and 0.91(2) ° for P(1) and P(3), respectively. Another important feature in the structure of **2.1** is provided by the short basal Ir(2)-Ir(3) bond of 2.6702(3) Å. In contrast, the two apical metal-metal distances are much longer, averaging 2.9913(3) Å. It is difficult to assign the coordination geometry of the two basal iridium centres since there seems to be a lack of guidelines for clusters, in terms of including the metal-metal interaction or not, which is reflected in different perspectives throughout the literature [34, 36]. Ignoring metal-metal interactions, the two iridium centres can be said to adopt a distorted tetrahedral geometry. If the iridium-iridium bond is taken into account a

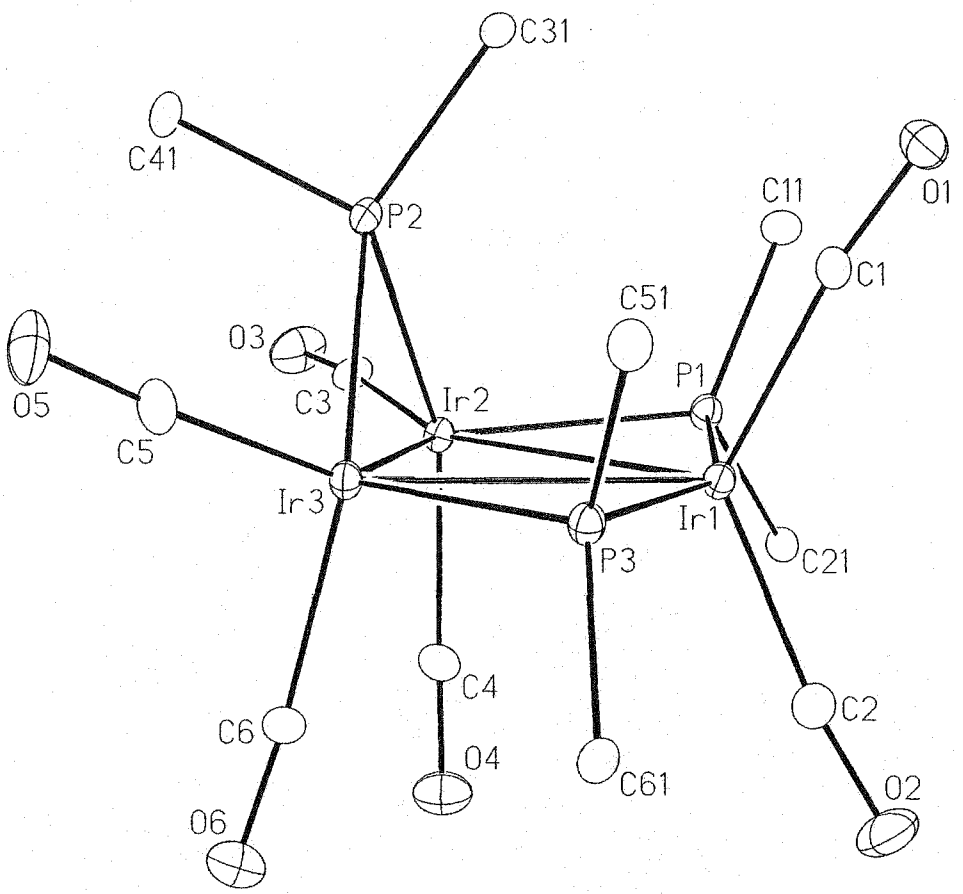

Figure 2.1.3 *Molecular structure of $[Ir_3(\mu\text{-}PPh_2)_3(CO)_6]$ (**2.1**). For clarity only the ipso-carbons of the phenyl rings are shown.*

A. Crystal Data

formula	$C_{42}H_{30}Ir_3O_6P_3$
formula weight	1300.17
crystal dimensions (mm)	0.36 × 0.25 × 0.23
crystal system	monoclinic
space group	$P2_1/n$ (an alternate setting of $P2_1/c$ [No. 14])
unit cell parameters	
a (Å)	15.8572 (10)
b (Å)	13.0942 (8)
c (Å)	19.9854 (13)
β (deg)	109.0748 (13)
V (Å^3)	3921.9 (4)
Z	4
ρ_{calcd} (g cm^{-3})	2.202
μ (mm^{-1})	10.32

B. Data Collection and Refinement Conditions

diffractometer	Bruker P4/RA/SMART 1000 CCD[b]
radiation (λ [Å])	graphite-monochromated Mo Kα (0.71073)
temperature (°C)	−80
total data collected	20934 ($-19 \le h \le 16$, $-16 \le k \le 16$, $-24 \le l \le 21$)
independent reflections	7995
number of observed reflections (NO)	7022 [$F_o^2 \ge 2\sigma(F_o^2)$]
R_1 [$F_o^2 \ge 2\sigma(F_o^2)$]	0.0254
wR_2 [$F_o^2 \ge -3\sigma(F_o^2)$]	0.0620

Table 2.1.1 *Crystallographic parameters and experimental details for* $[Ir_3(\mu\text{-}PPh_2)_3(CO)_6]$ (**2.1**)

Atoms	Distance	Atoms	Distance
Ir(1)-Ir(2)	2.9831(3)	Ir(2)-C(3)	1.880(5)
Ir(1)-Ir(3)	2.9995(3)	Ir(2)-C(4)	1.922(5)
Ir(2)-Ir(3)	2.6702(3)	Ir(3)-C(5)	1.868(5)
Ir(1)-P(1)	2.3113(11)	Ir(3)-C(6)	1.922(4)
Ir(1)-P(3)	2.3225(12)	O(1)-O(1)	1.150(5)
Ir(2)-P(1)	2.3180(11)	O(2)-C(2)	1.145(7)
Ir(2)-P(2)	2.3266(12)	O(3)-C(3)	1.137(6)
Ir(3)-P(2)	2.3204(12)	O(4)-C(4)	1.142(6)
Ir(3)-P(3)	2.3194(11)	O(5)-C(5)	1.152(6)
Ir(1)-C(1)	1.889(4)	O(6)-C(6)	1.141(5)
Ir(1)-C(2)	1.898(6)	Ir(1)-P(2)	3.522(20)

Atoms	Angles	Atoms	Angles
Ir(2)-Ir(1)-Ir(3)	53.014(6)	P(3)-Ir(3)-C(5)	102.76(14)
Ir(1)-Ir(2)-Ir(3)	63.808(6)	P(3)-Ir(3)-C(6)	98.67(14)
Ir(1)-Ir(3)-Ir(2)	63.178(6)	C(5)-Ir(3)-C(6)	99.9(2)
Ir(1)-P(1)-Ir(2)	80.24(4)	P(2)-Ir(3)-C(5)	94.19(16)
Ir(2)-P(2)-Ir(3)	70.14(3)	P(2)-Ir(3)-C(6)	143.47(13)
Ir(3)-P(3)-Ir(1)	80.51(4)	C(1)-Ir(1)-C(2)	127.9(2)
P(1)-Ir(1)-P(3)	152.13(4)	P(1)-Ir(1)-C(1)	93.38(14)
P(1)-Ir(2)-P(2)	105.90(4)	P(1)-Ir(1)-C(2)	98.20(15)
P(2)-Ir(3)-P(3)	110.88(4)	Ir(1)-C(1)-O(1)	171.4(4)

Table 2.1.2 *Selected bond distances (Å) and angles (°) for* $[Ir_3(\mu\text{-}PPh_2)_3(CO)_6]$ *(**2.1**). Estimated standard deviations are given in parentheses.*

trigonal bipyramidal geometry applies. The unique iridium centre, at which metal-metal bond contributions are much smaller, adopts an intermediate geometry that can neither be fully described as square planar nor tetrahedral. The molecular structure of **2.1** is very similar to that of $[Ir_3(\mu\text{-}PPh_2)_3(CO)_4(\mu\text{-dppm})]$ (**1.2**), which, together with $[Ir_3(\mu\text{-}PPh_2)_3(CO)_3(\mu\text{-dppm})(OH)(I)]$ represents the only other well characterized *tris*-μ^2-phosphido-bridged 48-electron cluster of rhodium or iridium [47]. **2.1** and **1.2** are essentially isostructural and possess very similar metal-metal distances; in **1.2** the basal and two apical iridium-iridium distances are 2.707(3), 2.996(3) and 2.982(3) Å respectively, while in **2.1** the same atoms are separated by 2.6702(3), 2.9995(3) and 2.9831(3) Å. Most notable is the agreement of the basal iridium sides, which in both clusters remain largely unaffected by the ligand addition even though this is the metal-metal bond spanned by the bidentate phosphine in **1.2**.

2.2 Decarbonylation of $[Ir_3(\mu\text{-}PPh_2)_3(CO)_6]$ (2.1)

As mentioned before, **2.1** can be transformed to the reactive pentacarbonyl (**2.2**) after extended periods in vacuum or by nitrogen purging of solutions containing the cluster mixture. The transformation is slow in benzene, faster in polar solvents such as dichloromethane or 1,2-dichloroethane and is carried out most conveniently in cyclohexane using a slow stream of dinitrogen to prevent excessive vaporization of the solvent. Over a period of two days the color of such

a solution gradually brightens from dark wine red to strawberry red indicating complete conversion. This slight color change is confirmed by comparison of the absorption maxima in the electronic spectra of the two clusters which shift from 503 nm for **2.1** to 506 nm for **2.2** . A very similar trend is found in the related isoelectronic clusters $[Ir_3(\mu\text{-}PPh_2)_3(\mu\text{-dppm})(CO)_4]$ and $[Ir_3(\mu\text{-}PPh_2)_3(\mu\text{-dppm})(CO)_3]$ which exhibit a strong absorption in the visible range as well. λ_{max} values for several clusters are given in Table 2.2.1.

Cluster	λ_{max} (nm)	Reference
$[Ir_3(\mu\text{-}PPh_2)_3(CO)_5]$ (**2.2**)	506[a]	[c]
$[Ir_3(\mu\text{-}PPh_2)_3(CO)_6]$ (**2.1**)	503[a]	[c]
$[Ir_3(\mu\text{-}PPh_2)_3(\mu\text{-dppm})(CO)_3]$ (**1.1**)	509[a]	[c]
$[Ir_3(\mu\text{-}PPh_2)_3(\mu\text{-dppm})(CO)_4]$ (**1.2**)	506[a]	[c]
$[Ir_2Rh(\mu\text{-}PPh_2)_3(CO)_5]$ (**5.1**)	519[a]	[c]
$[Ir_2Rh(\mu\text{-}PPh_2)_3(\mu\text{-dppm})(CO)_3]$ (**5.7**)	518[a]	[c]
$[Rh_2Ir(\mu\text{-}PPh_2)_3(\mu\text{-dppm})(CO)_3]$ (**5.8**)	566[b]	[44]
$[Rh_3(\mu\text{-}PPh_2)_3(\mu\text{-dppm})(CO)_3]$ (**5.9**)	632[b]	[44]

a) using cyclohexane, b) using dichloromethane, c) this work

Table 2.2.1 *UV absorption maxima of selected clusters in cyclohexane solution.*

^{31}P NMR data for **2.2** have been reported [28]. The downfield shift of the phosphorus resonances suggests the presence of iridium-iridium bonds and a small coupling constant $^{2}J\{PP\}$ of 15 Hz suggested a *cis* arrangement of the unique phosphido bridge bending out of the plane of the metal triangle as found in $[Rh_3(\mu\text{-}PPh_2)_3(CO)_5]$. This is in agreement with ^{13}C NMR data which clearly show the presence of three different carbonyl resonances as expected for the proposed structure shown in Table 2.2.2. A doublet at +180.2 ppm can be readily assigned to the two equivalent axial carbonyl ligands since extensive coupling to phosphorus at the unique phosphido bridge *trans* to these carbonyls is expected. In contrast, the two equatorial carbonyls which are in a *cis* relationship to both the unique and the two in-plane phosphido bridges only give rise to a weakly coupled doublet (see

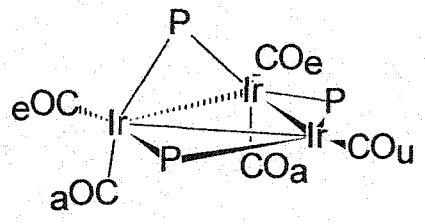

Assignment	δ (ppm)	$^{2}J\{CP\}$
CO_{unique}	183.3 (t)	<10 Hz
CO_{axial}	180.2 (d)	65 Hz
$CO_{equatorial}$	185.2 (d)	11 Hz

Table 2.2.2 *^{13}C NMR chemical shifts and coupling constants for $[Ir_3(\mu\text{-}PPh_2)_3(CO)_5]$ (**2.2**) in (C_6D_6)*

Table 2.2.2 for J values). $^{2}J\{C_{axial}P_{a}\}$ is smaller than the spectrum resolution of about 3 Hz. In a similar manner coupling of CO_{equat} is only resolved for either P_a or P_x. The unique carbonyl coordinated to the apical iridium centre appears as a poorly resolved triplet because of coupling to the two equivalent phosphorus nuclei of the in-plane PPh_2 groups.

FAB MS analysis of **2.2**, is, of course, very similar to that of the parent hexacarbonyl (**2.1**). A molecular ion is observed for **2.2** at (m/z) 1272 and fragments due to the subsequent loss of carbonyls and phenyl groups can be assigned.

Finally, the infrared spectrum of the **2.2** contrasts very strongly with that of **2.1** both in solution, and in the solid state. Five absorption bands are resolved in the region for terminal carbonyls using cyclohexane as a solvent. The absence of absorptions in the region typically associated with bridging carbonyl ligands strongly suggests that the **2.2** is isostructural with $[Rh_3(\mu\text{-}PPh_2)_3(CO)_5]$ [37], but not with $[Rh_3(\mu\text{-}^{t}Bu_2P)_3(\mu\text{-}CO)(CO)_4]$ [49]. This is reinforced by a more careful comparison of band pattern and stretching frequencies of clusters $[M_3(\mu\text{-}PPh_2)_3(CO)_5]$ (M_3=Ir_3,Rh_3 and Ir_2Rh), discussed in Chapter 5.

2.3 Discussion

In 1993 our group reported [47] that the average metal-metal distance in clusters **1.1**, **1.2** and **1.5** increased steadily as their electron count rose from 46 to 48 to 50, respectively. Structural data are now available on quite a number of 46 and 50-electron clusters bearing the $M_3(\mu\text{-}PPh_2)_3$ core (M=Rh, Ir) but 48-electron examples continue to be rare with **2.1** representing a welcome addition. Although the majority of these clusters seem to follow the trend of core expansion with increasing electron count there are limitations to this rule. The following discussion will be used to summarize experimental observations, attempt to rationalize the reasons behind this trend and to comment on the exceptions.

At different levels of theory, triangular transition metal clusters with single metal-metal bonds require a total valence electron count of 48 in order to be stable [50-52]. If fewer cluster valence electrons are present the cluster is considered unsaturated and this is often encountered especially amongst triangular clusters of platinum and palladium where numerous stable 42-electron clusters exist [53, 54]. Theoretical studies which examine why such highly unsaturated clusters are stable have appeared for triangular palladium and platinum systems [55] but studies concerning phosphido-bridged triangular clusters of the cobalt triad are rare [34]. A decrease in valence electron count from the stable 48-electron

Cluster	CVE[a]	Color[b]	M-M[c]	Type[d]	Ref.
$[Rh_3(\mu\text{-}P^tBu_2)_3(CO)_3]$	42	brown	2.65 Å	A	38
$[Rh_3(\mu\text{-}P^tBu_2)_3(\mu\text{-}CO)(CO)_4]$	46	green	2.94 Å	-[e]	49
$[Rh_3(\mu\text{-}PPh_2)_3(CO)_5]$	46	green	2.77 Å	B	37
$[Rh_3(\mu\text{-}PPh_2)_3(CO)_3(PPh_3)_2]$	46	green	2.78 Å	B	32
$[Rh_3(\mu\text{-}PPh_2)_3(CO)_3(\mu\text{-}dppm)]$	46	green	2.79 Å	B	28
$[Rh_3(\mu\text{-}PPh_2)_3(CO)_2\{P(OMe)_3\}_3]$	46	blue	2.78 Å	B	44
$[Ir_3(\mu\text{-}PPh_2)_3(CO)_3(\mu\text{-}dppm)]$	46	red	2.78 Å	B	28
$[Ir_3(\mu\text{-}P^tBu_2)_3(CO)_5]$	46	red	2.78 Å	B	39
$[Ir_3(\mu\text{-}PPh_2)_3(CO)_6]$	48	red	2.88 Å	B	[f]
$[Ir_3(\mu\text{-}PPh_2)_3(CO)_4(\mu\text{-}dppm)]$	48	red	2.89 Å	B	47
$[Ir_3(\mu\text{-}PPh_2)_3(CO)_3(\mu\text{-}dppm)(OH)(I)]$	48	red	2.85 Å	B	48
$[Co_3(\mu\text{-}PPh_2)_3(CO)_6]$	48	not available		D	34
$[Co_3(\mu\text{-}PMe_2)_3(CO)_6]$	48	green	2.61 Å	D	36
$[Co_3(\mu\text{-}PCy_2)_3(CO)_6]$	48	green	2.61 Å	D	34
$[Rh_3(\mu\text{-}PPh_2)_3(CO)_7]$	50	orange	3.14 Å	C	43
$[Rh_3(\mu\text{-}PPh_2)_3(CO)_6(HPPh_2)]$	50	orange	3.16 Å	C	43
$[Ir_3(\mu\text{-}PPh_2)_3(CO)_5(^tBuNC)_2]$	50	orange	3.23 Å	C	28
$[Ir_3(\mu\text{-}PPh_2)_3(CO)_4(tmBuNC)_3]$	50	yellow	3.24 Å	C	[g]

$[Ir_3(\mu\text{-}PPh_2)_3(CO)_4(^tBuNC)_3(CH_3)]I$	50	yellow	3.18 Å	C	48
$[Ir_3(\mu\text{-}PPh_2)_3(CO)_4(isoprNC)_3(CH_3)]I$	50	orange	3.19 Å	C	[g]
$[Ir_3(\mu\text{-}PPh_2)_3(CO)_4(^tBuNC)_3(CH_2Ph)]Br$	50	orange	3.19 Å	C	44
$[Rh_3(\mu\text{-}PPh_2)_3(\mu\text{-}I)_2(\mu\text{-}CO)(CO)_2(PPh_3)]$	50	red	2.80 Å	E	44
$[Rh_3(\mu\text{-}PPh_2)_3(\mu\text{-}Cl)_2(\mu\text{-}CO)(CO)_3]$	50	yellow	2.77 Å	E	45

Table 2.3.1. *Structurally characterized clusters with $M_3(\mu\text{-}PR_2)_3$ core (M=Co, Rh, Ir), a) their electron count (CVE), b) color in the solid state, c) average metal-metal distance, and d) Type of geometry at the cluster core (see Figure 2.3.1 for an illustration of types A-E) e) geometry cannot be described with structure types A-E f) this work, g) see Appendix,*

configuration that implies short internuclear distances also results in chemical behavior expected for an unsaturated compound. On the other hand, if the cluster valence electron count rises above the required 48 valence electrons metal-metal bonds are cleaved, the metal triangle expands and the cluster, having exhausted the ability to coordinate additional ligands behaves as a saturated system. Clusters with 48 electrons exhibit intermediate behavior. The metal-metal bonds are not fully cleaved and the clusters can both eliminate or add ligands. Table 2.3.1 gives a comprehensive account of the structurally

add ligands. Table 2.3.1 gives a comprehensive account of the structurally characterized clusters with the $M_3(\mu\text{-}PPh_2)_3$ core (M=Co, Rh, Ir, excluding the alkyne adducts which will be discussed in Chapters 3-4) their average metal-metal distances, electron count, geometry at the M_3P_3 core in the solid state and color. In comparing the data in Table 2.3.1 another relationship appears. Clusters with 48 or fewer electrons are, without exception, intensely colored compounds while 50-electron clusters are usually yellow or orange. It has been suggested that the strong electronic transitions responsible for the intense colors of the unsaturated phosphido bridged clusters of group 9 transition metals involve orbitals directly associated with metal-metal bonding [43]. Table 2.2.1, which includes λ_{max} values of the electronic spectra for selected 46-and 48-electron clusters provides indirect support for this suggestion since λ_{max} values shift significantly on metal substitution (rhodium for iridium) but are remarkably unchanged upon replacement of terminal ligands (eg, CO for dppm) .

On the basis of this experimental data it is tempting to suggest that electrons in excess of the required 48 valence electrons occupy molecular orbitals which exhibit metal-metal antibonding character, thus explaining the expansion of the metal triangle and the UV/vis data. At a basic level of theory it could be argued that the intense electronic transitions in those 48 electron cluster are caused by a σ to σ^* transition involving a set of molecular orbitals which have metal-metal

bonding and metal-metal antibonding character respectively. The addition of two electrons results in population of the σ^* level and thus elimination of the σ to σ^* transition. More sophisticated theoretical studies are however required to confirm these suggestions which at this point are merely suggested by the experimental evidence.

Exceptions

Although surprisingly consistent, the general trend of cluster core expansion with increasing valence electron count does not hold for all clusters bearing the $M_3(\mu\text{-}PPh_2)_3$ (M=Co, Rh, Ir) core. A few years ago these clusters seemed at odds but with the number of characterized phosphido-bridged group 9 carbonyl clusters rising the number of exceptions has increased as well and a general trend amongst these "odd" clusters is now becoming apparent.

Upon examining the geometry of the M_3P_3 core (M=Co, Rh, Ir) all clusters in Table 2.3.1, except one, can be categorized into five groups (A-E) depending on the relative orientations of the phosphido bridges with respect to the metal triangle as illustrated in Figure 2.3.2. Interestingly, each of the different M_3P_3 core geometries can be associated with a group of clusters of common valence electron count. In addition, clusters that follow the trend of core expansion as a

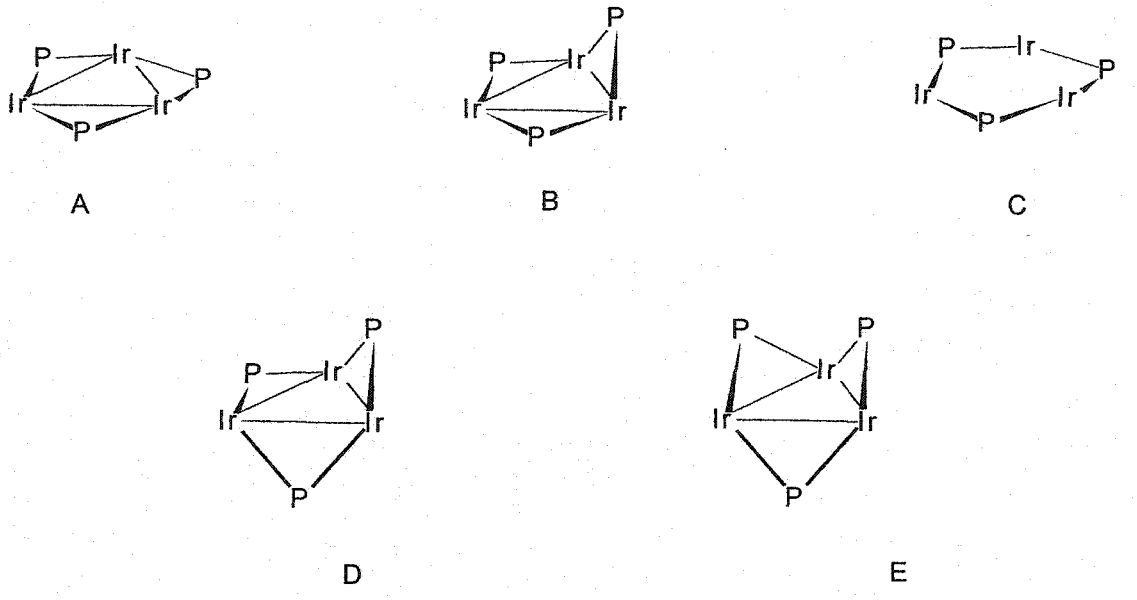

Figure 2.3.1 *Geometries of the $M_3(\mu\text{-}PR_2)_3$ core (M=Co, Rh, Ir) adopted by the clusters summarized in Table 2.3.1.*

consequence of rising valence electron count and those "odd" clusters that do not follow this general trend can be distinguished by their M_3P_3 core geometry even though they might possess an equal electron count. For example, all 50-electron clusters in Table 2.3.1 which have the expected non-bonding metal-metal distances adopt geometry C in the solid state while those 50-electron clusters with metal-metal bonds exhibit geometry E. Furthermore, the 48-electron clusters of the cobalt series that show unusually short cobalt-cobalt bonds adopt geometry D while those 46-and 48-electron clusters which exhibit geometry B show expected moderate metal-metal bond lengths on average. The geometry of

type B could be further divided for 46-electron clusters in which all metals are connected by strong metal-metal bonds and 48-electron clusters in which only the metal-metal bond bridged by the unique phosphido bridge is short. Finally, there is one interesting example of geometry A which exhibits a flat M_3P_3 core like, in the type C structure, except that all metal-metal distances are very short.

There is at present no explanation for the dramatic consequences on the metal-metal distances depending on the orientation of the phosphido bridges which seem to be most pronounced amongst the 50-electron clusters. The observations that a certain geometry is indicative of the magnitude of the metal-metal distances could be useful to predict the presence or absence of metal-metal bonds in clusters for which structural data are not available by use of ^{31}P NMR.

3. Novel trinuclear phosphido-bridged iridium alkyne clusters

3.1. Reaction of $[Ir_3(\mu\text{-}PPh_2)_3(CO)_6]$ with excess alkyne.

When deep red solutions of $[Ir_3(\mu\text{-}PPh_2)_3(CO)_6]$ (**2.1**) in benzene or dichloromethane were treated with dimethylacetylene, diphenylacetylene, 1-hexyne or methylbutynoate, no reaction could be induced at room temperature. Even after several days the infrared solution spectra of the mixtures remained unchanged, indicating no reaction. If, however, the electron deficient alkyne, dimethylacetylenedicarboxylate, (DMAD) was used in a 20-fold molar excess the initially deep red solution of **2.1** gradually brightened to orange-red and finally orange to yellow accompanied by a dramatic change in the solution infrared spectrum. Red prisms could be crystallized directly from the reaction mixture when pure **2.1** was used. If the reaction was carried out using crude **2.1**, it was necessary to first clean the reaction mixture by chromatography. FAB MS of the new cluster detected a molecular ion [M+H] at 1585 suggesting the addition of two molecules of alkyne to the hexacarbonyl. This stochiometry was confirmed by elemental analysis and integration of the proton NMR resonances. While the ^1H NMR of the hexacarbonyl cluster only exhibits aromatic resonances due to the diphenylphosphido bridges, the alkyne adduct exhibits three additional signals characteristic of the methoxy protons of coordinated DMAD. Integration of these new signals, which have a ratio of 1:2:1, suggests that one alkyne is coordinated symmetrically. In the other DMAD ligand however, the methoxy groups are in very different environments, giving rise to two individual signals

separated by over 1 ppm. The suggestion of two individually coordinated alkynes arises from the FAB MS spectrum, which is quite complex and yields a lot more information about the new cluster than just the molecular weight. The occurrence of four fragments in the spectrum that arise from loss of one DMAD ligand followed by the subsequent loss of 3 carbonyls (see Table 3.1.1) speaks against the possibility of alkyne coupling on the iridium centre which is frequently

m/z	intensity (%)	assignment
1585	100	[M+H]
1556	28	[M-CO]
1528	37	[M-2CO]
1500	52	[M-3CO]
1472	93	[M-4CO]
1442	48	[M-alkyne]
1414	20	[M-alkyne-CO]
1386	63	[M-alkyne-2CO]
1358	22	[M-alkyne-3CO]

Table 3.1.1 *Analysis of FAB MS spectrum of*

$[Ir_3(\mu\text{-}PPh_2)_3(CO)_5(\kappa^2\text{-}MeO_2C\underline{C}C(CO_2Me)\underline{C}(O)(\mu\text{-}DMAD)]$ ***(3.1)***

encountered in organometallic chemistry [56]. To rationalize the observed fragments from a structure with two coupled alkynes would necessarily involve the breakage of two stable carbon-carbon bonds to justify the loss of only one DMAD ligand, and such a situation is very unlikely to occur under the mild conditions of ionization employed in FAB MS. Furthermore, an iridacyclopentadienyl, for which two or four signals are expected, depending on the symmetry, is not in agreement with the 1:2:1 ratio for the methoxy protons as encountered in the proton NMR which is shown in Figure 3.1.1.

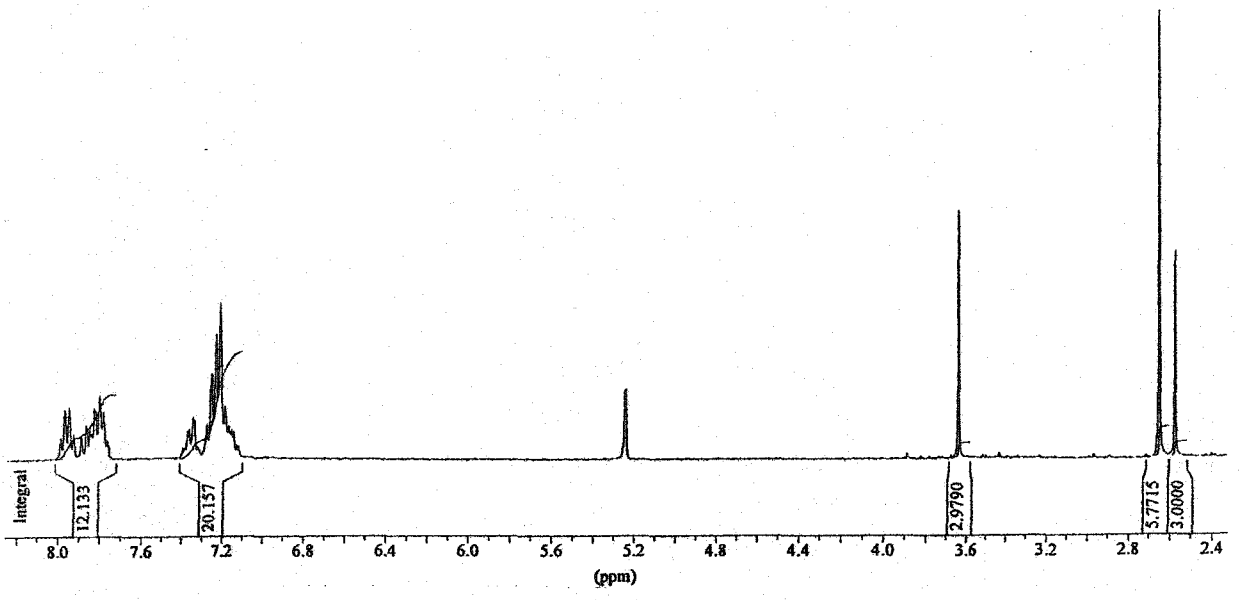

Figure 3.1.1 *^{1}H NMR of [$Ir_3(\mu\text{-}PPh_2)_3(CO)_5(\kappa^2\text{-}MeO_2C\underline{C}\underline{C}(CO_2Me)\underline{C}(O)(\mu\text{-}DMAD)]$ (**3.1**) in dichloromethane-d_2*

^{31}P NMR spectroscopy provides an important insight into the structure of the new cluster. Upon alkyne coordination, the singlet encountered in **2.1** gives way to an A_2X spin system in **3.1**. The ^{31}P resonances appear as a mutually coupled doublet and triplet at δ = -59.8 and -16.8 ppm respectively. The large coupling constant $^2J\{P_aP_x\}$ of 168 Hz suggests that all three phosphido bridges are now in the plane of the iridium triangle. These dramatic changes in the ^{31}P NMR are very similar to those encountered upon ^{t}BuNC addition to the hexacarbonyl cluster discussed in the introduction [28].

However, the infrared spectrum of **3.1**, which is shown in Figure 3.1.2, contrasts with that of $[Ir_3(\mu\text{-}PPh_2)_3(CO)_4(^t BuNC)_3]$ (**1.6**), providing important information about the alkyne adduct. Only terminal carbonyl absorptions are observed which appear in a narrow range and are net shifted to higher energy in comparison to $[Ir_3(\mu\text{-}PPh_2)_3(CO)_6]$ (**2.1**). In the isocyanide adduct $[Ir_3(\mu\text{-}PPh_2)_3(CO)_4(^t BuNC)_3]$ (**1.6**) the carbonyl stretching frequencies experience a net shift to lower energy. Such a shift for ν_{CO} to higher energy is typically encountered in iridium and rhodium chemistry upon oxidation of the metal centre, and is particularly well established for oxidative additions on mononuclear and dinuclear complexes which commonly involve changes from M(I) to M(III) and from M(I)-M(I) to M(II)-M(II), respectively [57]. In addition, absorptions diagnostic of CH_3, C-O-C and in particular C=O ($\nu_{C=O}$: 1716 and 1682 cm^{-1}), which are absent in $[Ir_3(\mu\text{-}PPh_2)_3(CO)_6]$ (**2.1**) confirm the coordination of DMAD to the cluster. It is

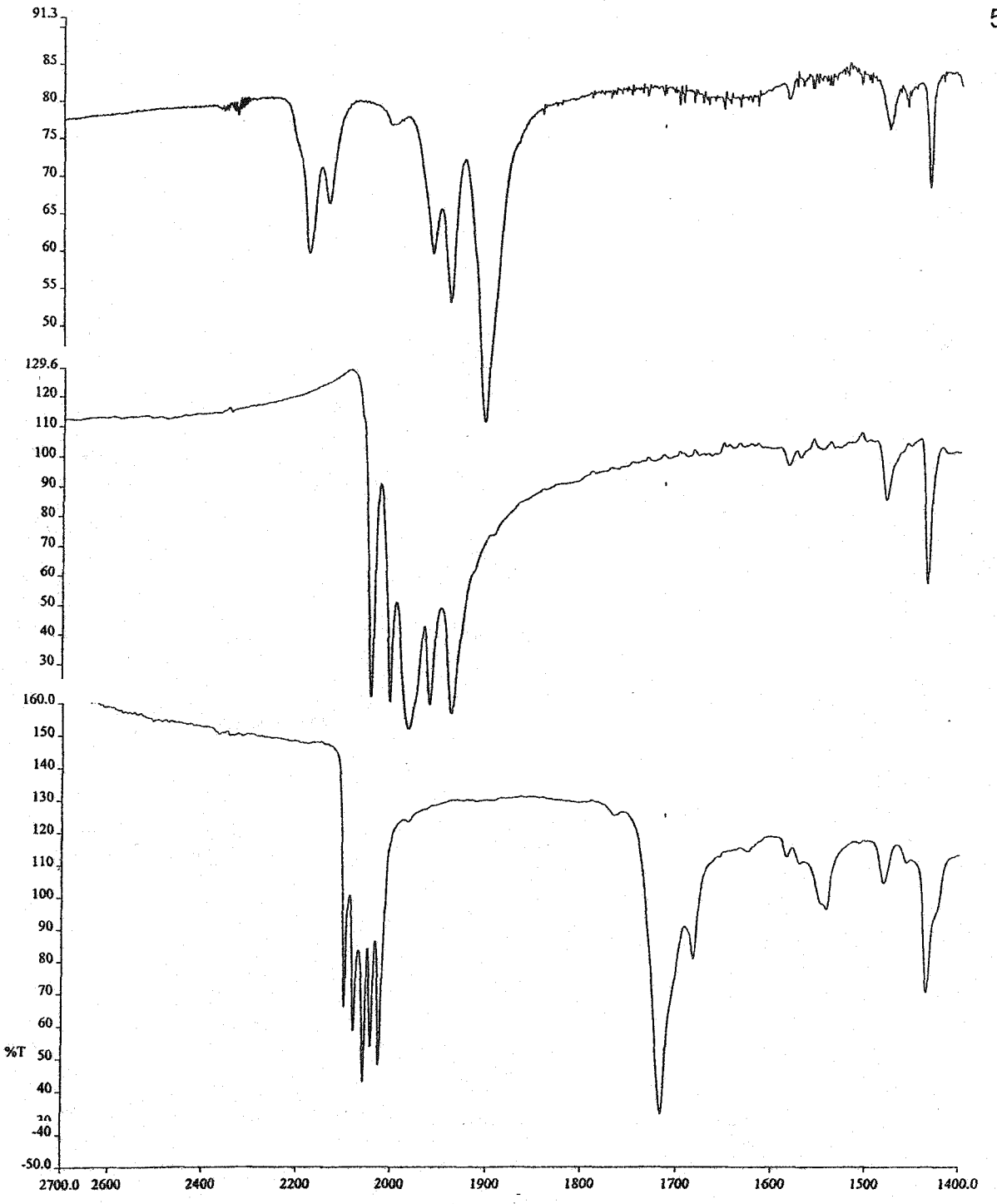

Figure 3.1.2 *Part of the infrared spectra of clusters* $[Ir_3(\mu\text{-}PPh_2)_3(CO)_4(^tBuNC)_3]$ (**1.6**) *top,* $[Ir_3(\mu\text{-}PPh_2)_3(CO)_6]$ (**2.1**) *middle and* $[Ir_3(\mu\text{-}PPh_2)_3(CO)_5$ (κ^2-$MeO_2C\underline{C}C(CO_2Me)\underline{C}(O)(\mu\text{-}DMAD)]$ (**3.1**) *bottom using KBr.*

interesting to note here that the number of CO bands decreases from six in the hexacarbonyl to five in the alkyne adduct. The weak band at 1540 cm^{-1} could be interpret as $\nu_{C=C}$ of the coordinated alkyne. A very useful tool in defining the coordination mode of the DMAD ligands is ^{13} C NMR spectroscopy. The complex spectrum will be analyzed in the structural discussion since it is of key importance in confirming solution and solid state structure of the new cluster.

Structural analysis

The requirement of one symmetric and one non-symmetric coordination mode for the DMAD ligands does not allow many possible structures if the overall A_2X symmetry of the phosphido bridges is to be preserved. A structure one could envision would have a bridging DMAD ligand bent out of the plane defined by the iridium triangle and the three phosphido bridges while the other alkyne coordinates to the apical iridium perpendicular to this plane, thus creating two different environments for the methoxy groups. Each metal atom would still bear two terminal carbonyl ligands to satisfy the observed IR data. Such a structure would be in agreement with proton and phosphorus NMR data. However the absence of signals in the ^{13}C NMR typically found for terminal or bridging alkynes and the presence of olefinic signals is in disagreement with such a formulation. To elucidate the coordination mode of the alkyne a crystal structure analysis would be invaluable. Although large, well-formed orange-red prisms of the cluster could be readily obtained either from dichloromethane/hexane or

benzene/hexane the crystals immediately collapsed when removed from the mother liquid. Bob McDonald finally succeeded in mounting a single crystal under a cold stream of nitrogen and was able to acquire sufficient data to solve the crystal structure of **3.1** which is shown in Figure 3.1.3. Important structural parameters as well as bond lengths and angles are given in Tables 3.1.2 and 3.1.3 respective. The cluster appears to crystallize without solvent which seems surprising since crumbling and loss of the brilliant appearance of single crystals upon removal from the mother liquor is most frequently a result of desolvation and must in this case arise from another cause. The most striking feature of the structure is the insertion of a single carbon monoxide ligand into a iridium alkyne bond creating a four membered ring, formally an iridacyclobutenone. The carbon-carbon bond length of 1.362(6) Å found in the DMAD fragment of this ring is well within the range for olefinic bonds, while both iridium carbon distances in the metallacycle compare well with those typically found for iridium-carbon sigma bonds. The inserted carbonyl forms a ketone-like fragment with a very short C=O bond of 1.199(5) Å. These data are in agreement with a well localized iridacyclobutenone structure and are strongly supported by ^{13}C NMR data of **3.1**, which exhibits three types of signals in the region between +150 and +170 ppm: singlets, triplets and multiplets. The triplets observed in the proton decoupled ^{13}C NMR spectrum must arise from coupling with two equivalent phosphorus nuclei. The only carbon atoms that are in an environment that allows coupling to two equivalent phosphorus atoms are those coordinated to the

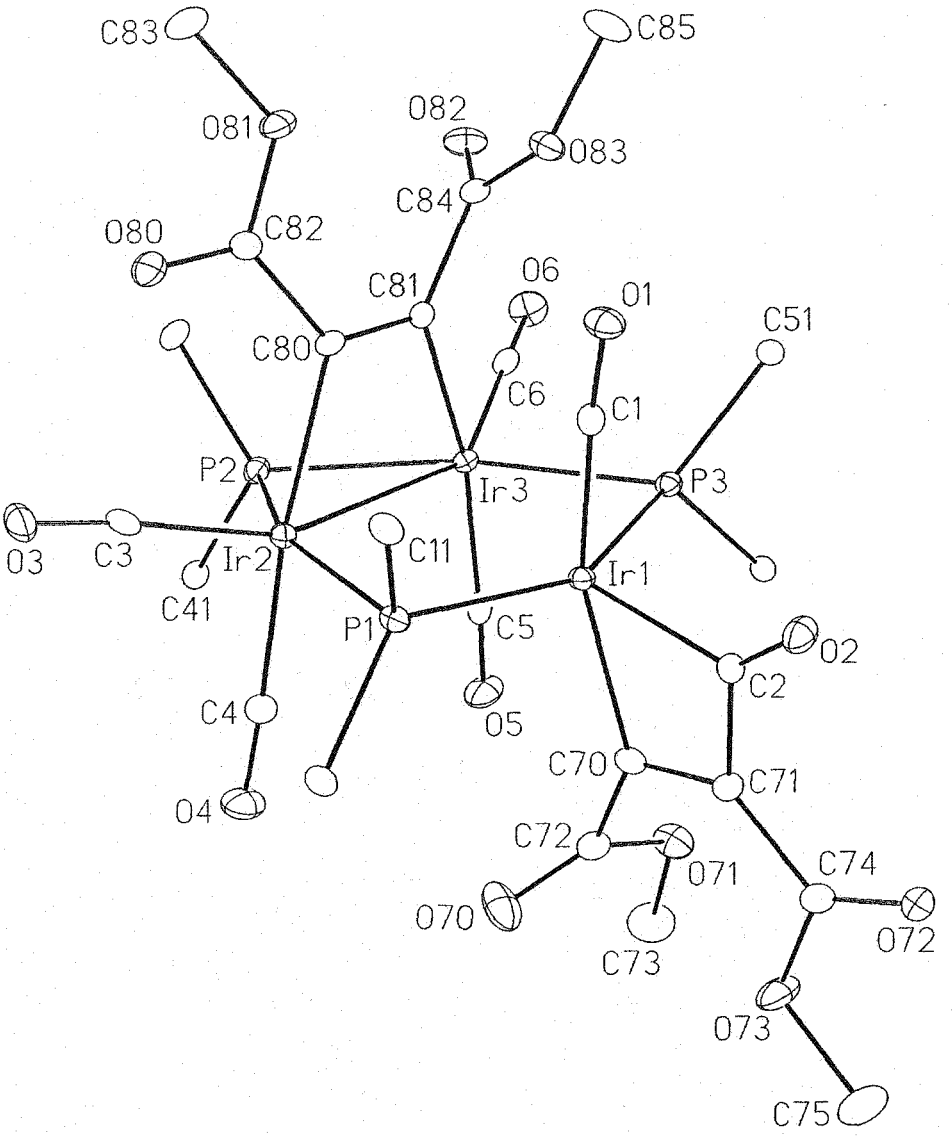

Figure 3.1.3 *ORTEP diagram showing the molecular structure of* $[Ir_3(\mu\text{-}PPh_2)_3(CO)_5(\kappa^2\text{-}MeO_2C\underline{C}C(CO_2Me)\underline{C}(O)(\mu\text{-}DMAD)]$ ***(3.1)***

For clarity only the ipso carbons of the phenyl groups are shown.

A. Crystal Data

formula	$C_{54}H_{42}Ir_3O_{14}P_3$
formula weight	1584.39
crystal dimensions (mm)	0.44 × 0.26 × 0.07
crystal system	monoclinic
space group	$P2_1/c$ (No. 14)
unit cell parameters	
a (Å)	11.6969 (5)
b (Å)	21.7377 (10)
c (Å)	21.2685 (9)
β (deg)	100.9618 (9)
V (Å^3)	5309.1 (4)
Z	4
ρ_{calcd} (g cm^{-3})	1.982
μ (mm^{-1})	7.657

B. Data Collection and Refinement Conditions

diffractometer	Bruker P4/RA/SMART 1000 CCD[b]
radiation (λ [Å])	graphite-monochromated Mo Kα (0.71073)
temperature (°C)	−80
total data collected	26117 ($-14 \le h \le 14$, $-25 \le k \le 27$, $-13 \le l \le 26$)
independent reflections	10875
number of observed reflections	(*NO*) 9016 [$F_o^2 \ge 2\sigma(F_o^2)$]
R_1 [$F_o^2 \ge 2\sigma(F_o^2)$]	0.0248
wR_2 [$F_o^2 \ge -3\sigma(F_o^2)$]	0.0531

Table 3.1.2 *Crystallographic experimental details for*

*[$Ir_3(\mu\text{-}PPh_2)_3(CO)_5(\kappa^2\text{-}MeO_2CC\underline{C}C(CO_2Me)\underline{C}(O)(\mu\text{-}DMAD)$] (**3.1**)*

Atoms	Distance	Atoms	Distance
Ir(1)-Ir(2)	3.2414(2)	Ir(2)-C(3)	1.872(5)
Ir(1)-Ir(3)	3.2295(2)	Ir(2)-C(4)	1.964(5)
Ir(2)-Ir(3)	2.9320(3)	Ir(2)-C(80)	2.107(4)
Ir(1)-P(1)	2.3181(11)	Ir(3)-C(5)	1.939(5)
Ir(1)-P(3)	2.3054(11)	Ir(3)-C(6)	1.915(4)
Ir(2)-P(1)	2.4169(11)	Ir(3)-C(81)	2.087(4)
Ir(2)-P(2)	2.3178(11)	C(80)-C(81)	1.350(6)
Ir(3)-P(2)	2.3476(11)	O(2)-C(2)	1.199(5)
Ir(3)-P(3)	2.3939(11)	C(70)-C(72)	1.484(6)
Ir(1)-C(1)	1.891(5)	C(71)-C(74)	1.480(6)
Ir(1)-C(2)	2.035(4)	C(80)-C(82)	1.482(6)
Ir(1)-C(70)	2.125(4)	C(81)-C(84)	1.498(6)
C(70)-C(71)	1.362(6)	O(1)-C(1)	1.140(5)
C(2)-C(71)	1.485(6)	O(72)-C(74)	1.197(5)

Atoms	Angles	Atoms	Angles
Ir(2)-Ir(1)-Ir(3)	53.886(7)	C(1)-Ir(1)-C(70)	159.57(17)
Ir(1)-Ir(2)-Ir(3)	62.850(7)	C(1)-Ir(1)-C(2)	95.35(17)
Ir(1)-Ir(3)-Ir(2)	63.264(7)	C(2)-Ir(1)-C(70)	64.38(17)
Ir(1)-P(1)-Ir(2)	86.37(4)	C(4)-Ir(2)-C(80)	167.65(17)
Ir(2)-P(2)-Ir(3)	77.87(3)	C(3)-Ir(2)-C(4)	95.15(18)
Ir(3)-P(3)-Ir(1)	86.80(4)	C(3)-Ir(2)-C(80)	95.32(17)
P(1)-Ir(1)-P(3)	148.67(4)	Ir(2)-C(80)-C(81)	111.7(3)
P(1)-Ir(2)-P(2)	159.24(5)	Ir(3)-C(81)-C(80)	112.4(3)
P(2)-Ir(3)-P(3)	158.93(5)	C(5)-Ir(3)-C(81)	167.10(17)

Table 3.1.3 *Selected internuclear distances (Å) and angles (°) for* $[Ir_3(\mu\text{-}PPh_2)_3(CO)_5(\kappa^2\text{-}MeO_2C\underline{C}\underline{C}(CO_2Me)\underline{C}(O)(\mu\text{-}DMAD)]$ ***(3.1)***

Estimated standard deviations are given in parentheses.

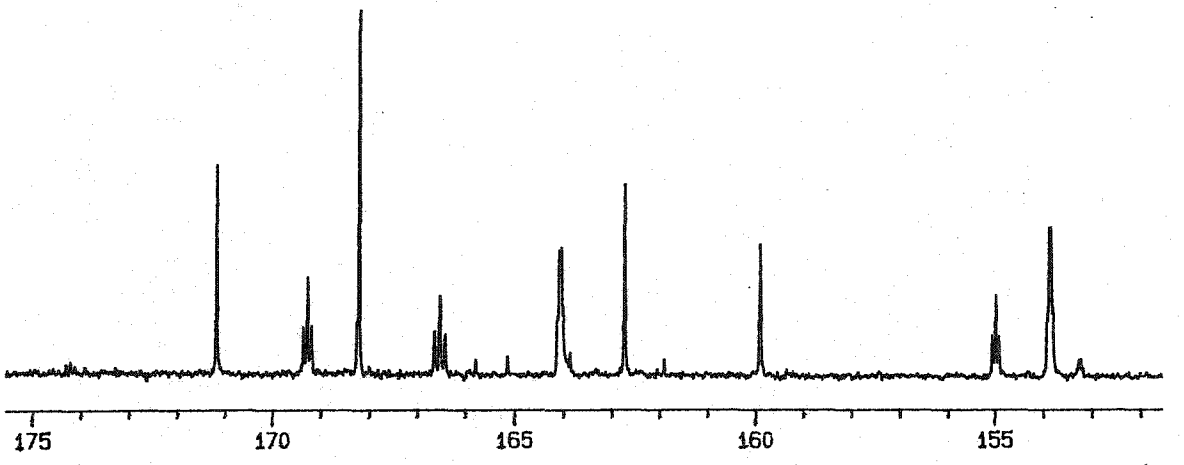

Figure 3.1.4 *Olefinic region of the $^{13}C\{^1H\}$ NMR spectrum of $[Ir_3(\mu\text{-}PPh_2)_3(CO)_5(\kappa^2\text{-}MeO_2C\underline{C}\underline{C}(CO_2Me)\underline{C}(O)(\mu\text{-DMAD})]$ (**3.1**) in CD_2Cl_2.*

apical iridium centre. Three triplets are resolved at δ = 169.3, 166.5 and 155.0 ppm with values of $^2J\{CP\}$ = 8, 10 and 6 Hz respectively. These coupling constants are in the normal range for two bond phosphorus-carbon *cis*-coupling and can only arise from C1, C2 and C70. An unambiguous assignment of the resonances is not possible without ^{13}C labeling experiments but an intuitive assignment made by comparison with related clusters will be discussed later. In principle, C71, which is part of the metallacycle should also be affected by the

two equivalent phosphido bridges. In an attempt to resolve $^{3}J\{CP\}$ and therefore assign C71 precisely, the sweep width was minimized to gain resolution which resulted in a strongly improved spectrum. Although a fourth triplet could not be resolved, the resonance at δ = 159.9 ppm appears very much in the shape of a unresolved triplet with $^{3}J\{CP\} < 2$ Hz and is therefore assigned to C71. The chemical shifts encountered for the DMAD portion of the metallacycle reflect the olefinic character of this bond as suggested on the basis of the bond distance.

The other alkyne is bridging the two basal iridium atoms of the cluster, a coordination mode very frequently encountered in di- and polynuclear transition metal alkyne chemistry. The carbon-carbon bond length of 1.350(6) Å found in the bridging DMAD ligand is similar to those normally encountered in dimetallacyclobutenes [58]. Overall the cluster core expanded significantly during the alkyne addition. All three phosphido bridges are now coplanar with the iridium triangle, thus explaining the large $^{2}J\{P_aP_x\}$ value of 168 Hz. The iridium-iridium distances in **3.1** average 3.134 Å which is very similar to an average 3.236 Å in $[Ir_3(\mu\text{-}PPh_2)_3(CO)_5(tBuNC)_2]$ (**1.5**).

It is worthwhile to examine the individual metal-metal distances in **3.1** and **1.5** more closely. Let's first consider the apical iridium centre in both clusters and the two metal-metal distances that span this unique atom and the two basal iridium

centres. In both clusters, the geometry of the unique iridium is very similar and can be considered, without metal-metal bonding contributions, to be distorted trigonal bipyramidal. However, it should be noted that deviation from the idealized 180 ° angle for the axial sites is much more pronounced in the alkyne adduct than in the ^{t}BuNC system, presumably induced by the steric constraints of the four-membered ring. The metal-metal distances that span between this site and the basal iridium centres are remarkably similar despite the different steric and electronic influences of the ligands (see Figure 3.1.5).

During the addition of ^{t}BuNC to the parent cluster $[Ir_3(\mu\text{-}PPh_2)_3(CO)_5]$ the oxidation state of the apical atom does not change and the reaction is best understood in terms of two-electron addition to the cluster count. In contrast, formation of the iridacyclobutenone involves oxidation of the metal centre from Ir(I) in the hexacarbonyl to Ir(III) in the alkyne adduct. Despite similarities in the average metal-metal bond lengths, the basal sides of the iridium triangles in clusters (**3.1**) and (**1.5**) are very different. The ^{t}BuNC cluster experiences the most dramatic iridium-iridium bond elongation at the basal side, away from the metal centre that underwent ligand addition. In the corresponding alkyne adduct the other DMAD ligand mimics the chemistry of dinuclear rhodium and iridium complexes and oxidatively adds across the base of the iridium-iridium triangle (see Figure 3.1.5). The discussion (Section 3.5) will be used to comment further on this oxidative addition.

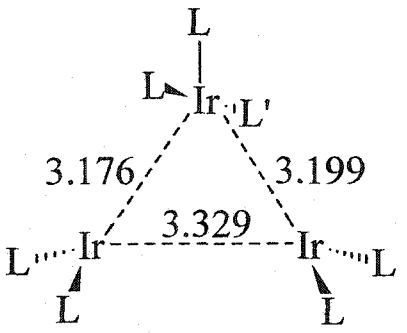

1.5

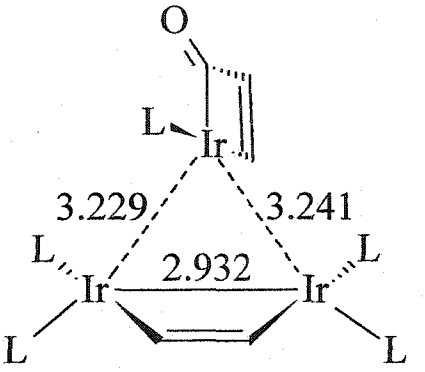

3.1

Figure 3.1.5

*Streochemistry and iridium-iridium distances of clusters (**1.5**) left and (**3.1**) right.*

(L= CO, L'= ^{t}BuNC; phosphido bridges and COOMe groups omitted for clarity.)

3.2. Stoichiometric reactions of $[Ir_3(\mu\text{-}PPh_2)_3(CO)_6]$ (2.1) with DMAD

The isolation of **3.1** immediately raised questions about the mechanism of formation. It seemed unlikely that both the addition of two molecules of alkyne as well as the CO insertion reaction would proceed simultaneously. In terms of gaining mechanistic information adding stoichiometric amounts of DMAD to **2.1** would be very interesting because it might reveal the primary processes involved in the formation of **3.1**.

Treatment of wine-red solutions of the **2.1** in either dichloromethane or benzene with one molar equivalent of DMAD results in a very slow transformation that produces a mixture of clusters as indicated by ^{31}P NMR. After one week the proton NMR of the mixture confirms the consumption of all free DMAD. Phosphorus NMR data show only a trace of starting material, **2.1**, beside a minor amount of the CO-inserted dialkyne adduct, **3.1**. The major resonances in the ^{31}P NMR spectrum of the mixture consist of a mutually coupled doublet and triplet at +12.2 and -68.0 ppm, respectively. These signals are very similar to those observed for **3.1**, except much broader, and are in agreement with the formation of a new compound, **3.3**. The large phosphorus-phosphorus coupling constant of $^2J\{P_aP_x\}$ = 164 Hz, found in **3.3**, is also extremely similar to the 168 Hz encountered in **3.1** and suggests a planar arrangement of the three phosphido bridges with respect to the metal triangle.

The new cluster readily crystallizes from concentrated dichloromethane or benzene solution upon hexane addition to form large bright yellow prisms. Subsequent analysis of the NMR, infrared and FAB MS spectra allowed the assignment of the new cluster the formula $[Ir_3(\mu\text{-}PPh_2)_3(CO)_6(DMAD)]$ which is also in good agreement with analytical data.

The infrared spectrum of **3.3**, shown in Figure 3.2.1, exhibits six terminal carbonyl absorptions which, on average, shift slightly to higher energy when compared with the parent hexacarbonyl (**2.1**) indicating oxidation of at least one metal centre. Two well resolved infrared bands at 1707 and 1682 cm^{-1} are

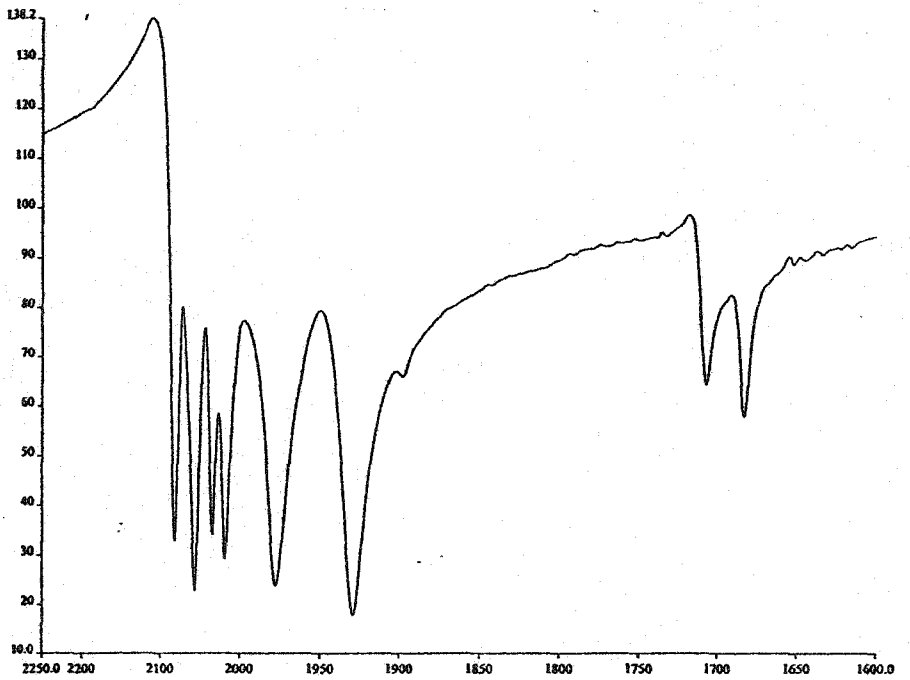

Figure 3.2.1 *Part of the infrared spectrum of* $[Ir_3(\mu\text{-}PPh_2)_3(CO)_6(\mu\text{-}DMAD)]$ (**3.3**) *in KBr.*

assigned to the carboxylates of the DMAD ligand and confirms coordination. Proton NMR data for **3.3** are in agreement with the addition of only one molecule of alkyne to the cluster core. A single resonance, integrating for six protons, is observed for the two methoxy groups of the coordinating DMAD ligand.

Structural analysis of $[Ir_3(\mu\text{-}PPh_2)_3(CO)_6(\mu\text{-}DMAD)]$ (3.3)

The crystal structure of **3.3** was determined by Bob McDonald and is shown in Figure 3.2.2. Relevant structural parameters are given in Table 3.2.1, while selected bond lengths and angles are listed in Table 3.2.2.

The addition of one molecule of DMAD is confirmed and shown to have proceeded via oxidative addition across the basal side of the iridium triangle. It is most interesting to note that the two apical iridium-iridium bonds of the 50 electron cluster have been broken during the oxidative addition (3.3317(3) and 3.2000(3) Å), which is in good agreement with the isoelectronic $[Ir_3(\mu\text{-}PPh_2)_3(CO)_4(^tBuNC)_3]$, while the basal site, which is now bridged by the DMAD ligand, contains a metal-metal bond (2.8641(3) Å). It is not immediately obvious from ^{31}P NMR data whether to assign a metal-metal bond to the basal site of the iridium triangle since the unique phosphido bridge in **3.3** resonates at -68 ppm. This data clearly demonstrates, that the deshielding of the phosphorus nucleus by the electron pair in the metal-metal bond is an oversimplification and that the down-field shift of the phosphorus nucleus usually encountered in phosphido-bridged metal-metal bonded di-and trinuclear systems does not hold for all

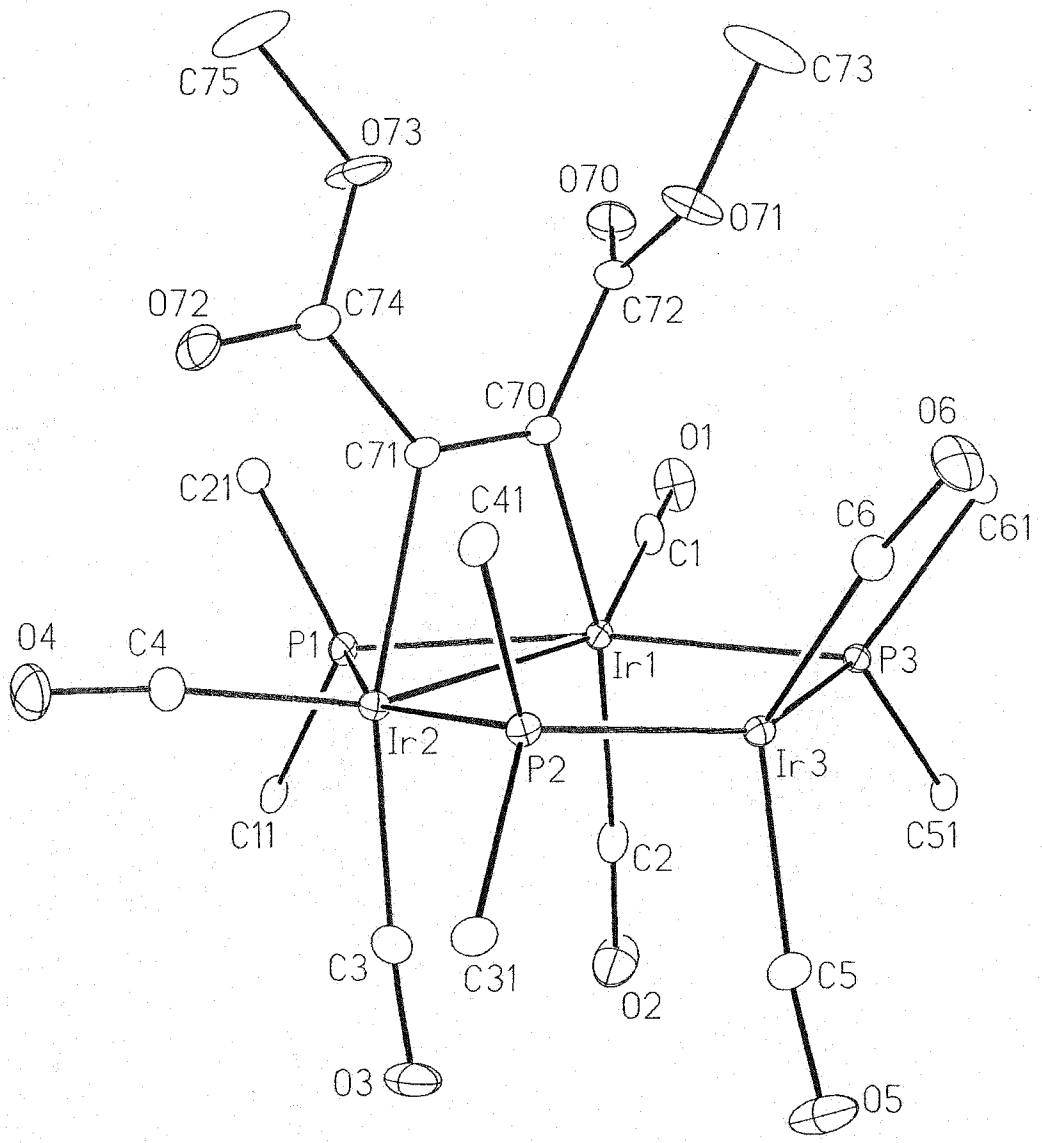

Figure 3.2.2 *Molecular structure of* $[Ir_3(\mu\text{-}PPh_2)_3(CO)_6(\mu\text{-}DMAD)]$ (**3.3**).

For clarity only the ipso-carbons of the phenyl rings are shown.

A. Crystal Data

formula	$C_{48}H_{36}Ir_3O_{10}P_3$
formula weight	1442.28
crystal dimensions (mm)	0.40 × 0.36 × 0.21
crystal system	monoclinic
space group	$P2_1/n$ (an alternate setting of $P2_1/c$ [No. 14])
unit cell parameters	
a (Å)	11.5406 (6)
b (Å)	31.9684 (16)
c (Å)	13.2842 (7)
β (deg)	106.8731 (10)
V (Å^3)	4690.0 (4)
Z	4
ρ_{calcd} (g cm^{-3})	2.043
μ (mm^{-1})	8.651

B. Data Collection and Refinement Conditions

diffractometer Bruker	PLATFORM/SMART 1000 CCD[b]
radiation (λ [Å])	graphite-monochromated Mo Kα (0.71073)
temperature (°C)	−80
total data collected	23288 ($-14 \le h \le 14$, $-39 \le k \le 40$, $-11 \le l \le 16$)
independent reflections	9616
number of observed reflections (*NO*)	8393 [$F_o^2 \ge 2\sigma(F_o^2)$]
R_1 [$F_o^2 \ge 2\sigma(F_o^2)$]	0.0272
wR_2 [$F_o^2 \ge -3\sigma(F_o^2)$]	0.0643

Table 3.2.1 *Crystallographic experimental details for* $[Ir_3(\mu\text{-}PPh_2)_3(CO)_6(\mu\text{-}DMAD)]$ (**3.3**).

Atoms	Distance	Atoms	Distance
Ir(1)-Ir(2)	2.8641(3)	Ir(2)-C(3)	1.954(5)
Ir(1)-Ir(3)	3.2000(3)	Ir(2)-C(4)	1.874(5)
Ir(2)-Ir(3)	3.3317(3)	Ir(3)-C(5)	1.890(5)
Ir(1)-P(1)	2.3500(11)	Ir(3)-C(6)	1.859(5)
Ir(1)-P(3)	2.4120(11)	Ir(1)-C(70)	2.100(4)
Ir(2)-P(1)	2.3236(12)	Ir(2)-C(71)	2.093(4)
Ir(2)-P(2)	2.3945(12)	C(70)-C(71)	1.332(6)
Ir(3)-P(2)	2.2885(11)	C(70)-C(72)	1.489(6)
Ir(3)-P(3)	2.2826(11)	C(72)-O(70)	1.211(6)
Ir(1)-C(1)	1.882(5)	O(1)-C(1)	1.139(6)
Ir(1)-C(2)	1.943(5)	O(2)-C(2)	1.128(6)

Atoms	Angles	Atoms	Angles
Ir(2)-Ir(1)-Ir(3)	66.385(6)	C(1)-Ir(1)-Ir(2)	149.96(14)
Ir(1)-Ir(2)-Ir(3)	61.647(6)	C(2)-Ir(1)-C(70)	164.0(2)
Ir(1)-Ir(3)-Ir(2)	51.968(6)	P(1)-Ir(1)-C(1)	102.00(14)
Ir(1)-P(1)-Ir(2)	75.59(3)	P(3)-Ir(1)-C(1)	94.91(14)
Ir(2)-P(2)-Ir(3)	90.68(4)	P(3)-Ir(1)-C(2)	88.61(14)
Ir(3)-P(3)-Ir(1)	85.89(4)	P(1)-Ir(1)-C(2)	89.53(14)
P(1)-Ir(1)-P(3)	163.07(4)	Ir(2)-Ir(1)-C(2)	96.26(17)
P(1)-Ir(2)-P(2)	156.32(4)	Ir(2)-Ir(1)-C(70)	67.79(12)
P(2)-Ir(3)-P(3)	144.63(4)	Ir(1)-C(70)-C(71)	112.1(3)

Table 3.2.2 *Selected internuclear distances (Å) and angles (°) for* $[Ir_3(\mu\text{-}PPh_2)_3(CO)_6(\mu\text{-}DMAD)]$ (**3.3**). *Estimated standard deviations are given in parentheses*

cases. The three phosphido bridges lie within the plane of the iridium triangle which is in good agreement with the large phosphorus-phosphorus coupling constant observed by NMR. P(2) exhibits the greatest deviation from planarity, resting 0.3810(11) Å out of the Ir_3 plane. In contrast, the DMAD ligand, which is bridging the basal side of **3.3** is orthogonal to this metal plane, with a dihedral angle of 88.73(9) °. The coordination sphere around each of the basal iridium centres is roughly octahedral and overall very similar to the geometry encountered in numerous dinuclear μ-η^2 type alkyne-bridged complexes [59]. Finally, the unique iridium centre in **3.3**, which can formally be assigned a 16-valence electron count, is still coordinatively unsaturated and exhibits distorted tetrahedral geometry. It is thus not difficult to understand the reactivity of **3.3** in the transformation to **3.1**, which involves addition of another DMAD molecule and subsequent CO insertion at the unsaturated metal centre [109].

^{13}C NMR data for the alkyne **3.3** are in agreement with the molecular structure determined in the solid state. The acquisition of a ^{13}C NMR spectrum for an alkyne cluster in sufficient detail for analysis, is not a trivial exercise. It was especially difficult for **3.3** which exhibits broad NMR resonances for reasons not clearly understood at present. Two broad, weak signals at +188.2 and +185.4 ppm can be assigned to the two terminal carbonyl ligands of the unique iridium centre. Non-equivalence of these nuclei arises because carbonyl C_a (see

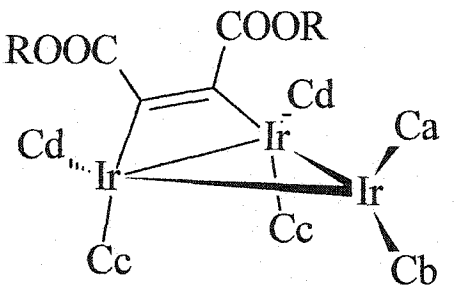

Figure 3.2.3 *Atomic labeling scheme for [$Ir_3(\mu\text{-}PPh_2)_3(CO)_6(\mu\text{-}DMAD)$] (**3.3**) used in ^{13}C NMR discussion.*

δ (ppm)	CO_c	CO_d	COOMe
(**3.3**)	165.4 (m)	153.3 (m)	168.0 (s)
(**3.1**)	164.1 (m)	153.8 (m)	168.2 (s)

Table 3.2.3 *Selected ^{13}C NMR shifts of clusters [$Ir_3(\mu\text{-}PPh_2)_3(CO)_6(\mu\text{-}DMAD)$] (**3.3**) and [$Ir_3(\mu\text{-}PPh_2)_3(CO)_5(\kappa^2\text{-}MeO_2CCC(CO_2Me)C(O)(\mu\text{-}DMAD)$] (**3.1**).*

numbering scheme in Figure 3.2.3) is close to the bridging alkyne which provides a different environment than the terminal axial carbonyl ligands C_c which are close to C_b. The values for the observed chemical shifts for C_a and C_b are close to the average carbonyl resonance of 182.1 ppm found at room temperature for

hexacarbonyl (**2.1**), suggesting that the apical iridium centre, which is coordinatively very similar to that in **3.3** remains largely undisturbed during the DMAD addition. A relatively sharp singlet at +168.0 ppm is easily assigned to the two equivalent carboxylate carbons of the bridging DMAD ligand, while two broad multiplets at +165.4 and +153.3 ppm arise from the two pairs of equivalent axial and equatorial carbonyls $2C_c$ and $2C_d$.

The olefinic resonances due to DMAD carbons of the metallacycle cannot be resolved and are most likely obscured by the intense signals resulting from the diphenylphosphido groups.

There is an apparent similarity in the ^{13}C NMR spectra of **3.1** and **3.3**. concerning the ligand sets of the two basal iridium centres as shown in Table 3.2.3. The basal sites in those two clusters possess not only the same ligand set but exhibit overall very similar stereochemistry which most likely accounts for the similar chemical shifts observed.

3.3. Decarbonylation of $[Ir_3(\mu\text{-}PPh_2)_3(CO)_6(\mu\text{-}DMAD)]$ (3.3)

Surprisingly, upon purification of **3.3** via multiple recrystallization procedures, a minor impurity became more and more noticeable in the proton and phosphorus NMR spectra, especially when crystals of the sample had been under vacuum to

remove trace amounts of hexane employed in the recrystallization. Evaporation of solutions containing **3.3** and extensive pumping on the resulting powder produced, in fact, a new compound, **3.2**, presumably the decarbonylation product of **3.3**. The transformation, which was found to proceed very cleanly is also fully reversible. Thus, introducing a CO atmosphere over solutions of **3.2** instantly regenerates **3.3**, with a corresponding color change from orange to yellow. It is interesting to note here that, for reasons not clearly understood, the NMR signals of **3.3** significantly broaden when excess CO is present.

A dynamic equilibrium involving addition and loss of a terminal carbonyl to interconvert **3.2** and **3.3** seems not unreasonable since the very same process is encountered in the parent systems **2.1** and **2.2** as well as the related bis-diphenylphosphinomethane substituted derivatives **1.1** and **1.2** (Equation 3.3.1) and is generally quite common in trinuclear phosphido-bridged cluster chemistry of group 9 transition metals as discussed in detail in the introduction.

$$[Ir_3(\mu\text{-}PPh_2)_3(CO)_3(\mu\text{-dppm})] + CO \rightleftharpoons [Ir_3(\mu\text{-}PPh_2)_3(CO)_4(\mu\text{-dppm})] \quad (3.3.1)$$

An experiment to prove that **3.2** is indeed the decarbonylation product of **3.3** was carried out and involved the addition of one molar equivalent of DMAD to the pentacarbonyl $[Ir_3(\mu\text{-}PPh_2)_3(CO)_5]$ (**2.2**). Treatment of strawberry red solutions

of **2.2** with one molar equivalent of DMAD results in an instant color change to orange. Spectroscopic properties of the orange product were found to be identical to those obtained for **3.2** and will be discussed later. Furthermore, **3.2** instantly converts to **3.3** upon exposure to 1 atm of CO, opening up an alternative and much more convenient synthesis for this cluster. The rapid formation of **3.3** in two steps from the **2.2** contrasts with the extremely slow transformation involving stoichiometric alkyne addition to **2.1**. Scheme 3.3.1 summarizes the equilibria and reaction sequences encountered in the mono alkyne systems.

Given the experimental evidence, especially the surprising observation that the pentacarbonyl (**2.2**) adds only one alkyne even when a hundred molar equivalents of DMAD are present, it seems possible to make some valid statements about the formation of **3.1**. It is assumed that the hexacarbonyl (**2.1**), which is quite inert, dissociates one carbonyl at first giving **2.2** and free CO gas. Because the rate of dissociation is slow the CO remains dissolved. The highly reactive pentacarbonyl immediately reacts with available DMAD to generate **3.2** which competes with **2.2** in the uptake of free CO from the solution to form **3.3**. This assumption is also supported by the observation that excess DMAD accelerates the overall reaction, leading to **3.1**, but excess CO gas does not lead to rate enhancement. Since CO insertion into the metal-alkyne bond of **3.3**

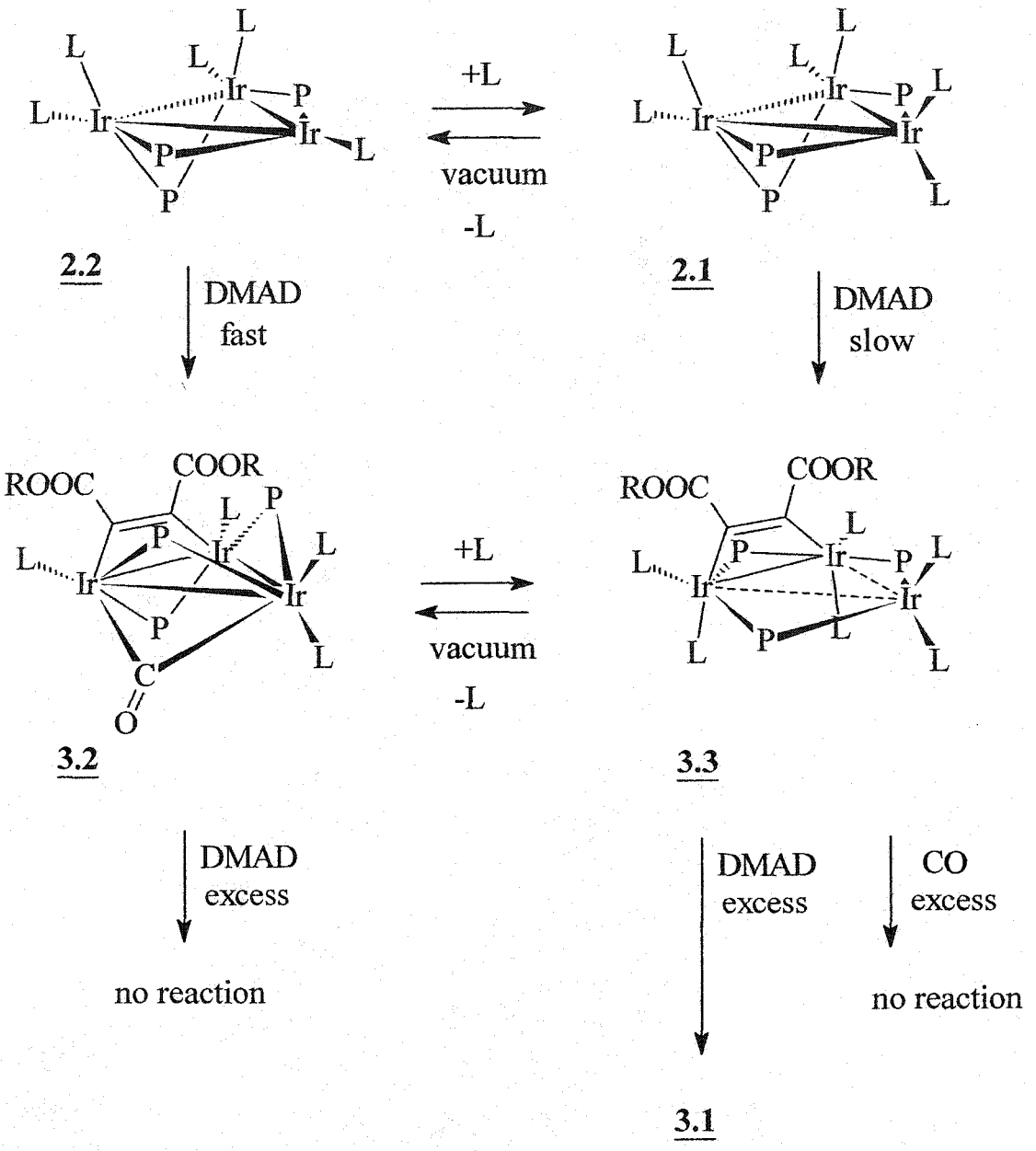

Scheme 3.3.1 *Interconversions of clusters $[Ir_3(\mu\text{-}PPh_2)_3(CO)_6]$ (**2.1**) and $[Ir_3(\mu\text{-}PPh_2)_3(CO)_5]$ (**2.2**) as well as $[Ir_3(\mu\text{-}PPh_2)_3(CO)_6(\mu\text{-}DMAD)]$ (**3.3**) and $[Ir_3(\mu\text{-}PPh_2)_3(CO)_5(\mu\text{-}DMAD)]$ (**3.2**) and reactivity of those clusters towards CO and DMAD, L=CO, P=PPh_2, R=OMe*

cannot be induced, not even under a CO atmosphere, it seems reasonable to suggest that coordination of a second DMAD molecule to **3.3** proceeds next, followed by CO insertion, leading to the final product **3.1** [109].

Spectroscopic analysis

^{31}P NMR parameters of **3.2**, **3.3** and **3.1** as well as relevant atomic numbering schemes are given in Table 3.3.1. Assignment of the observed ^{31}P NMR resonances is straightforward for **3.1** and **3.3** because the overall symmetry of the clusters does not permit an alternative interpretation. The situation is however more complicated for **3.2** which exhibits three phosphorus NMR signals indicating three inequivalent phosphido bridges.

Given the structural information for the closely related **3.3** it was assumed at first that **3.2** should be isostructural with **3.3** differing only in the absence of a terminal carbonyl, which caused the loss of symmetry as indicated by phosphorus, proton and carbon NMR spectroscopy. A more careful analysis however, especially of the infrared spectrum and ^{31}P NMR parameters, was not in agreement with the initially anticipated structure.

Although infrared spectra for **3.2** and **3.3** are quite similar, **3.3** exhibits a strong absorption band at 1849 cm $^{-1}$ typical of a bridging carbonyl ligand, in addition to

four terminal CO bands (see Figure 3.3.1). Two bands at 1706 and 1686 cm^{-1} associated with the two carboxylate groups of the DMAD ligand, confirm the coordination of the alkyne. The carboxylate bands are essentially identical in shape and energy to those found in **3.3**. The absorption at 1657 cm^{-1} could be assigned to the symmetric C=C stretch of the bridging alkyne, but such an absorption is absent in the IR spectrum of **3.3**.

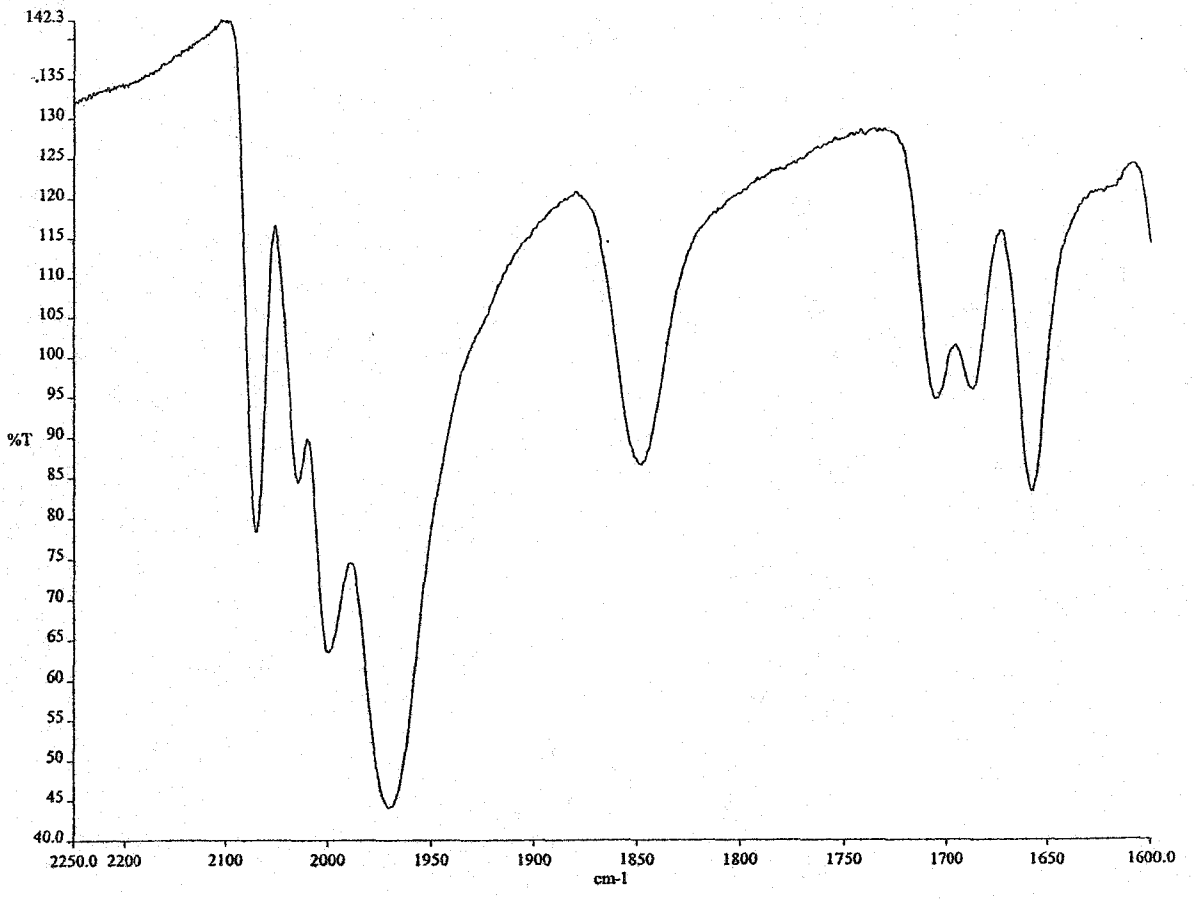

Figure 3.3.1 *Part of the solid state infrared spectrum of*

*$[Ir_3(\mu\text{-}PPh_2)_3(\mu\text{-}CO)(CO)_4(\mu\text{-}DMAD)]$ (**3.2**) (KBr)*

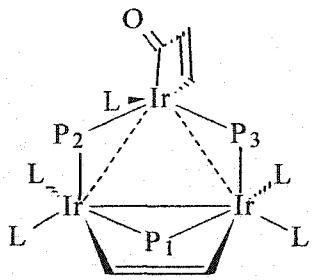

3.1

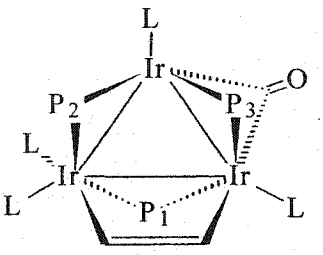

3.2

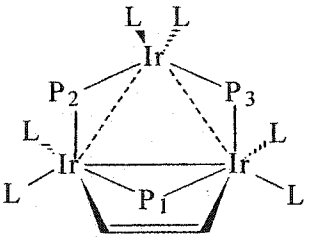

3.3

Compound	(3.1)[a]	(3.2)[b]	(3.3)[a]
δ_1 (ppm)	-59.8 (t)	+80.5 (d of d)	-68.0 (t)
δ_2 (ppm)	-16.8 (d)	+31.7 (d)	+12.2 (d)
δ_3 (ppm)	-16.8 (d)	+142.8 (d)	+12.2 (d)
$^2J(1,2)$ (Hz)	168	140	164
$^2J(1,3)$ (Hz)	168	c	164
$^2J(2,3)$ (Hz)	d	174	d

[a] CD_2Cl_2, [b] C_6D_6, [c] smaller than spectrum resolution of about 2 Hz,

[d] not available from observed spectrum

Table 3.3.1 *^{31}P NMR parameters for 3.1-3.3 with atomic numbering scheme.*

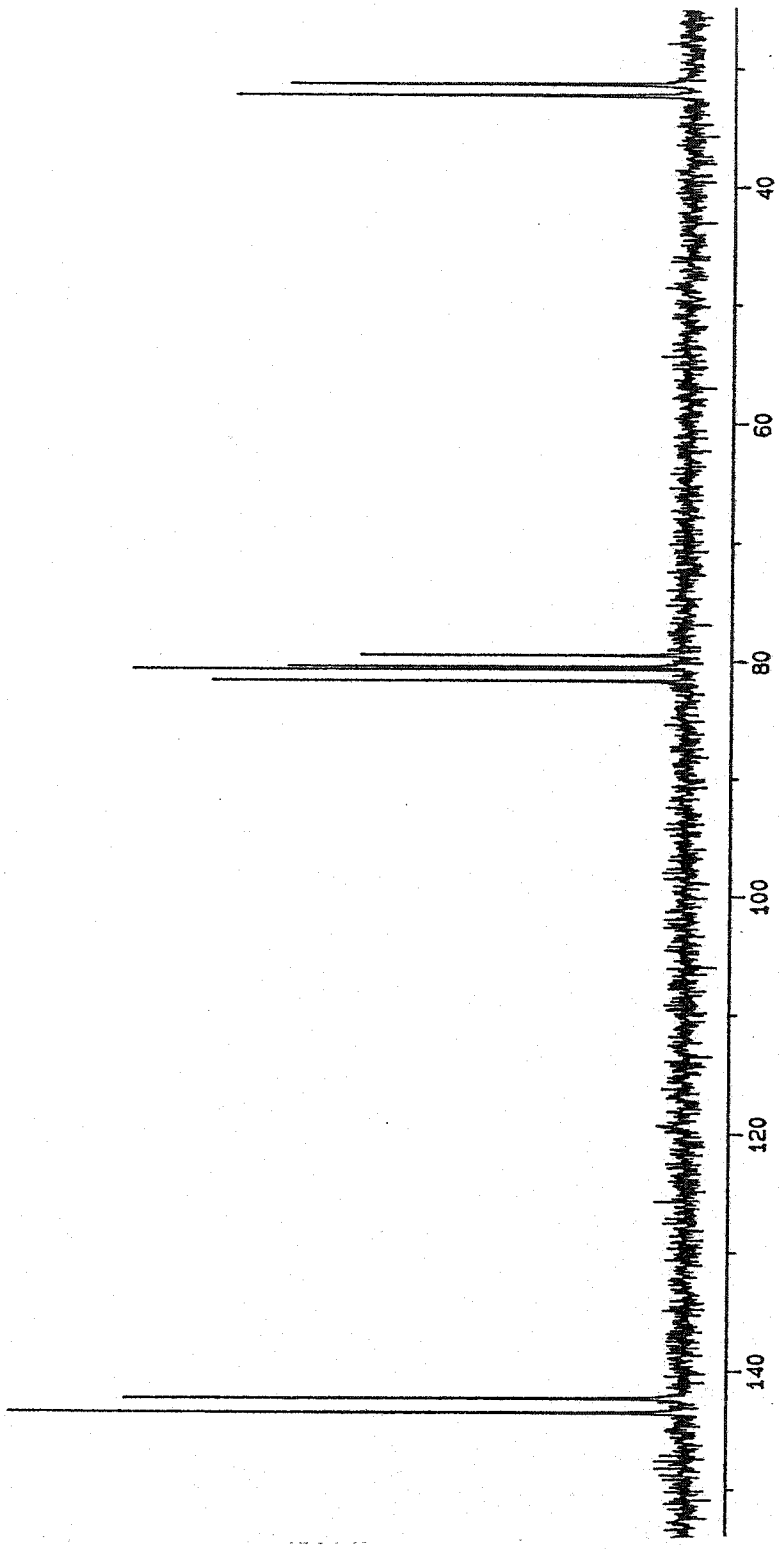

Figure 3.3.2 *^{31}P NMR spectrum of $[Ir_3(\mu\text{-}PPh_2)_3(\mu\text{-}CO)(CO)_4(\mu\text{-}DMAD)]$ (**3.2**) in benzene-d_6.*

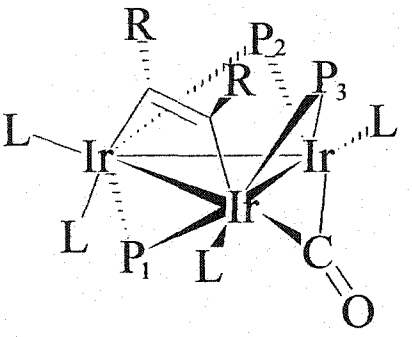

Figure 3.3.3 *Possible structure of $[Ir_3(\mu\text{-}PPh_2)_3(\mu\text{-}CO)(CO)_4(\mu\text{-}DMAD)]$ (**3.2**)*

An important insight into the structure of **3.2** arises from ^{31}P NMR parameters (see Figure 3.3.2 for spectrum and Table 3.3.1 for atomic numbering scheme). P_1 is mutually coupled to P_2 and P_3, giving rise to a doublet of doublets, while both P_2 and P_3 only appear as simple doublets coupling to P_1 but not to each other. This observation clearly implies that the phosphido bridges are no longer in the plane of the iridium triangle. Since $^2J\{P_2P_3\}$ is smaller than the spectrum resolution of about 2 Hz, P_2 and P_3 must be in a *cis* relationship to each other. At the same time the large coupling observed between P_1 and P_2 as well as P_1 and P_3 implies a trans geometry between those atoms. Thus **3.2** is anticipated to have a structure similar to the one shown in Figure 3.3.3. An unambiguous assignment of the observed phosphorus resonances for P_2 and P_3 cannot be made at this point and assignments in Table 3.3.1 have been made based on comparison with ^{31}P NMR parameters for the closely related $[Rh_3(\mu\text{-}PPh_2)_3(\mu\text{-}CO)(CO)_2(\mu\text{-}I)_2(PPh_3)]$ [44].

Other closely related clusters possessing 50 valence electrons and an *open winged* geometry of the phospido bridges include $[Rh_3(\mu\text{-}PPh_2)_3(\mu\text{-}CO)(CO)_3(\mu\text{-}Cl)_2]$ [45] and $[Ir_3(\mu\text{-}PPh_2)_3(CO)_5(\mu\text{-}DMAD)_2]$ (**4.1**) discussed in Chapter 4. The presence of bridging ligands other than the phosphido groups seems to be a common feature amongst such *open winged* clusters (see also Table 2.3.1, Type E geometry) and include μ-Cl, μ-I, μ-CO and μ-DMAD ligands.

Unfortunately several attempts to obtain even small crystals of **3.2** proved unsuccessful. The material precipitates as an orange-red powder from solvent mixtures such as benzene/hexane or dichloromethane/pentane. At present, studies are underway to obtain an isoelectronic and hopefully isostructural triphenylphosphine derivative of **3.2** employing the addition of one mole of DMAD to $[Ir_3(\mu\text{-}PPh_2)_3(CO)_3(PPh_3)_2]$. If this reaction is carried out using excess alkyne and 1 atm of CO **3.1** can be isolated in good yield and it is expected that without additional CO or alkyne a synthetic method to triphenylphosphine substituted derivatives of **3.2** can be established.

3.4 Reaction of $[Ir_3(\mu\text{-}PPh_2)_3(CO)_{5-n}(^tBuNC)_{2+n}]$ (n=0, 1.5; n=1, 1.6) with DMAD

Solutions of the isocyanide clusters **1.5** and **1.6** in benzene or dichloromethane react with DMAD causing a color change from bright yellow to orange over a period of several hours. This reaction contrasts with the clean transformation encountered upon alkyne addition to $[Ir_3(\mu\text{-}PPh_2)_3(CO)_6]$ (**2.1**) since mixtures of new clusters are obtained upon DMAD addition to **1.5** and **1.6** as indicated by ^{31}P NMR (see Equations 3.4.1 and 3.4.2)

1.5 +xs DMAD → **3.4a** + **3.4b** (3.4.1)

1.6 +xs DMAD → **3.5a** + **3.5b** (3.4.2)

Initial attempts to separate the cluster mixtures using fractional crystallization proved only partially useful, unfortunately, with a great reduction of the overall yield. Complete separation was never achieved by this method. The observation that the new cluster mixtures **3.4a-b** and **3.5a-b** did not elute from alumina with either benzene, or dichloromethane, but with oxygen donor solvents such as acetone or THF, led to an extensive search for a mixture of these solvents which would separate the clusters. It was subsequently discovered that a yellow band could be eluted upon introducing cluster mixture **3.5a-b** on to an alumina column using benzene : THF (ratio of 5:1) as the mobile phase. This yellow band contained **3.5a** only. After collecting all of the yellow band and increasing the THF concentration another band could be eluted which contained the orange

3.5b exclusively. Using higher THF concentrations accelerated the movement but proved impractical since the new cluster readily decomposed in pure THF in the presence of even small amounts of oxygen. Therefore all procedures were carried out using carefully deoxygenated solvents and the THF concentration was kept as low as possible.

Spectroscopic analysis of 3.5a and 3.5b

The spectroscopic properties of the DMAD adducts of the *tris*-isocyanide cluster $[Ir_3(\mu\text{-}PPh_2)_3(CO)_4(^tBuNC)_3]$ (**1.6**) will first be discussed. FAB MS spectra of the two new alkyne clusters **3.5a** and **3.5b**, shown in Figure 3.4.1, gave the same molecular ion at 1778 indicative of the net addition of two molecules of DMAD to both clusters. The spectra are extremely similar with the same fragment peaks being encountered with only slight variations in their relative intensities (see Table 3.4.1 for detailed analysis). Solid state infrared spectra of the two new clusters appear, at first sight, superimposable between 400 and 4000 cm^{-1}. A more detailed analysis shows minor band shifts with the greatest deviation being 10 cm^{-1} for an isocyanide band. These results clearly suggest that the two new alkyne clusters are isomers having the stochiometry $[Ir_3(\mu\text{-}PPh_2)_3(CO)_4(^tBuNC)_3(DMAD)_2]$. Analytical data of the dichloromethane solvates are essentially identical.

The infrared spectra of **3.5.a** and **3.5b** also give an important insight into the structure of the new alkyne adducts. Three bands around 2200 cm^{-1} with a

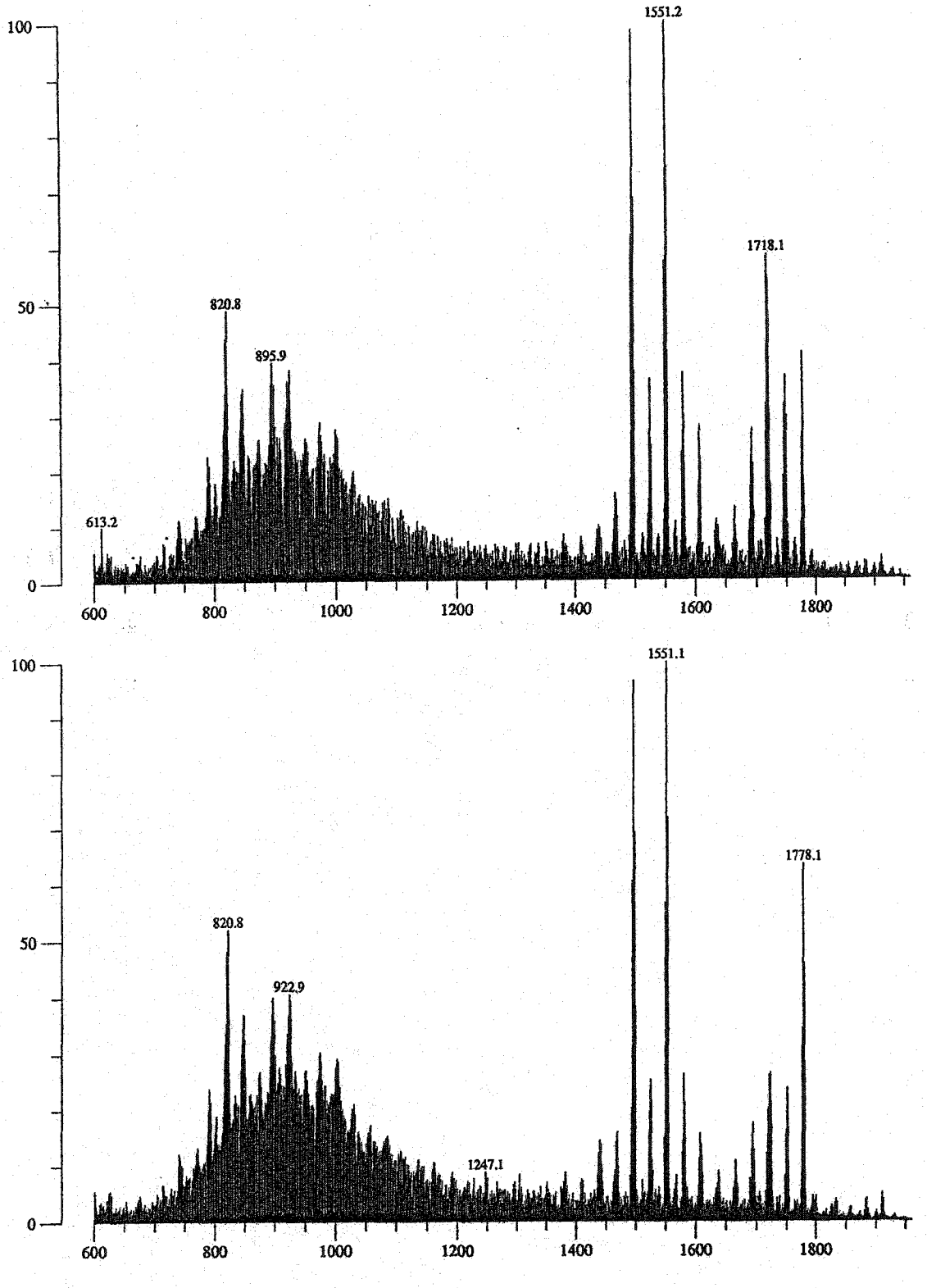

Figure 3.4.1 *FAB MS spectra of **3.5a** top, and **3.5b** bottom.*

Ion (m/z)	Intensities in % for 3.5a	3.5b	Assignment
1778	41	67	[M+H]
1749	30	24	[M-CO]
1721	47	27	[M-2CO]
1720	56	26	[M-^{t}Bu]
1718	60	22	[M-CO_2Me]
1693	28	18	[M-3CO]
1665	13	12	[M-4CO]
1607	28	17	[M-alkyne-CO]
1579	38	27	[M-alkyne-2CO]
1551	100	100	[M-alkyne-3CO]
1524	37	25	[M-alkyne-^{t}BuNC-CO]
1496	98	97	[M-alkyne-^{t}BuNC-2CO]
1468	17	17	[M-alkyne-^{t}BuNC-3CO]
1440	10	14	[M-alkyne-^{t}BuNC-4CO]

Table 3.4.1 *Analysis of the FAB MS spectra for **3.5a** and **3.5b***

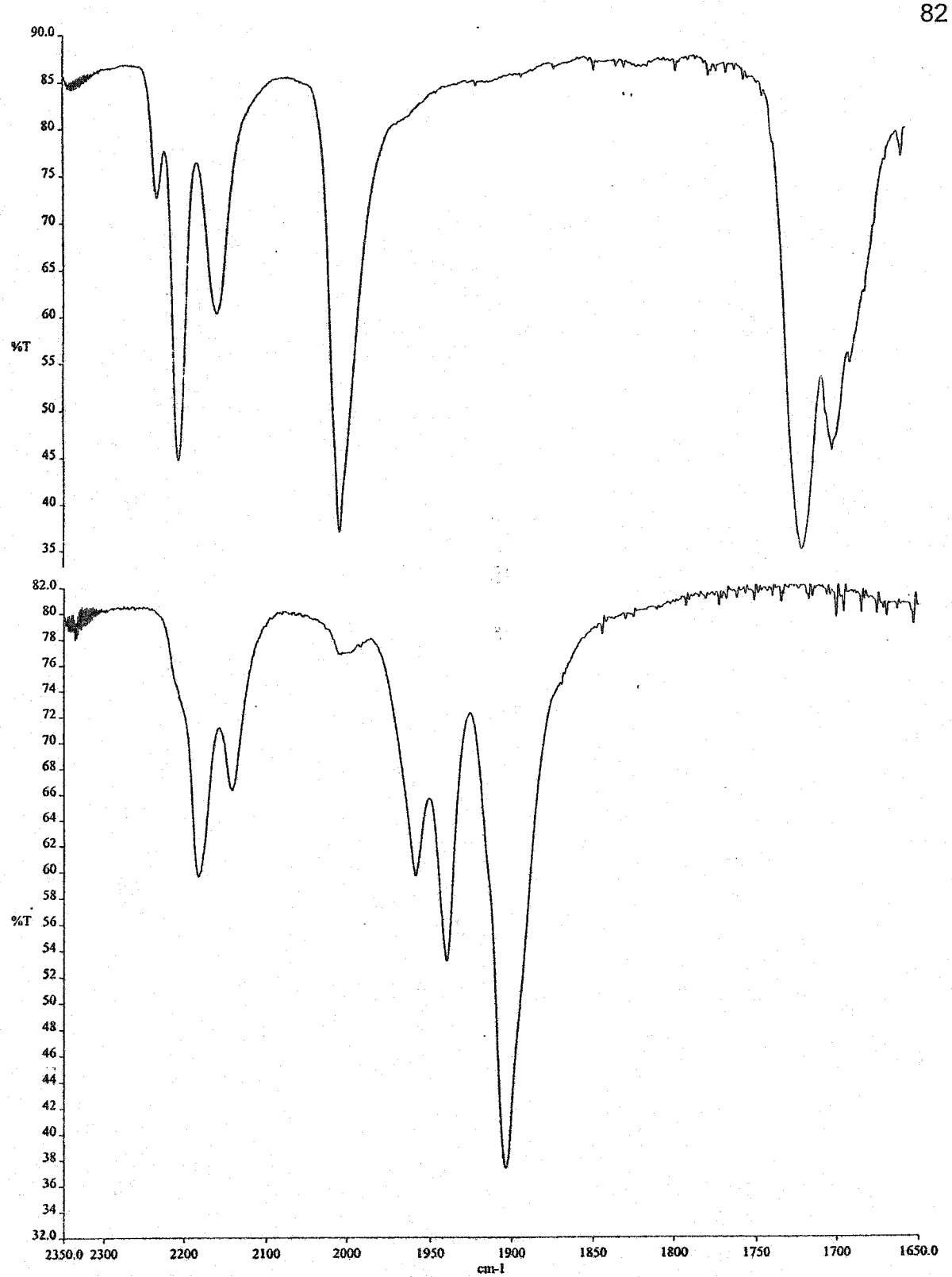

Figure 3.4.2 *Infrared spectra of* ***3.5a*** *top, and the DMAD free* ***1.6*** *bottom (KBr).*

pattern extremely similar to that observed for the parent **1.6** suggests that the three isocyanide ligands are still coordinating to the apical iridium centre which presumably remains largely undisturbed during the reaction. In contrast, a dramatic change is observed in the terminal carbonyl region of the infrared spectrum. The multiple band structure in the carbonyl region that predominates the spectrum of **1.6** essentially collapses into one strong absorption band at 2003 cm^{-1} which is found in both isomers. Figure 3.4.2 illustrates those changes by comparing the infrared spectra of **3.5a** with that of the DMAD free parent **1.6**.

The similarity between IR and FAB MS data initially caused doubt on whether the separation was successful, but ^{31}P and ^{1}H NMR analysis confirmed the two new clusters which exhibit different NMR parameters.

Phosphorus NMR parameters of the new clusters change little when compared with their parents, as shown in Table 3.4.2, suggesting that the overall geometry of the cluster core remains similar with non-bonding iridium-iridium distances and all three phosphido bridges in the plane of the metal triangle. However, proton NMR gives a very important insight into the symmetry of the two isomers. Isomer **3.5a**, the fast eluting yellow band, exhibits two resonances in a 1:2 ratio for the *tert*-butyl protons of the coordinating isocyanide ligands, resembling the ^{1}H NMR spectrum of the parent **1.6**. In the latter cluster two signals arise because of the different chemical environments of equatorial and axial ^{t}BuNC

Compound	$\delta_{1,2}$ (ppm)	δ_3 (ppm)	$^2J\{P_aP_x\}$	comments
(**3.4a**)	-43.8 (d)	+13,0 (t)	200 Hz	yellow flakes
(**3.4b**)	-34.7 (d)	+9.7 (t)	200 Hz	yellow prisms
(**3.5a**)	-39.4 (d)	+6.2 (t)	195 Hz	yellow needles
(**3.5b**)	-30.6 (d)	-16.7 (t)	196 Hz	orange prisms
(**1.5**)[b]	-8.2 (d)	+38.0 (t)	144 Hz	yellow needles
(**1.6**)[b]	-1.6 (d)	+36.4 (d)	141 Hz	yellow needles

[a] solvent CD_2Cl_2, [b] from reference [44]

Table 3.4.2

*^{31}P NMR parameters[a] for clusters **3.4a** - **3.5b** and the DMAD free **1.5** - **1.6**.*

groups coordinated to the apical iridium centre. Both axial groups are related by a symmetry plane that passes through the metal triangle, as well as a C_2 axis passing through the unique iridium centre and bisecting the metal triangle, thus causing the 1:2 ratio of the signals.

In contrast, isomer **3.5b**, the late eluting orange band, exhibits three signals for the three coordinated isocyanide groups which appear in a 1:1:1 ratio, clearly indicating different cluster symmetry. Yet, only two resonances corresponding to

the four methoxy groups of the two coordinating alkynes appear in the proton NMR spectra of **3.5a** and **3.5b**.

Furthermore, the A_2X spin system encountered in the phosphorus NMR of both isomers in conjugation with the proton NMR data imply that the loss of the symmetry element in cluster **3.5b** that causes the inequivalence of the two axial isocyanide ligands must be accompanied by the gain of another one, to account for the overall symmetry in the cluster.

Attempts to obtain single crystals proved successful only for the late eluting orange band, isomer **3.5b**. However, the large, very well formed orange prisms, obtained upon diffusing hexane into dichloromethane solutions of **3.5b**, were found to be extremely sensitive and lost their brilliant appearance immediately upon removal from the mother liquor, preventing further characterization by crystallographic techniques. Structural data would be invaluable to determine the overall stereochemistry of the clusters as well as the coordination mode of the alkynes. Thus a major effort was undertaken to obtain crystals from the DMAD adducts of the closely related di-isocyanide system **1.5** (see Equation 3.4.1) which resembles the chemistry of the tris-^{t}BuNC cluster **1.6** (Equation 3.4.2).

Again separation of two isomers was achieved on an alumina column using very similar conditions as employed for the separation of **3.5a** and **3.5b**. FAB MS and infrared spectra of the two new isomers, **3.4a** and **3.4b**, were again extremely

similar with the most notable feature of the infrared spectra being the collapse of the multiple band structure in the carbonyl region into one major band. Finally, and most importantly, proton NMR spectra of the two new isomers **3.4a** and **3.4b**, which are shown in Figure 3.4.3, mirrors the symmetry changes encountered in the tris-^{t}BuNC substituted isomers **3.5a** and **3.5b**. While the fast eluting yellow band, isomer **3.4a**, only exhibits one signal for the two axial isocyanide ligands, the slow eluting yellow band, isomer **3.4b**, shows two resonances in a 1:1 ratio implying again the loss of a symmetry element.

Finally, ^{31}P NMR parameters of **3.4a** and **3.4b**, which are given in Table 3.4.2, as well as ^{13}C NMR spectra, discussed in the structural analysis, are very similar to those of clusters **3.5a** and **3.5b**.

Structural analysis of 3.4b

Prisms that formed readily upon diffusion of pentane into dichloromethane solutions of **3.4b**, were found to be much less sensitive than crystals of **3.5b** and could be handled out of the mother liquor without apparent deterioration. The crystal structure of **3.4b** was solved by Bob McDonald and is shown in Figure 3.4.4. Crystallographic parameters and selected bond lengths and angles are given in Tables 3.4.3 and 3.4.4 respectively.

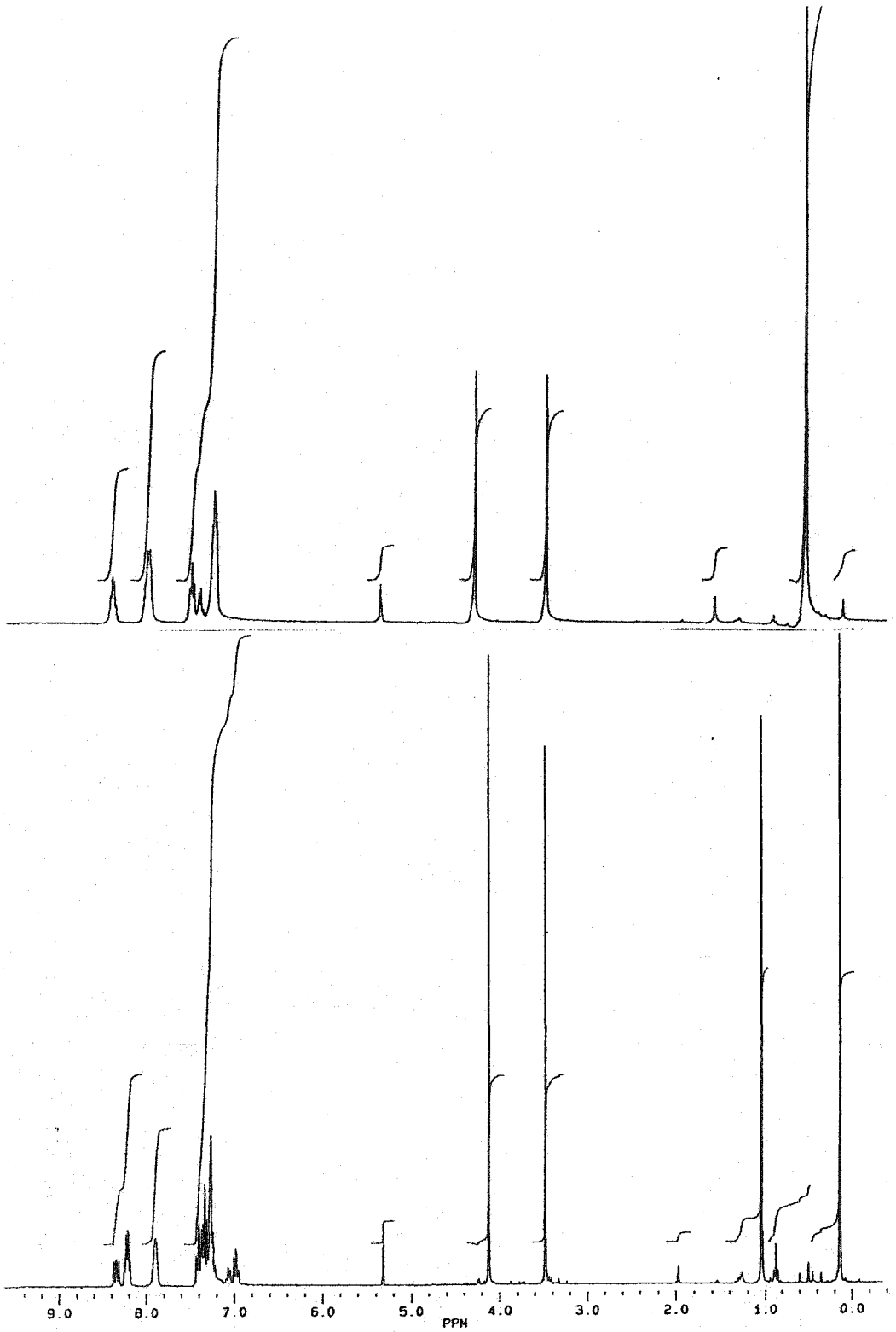

Figure 3.4.3 *^{1}H NMR spectra of **3.4a** bottom, and **3.4b** top, in dichloromethane-d_2.*

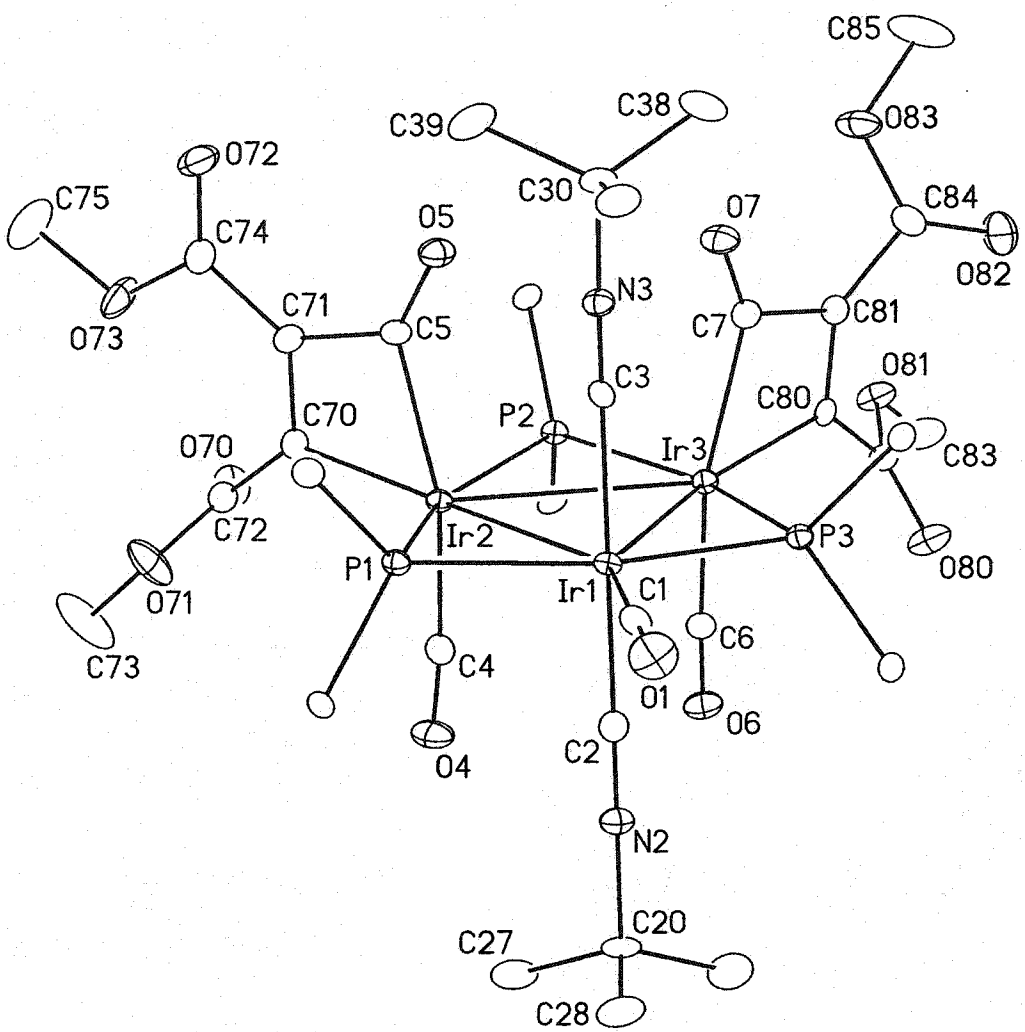

Figure 3.4.4 *Molecular structure of*

$[Ir_3(\mu\text{-}PPh_2)_3(CO)_3(^tBuNC)_2\{\kappa^2\text{-}MeO_2C\underline{C}\underline{C}(CO_2Me)\underline{C}(O)\}_2]$ ***(3.4b)***

For clarity only the ipso-carbons of the phenyl groups are shown.

A. Crystal Data

formula	$C_{66.5}H_{68}Cl_2Ir_3N_2O_{13}P_3$
formula weight	1843.64
crystal dimensions (mm)	0.24 × 0.14 × 0.13
crystal system	monoclinic
space group	$P2_1/c$ (No. 14)
unit cell parameters	
a (Å)	12.1499 (5)
b (Å)	23.4744 (10)
c (Å)	23.9287 (9)
β (deg)	99.9945 (11)
V (Å^3)	6721.2 (5)
Z	4
ρ_{calcd} (g cm^{-3})	1.822
μ (mm^{-1})	6.139

B. Data Collection and Refinement Conditions

diffractometer	Bruker P4/RA/SMART 1000 CCD[b]
radiation (λ [Å])	graphite-monochromated Mo Kα (0.71073)
temperature (°C)	−80
total data collected	33176 (-15 ≤ h ≤ 12, -27 ≤ k ≤ 29, -29 ≤ l ≤ 20)
independent reflections	13736
number of observations (*NO*)	10553 [$F_o^2 \geq 2\sigma(F_o^2)$]
R_1 [$F_o^2 \geq 2\sigma(F_o^2)$]	0.0319
wR_2 [$F_o^2 \geq -3\sigma(F_o^2)$]	0.0755

Table 3.4.3 *Crystallographic experimental detail for*

*$[Ir_3(\mu\text{-}PPh_2)_3(CO)_3(^tBuNC)_2\{\kappa^2\text{-}MeO_2CCC(CO_2Me)C(O)\}_2]$ (**3.4b**)*

Atoms	Distance	Atoms	Distance
Ir(1)-Ir(2)	3.1678(3)	Ir(2)-C(4)	1.932(6)
Ir(1)-Ir(3)	3.1408(3)	Ir(3)-C(6)	1.940(6)
Ir(2)-Ir(3)	3.1762(3)	Ir(3)-C(7)	2.111(6)
Ir(1)-P(1)	2.3733(15)	Ir(3)-C(80)	2.030(6)
Ir(1)-P(3)	2.3693(15)	C(7)-O(7)	1.209(7)
Ir(2)-P(1)	2.3081(15)	C(7)-C(81)	1.521(8)
Ir(2)-P(2)	2.3339(15)	C(80)-C(81)	1.347(8)
Ir(3)-P(2)	2.3466(14)	Ir(1)-C(2)	1.988(6)
Ir(3)-P(3)	2.3048(15)	Ir(1)-C(3)	2.010(6)
Ir(2)-C(5)	2.125(5)	C(2)-N(2)	1.142(7)
Ir(2)-C(70)	2.030(5)	C(3)-N(3)	1.128(6)
C(5)-C(71)	1.499(8)	C(84)-O(82)	1.179(7)
C(70)-C(71)	1.351(8)	C(1)-O(1)	1.110(7)
C(5)-O(5)	1.203(7)	Ir(1)-C(1)	1.894(7)

Atoms	Angles	Atoms	Angles
Ir(2)-Ir(1)-Ir(3)	60.457(7)	C(2)-Ir(1)-C(3)	179.5(2)
Ir(1)-Ir(2)-Ir(3)	59.351(7)	C(1)-Ir(1)-C(2)	90.2(2)
Ir(1)-Ir(3)-Ir(2)	60.192(7)	C(1)-Ir(1)-C(3)	89.3(2)
Ir(1)-P(1)-Ir(2)	81.16(5)	C(4)-Ir(2)-C(5)	165.0(2)
Ir(2)-P(2)-Ir(3)	85.47(5)	C(4)-Ir(2)-C(70)	101.6(2)
Ir(3)-P(3)-Ir(1)	84.43(5)	C(5)-Ir(2)-C(70)	63.5(2)
P(1)-Ir(1)-P(3)	153.91(5)	Ir(2)-C(70)-C(71)	102.8(4)
P(1)-Ir(2)-P(2)	154.09(5)	C(5)-C(71)-C(70)	100.2(5)
P(2)-Ir(3)-P(3)	155.26(5)	Ir(2)-C(5)-C(71)	93.6(4)

Table 3.4.4 *Selected bond distances (Å) and angles (°) for*

$[Ir_3(\mu\text{-}PPh_2)_3(CO)_3(^tBuNC)_2\{\kappa^2\text{-}MeO_2CC\underline{C}C(CO_2Me)\underline{C}(O)\}_2]$ ***(3.4b)***

Estimated standard deviations are given in parentheses.

The most noticeable feature in the molecular structure of **3.4b** is the insertion of two CO ligands into two separate iridium-alkyne bonds creating two independent metallacycles. This immediately accounts for the simplicity of the carbonyl region of the infrared spectra encountered in this series of compounds since the carbonyl stretching frequency of the inserted carbonyl, which now exhibits more ketonic character, moves several hundred wave numbers to lower energy, appearing between 1650 and 1730 cm^{-1}.

The structure also explains the loss of equivalence of the two axial isocyanide ligands in **3.4b** as indicated initially by proton and carbon NMR data. While one ^{t}BuNC group, pointing out of the plane of the iridium triangle, is adjacent to two metallacycles the other axial isocyanide ligand is in a different environment, experiencing the influence of nearby terminal carbonyl ligands.

The observed doublet triplet pattern in the ^{31}P NMR, as well as the occurrence of only two signals for the four methoxy groups of the metallacycles observed in the proton NMR, requires a symmetry element in the cluster. Although there is no perfect crystallographic mirror plane in the solid state structure of **3.4b**,it can be anticipated that, at least in solution, molecular motion will produce an effective symmetry plane that is perpendicular to the iridium triangle and passes through the unique metal centre as well as the midpoint of the basal iridium-iridium bond. Thus the slow eluting isomer, **3.4b**, possesses C_s symmetry in solution.

The other isomer, **3.4a**, in which the two axial isocyanide ligands are related by symmetry, gives rise to only one resonance in the proton NMR and must therefore possess a different element of symmetry. Since the infrared spectra of the two isomers are extremely similar, exhibiting the same band structure, the bond skeleton of the two isomers must remain unchanged. This allows only for the possibility that **3.4a** and **3.4b** are stereoisomers, differing only in the spatial orientation of ligands. The most likely structure for the fast eluting yellow band, isomer **3.4a**, would possess a C_2 axis that passes through the midpoint of the basal iridium-iridium bond and the unique metal centre, bisecting the iridium triangle (see Figure 3.4.5). In such a structure, the two metallacycles are in a *transoid* orientation with respect to the basal iridium centres and are related by a C_2 operation. Similarly the two axial isocyanide ligands are superimposable upon each other after a 180 ° rotation, giving rise to only one proton NMR signal for both axial ^{t}BuNC groups.

The geometry of the metallacyclobutenones in **3.4b** and the ^{t}BuNC free **3.1** are very similar, showing localized carbon-carbon double bonds for the alkyne fragment of the four membered rings while the remaining iridium-carbon bonds and the C-C bond linking the inserted carbonyl to the DMAD fragment exhibit the expected single bond character. In addition, the iridium centres involved with the metallacycles exhibit distorted trigonal bipyramidal geometry in both clusters. It is therefore not surprising that the chemical shifts of the carbon nuclei involved

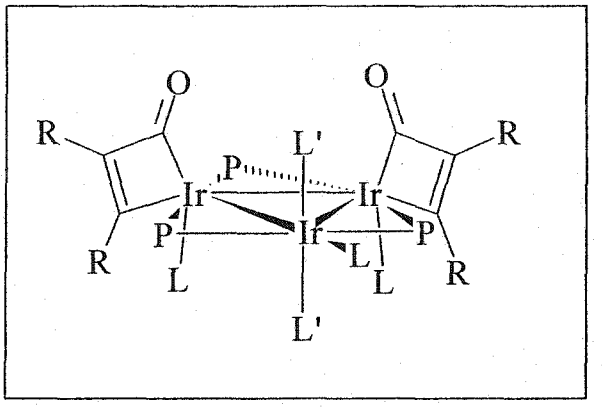

3.4b C_s

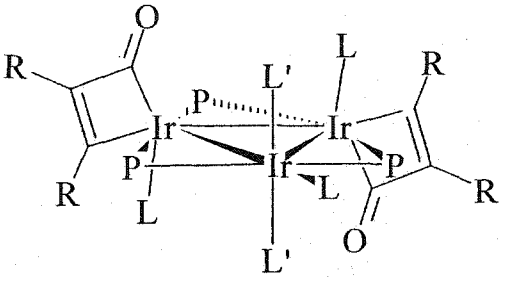

3.4a C_2

Figure 3.4.5

*Schematic representation of observed (framed) and anticipated structure for clusters **3.4b** and **3.4a** respectively (L=CO, L'=^{t}BuNC, P=PPh_2, R=COOMe).*

in the metallacycle appear at frequencies very similar to those observed in the ^{t}BuNC free **3.1**. Unfortunately, an unambiguous assignment of all resonances remains impossible without isotopic labeling experiments. Nevertheless, it appears reasonable to assign the multiplet furthest downfield to the terminal

carbonyls C4 and C6 (see ORTEP diagram in Figure 3.3.4 for atomic numbering used in NMR discussion) while the sharp singlet must clearly arise from the carboxylate carbons C74 and C84 which are four bonds away from the nearest ^{31}P nucleus. In contrast, carboxylate carbons C72 and C82, as well as olefinic C71 and C81, which are only separated by three bonds from P1 or P2, appear much broader. The remaining two multiplets, presumably doublets of doublets, must belong to olefinic C70 and C80 as well as to the inserted carbonyls C5 and C7.

Broad signals between 90 and 110 ppm are found in the ^{13}C NMR spectra of **3.4a**, **3.4b**, **3.5b** and **3.5b**) and arise from the isonitrile carbons of the coordinated ^{t}BuNC ligands, reflecting the symmetry of each isomer. For example, only one resonance appears in the C_2 isomer **3.5a** while two isocyanide resonances can be observed in the C_s isomers **3.5b**. The unusually large 50 ppm upfield shift of these resonances relative to free ^{t}BuNC implies that σ-donation plays an important role in the stabilization of the isocyanide-iridium bond while little electron density is π-back donated. This is supported by the CN stretching frequency which changes very little when comparing wave numbers for the coordinated isocyanide with those of the free ligand.

3.5 Discussion

Investigations on the reactivity of acetylenes towards low valent transition metal complexes have received considerable attention, and led to important industrial transformations. Examples include the cyclooligomerization of alkynes, initially discovered by Reppe [60, 61] and reinvestigated by Wilke [62, 63], Schrock's pioneering contributions on carbyne complexes which led to reliable homogeneous catalysis for alkyne metathesis [64] and Bönnemanns strategy to prepare substituted pyridines via cyclooligomerization of alkynes with nitriles [65]. Although Reppe's original benzene synthesis via cyclotrimerization of acetylene has long been abandoned due to the much cheaper and safer dehydrogenation of cyclohexane, cyclooligomerization is still attractive for the synthesis of cyclooctatetraene and highly substituted benzenes [62, 63]. Other transition metal complexes have since been found to catalyze the cyclotrimerization of alkynes [56, 66, 67] and it is now generally accepted that many of these cyclooligomerization reactions proceed via a series of alkyne

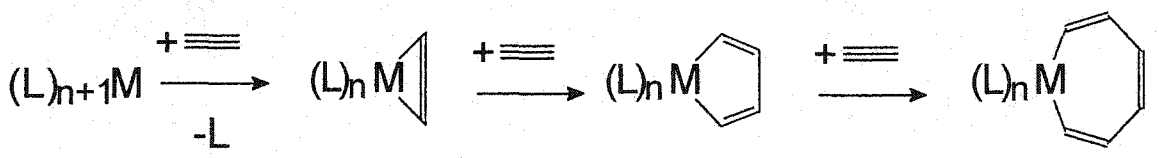

Figure 3.5.1

Sequential acetylene insertion in cyclooligomerization reaction.

insertion steps that involve the formation of metallacyclic intermediates as shown in Figure 3.5.1. $[Pd(dba)_2]$ represents an especially well studied system which helped elucidate the mechanism of sequential alkyne insertion [56]. Addition of one and two molar equivalents of DMAD to $[(dba)PdL_2]$ (A) led to the isolation of intermediates (B) and (C), respectively, as illustrated in Figure 3.5.2. Numerous other metallacyclopropene (B) and metallacyclopentadiene (C) complexes have since been isolated and characterized.

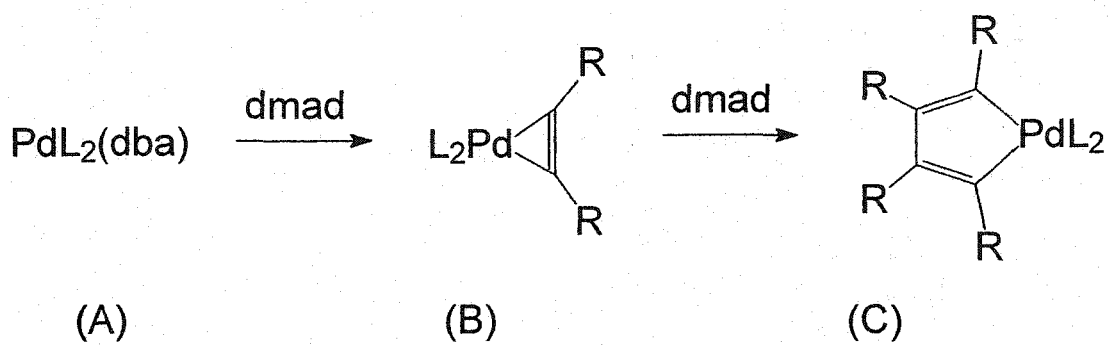

Figure 3.5.2.

Sequential DMAD addition to $[Pd(dba)L_2]$, L = PPh_3, R= COOMe [56].

A very similar sequence of substrate insertions can be proposed for Bönnemann's catalytic pyridine synthesis except that the insertion of nitrile now competes with that of alkyne, leading predominantly to pyridine formation for M=CoCp [65] as shown in Scheme 3.5.1.

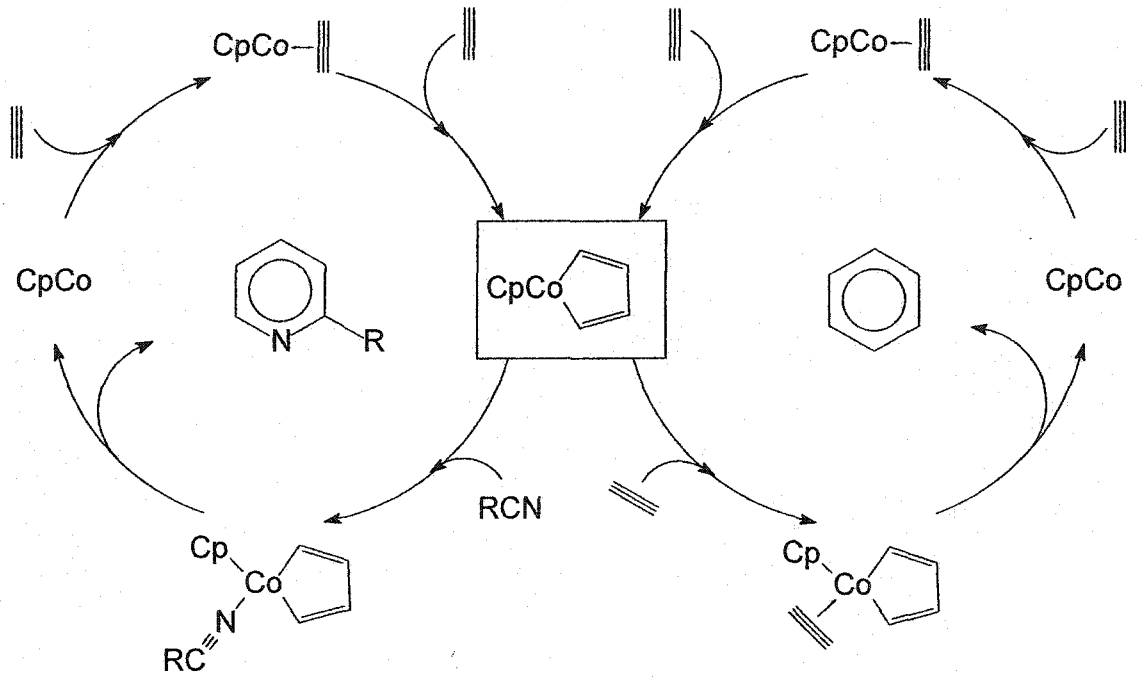

Scheme 3.5.1.

Competitive catalytic formation of pyridine and benzene [65]

Insertion of other substrates such as CO or isocyanide can also compete with alkyne insertion, leading to new metallacycles. Thus insertion of CO into a metallacyclopropene can result in metallacyclobutenone formation [68, 69] while double insertion of CO can yield the metallacyclpentenediones [68, 70, 71]. Interestingly isolated four-membered metallacycles of type (A) and (D) (see Figure 3.5.3) are only obtained for the heaviest members of the cobalt and nickel triad (eg. for Ir and Pt). Compounds of type (B) and (C) are the isolated products for M = Co or Ni for which the metallacyclobutenone structure of (A) has often been postulated as the reactive intermediate [72-74].

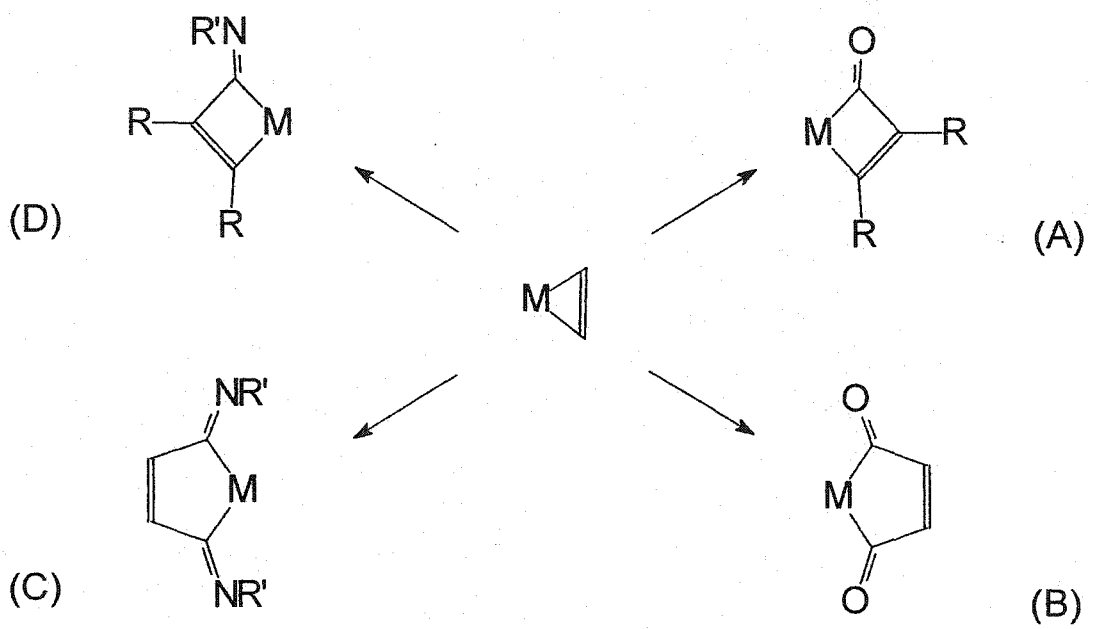

Figure 3.5.3.

Formation of four and five membered metallacycles (A)-(D).

When our group became interested in iridacycles we were surprised to learn that relatively few metallacyclobutenones were known [68, 76, 77] and structurally characterized [78]. A short review of this class of metallacycle therefore seems appropriate. General and detailed reviews on metallacyles of the transition elements have appeared [79, 80], including metallacyclobutanes [81]. Interestingly most of the early metallacyclobutenones were accessed indirectly via insertion of platinum into the C-C-single bond of cyclopropenones. In one particular case which involved methylcyclopropenone, the initially expected π-olefin complex (B), Figure 3.5.4, could be detected at very low temperature. At

temperatures above -30 °C, (B) quickly rearranged to the platinacylobutenone (C) [76].

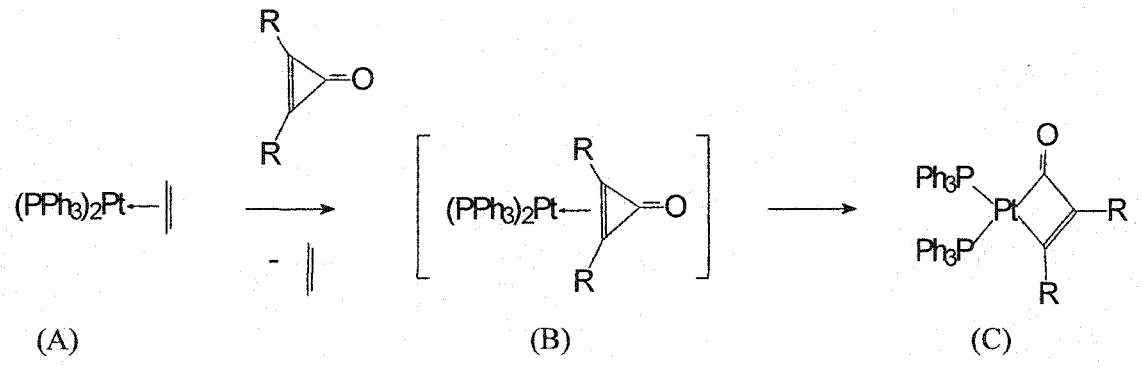

Figure 3.5.4.

Formation of platinacyclobutenones via metal insertion in cyclopropenones

Comprehensive investigations on the reactivity of low-valent transition metal carbonyls with hexafluorobut-2-yne carried out by Green [68] led to the isolation of a wide variety of metallacyclic products depending on the nature of the metal involved and the alkyne concentration as shown in Figure 3.5.5. With one molar equivalent of hexafluorobutyne the ruthenacyclobutenone (B) was obtained, which might be regarded as the first metallacyclobutenone formed via insertion of CO into a metal-alkyne bond. In a similar fashion, Dickson and coworkers obtained an iridacyclobutenone from hexafluorobut-2-yne and a cyclopentadienyl iridium carbonyl precursor [77].

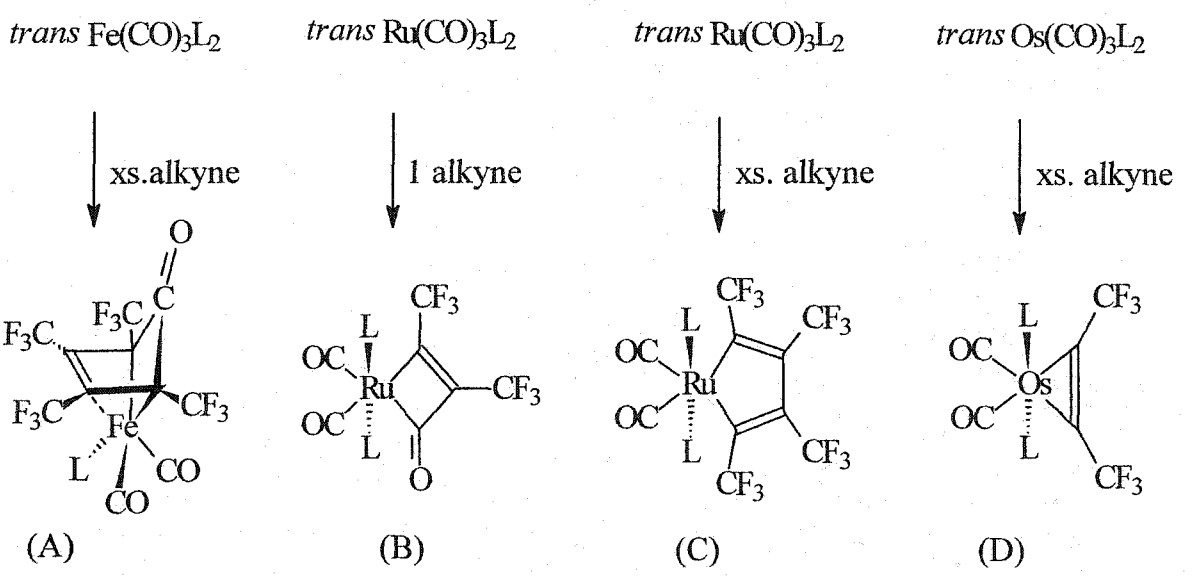

Figure 3.5.5.

Photolysis reactions of hexafluorobut-2-yne with zero-valent trans-$[M(CO)_3L_2]$, M=Fe, Ru or Os; L=$P(OMe)_3$.

Not many metallacyclobutenones have been prepared since. Chapter 4 will deal with some of them, including the limited chemistry that has been established for this class of metallacycle.

An exception is the very recent study from Joe Takats' laboratory, which shows that intramolecular CO insertion into a metallacyclopropene can also be induced by ligand substitution [69]. Addition of tertiary phosphines to solutions of $[Os(CO)_4(\eta^2\text{-}C_2H_2)]$, (A), see Figure 3.5.6, results in an unexpected diversity of products which depends mainly on the nature and concentration of the

phosphine. Thus, addition of one equivalent of PMe_3 at 0 °C yields the substitution product (B) which slowly forms the dinuclear complex (C) at ambient temperature. With excess PMe_3, the bis(phosphine) complex (D) as well as two

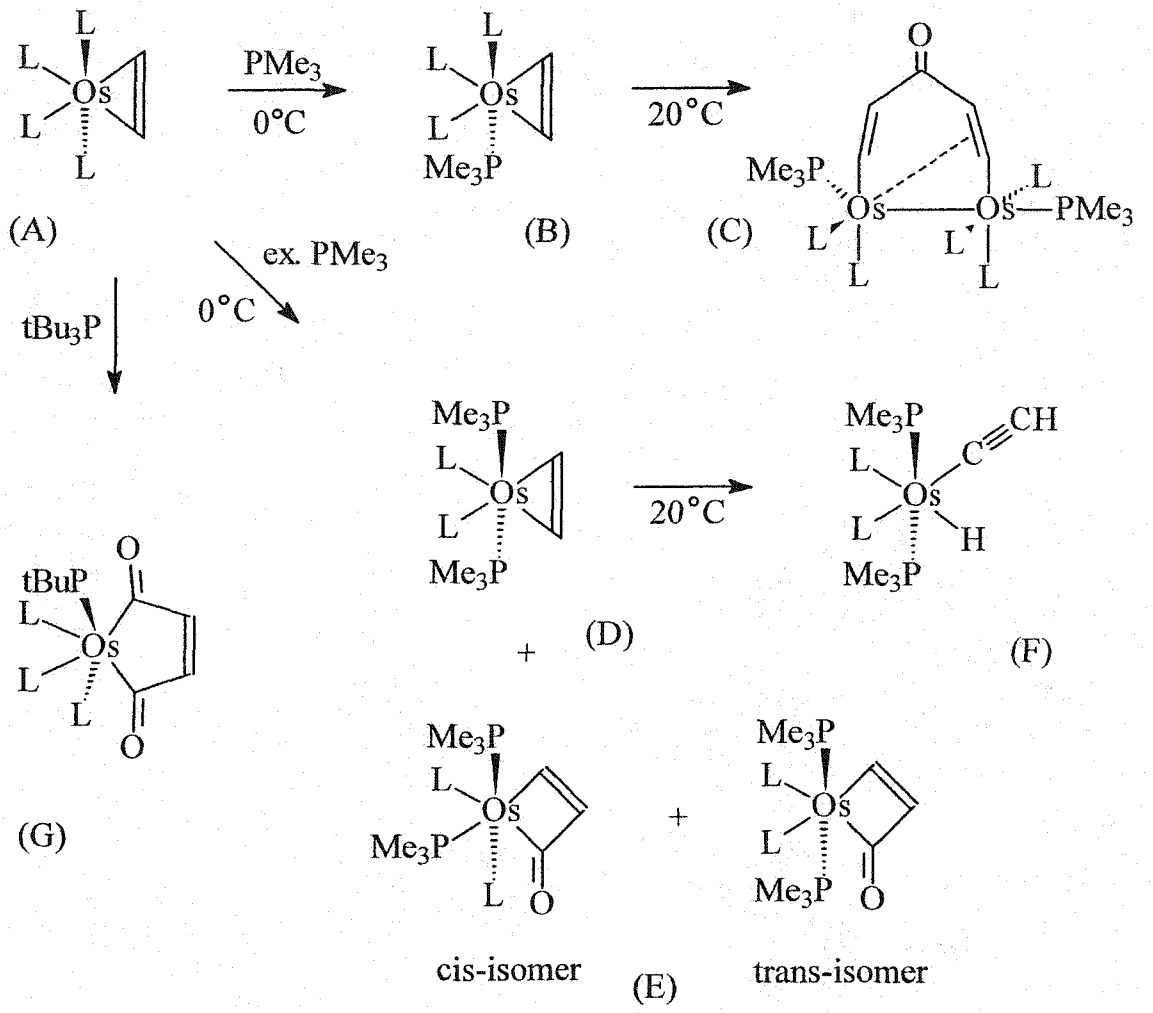

Figure 3.5.6.

Reaction of $[Os(CO)_4(\eta^2\text{-}C_2H_2)]$ with Me_3P and $^tBu_3P$ under different experimental conditions, L=CO.

isomeric forms of the CO inserted osmacyclobutenone (E) result. At ambient temperature (D) rearranges to the hydride complex (F). Surprisingly, addition of excess $^{t}Bu_3P$ to $[Os(CO)_4(\eta^2\text{-}C_2H_2)]$ gives the doubly CO inserted osmacyclopentenedione (G) as the only isolated product.

Figures 3.5.3 -3.5.5 include stable metallacyclobutenones which do not show any tendency towards further insertion of either CO or alkyne. It is not immediately obvious why such an insertion, which would produce a less strained metallacycle, does not occur even when CO is available through an intramolecular rearrangement.

Our clusters involving the metallacyclobutenone fragment seem to follow this trend and are reluctant to insert either DMAD or CO even under more severe conditions. Solutions of **3.5a** are especially inert, remaining unaffected by excess CO or DMAD in refluxing toluene or under UV light. The other clusters, however, will not stand up to such treatment. **3.4a-b** quickly decompose after being exposed to UV light for short periods of time, while yellow benzene solutions of **3.1** cleanly decarbonylate under such conditions to give a new cluster, which will be described later. Thermally **3.1** is unstable as indicated by a darkening of solutions to red at temperatures above 50 °C to afford a very complex product mixture. Although it was found that this process proceeded much faster when excess DMAD was present, the ^{31}P NMR of the reaction mixture indicated the

formation of at least six different species and it was subsequently judged impractical to carry out more investigations into the thermal chemistry of cluster **3.1**.

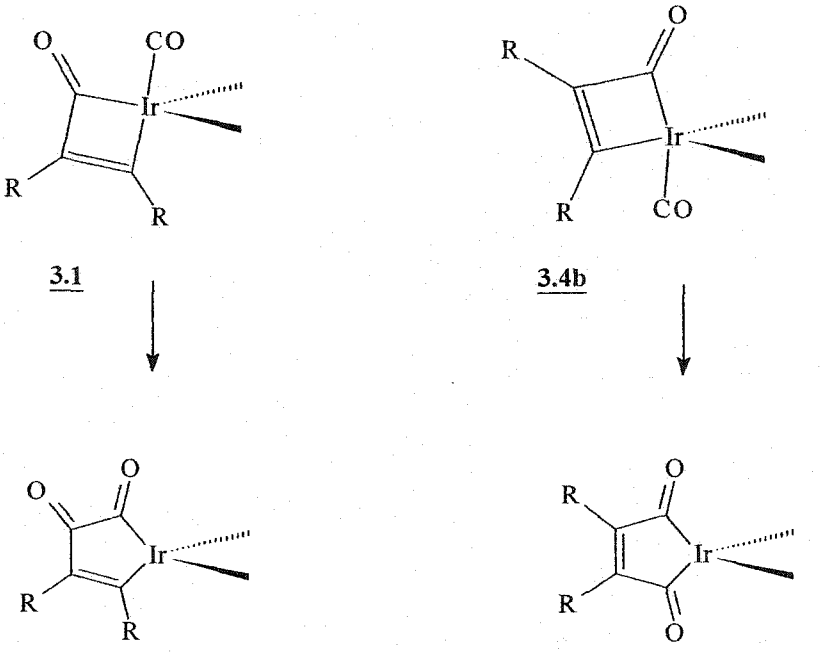

Figure 3.5.7

*Schematic representation of the immediate geometry of the iridium centre in clusters **3.4b** and **3.1** that are involved in the iridacyclobutenone ring (top) and the structure of their CO insertion products (bottom).*

Figure 3.5.7 highlights the immediate geometry at the metal centre in clusters **3.1** and **3.4b** that are involved in the metallacycle. In both clusters the coordination sphere around the iridium(III) centre can be regarded as distorted trigonal

bipyramidal. The important difference between the two clusters however, concerns the ligand arrangement within this trigonal bipyramid. In cluster **3.1** the remaining terminal carbonyl ligand is bound *cis* to the inserted carbonyl and *trans* to the olefinic carbon of the DMAD unit. Thus, without rearrangement, intramolecular insertion of a second CO would produce an α-β-diketonic metallacycle (Figure 3.5.7). Although many metal-catalyzed double carbonylation reactions that lead to α-β-diketones have been reported, examples of well characterized α-β-diketonic metallacycles that result from direct insertion of CO into the metal acyl bond are rare [82, 83]. Alternatively, such complexes have been obtained via oxidative addition of substituted cyclobutene-1,2-dione to platinum (0) centres [84]. This route however cannot be applied in general. It has been found that the same reaction also produces metallacyclopentenediones [85], which are in general the more preferred products of the double insertions of CO in to metal-alkyne bonds (Figure 3.5.3), and for which numerous examples exist [69]. In contrast to cluster **3.1**, the coordinated terminal carbonyl in **3.4b** is bound *cis* to the olefinic carbon of the DMAD unit and in a *trans* relationship to the inserted carbonyl. This represents a very favorable geometry for iridacyclopentadione formation since no rearrangement of ligands is necessary and the "migration" of a single bond would lead to the less strained five-membered ring. Such a transformation is, however, not observed. It is worth mentioning here that the resulting tetrahedral geometry of the subsequent iridacyclopentenedione is not common for an iridium

(III) centre in phosphido-bridged cluster chemistry which might disfavor the double insertion.

The structural characterization of the new alkyne clusters **3.1**, **3.3** and **3.4b** as well as the alkyne-free **2.1** provides an opportunity for testing the correlation between cluster valence-electron count and average metal-metal bond length, that had been established in our group previously. Formally the three new alkyne clusters all possess 50 valence electrons which correlates exceedingly well with the average iridium-iridium distance of 3.134, 3.132 and 3.162 Å for **3.1**, **3.3** and **3.4b**, respectively. For comparison, **1.5**, the parent of **3.4b**, which also possesses 50 valence electrons, exhibits average metal-metal distances of 3.234 Å, while in isoelectronic $[Rh_3(\mu\text{-}PPh_2)_3(CO)_6(HPPh_2)]$, the average rhodium-rhodium separation is 3.165 Å. In contrast the 48-electron cluster **2.1**, has a much shorter average metal-metal bond of 2.884 Å, in good agreement with 2.916 Å found in isoelectronic and isostructural **1.2**. The latter represents another rare example of a well characterized tris-phosphido-bridged 48-electron cluster of iridium.

Although surprisingly consistent when applied, the relation between cluster valence-electron count and average metal-metal distance does not take into account the deviations of individual iridium-iridium bonds within the metal triangle, which are often substantial. In the following paragraphs an attempt is

made to understand the reactivity and observed internuclear metal-metal distances in terms of local bonding. Although there is a danger associated with assigning local electron counts in clusters, the model provides a helpful tool and the resulting conclusions are in good agreement with experimental data.

The basal side in **2.1**, consists of two roughly tetrahedral iridium centres linked by a very short bond of 2.6702(3) Å, while the remaining apical sides have much longer metal-metal distances averaging 2.991 Å. In dinuclear chemistry such short distances are found in a series of complexes that contain a formal metal-metal-double bond. The phosphido and arsino bridged doubly bonded group 9 transition metal dimers are most relevant and a schematic representation of the geometry encountered in these complexes is shown in Figure 3.5.8, while relevant internuclear bond lengths of selected dimers are given in Table 3.5.1. If viewed as an isolated bimetallic unit, the basal side in **2.1** closely mirrors the geometry of a type A structure. It is therefore not surprising, that oxidative addition of DMAD to this "iridium-iridium double bond" results in diiridacyclobutene formation, which formally represents the product of a 2+2 cycloaddition, and for which examples exist in the literature [86]. During the cycloaddition, the bond order between the two iridium centres decreases, as expected, from two to one, in excellent agreement with the crystallographically determined Ir-Ir bond lengths of 2.6702(3) and 2.8641(3) Å for **2.1** and **3.3**, respectively.

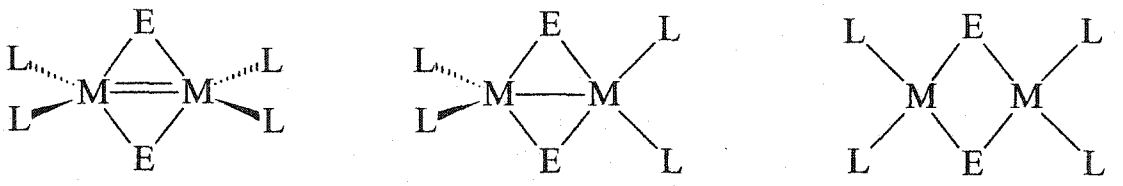

Figure 3.5.8.

Geometry of isoelectronic doubly-(Type A), singly-(Type B), and non-metal-metal bonded (Type C) group IX transition metal dimers (E=PR_2, L_2=2CO, 2PR_3, COD).

Type	M-M distance (Å)	M_2	E	L	Reference
A	2.551(1)	Ir_2	PPh_2	CO, PPh_3	[87]
A	2,545(1)	Ir_2	P^tBu_2	CO	[39]
A	2.343(2)	Co_2	PPh_2	CO, PPh_2Et	[88]
A	2.629(2)	Ru_2	PPh_2	NO, PPh_2Me	[89]
B	2.752(1)	Rh_2	PPh_2	PEt_3, COD	[90]
B	2.7609(9)	Rh_2	P^tBu_2	CO	[91]
C	3.717(1)	Rh_2	P^tBu_2	CO	[91]
C	3.89(1)	Ir_2	As^tBu_2	CO	[39]

Table 3.5.1

Metal-metal distances of selected (μ-$ER_2)_2$-bridged group 9 dimers of Type (A-C)

Alternatively, oxidative addition of alkyne to a type C dimer, Figure 3.5.8, would result in the formation of a dinuclear complex containing a metal-metal bond, by a bond-making, rather than a bond-breaking process. The presence of two square planar non-bonded metal centres does not offer a reasonable comparison to the basal site in **2.1**.

Aside from the two oxidized basal Ir(II) centres, the unique Ir(I) atom in **3.3** remains coordinatively unsaturated and should be susceptible to oxidative addition as well. This is readily observed when more DMAD is added to solutions of **3.3** resulting in formation of **3.1**. During this transformation, which involves alkyne addition as well as CO insertion, the unique iridium atom formally undergoes two-electron oxidation to give a 16-electron iridium (III) centre. This oxidation induces little disturbance in the cluster core. Most notable is the retention of the basal metal-metal bond, which is similar to the observed iridium-iridium bond preservation upon oxidation of **1.** with iodine and subsequent hydrolysis of one of the iridium-iodine bonds (see Figure 3.5.9). The trinuclear $[Os_3(\mu\text{-}H)_2(CO)_9L]$ (L=CO, PPh_3) represents a rare example of a well studied cluster with a formal metal-metal double bond [92] and should exhibit chemistry similar to that of **2.1**. The presence of two bridging hydride ligands, however, prevents a simple 2+2 cycloaddition product in the addition of alkyne. The outcome of the reaction is strongly dependent on the nature of the alkyne, and often involves hydride migration or CO insertion products [93].

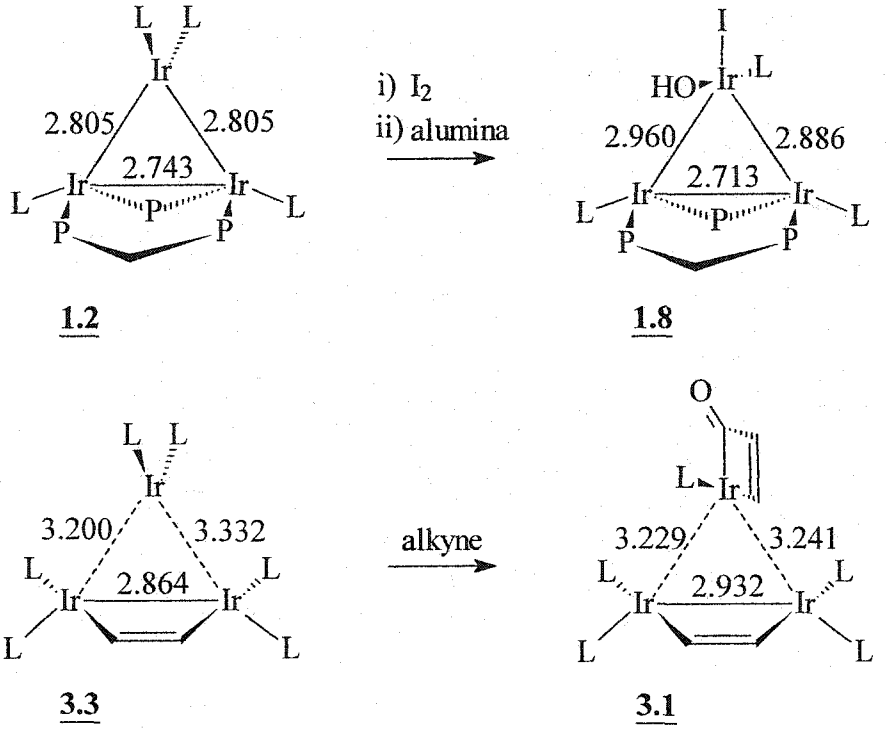

Figure 3.5.9.

*Metal-metal bond lengths in $[Ir_3(\mu\text{-}PPh_2)_3(CO)_4(\mu\text{-}dppm)]$ **1.2** and $[Ir_3(\mu\text{-}PPh_2)_3(CO)_4(\mu\text{-}dppm)(I)(OH)]$ **1.8** (top), as well as $[Ir_3(\mu\text{-}PPh_2)_3(CO)_5\{\kappa^2\text{-}MeO_2C\underline{C}C(CO_2Me)\underline{C}(O)\}(\mu\text{-}DMAD)]$ **3.1** and $[Ir_3(\mu\text{-}PPh_2)_3(CO)_6(\mu\text{-}DMAD)]$ **3.3** (bottom). L=CO; in-plane PPh_2 bridges and COOMe groups of the DMAD ligand omitted for clarity.*

4. Chemistry of the new iridacyclobutenone clusters

4.1. Introduction

Since there are few metallacyclobutenones, the chemistry of this group of metallacycles is not very well established. The role that these compounds play as intermediates in the formation of a five- or six-membered metallacycles or of organic systems such as quinones and cyclopentadienones has been mentioned in Section 3.5. Wojcicki and co-workers have shown [78], that the inserted carbonyl in the anionic rhenacyclobutenone $Na[(CO)_4ReC(R)C(CO_2Me)C(O)]$ can be alkylated without ring opening during the formation of a cyclic carbene as illustrated in Figure 4.1.1.

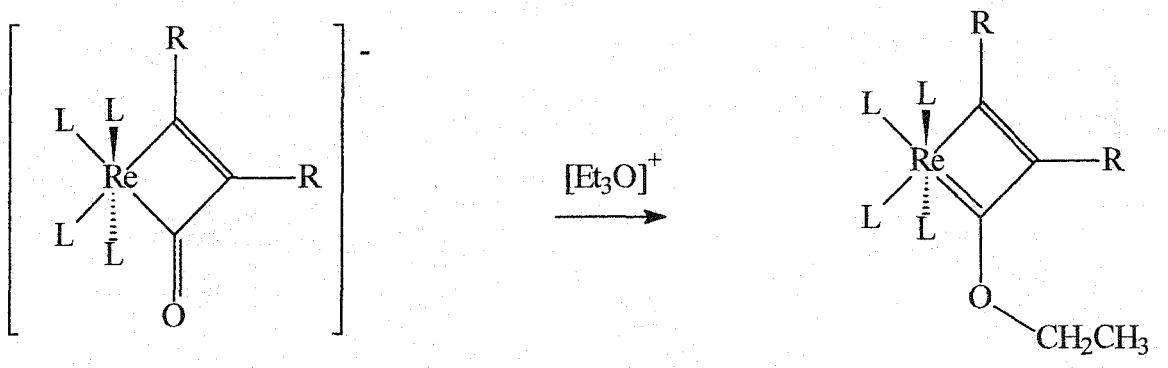

Figure 4.1.1

Formation of a cyclic carbene via alkylation of the rhenacyclobutenone [78]

It has also been demonstrated by Puddephatt [94], that the related dimetalla-cyclopentenone shown in Figure 4.1.2 can be decarbonylated thermally. Interestingly, the decarbonylation is fully reversible and the thermal product

completely regenerates the dimetallacyclopentenone upon exposure to a CO atmosphere.

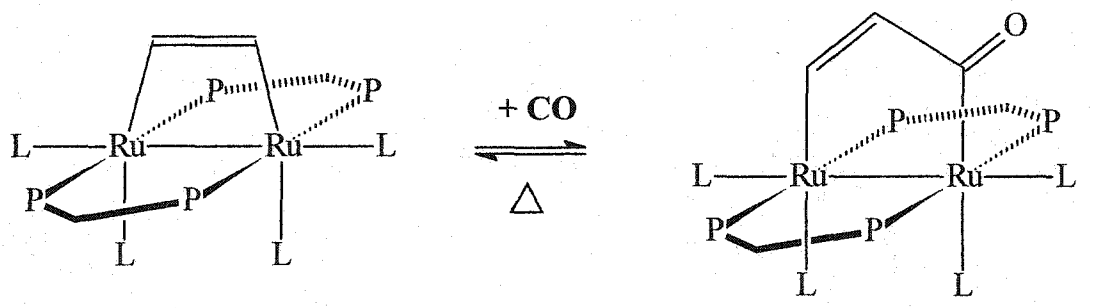

Figure 4.1.2

Equilibrium between dimetallacyclopentenone and dimetallacyclobutene [94].

Using VT NMR analysis Knox and co-workers demonstrated [95] that the fluxional behaviour in the crystallographically characterized tungsten dimer shown in Figure 4.1.3 arises from an oscillation of the metallacyclobutenone

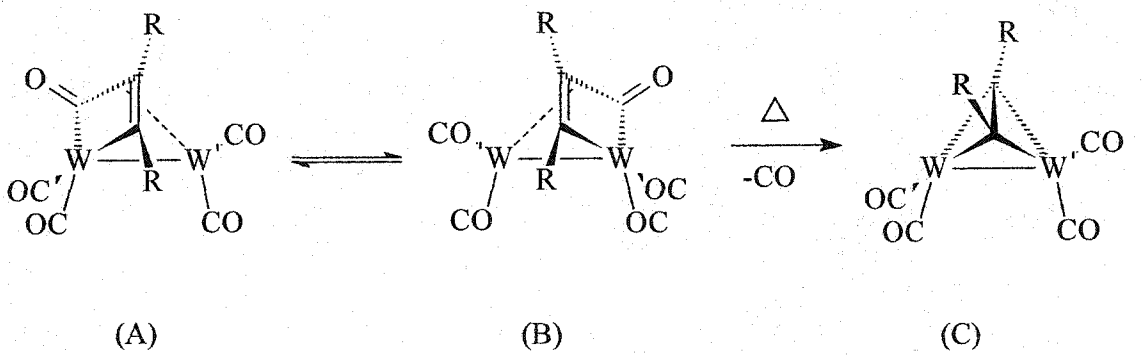

Figure 4.1.3.

Oscillation of the metallacyclobutenone between two tungsten centres (A)-(B) and main product of photochemical decarbonylation (C), W=(η^5-Cp)W [95].

unit between both metal atoms, which proceeds without rupturing of the alkyne-carbonyl link (A) and (B). The dimer, which was prepared by UV irradiation of a solution containing $[W_2(CO)_6(Cp)_2]$ and DMAD, is not stable under UV light. Thus prolonged irradiation leads to the DMAD-bridged dimer (C), presumably via decarbonylation of the metallacyclobutenone complex (A)-(B) [95]. Similar dinuclear complexes of type (A)-(B) have been characterized for Pt_2 [96], Rh_2 [97] and NiMo [98] but the fluxional behavior of the tungsten dimer seems to be unique.

4.2. Photochemical decarbonylation of 3.1

As mentioned in Section 3.5, the new clusters, involving metallacyclobutenone rings, **3.1** and **3.4a**-**3.5b** are reluctant to further insert either alkyne or CO under normal conditions. At elevated temperatures, decomposition of cluster **3.1** occurred, while **3.4a** remained intact in boiling toluene for several hours. In contrast, the photolysis of solutions of **3.5a-b** resulted in decomposition, while **3.1** transformed into a new product after several hours under UV light. The latter reaction, which proceeds cleanly in benzene, is conveniently monitored in solution via infrared spectroscopy. The new product, **4.1**, exhibits only terminal carbonyl stretching frequencies, as well as a broad band indicative of several overlapping carboxylate vibrations. FAB MS shows a molecular ion at 1557 (m/z), which is 28 mass units less than that of the parent **3.1** and strongly suggests that it contains one less carbonyl ligand. This is further supported by

analytical data. Proton NMR spectroscopy of the new product confirms the presence of two DMAD ligands via integration of the characteristic methoxy signals of the coordinated alkyne. The appearance of four methoxy signals in the proton NMR, having a 1:1:1:1 ratio, indicates a loss of symmetry compared with the parent cluster. A strong insight into the structure of the photolysis product arises from the ^{31}P NMR spectrum, which exhibits two doublets and a doublet of doublets consistent with an AMX spin system. The doublet of doublets encountered for P_m couples strongly to P_a and P_x, suggesting a *trans* relationship between these nuclei. In contrast, $^{2}J\{P_a\ P_x\}$ is smaller than the spectrum resolution of about 2 Hz, indicating a *cis* geometry between P_a and P_x.

Unfortunately, the new cluster is not stable in solution for long periods of time. It rearranges to a give a mixture of products, accompanied by a darkening of the initially bright yellow solutions to orange and finally, after a period of about two weeks, deep red. It seems worth mentioning here, that some of the resonances found in the proton and phosphorus NMR spectra of the deep red mixture, containing the decomposition or isomerization products of **4.1**, are also present in the mixture that arises from thermolysis reactions of **3.1**. The instability of the new cluster in common solvents has made reliable ^{13}C NMR analysis difficult. **4.1** does, however, exhibit reproducible resonances between +112 and +115 indicative of at least one DMAD ligand bridging two iridium centres. The appearance of four carbon signals corresponding to four distinct methoxy

carbons of the two coordinated alkynes is consistent with the proton NMR spectrum.

Structural analysis of $[Ir_3(\mu\text{-}PPh_2)_3(CO)_5(\mu\text{-}DMAD)_2]$ (4.1)

Although the spectroscopic properties of **4.1** give several important clues regarding the orientation of the phosphido bridges and the coordination mode of one DMAD ligand, it is not possible to make a structural proposal for **4.1** with much confidence, based on the spectral data alone. Fortunately, yellow prisms, suitable for crystallographic analysis, form upon diffusion of pentane into dichloromethane solutions of **4.1**. Because of the instability of **4.1**, which crystallizes first, it took several attempts to obtain suitable prisms. When a narrow diffusion tube was chosen, usually reliable in giving X-ray quality crystals, a dark red precipitate formed after four days, which rapidly covered most of the yellow prisms. A compromise was achieved by using an NMR tube, which still provided a diffusion rate slow enough to grow suitable prisms of **4.1** but in a much shorter time, thus preventing excessive decomposition.

The crystal structure of **4.1** was solved by Dr. Bob McDonald and is shown in Figure 4.2.1. Crystallographic experimental details and selected internuclear distances including bond angles are given in Tables 4.2.1 and 4.2.2 respectively. The molecular structure of **4.1** clarifies the outcome of the photolysis reaction.

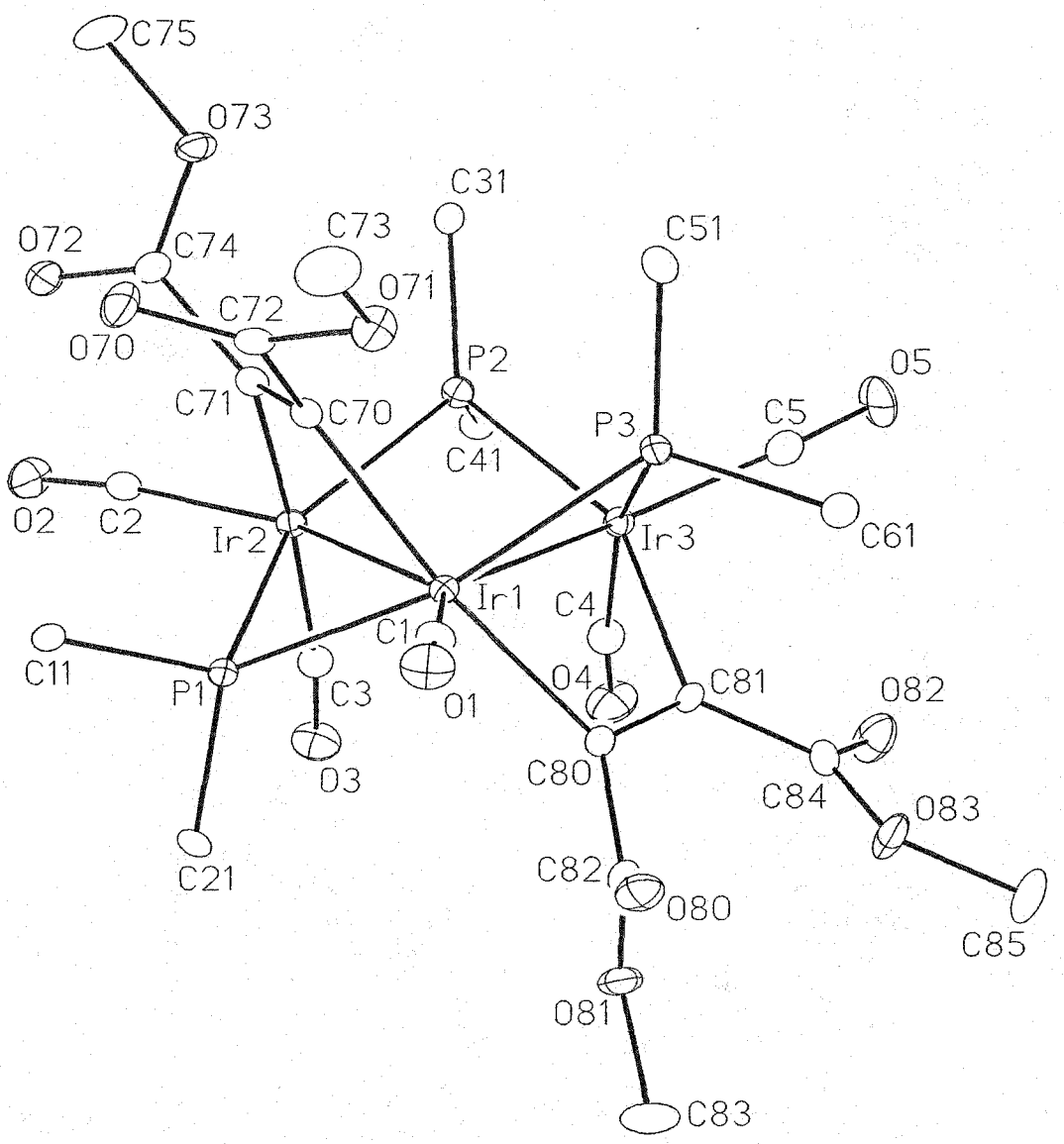

Figure 4.2.1 *Molecular structure of $[Ir_3(\mu\text{-}PPh_2)_3(CO)_5(\mu\text{-}DMAD)_2]$,* ***4.1****.*

Only the ipso carbons of the phenyl rings are shown.

A. Crystal Data

formula	$C_{59}H_{48}Ir_3O_{13}P_3$
formula weight	1634.48
crystal dimensions (mm)	0.30 × 0.11 × 0.07
crystal system	triclinic
space group	*P*-1 (No. 2)
unit cell parameters	
a (Å)	11.6776 (7)
b (Å)	11.9738 (7)
c (Å)	21.2299 (13)
a (deg)	80.3405 (10)
b (deg)	85.5666 (11)
g (deg)	84.0005 (13)
V (Å^3)	2905.0 (3)
Z	2
r_{calcd} (g cm^{-3})	1.869
μ (mm^{-1})	6.999

B. Data Collection and Refinement Conditions

diffractometer	Bruker P4/RA/SMART 1000 CCD
radiation (*l* [Å])	graphite-monochromated Mo K*a* (0.71073)
temperature (°C)	–80
total data collected	14493 (-14 <*h* < 6, -13 < *k* < 14, -26 < *l* < 26)
independent reflections	11789
number of observed reflections (*NO*)	9348 [$F_o^2 > 2s(F_o^2)$]
R_1 [$F_o^2 > 2s(F_o^2)$]	0.0334
wR_2 [$F_o^2 > -3s(F_o^2)$]	0.0739

Table 4.2.1 *Crystallographic experimental details for* $[Ir_3(\mu\text{-}PPh_2)_3(CO)_5(\mu\text{-}DMAD)_2]$, ***4.1***.

Atoms	Distance	Atoms	Distance
Ir(1)-Ir(2)	3.0070(3)	Ir(2)-C(3)	1.942(6)
Ir(1)-Ir(3)	3.0144(3)	Ir(3)-C(4)	1.950(6)
Ir(2)-Ir(3)	3.1258(4)	Ir(3)-C(5)	1.866(7)
Ir(1)-P(1)	2.3170(15)	Ir(1)-C(70)	2.111(6)
Ir(1)-P(3)	2.3408(16)	Ir(1)-C(80)	2.113(6)
Ir(2)-P(1)	2.3581(14)	Ir(2)-C(71)	2.102(4)
Ir(2)-P(2)	2.3590(15)	Ir(3)-C(81)	2.124(6)
Ir(3)-P(2)	2.3768(16)	C(70)-C(71)	1.329(7)
Ir(3)-P(3)	2.3710(15)	C(80)-C(81)	1.353(8)
Ir(1)-C(1)	1.837(6)	O(1)-C(1)	1.155(6)
Ir(1)-C(2)	1.879(6)	O(2)-C(2)	1.144(7)

Atoms	Angles	Atoms	Angles
Ir(2)-Ir(1)-Ir(3)	62.547(8)	P(1)-Ir(1)-C(70)	78.92(16)
Ir(1)-Ir(2)-Ir(3)	58.843(8)	P(3)-Ir(1)-C(70)	90.40(16)
Ir(1)-Ir(3)-Ir(2)	58.611(8)	P(1)-Ir(2)-C(71)	81.32(15)
Ir(1)-P(1)-Ir(2)	80.06(5)	P(2)-Ir(2)-C(71)	91.18(15)
Ir(2)-P(2)-Ir(3)	82.61(5)	C(3)-Ir(2)-C(71)	172.4(2)
Ir(3)-P(3)-Ir(1)	79.54(5)	P(2)-Ir(3)-C(81)	154.81(16)
P(1)-Ir(1)-P(3)	152.35(5)	P(3)-Ir(3)-C(4)	158.2(2)
P(1)-Ir(2)-P(2)	149.05(5)	P(3)-Ir(3)-C(81)	77.06(15)
P(2)-Ir(3)-P(3)	110.71(5)	Ir(1)-C(70)-C(71)	112.9(4)
C(70)-Ir(1)-C(80)	168.5(2)	Ir(2)-C(71)-C(70)	113.5(4)

Table 4.2.2. *Selected bond distances (Å) and angles (°) for* $[Ir_3(\mu\text{-}PPh_2)_3(CO)_5(\mu\text{-}DMAD)_2]$, ***4.1***.

Estimated standard deviations are given in parentheses.

3.1 photochemically decarbonylated to give **4.1** in which the alkyne ligands, including the DMAD that was formerly involved in the iridacyclobutenone ring, bridge different sides of the metal triangle forming two independent diiridacyclobutenes. The phosphido bridges are no longer in the plane of the metal triangle. P(1) lies 0.983(2) Å below the Ir_3 plane, while P(2) and P(3) are 1.070(2) and 1.251(2) Å above the Ir_3 plane, respectively (see ORTEP diagram in Figure 4.2.1 for atomic numbering scheme). The terms below and above metal triangle refer to the positions of the two unique axial carbonyl ligands which are assigned as lying below the iridium triangle.

Although the angles of 152.35(5) and 149.05(5) °, for P(1)-Ir(1)-P(3) and P(1)-Ir(2)-P(2) respectively, differ significantly from linearity, P(1) is best understood as being pseudo *trans* to P(2) and P(3), resulting in the doublet of doublets observed at 52.7 ppm for P(1) in the ^{31}P NMR of **4.1**. P(2) and P(3) on the other hand are in a *cis* relationship, as indicated by a P(2)-Ir(3)-P(3) angle of 110.71(5) °, thus explaining the two ^{31}P NMR doublets for P(2) and P(3), mutually coupled to P(1), but not to each other. The doublet at 80.0 ppm is assigned to P(3), which is in a very similar chemical environment, compared to P(1). P(2) resonates at higher field, causing the doublet at -7.3 ppm, because it is bridging a non-bonding iridium-iridium distance. The two DMAD ligands that are bridging different sides of the iridium triangle form nearly planar iridacyclobutene rings

that subtend dihedral angles of 63.70(11) ° above and 51.92(11) ° below the Ir_3 plane. The alkyne carbon C(81) is pseudo *trans* to P(2), which should result in significant phosphorus-carbon coupling.

Although significant amounts of **4.1** decomposed during the long ^{13}C NMR experiment, only two signals were observed between +60 and +126 ppm in benzene solution, a doublet at +113.9 and a multiplet at +112.5 ppm. Interestingly, the doublet exhibits a J value of 44 Hz which could be attributed to the two-bond coupling between P(2) and C(81). Similarly C(4) of the terminal carbonyl ligand bound to Ir(3), is the only other atom in **4.1**, other than phosphorus, that is in a pseudo *trans* relationship with a phosphido bridge and thus, subject to large spin-spin coupling. An unambiguous assignment for C(4) was however, not possible from the observed spectrum, which exhibits a large number of signals in the olefinic region due to the low symmetry of the cluster.

The coordination sphere around each iridium centre can be described as distorted square pyramidal. Each of the axial sites of the square pyramids is occupied by one of the three terminal carbonyls that rest closely within the Ir_3 plane. Ir(1), which is involved in both metallacycles, represents an Ir(III) centre, while the two remaining metal atoms have formal oxidation states of (II).

Overall, the geometry of **4.1** is extremely similar to that of isoelectronic [$Rh_3(\mu$-$PPh_2)_3(\mu$-$CO)(CO)_2(\mu$-$I)_2(PPh_3)$], prepared by our group [44] and [$Rh_3(\mu$-$PPh_2)_3(\mu$-$CO)(CO)_3(\mu$-$Cl)_2$], reported by Haines [45], differing only in the absence of the bridging carbonyl ligand, and the nature of the non-phosphido bridging groups. Two axial carbonyl ligands are accommodated in place of the absent bridging carbonyl thus introducing an additional ligand to **4.1**.

50-electron counts for the three related clusters arise because the two μ^2-halides donate three electrons each to the tri rhodium cluster, while the μ^2-DMAD ligands are two-electron donors.

There is, however, an important difference between the two Rh_3 systems and **4.1** concerning the metal-metal distances. The former represent rare examples of 50-electron clusters exhibiting short metal-metal bonds, averaging, for example 2.798 Å for the diiodo-bridged rhodium cluster. In contrast, the iridium-iridium distances in **4.1** are much longer. The two sides of the metal triangle that are bridged by the DMAD ligands still exhibit a weak iridium-iridium bond, as indicated by an average separation of 3.011 Å. The iridium atoms which are only bridged by the phosphido group are 3.1258(4) Å apart and therefore not strongly metal-metal bonded.

4.3. Addition of isocyanide to 3.1

Solutions of **3.1** cleanly react with ^{t}BuNC to afford a new product of stoichiometry $[Ir_3(\mu\text{-}PPh_2)_3(CO)_6(DMAD)_2(^t BuNC)]$, **4.2**. The transformation is quite slow, taking several days for completion when one equivalent of isocyanide is used. Since excess ^{t}BuNC does not affect the outcome of the reaction, **4.2** is most conveniently synthesized by using a 20-fold molar excess of isocyanide, which yields **4.2** within a few hours. The infrared spectrum of the new cluster exhibits a strong absorption band at 2208 cm^{-1}, characteristic of terminally coordinated isocyanide. Four distinct terminal carbonyl absorptions can be observed in the solid state and in solution, with no indication of bridging carbonyls. Finally, a broad band between 1685 and 1745 cm^{-1} is indicative of several overlapping ester carbonyl stretches of the coordinating DMAD ligand.

The presence of a single molecule of ^{t}BuNC is further confirmed by analytical and proton NMR data for **4.2**. The ^{1}H NMR spectrum exhibits a sharp singlet with the appropriate integration, 1.13 ppm downfield from TMS indicative of the nine equivalent protons of the t-butyl group. The four methoxy groups of the DMAD ligands give rise to four distinct signals indicating non-symmetrical binding modes for both alkynes. Understanding ^{31}P NMR data for **4.2** represents a challenge. The observed spectrum is of ABX type and consists of two overlapping doublets at -59.9 and -60.2 ppm for P_b and P_a, respectively.

Both P_b and P_a are mutually coupled to P_x, which appears as a doublet of doublets, but not to each other. The unusual feature of the spectrum is the chemical shift encountered for P_x which appears more than 200 ppm downfield from P_a and P_b, at +151.8 ppm.

FAB MS spectroscopy of **4.2** confirms the formal addition of a ^{t}BuNC molecule to **3.1**. A careful analysis of the complex spectrum gives important information about the structure of **4.2**. Table 4.3.1 lists prominent fragment peaks including intensities and assignments. The appearance of a fragment family, caused by the loss of a single DMAD ligand followed by sequential loss of three to six carbonyls strongly suggests the presence of two separate alkyne units in **4.2**.

Finally ^{13}C NMR data, although not fully interpretable without the determination of the molecular structure of **4.2**, allow an important conclusion regarding the coordination mode of at least one alkyne. The low symmetry of the cluster is manifested in the appearance of many resonances in the olefinic region of the carbon NMR spectrum. In fact, a total of 12 signals are observed, between +156 and +177 ppm (confirmed in several independent experiments). **4.2** possesses a total of fourteen carbon nuclei, that could possibly resonate in this narrow region of the spectrum, including the six carbonyl ligands, as well as the four non-equivalent alkyne and carboxylate carbons each. Considering this evidence,

Ion (m/z)	Intensity (%)	Assignment
1668	38	[M+H]
1639	23	[M-CO]
1636	21	[M-MeO]
1611	32	[M-2CO]
1610	32	[M-^{t}Bu]
1608	30	[M-CO_2Me]
1583	35	[M-3CO]
1555	58	[M-4CO]
1527	68	[M-5CO]
1525	54	[M-alkyne]
1496	54	[M-CO_2Me-4CO]
1470	37	[M-^{t}Bu-5CO]
1441	100	[M-alkyne-3CO]
1413	33	[M-alkyne-4CO]
1386	28	[M-alkyne-5CO]
1356	21	[M-alkyne-6CO]

Table 4.3.1 *Analysis of the FAB MS spectrum of* $[Ir_3(\mu\text{-}PPh_2)_3(CO)_5(\mu\text{-}DMAD)_2(^tBuNC)]$, ***4.2***.

it seems unlikely that the DMAD ligands occupy bridging positions. It is worth mentioning that the alkyne carbons of the bridging DMAD ligands in the *open winged* clusters **3.2** and **4.1** resonate between +112 and +115 ppm although a substantial downfield shift occurs for **3.3**, where all phosphido bridges are in plane with the iridium triangle. Unfortunately, all attempts to obtain crystals of **4.2** have proven unsuccessful. Preliminary investigations have shown that other isocyanides such as isopropylisocyanide afford very similar products with **3.1** and studies are underway to determine whether these compounds can be obtained in a crystalline state.

4.4. Discussion

The identification and characterization of photolysis product **4.1** represents a major accomplishment in the context of this thesis. The following paragraphs comment on a possible mechanism for this reaction. It is well known that cyclobutanones undergo photochemical decarbonylation. The influence of a hetero atom usually accelerates this process. From an organic point of view, metallacyclobutenones are cyclic four membered ketones with a metallic hetero atom in α-position with respect to the carbonyl, and should therefore be expected to undergo photochemical decarbonylation. In organometallic chemistry, however, the metallacyclobutenones generally represent reactive intermediates that undergo further reactions like double insertion of carbonyls or other

substrates as discussed previously. It is therefore especially interesting to find that the reactivity of the cyclic ketone in **3.1** can be understood in terms of organic photochemistry and resembles the chemistry of other metallacyclobutenones, discussed in Section 4.1, which are also prone to photochemical decarbonylation.

The molecular structure of **4.1** provides important information regarding a possible mechanism for the decarbonylation. It is not immediately obvious if the eliminated carbonyl was incorporated in the metallocyclobutenone ring, or if instead, a terminal carbonyl dissociated from the cluster. Scheme 4.4.1 compares two alternative pathways that both describe the photochemical formation of **4.1**. If the eliminated carbonyl originated from the iridacyclobutenone ring, a subsequent rearrangement of the resulting chelating μ^1-η^2- to the bridging μ^2-η^2-alkyne would not produce **4.1** immediately, but would have to include a carbonyl migration that could possibly proceed via steps (iv - vi) as shown in scheme 4.4.1. The need of a carbonyl rearrangement together with the requirement of the μ^2-η^2-alkyne fragment to, at least temporarily, bind to a coordinatively saturated iridium centre, as outlined in structure **C**, makes this route unfavorable. Alternatively, the initial step (i) could involve photo-induced dissociation of a terminal carbonyl not bonded to the iridium atom involved in the metallacycle. Photolysis of organometallic complexes resulting in

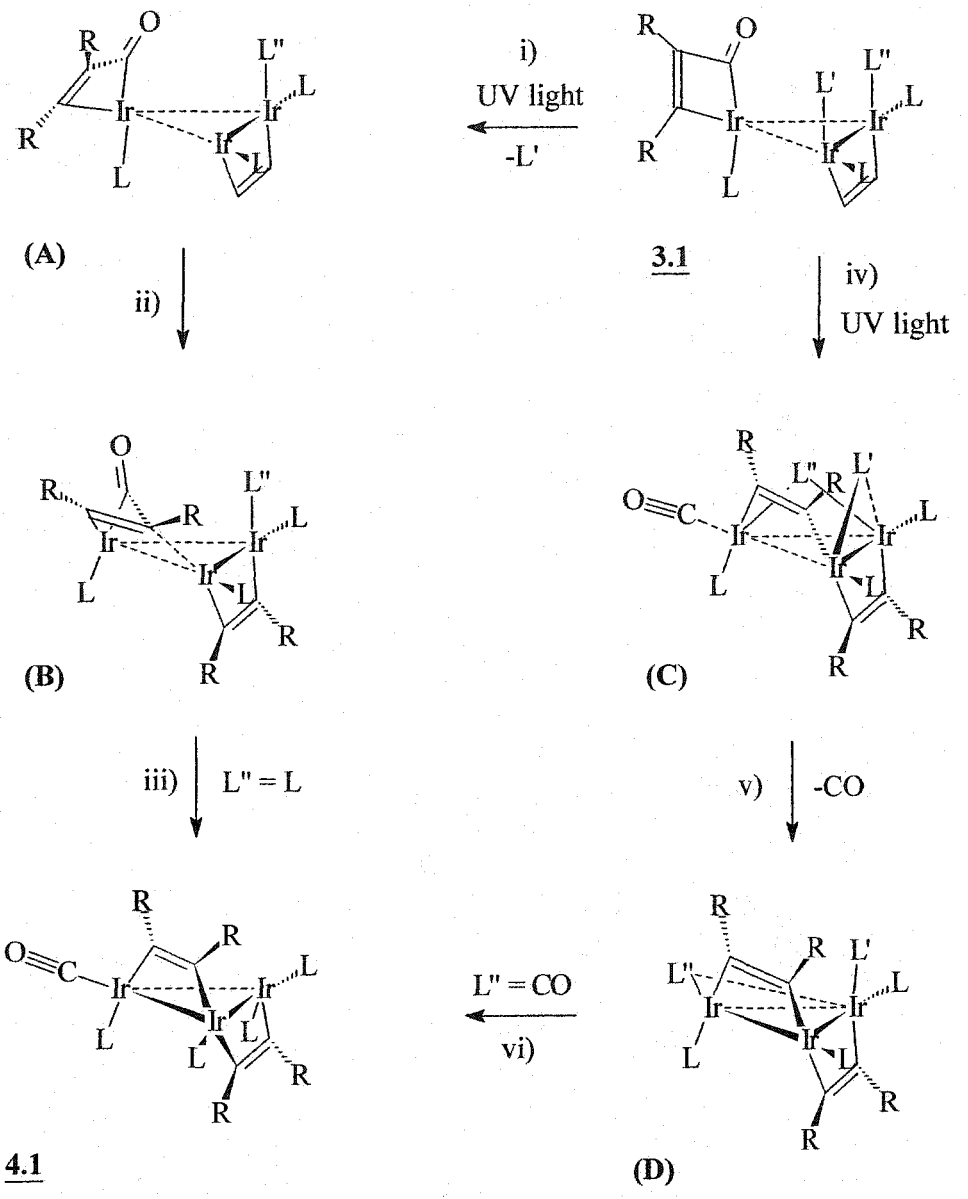

Scheme 4.4.1 *Alternative pathways concerning the decarbonylation of* ***3.1****.*

For clarity PPh_2 have been groups omitted (L, L,' L''= CO).

decarbonylation is not uncommon and has been observed, for example, in flash photolysis of $[(H_3C)Mn(CO)_5]$ [99]. CO loss from **3.1** could proceed before or simultaneously with the alkyne rearrangement, leading directly to **4.1** via a sigma bond migration as illustrated schematically through steps i-iii (Scheme 4.4.1). Since it has been demonstrated that the related hexacarbonyl **3.3** readily decarbonylates in vacuum, the initial photo-induced loss of CO from **3.1** (step i) followed by sigma bond migration of the alkyne fragment of the metallacyclobutenone (steps ii, iii) seems feasible. Isotopic labeling experiments on the mononuclear manganese acyl complex $[(CO)_5MnC(O)CH_3]$ have also demonstrated that the acyl carbonyl remains in the decarbonylation product, $[(CO)_5MnCH_3]$. First dissociation of a terminal carbonyl, in this case induced thermally, leads to a reactive five-coordinated acyl complex that subsequently undergoes methyl migration to produce a stable octahedral methyl-manganese-pentacarbonyl complex [100].

The outcome of the ^{t}BuNC addition to **3.1** is, at present, not as well understood. There are however several features of the reaction that need comment. Spectroscopic data for **4.2** are in support of a terminal isocyanide, yet all metal centres in **3.1** are formally coordinatively saturated. Thus a simple ligand addition seems highly unlikely. A rearrangement of the bridging alkyne in **3.1** could however offer an additional coordination site if it involved, for example, CO

insertion to yield diiridacyclopentenone **A** or iridacyclobutenones **B** or **C** as shown in Scheme 4.4.2. Possible formation of **A-C** would create a vacant coordination side that could subsequently be occupied by the incoming isocyanide ligand.

If the geometry of **4.2** is similar to that represented by structures **B** or **C**, then it would be expected to accommodate all phosphido bridges within the plane of the iridium triangle, as seen in the closely related iridacyclobutenone clusters **3.4a**-**3.5b**, discussed in Chapter 3. This assumption is clearly in contrast with ^{31}P NMR data, which are indicative of an *open winged* orientation of the phosphido bridges in **4.2**. Furthermore, if structures **B** or **C** represent **4.2**, it would be expected that at least one additional isocyanide ligand could be introduced via substitution of a terminal carbonyl to yield a cluster similar to **3.4a** or **3.4b**. Such a transformation was never observed, even when a large excess of isocyanide was provided.

Structure **A**, which is notably different from **B** and **C**, represents an alternative proposal for the geometry of **4.2**. It offers an explanation of the 200 ppm downfield shift of one of the phosphorus nuclei in **4.2** since **A** is expected to possess a metal-metal bond within the diiridacyclopentenone unit.

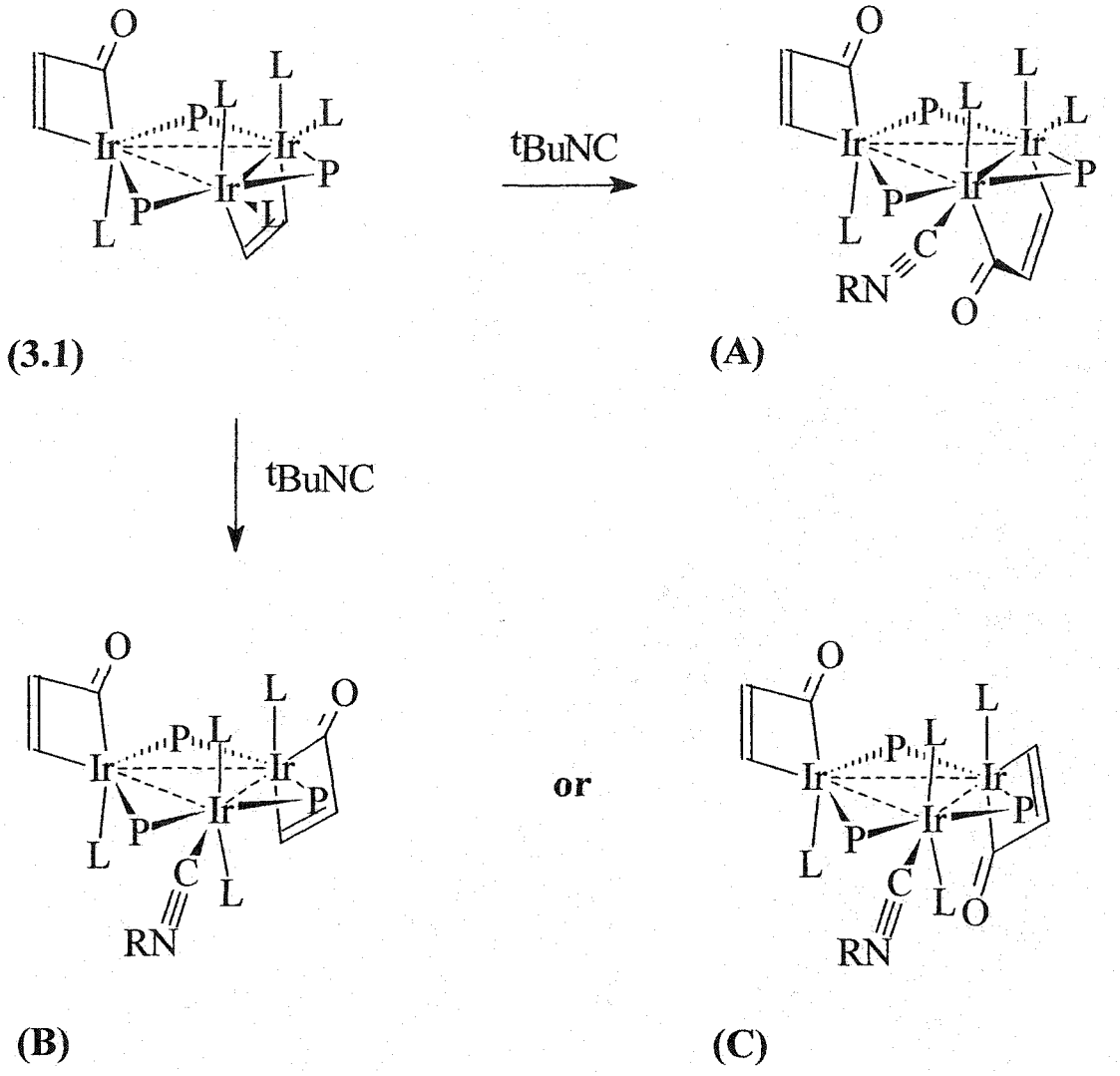

Scheme 4.4.2

*Intramolecular CO-insertion pathways for **3.1** followed by isocyanide coordination resulting in diiridacyclopentenone **A** and iridacyclobutenones **B-C**.*

In contrast, all iridium-iridium bonds should be broken in structures (**B**) and (**C**).

Unfortunately a crystallographic study, which could unambiguously establish the molecular structure of **4.2**, has not yet been possible due to the lack of suitable crystals. Preliminary results have shown that other isocyanides form similar products with **3.1** and current efforts are underway to induce crystallinity by changing the nature of the isocyanide.

5. Iridium and rhodium mixed-metal phosphido-bridged *triangulo*-clusters.

5.1. Introduction

Our group has a great interest and a long history in preparing heterometallic clusters involving metals from either group 9 or 10. Early investigations lead to the preparation and structural characterization of $[Pd_2Pt(\mu\text{-}PPh_2)_2(\mu\text{-}Cl)(PPh_3)_3]$, the first phosphido-bridged heteronuclear cluster involving palladium and platinum [101]. More recently, mixtures of the mixed-metal rhodium and iridium clusters $[M_3(\mu\text{-}PPh_2)_3(CO)_3L_2]$, (M=Rh, Ir; L_2=2CO, $2PPh_3$ or dppm), as well as the isocyanide adducts $[M_3(\mu\text{-}PPh_2)_3(CO)_{5-n}(^tBuNC)_{2+n}]$, (M=Rh, Ir; n=0,1) were prepared and analyzed with the aid of two dimensional ^{31}P COSY NMR spectroscopy [44]. Unfortunately, separation of the initial cluster mixture $[M_3(\mu\text{-}PPh_2)_3(CO)_5]$ (M_3=Rh_3, **5.1b**; Rh_2Ir, **5.1a**; $RhIr_2$, **5.1**; Ir_3, **2.2**) was never accomplished, which prevented a systematic investigation of this class of compounds. It was, however, clearly demonstrated that coordination of certain ligands to the mixed metal clusters occurred preferentially at iridium over rhodium as shown in Scheme 5.1.1, and that some of these heterometallic clusters exhibited a unique chemistry, markedly different from that of their homometallic analogues (Scheme 5.1.2). The observation that clusters (G) and (H) (see Scheme 5.1.1) were absent in the reaction mixture obtained upon addition of mono- or bidentate phosphines to the cluster mixture $[M_3(\mu\text{-}PPh_2)_3(CO)_5]$ (M=Rh,Ir), was not readily predicted. Similarly, addition of ^{t}BuNC to the mixed-metal clusters (B) and (C) resulted in coordination at the

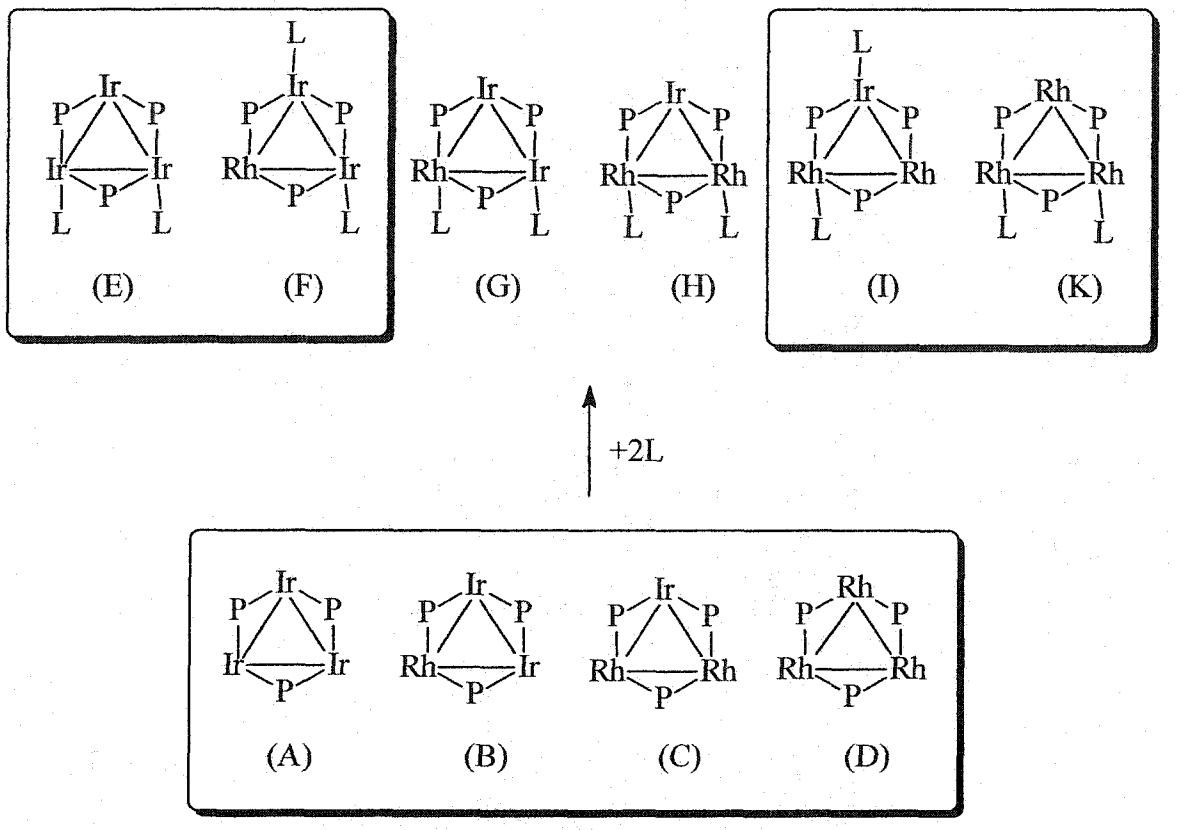

Scheme 5.1.1

Possible (E)-(K) and observed (E), (F), (I), (K) substitution products in the reaction of $[M_3(\mu\text{-}PPh_2)_3(CO)_5]$ (M=Rh,Ir) with phosphine (terminal carbonyl ligands omitted for clarity, P=PPh_2, 2L =$2PPh_3$ or dppm).

iridium centre only. The reasons behind the preference of iridium for binding phosphines or isocyanides are not fully understood at present. More dramatic changes are encountered in the reactivity of the mixed-metal clusters towards

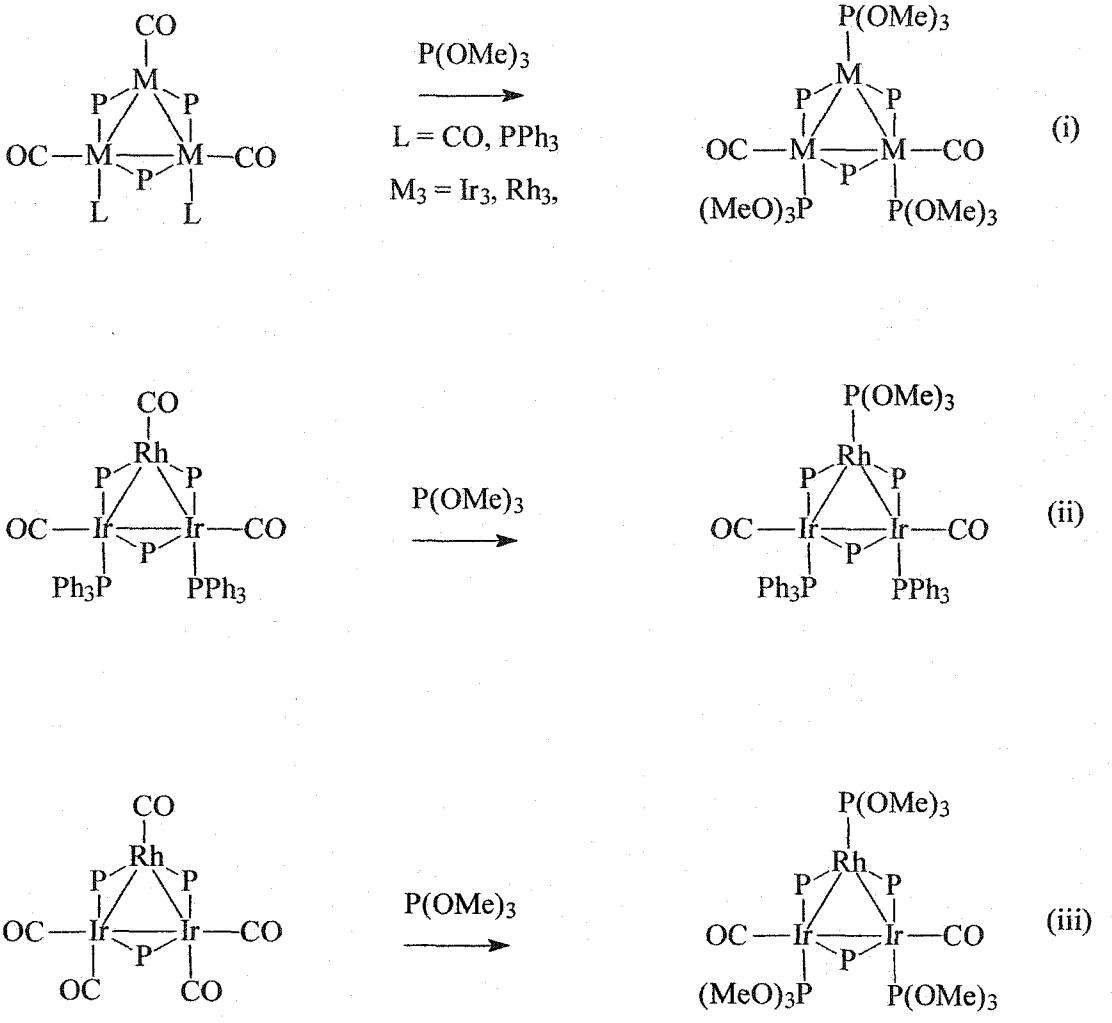

Scheme 5.1.2

Reactions of $[M_3(\mu\text{-}PPh_2)_3(CO)_3L_2]$, ($M_3$=$Ir_3$, Rh_3; L = CO or PPh_3); $[Ir_2Rh(\mu\text{-}PPh_2)_3(CO)_3(PPh_3)_2]$ and $[Ir_2Rh(\mu\text{-}PPh_2)_3(CO)_5]$ with $P(OMe)_3$, Equations (i)-(iii).

CO and $P(OMe)_3$ (see Scheme 5.1.2). For example, in $[Ir_2Rh(\mu\text{-}PPh_2)_3(CO)_5]$ (**5.1**) three carbonyl ligands are replaced by three $P(OMe)_3$ ligands, one on each metal, Equation (iii). This substitution reaction resembles the chemistry of the

homometallic trirhodium and triiridium parents (Equation i). In contrast, $P(OMe)_3$ addition to the bis-(triphenylphosphine) substituted derivative $[Ir_2Rh(\mu\text{-}PPh_2)_3(CO)_3(PPh_3)_2]$ causes substitution of the rhodium-bound carbonyl only [44] (Equation ii). This situation is entirely different from that in the homometallic parent complexes, in which both triphenylphosphine ligands are replaced as well.

Site selective reactivity in polynuclear mixed-metal complexes is an area of great interest in organonetallic chemistry. Recently, Adams *et al.* reported that the heterometallic cluster $[CpMo_2Ru(\mu_3\text{-}C_2HR)(CO)_7]$ on treatment with $PMePh_2$ underwent carbonyl substitution selectively at the ruthenium centre [102] while Fumagally *et al.* demonstrated that in the triruthenium-rhodium cluster anion, $[Ru_3Rh(\mu\text{-}CO)_3(CO)_{10}]^-$, carbonyl substitution caused by PPh_3 occurs on the rhodium centre only [103].

Finally the finding that the mixed-metal clusters $[M_3(\mu\text{-}PPh_2)_3(CO)_3L_2]$ (M=Ir, Rh; L_2=2CO or dppm) are not affected by CO contrasts with both the triiridium and trirhodium parents which readily and reversibly bind additional CO as discussed in Chapters 1 and 2.

5.2. Development of a strategy to separate mixed-metal rhodium and iridium clusters based upon their different chemical reactivity

Intensive efforts to separate mixtures of clusters $[M_3(\mu\text{-}PPh_2)_3(CO)_5]$, (M=Rh, Ir), using chromatographic or fractional recrystallization techniques proved unsuccessful. Although the hexane solubility of the clusters, which increases slightly as more rhodium is incorporated in the metal triangle, seemed to offer possibilities, no practical separation could be achieved. A series of observations, outlined below, led to the development of a strategy to separate the mixed-metal clusters based upon their different chemical reactivity.

1) $[Rh_3(\mu\text{-}PPh_2)_3(CO)_5]$ reacts instantaneously with DMAD,
2) The analogous reaction employing $[Ir_3(\mu\text{-}PPh_2)_3(CO)_6]$ needs several days for completion.
3) The clusters $[M_3(\mu\text{-}PPh_2)_3(CO)_3L_2]$, (M=Ir, Rh; L_2=2CO, $2PPh_3$ or dppm), as well as the isocyanide aducts $[M_3(\mu\text{-}PPh_2)_3(CO)_{5-n}(^t\text{BuNC})_{2+n}]$, (n=0,1) can be eluted on an alumina column using benzene.
4) All previously synthesized Ir_3-DMAD adducts or insertion products elute with THF on an alumina column but <u>not</u> with benzene.

Observations 1 and 2 two gave strong reason to assume different reactivity between the heteronuclear clusters towards DMAD, while the different physical properties of the DMAD adducts and their alkyne-free counterparts offered

possibilities in view of a practical and efficient separation. Thus, if the reactivities between the individual clusters $[Ir_3(\mu\text{-}PPh_2)_3(CO)_6]$ (**2.1**); $[Ir_2Rh(\mu\text{-}PPh_2)_3(CO)_5]$, (**5.1**); $[IrRh_2(\mu\text{-}PPh_2)_3(CO)_5]$, (**5.1a**) and $[Rh_3(\mu\text{-}PPh_2)_3(CO)_5]$, (**5.1b**) towards DMAD, are different enough, time-dependent chromatography could be employed to accomplish separation of the cluster mixture.

Because $[Rh_3(\mu\text{-}PPh_2)_3(CO)_5]$ (**5.1b**) was found to react so rapidly with DMAD, it was expected that the incorporation of more iridium in the metal triangle would slow down the reactivity towards alkyne. It is worth mentioning that, when this experiment was designed it was not known that isoelectronic and presumably isostructural $[Ir_3(\mu\text{-}PPh_2)_3(CO)_5]$ (**2.2**) also reacts instantly with molar quantities of DMAD.

5.3 Isolation and characterization of $[Ir_2Rh(\mu\text{-}PPh_2)_3(CO)_5]$ (5.1)

Because the DMAD chemistry of the triiridium cluster **2.1** was well established and a large spectroscopic database existed for both products and precursors, it was decided to first prepare a cluster mixture consisting predominantly of $[Ir_3(\mu\text{-}PPh_2)_3(CO)_6]$ (**2.1**) and $[Ir_2Rh(\mu\text{-}PPh_2)_3(CO)_5]$ (**5.1**). This was achieved by using a 1:4 molar ratio for Rh:Ir and employing the reaction sequence described in detail in the experimental section. Statistically, such a molar ratio of the metals should give the Ir_3, Ir_2Rh, $IrRh_2$ and Rh_3 clusters **2.1**, **5.1**, **5.1a** and **5.1b** in 51.2, 38.4, 9.6 and 0.8 % yield respectively. However, it was established in several

independent experiments that the actual amount of clusters produced deviated substantially from this prediction, strongly favoring $[Ir_2Rh(\mu\text{-}PPh_2)_3(CO)_5]$ (**5.1**). The relative ratios, as estimated by integration of the ^{31}P NMR signals, indicated that **2.1** and **5.1** were produced in relative yields of 30 and 70 % respectively, while only trace amounts of **5.1a** were present and no **5.1b** was detected.

Subsequent addition of small amounts of DMAD resulted in an immediate brightening of the initially deep red solution. ^{31}P NMR data obtained 12 minutes after alkyne addition to the cluster mixture disclosed surprising results. The ^{31}P NMR signals corresponding to $[Ir_2Rh(\mu\text{-}PPh_2)_3(CO)_5]$ (**5.1**). remained unchanged, while the singlet for $[Ir_3(\mu\text{-}PPh_2)_3(CO)_6]$ (**2.1**) was completely absent from the spectrum. Instead, a broad, mutually coupled doublet and triplet appeared, identical to the signals observed for $[Ir_3(\mu\text{-}PPh_2)_3(CO)_6(\mu\text{-}DMAD)]$ (**3.3**). It is interesting to note that it takes up to a week to prepare **3.3** directly from **2.1**, using similar conditions but in the absence of mixed-metal clusters.

The resulting cluster mixture was introduced to an alumina column, and a purple band, eluting with benzene was found to contain **5.1** in good yield. Figure 5.3.1 compares the ^{31}P NMR spectra for the sequence of steps described above.

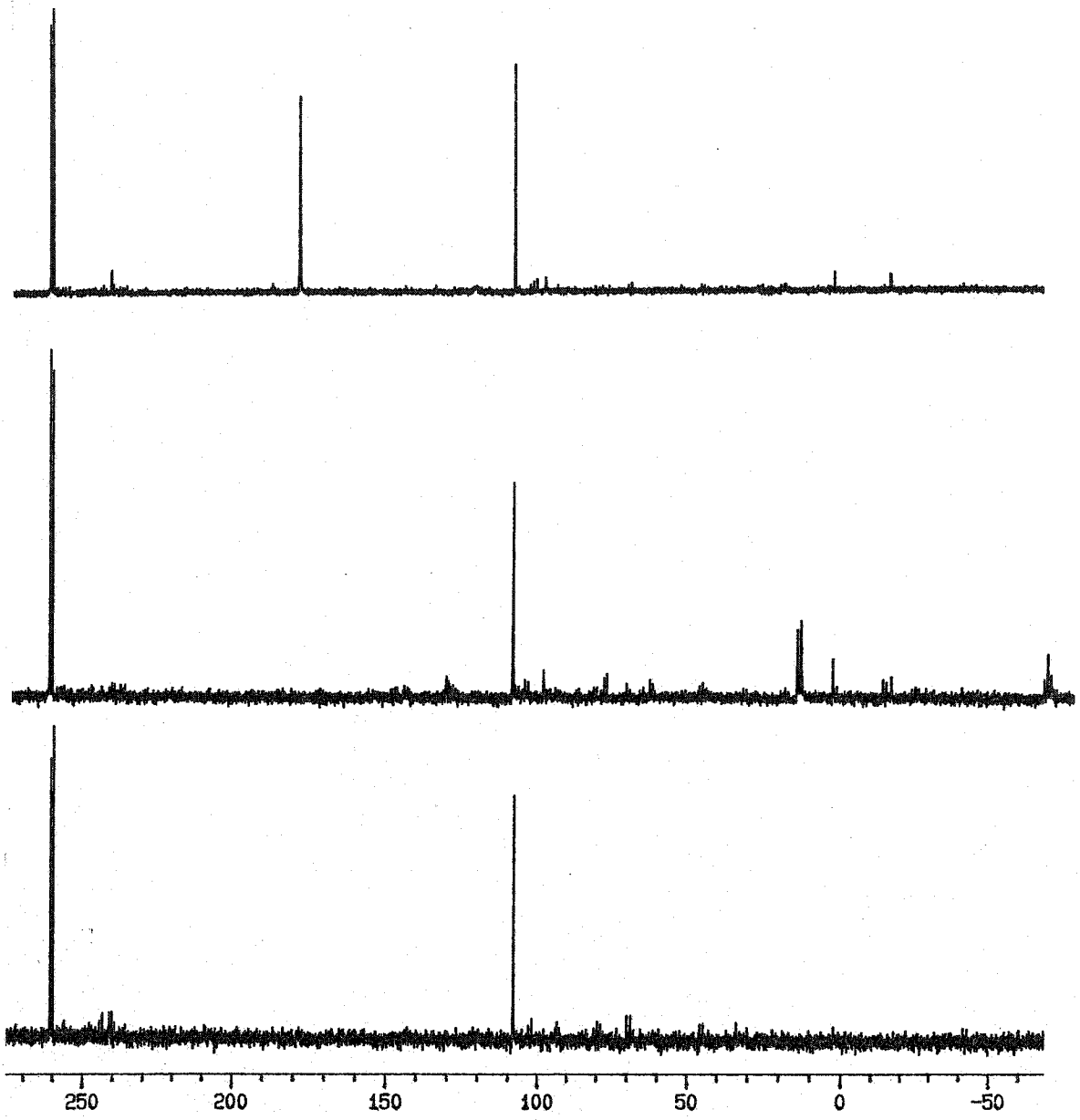

Figure 5.3.1

^{31}P NMR spectra of a cluster mixture prepared using a molar Ir:Rh ratio of 4:1 before DMAD addition (top), immediately after DMAD addition (middle) and after chromatography (bottom) using a molar ratio of 1:1 for DMAD : ***2.1****.*

Spectroscopic analysis of $[Ir_2Rh(\mu\text{-}PPh_2)_3(CO)_5]$ (5.1).

The ^{31}P NMR spectrum of **5.1** is essentially very similar to that of its homometallic triiridium analogue **2.2**, discussed in Chapter 2, except for the large additional splitting of the low field resonance, P_a due to one-bond coupling to rhodium (100% ^{103}Rh, I=1/2), which is of course absent in the spectrum of **2.2**. A comparison of relevant ^{31}P NMR parameters is given in Table 5.3.1.

Atomic labeling scheme		atom	δ (ppm)	$^2J\{P_aP_x\}$	$^1J\{P_aRh\}$
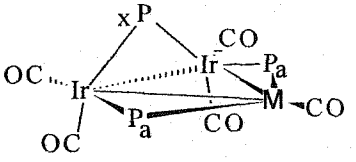	**5.1**	P_a	+259.0 (d of d)	13 Hz	119 Hz
	M=Rh	P_x	+107.9 (t)	13 Hz	0 Hz
	2.2	P_a	+240.5 (d)	15 Hz	----
	M=Ir	P_x	+100.5 (t)	15 Hz	----

Table 5.3.1

*Comparison of ^{31}P NMR parameters for **5.1** and **2.2** in benzene-d_6 and dichloromethane-d_2 respectively.*

The similarity in chemical shifts and coupling constants given in Table 5.3.1 strongly suggests that **2.2** and **5.1** are isostructural, adopting the geometry shown in Table 5.3.1, the same as found in the crystallographically characterized

$[Rh_3(\mu\text{-}PPh_2)_3(CO)_5]$ (**5.1b**), prepared by Haines and co-workers [37]. The small two-bond phosphorus-phosphorus coupling constant ($^2J\{P_aP_x\}$, 13 Hz) is indicative of an orthogonal orientation of the unique phosphido bridge with respect to the metal triangle, while the remaining phosphido groups lie closely within the M_3 plane. The overall symmetry of the ^{31}P NMR spectrum implies that the rhodium atom coordinates only one of the five cluster carbonyls, since any other reasonable alternative structure, involving terminal carbonyls only, would result in a more complicated spin system. This is furthur supported by infrared data. Infrared spectra for **5.1** and **2.2** (Figure 5.3.2) are very similar for both clusters differing in one important detail only. The low energy vibration at 1964 cm^{-1} encountered in **2.2** is absent in the spectrum of **5.1**. Instead, **5.1** exhibits a very strong band at 1975 cm^{-1}, which is close in energy and similar in shape to the strong absorption at 1977 cm^{-1} found in $[Rh_3(\mu\text{-}PPh_2)_3(CO)_5]$ (**5.1b**) [43] (see Table 5.3.2 for a comparison of all carbonyl stretching frequencies) .

Based on these results, the carbonyl vibration at 1964 cm^{-1} found in **2.2**, is assigned to the terminal carbonyl ligand of the unique iridium atom. This band shifts to 1975 cm^{-1} in **5.1** in which the unique carbonyl binds rhodium. Tentative evidence for this assignment is also provided by the very similar absorption band at 1977 cm^{-1} found in $[Rh_3(\mu\text{-}PPh_2)_3(CO)_5]$.

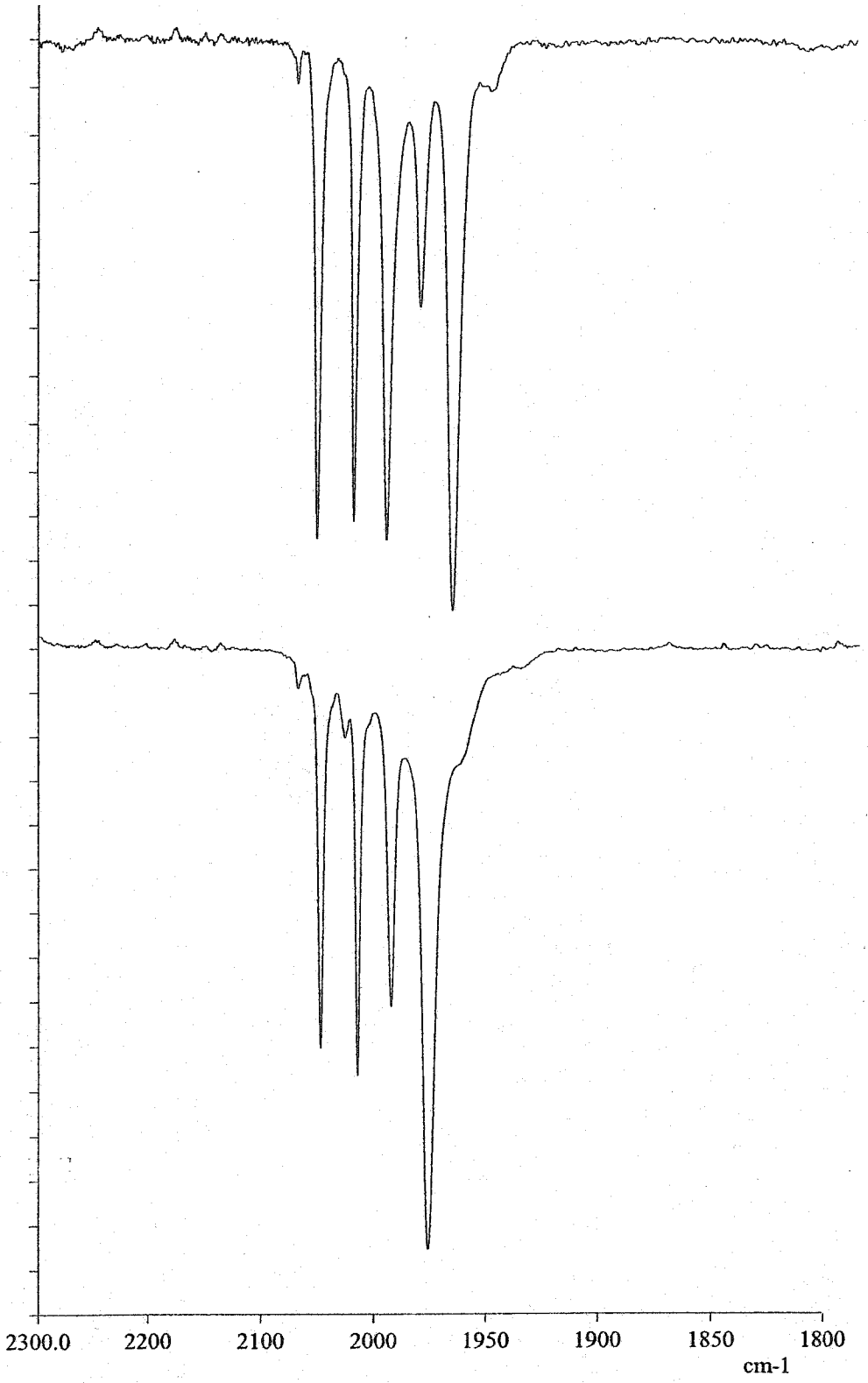

Figure 5.3.2 *Carbonyl region of the infrared spectra of $[Ir_3(\mu\text{-}PPh_2)_3(CO)_5]$ (**2.2**), top and $[Ir_2Rh(\mu\text{-}PPh_2)_3(CO)_5]$ (**5.1**), bottom (cyclohexane solution).*

2.2 [a]	**5.1** [a]	**5.1b** [b]
2050 (s)	2047 (s)	2044 (s)
2017 (s)	2014 (s)	2013 (s)
1994 (s)	1992 (s)	2000 (ms)
1979 (s)	1975 (vs)	1993 (w)
1964 (s)		1977 (vs)

Table 5.3.2

*Terminal carbonyl stretching frequencies (cm^{-1}) for clusters $[Ir_3(\mu\text{-}PPh_2)_3(CO)_5]$ (**2.2**), $[Ir_2Rh(\mu\text{-}PPh_2)_3(CO)_5]$ (**5.1**) and $[Rh_3(\mu\text{-}PPh_2)_3(CO)_5]$ (**5.1b**).*

a) cyclohexane solution, b) hexane solution (from reference [43])

A ^{13}C NMR analysis was carried out to confirm the proposed coordinative arrangement of the five carbonyl ligands in **5.1**. Relevant ^{13}C NMR parameters are summarized in Table 5.3.3. The spectrum is essentially similar to that of **2.2**, but shows additional splitting of the unique carbonyl resonance due to the strong one-bond coupling to rhodium causing a doublet of triplets. The two equivalent axial carbonyls, which are pseudo *trans* to the phosphorus atom of the unique phosphido bridge, give rise to a doublet with substantial coupling ($^2J\{CP\}$ =67 Hz). In contrast, the two equivalent equatorial carbonyls which are *cis* to both

Atomic labeling scheme	Atom	δ (ppm)	^{2}J{CP}	J{CRh}
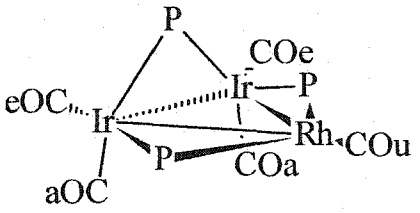	CO_{unique}	194.1 (d of t)	9 Hz	86 Hz
	CO_{equat}	184.1 (d)	8 Hz	0
	CO_{axial}	183.1 (d)	67 Hz	0

Table 5.3.3

*Selected ^{13}C NMR parameters for cluster (**5.1**) in benzene-d_6.*

the unique and the apical phosphido bridges, are subject to much smaller carbon-phosphorus coupling (^{2}J{CP} =8 Hz).

Finally, FAB MS spectroscopy unambiguously verifies the incorporation of one rhodium atom into cluster **5.1**. The spectrum exhibits dominant fragment peaks that are very similar to those observed for the homonuclear triiridium parent, **2.2**, except 91 mass units less, which can only be accounted for by the replacement of one iridium by rhodium. Furthermore, the isotopic distribution of the fragment peaks, which is very different for both clusters, can only be satisfactory simulated when one rhodium atom is included.

5.4 The reactivity of $[Ir_2Rh(\mu\text{-}PPh_2)_3(CO)_5]$ (5.1), towards DMAD

Although some of the ligand addition and substitution products of **5.1** had already been identified spectroscopically in cluster mixtures using 2D COSY ^{31}P NMR, the isolation of **5.1** in reasonable yield justified a reinvestigation and extension of the existing chemistry. It seemed especially interesting and relevant in the context of this thesis to investigate the reactivity of **5.1** and derivatives towards DMAD, which would allow for a direct comparison with the homonuclear iridium analogue. Such investigations were spurred by the observation that **5.1** was not completely inert to DMAD as initially assumed from the successful separation of **5.1** and **2.1**. Given enough time, **5.1** reacts with DMAD to form a new product that has spectroscopic properties extremely similar to that of **3.2**.

$$[Ir_2Rh(\mu\text{-}PPh_2)_3(CO)_5] \quad + \quad DMAD \quad \longrightarrow \quad [Ir_2Rh(\mu\text{-}PPh_2)_3(DMAD)(CO)_5] \ (\mathbf{5.2})$$

The stoichiometry of **5.2** was confirmed by proton NMR spectroscopy and FAB MS analysis. Relevant ^{31}P NMR parameters are given in Table 5.4.1 which also includes an atomic numbering scheme for **5.2**. The first order spectrum consists of a doublet at +128.3 ppm, a doublet of doublets at +43.7 ppm and a doublet of doublet of doublets at +104.0 ppm. The low field doublet is easily assigned to P_a which is not involved in coupling to the rhodium atom, while the remaining two signals clearly involve the phosphorus nuclei that bridge between the rhodium

and iridium atoms. The doublet of doublets corresponds to P_x which couples to rhodium and P_m but not P_a. The remaining doublet of doublet of doublets, assigned to P_m, arises from coupling to both neighboring phosphido bridges as well as the rhodium atom. Thus, P_m must be in a *trans* relationship to both P_a and P_x as indicated by the large coupling constants of 158 and 172 Hz, respectively. Since no coupling is observed between P_a and P_x it is assumed that those two nuclei are *cis* to each other.

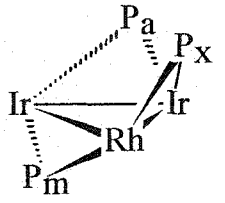

atom	δ [ppm]	^{2}J{PP}	[Hz]	J{PRh}	[Hz]
P_a	+128.3	P_aP_x	<2[a]	P_aRh	<2[a]
P_m	+104.0	P_mP_a	158	P_mRh	112
P_x	+ 43.7	P_xP_m	172	P_xRh	87

a) smaller than the spectrum resolution of about 2 Hz

Table 4.2.1

*^{31}P NMR parameters for $[Ir_2Rh(\mu\text{-}PPh_2)_3(CO)_5(DMAD)]$ (**5.2**) in benzene-d_6.*

Although the ^{31}P NMR parameters allow the assignment of the relative orientations of the phosphido bridges it is not possible to reach conclusions about the coordination mode of the alkyne which is, of course, of special interest especially in regard as to which metal atoms are involved in binding the DMAD ligand. The similarity between the ^{31}P NMR parameters of clusters **5.2** and **3.2**

has already been noted. ^{1}H NMR spectra of both clusters are at first sight superimposable which strongly suggests, that **5.2** and **3.2** are isostructural. A comparison of FAB MS spectra gives additional support for this assumption. **5.2** exhibits the same prominent fragment peaks as **3.2**, except that those fragments occur 92 mass units less than those of **3.2** due to the presence of one rhodium atom in **5.2**. Unfortunately, **5.2** is not stable for long periods of time and decomposes during an overnight ^{13} C NMR experiment, preventing further characterization.

5.5 Reactions of $[Ir_2Rh(\mu\text{-}PPh_2)_3(CO)_5]$ (5.1) with tert-butylisocyanide.

After identifying the reactivity of **5.1** towards DMAD it became important, in the context of a systematic investigation, to study the reactivity of $[Ir_2Rh(\mu\text{-}PPh_2)_3(CO)_4(^tBuNC)_3]$ (**5.3**) towards DMAD. For that reason it was necessary to first prepare and fully characterize this bimetallic isocyanide cluster that had previously only been observed spectroscopically in a cluster mixture [44].

Deep red purple solutions of **5.1** react immediately with excess ^{t}BuNC to afford bright yellow $[Ir_2Rh(\mu\text{-}PPh_2)_3(CO)_4(^tBuNC)_3]$ (**5.3**). If three molar equivalents of isocyanide are added, a mixture of **5.3** and the disubstituted isocyanide cluster, $[Ir_2Rh(\mu\text{-}PPh_2)_3(CO)_5(^tBuNC)_2]$ (**5.4**), is found to coexist in solution for several hours allowing the extraction of ^{31}P NMR parameters for **5.4**, which was previously unknown. The proton NMR and infrared spectra of **5.3** are extremely

similar to those of the triiridium parent **1.6**, as might be expected, but the incorporation of the rhodium atom has a dramatic effect on the ^{31}P NMR spectrum of **5.3**, which is markedly different from that of **1.6**. Phosphorus NMR data for **5.3** and **5.4** are given in Table 5.6.1. The spectroscopic identification of **5.4** had important implications because it allowed an unambiguous assignment of the ^{31}P NMR resonances for **5.3** which was previously not accessible. A detailed analysis is given in Section 5.6.

Unfortunately, **5.3** is not stable for long periods of time. Bright yellow benzene or dichloromethane solutions quickly darken to orange after an hour and to deep red overnight, giving a new, as yet uncharacterized product. Even in the solid state, canary yellow microcrystals of **5.3** darken to orange-red after two days preventing further characterization. The instability of the isocyanide cluster, which resembles that of $[Rh_3(\mu\text{-}PPh_2)_3(CO)_4(^tBuNC)_3]$, prepared previously by our group [44], presented a major problem for the investigation of the DMAD chemistry of **5.3**. It was therefore decided to attempt the synthesis of a more stable heterometallic isocyanide cluster by introducing more streric bulk on the isocyanide groups.

5.6 Reations of $[Ir_2Rh(\mu\text{-}PPh_2)_3(CO)_5]$ (5.1), with 1,1,3,3,-tetramethylbutyl isocyanide (tmBuNC).

The choice of isocyanide, that could possibly lead to a more stable analog of **5.3**, was preceded by a comprehensive study that included the synthesis and characterization of the new triiridium isocyanide clusters $[Ir_3(\mu\text{-}PPh_2)_3(CO)_{5-n}(RNC)_{2+n}]$, (n=1: R=isopr, **6.3**; cy, **6.5**; xy, **6.6**; tmBuNC, **6.1**; n=0: R=isopr, **6.2**; cy, **6.4**) which are described separately (see Appendix). 1,1,3,3- tetramethylbutyl isocyanide (tmBuNC), also referred to as isooctylisocyanide in the literature, was subsequently considered because it formed the very stable adduct $[Ir_3(\mu\text{-}PPh_2)_3(CO)_4(tmBuNC)_3]$ (**6.1**) which, in contrast to the other new isocyanide clusters **6.2**-**6.6**, possessed very high crystallinity, a property that proved extremely useful for purification purposes.

5.1 reacts with excess tmBuNC to afford the new heterometallic cluster $[Ir_2Rh(\mu\text{-}PPh_2)_3(CO)_4(tmBuNC)_3]$ (**5.5**) in high yield. A substantial excess of isocyanide is necessarily to quantitatively generate **5.5**. At lower isocyanide concentrations the disubstituted $[Ir_2Rh(\mu\text{-}PPh_2)_3(CO)_5(tmBuNC)_2]$ (**5.6**) predominates, suggesting that it becomes considerably more difficult for a third bulky isocyanide ligand to substitute a carbonyl. Unfortunately, severe overlap of the signals in the cluster mixture of **5.6** and **5.5** prevented the analysis of the ^{31}P NMR spectrum of **5.6**. As observed for the triiridium analogue, **5.5** readily crystallizes from benzene or dichloromethane solutions. Most importantly, however, the new isocyanide

cluster is much more stable than **5.3**, especially in the solid state, which allowed for a thorough characterization. Table 5.6.1 compares ^{31}P NMR parameters for **5.5** with that of the ^{t}BuNC analogs **5.3** and **5.4** discussed in the previous section.

	(**5.3**)	(**5.5**)	(**5.4**)	
δ (1)	+53.2	+55.8	+41.7	(d of d of d)
δ (2)	+18.1	+20.4	+9.2	(d of d)
δ (3)	+88.1	+92.7	+86.4	(d of d of d)
$^{2}J\{P_1P_2\}$	134	137	153	
$^{2}J\{P_1P_3\}$	168	167	169	
$^{2}J\{P_1Rh\}$	101	102	103	
$^{2}J\{P_2P_3\}$	147	146	148	
$^{2}J\{P_2Rh\}$	<2	<2	<2	
$^{2}J\{P_3Rh\}$	85	86	82	

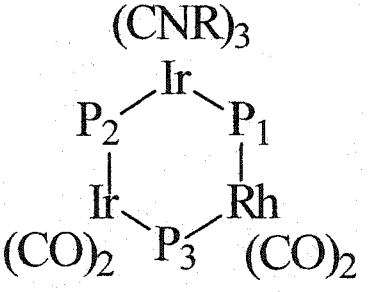

Table 5.6.1 *^{31}P NMR parameters for $[Ir_2Rh(\mu\text{-}PPh_2)_3(CO)_{5-n}(^{t}BuNC)_{2+n}]$ (n=0, **5.4**; n=1, **5.3**) and $[Ir_2Rh(\mu\text{-}PPh_2)_3(CO)_4(tmBuNC)_3]$ (**5.5**) with atomic numbering scheme adopted from the ORTEP diagram for **5.5** (Figure 5.6.1).*

The ^{31}P NMR spectrum of cluster **5.5** is extremely similar to that of **5.3** indicating that the nature of the alkyl group on the isocyanide ligand has little influence on the chemical shift of the phosphorus atom of the phosphido bridges. The doublet of doublets observed for **5.3** - **5.5** is easily assigned to P(2) since coupling to the rhodium atom is absent.

Assignment of P(1) and P(3) involves a comparison of the very similar chemical shifts of the tris-isocyanide adducts **5.3** and **5.5**, with that of the bis-isocyanide adduct **5.4**. The chemical shift for P(3) in **5.3** - **5.5** experiences minimal disturbance upon changing the number of coordinating isocyanides from 2 to 3 or changing the isocyanide from ^{t}BuNC to tmBuNC. In contrast, the resonances corresponding to P(1) and P(2) shift about 10 ppm downfield going from the bis-isocyanide **5.4** to the tris-isocyanide substituted **5.3** and **5.5**. These results clearly indicate that both P(1) and P(3), which are sensitive to substitution at the unique iridium centre, bind directly to the iridium atom bearing the isocyanide ligands while P(3), which is insensitive to such changes, bridges the carbonyl bearing metal centres. Thus, the downfield doublet of doublet of doublets is assigned to P(3) while the upfield doublet of doublet of doublets arises from P(1).

Crystallographic analysis of $[Ir_2Rh(\mu\text{-}PPh_2)_3(CO)_4(tmBuNC)_3]$ (5.5)

To unambiguously confirm the isostructural relationship between **5.5** and the

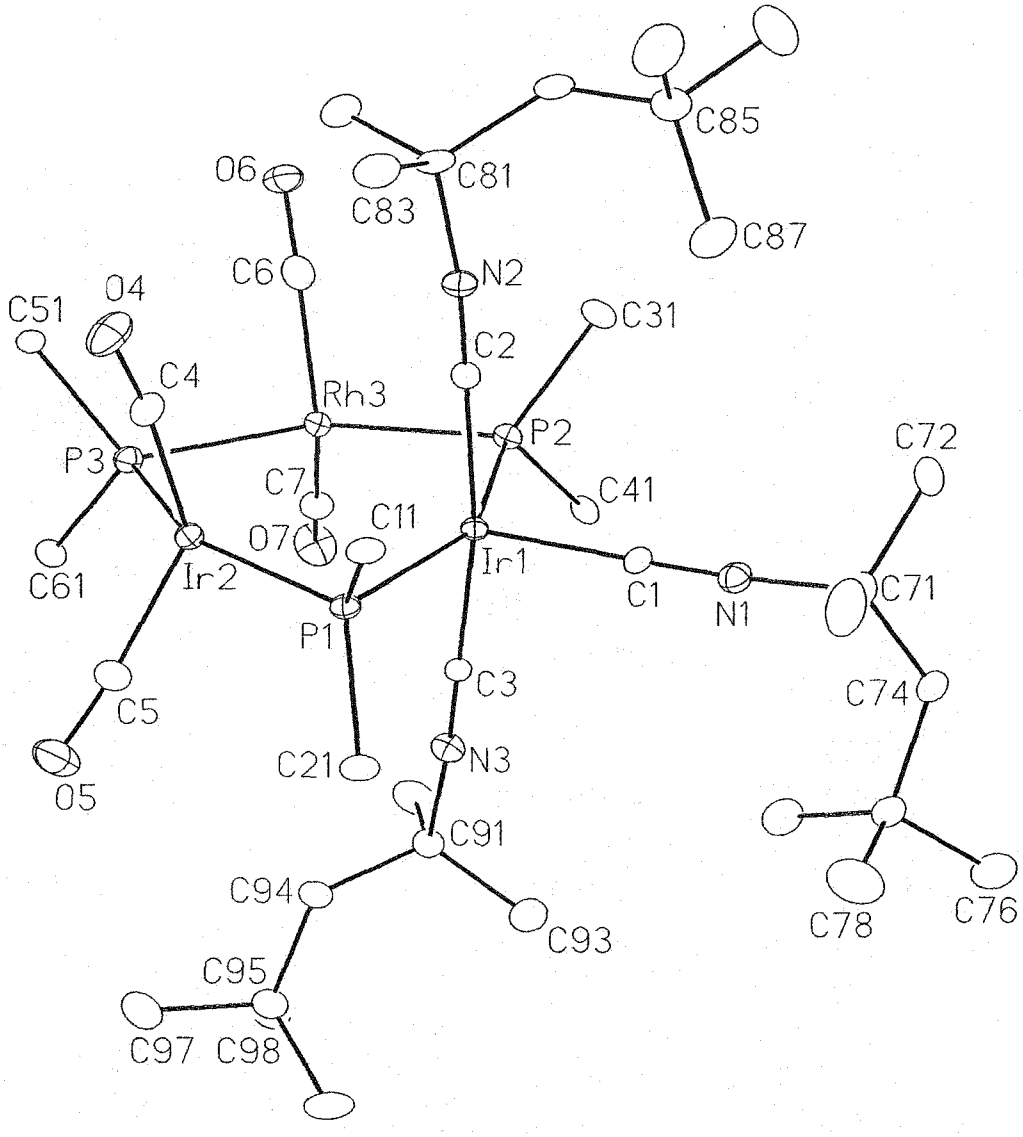

Figure 5.6.1.

*Molecular structure of $[Ir_2Rh(\mu\text{-}PPh_2)_3(CO)_4(tmBuNC)_3]$ (**5.5**).*

For clarity only the ipso carbons of the phenyl rings are shown.

A. Crystal Data

formula	$C_{67}H_{81}Ir_2N_3O_4P_3Rh$
formula weight	1572.57
crystal dimensions (mm)	0.46 × 0.33 × 0.26
crystal system	monoclinic
space group	$P2_1$ (No. 4)
unit cell parameters	
a (Å)	12.6763 (10)
b (Å)	22.6066 (18)
c (Å)	12.8217 (10)
β (deg)	117.7939 (13)
V (Å^3)	3250.4 (4)
Z	2
ρ_{calcd} (g cm^{-3})	1.607
μ (mm^{-1})	4.457

B. Data Collection and Refinement Conditions

diffractometer	Bruker P4/RA/SMART 1000 CCD
radiation (λ [Å])	graphite-monochromated Mo Kα (0.71073)
temperature (°C)	–80
total data collected	16812 ($-15 \le h \le 15$, $-24 \le k \le 28$, $-12 \le l \le 16$)
independent reflections	12037
number of observed reflections (*NO*)	11052 [$F_o^2 \ge 2\sigma(F_o^2)$]
R_1 [$F_o^2 \ge 2\sigma(F_o^2)$]	0.0258
wR_2 [$F_o^2 \ge -3\sigma(F_o^2)$]	0.0578

Table 5.6.2.

*Crystallographic experimental details for [$Ir_2Rh(\mu$-$PPh_2)_3(CO)_4(tmBuNC)_3$] (**5.5**).*

Atoms	Distance	Atoms	Distance
Ir(1)-Ir(2)	3.2106(4)	Ir(1)-C(3)	1.975(5)
Ir(1)-Rh(3)	3.1989(4)	Ir(2)-C(4)	1.874(6)
Ir(2)-Rh(3)	3.2905(4)	Ir(2)-C(5)	1.857(6)
Ir(1)-P(1)	2.3456(12)	Rh(3)-C(6)	1.864(6)
Ir(1)-P(2)	2.3478(12)	Rh(3)-C(7)	1.841(7)
Ir(2)-P(1)	2.2812(14)	N(1)-C(1)	1.150(6)
Ir(2)-P(3)	2.3173(13)	N(2)-C(2)	1.148(7)
Rh(3)-P(2)	2.2857(15)	N(3)-C(3)	1.136(7)
Rh(3)-P(3)	2.3171(14)	O(4)-C(4)	1.155(8)
Ir(1)-C(1)	1.963(5)	O(5)-C(5)	1.157(7)
Ir(1)-C(2)	1.978(5)	O(6)-C(6)	1.167(7)

Atoms	Angles	Atoms	Angles
Ir(2)-Ir(1)-Rh(3)	61.778(7)	C(1)-Ir(1)-C(2)	93.4(2)
Ir(1)-Ir(2)-Rh(3)	58.936(7)	C(1)-Ir(1)-C(3)	96.1(2)
Ir(1)-Rh(3)-Ir(2)	59.286(7)	C(2)-Ir(1)-C(3)	170.5(2)
Ir(1)-P(1)-Ir(2)	87.87(4)	P(1)-Ir(1)-C(1)	103.72(14)
Ir(1)-P(2)-Rh(3)	87.31(5)	P(2)-Ir(1)-C(1)	103.70(14)
Ir(2)-P(3)-Rh(3)	90.47(5)	Ir(1)-C(1)-N(1)	178.5(6)
P(1)-Ir(1)-P(2)	152.53(5)	Ir(1)-C(2)-N(2)	178.2(4)
P(1)-Ir(2)-P(3)	150.13(5)	Ir(1)-C(3)-N(3)	179.6(4)
P(2)-Rh(3)-P(3)	151.04(4)	C(4)-Ir(2)-C(5)	131.7(3)

Table 5.6.3. *Selected bond distances (Å) and angles (°) for* $[Ir_2Rh(\mu\text{-}PPh_2)_3(CO)_4(tmBuNC)_3]$ (**5.5**).

Estimated standard deviations are given in parentheses.

triiridium analogue $[Ir_3(\mu\text{-}PPh_2)_3(CO)_4(tmBuNC)_3]$ (**6.1**), (see Appendix for X-ray data for **6.1**) and to prove that the isocyanide ligands are indeed coordinated to iridium and not rhodium, as suggested by NMR data, a crystallographic analysis was carried out.

The molecular structure of **5.5** was determined by Dr. Bob McDonald and is shown in Figure 5.6.1. Crystallographic experimental details and selected internuclear distances and bond angles are given in Tables 5.6.2 and 5.6.3 respectively. The ORTEP diagram in Figure 5.6.1 represents 50 % of the molecules in the lattice of **5.5**. The other 50 % bear the rhodium atom Rh(3) in place of the iridium atom Ir(2) and *vice versa*. The structure is very similar to that of cluster (**1.5**) reported previously by our group [28] and that of the closely related cluster $[Ir_3(\mu\text{-}PPh_2)_3(CO)_4(tmBuNC)_3]$ (**6.1**) described in the Appendix. As in the triiridium systems, addition of isocyanide to the heterometallic cluster resulted in significant expansion of the metal triangle. The metal-metal distances of 3.2106(4), 3.1989(4) and 3.2905(4) Å found for Ir(1)-M(2), Ir(1)-M(3), and Ir(2)-Rh(3) = Ir(3)-Rh(2), (M = Rh, Ir) which can be regarded as metal-metal contacts compare exceedingly well with the iridium-iridium distances in the isostructural $[Ir_3(\mu\text{-}PPh_2)_3(CO)_4(tmBuNC)_3]$ (**6.1**) which were determined at 3.2147(3), 3.2046(3) and 3.3122(3) Å corresponding to Ir(1)-Ir(2), Ir(1)-Ir(3), and Ir(2)-Ir(3) (see Appendix). These minimal deviations can readily be explained by the

slightly smaller covalent radius encountered for the rhodium atom. The steric crowding of the three isooctylisocyanide groups bound to Ir(1) results in a "water wheel" like arrangement of the isocyanide ligands caused by the bending of the isooctyl chains in the solid state. Despite the steric demands of the isocyanide ligands the Ir-C-N bond angles remain surprisingly linear with a maximal deviation (from idealized 180 °) of 1.8(4) ° encountered for Ir(1)-C(2)-N(2).

5.7. Reactivity of $[Ir_2Rh(\mu\text{-}PPh_2)_3(CO)_4(^tBuNC)_3]$ (5.3) and $[Ir_2Rh(\mu\text{-}PPh_2)_3(CO)_4(tmBuNC)_3]$ (5.5) towards DMAD.

Bright yellow solutions of **5.5** are stable in dichloromethane or benzene for about one day. Decomposition becomes evident after a few days when solutions darken but is complete, on the basis of NMR, only after several weeks. Adding DMAD to dichloromethane solutions of **5.5** does not result in product formation even if a large excess of alkyne is used. Proton and phosphorus NMR spectra of the reaction mixture only identify signals due to unreacted starting material and free DMAD. If the mixture is allowed to stand for several days decomposition of **5.5** starts to occur. Similarly, only decomposition products of **5.3** are observed upon DMAD addition.

5.8. Reactivity of $[Ir_3(\mu\text{-}PPh_2)_3(CO)_4(tmBuNC)_3]$ (6.1) towards DMAD.

The three isooctylisocyanide ligands substantially increase steric crowding in **5.5**, which presumably causes the greater observed stability of the cluster compared to the tris ^{t}BuNC analog **5.3**. However, the lack of reactivity of **5.5** towards DMAD cannot be rationalized on steric grounds alone.

$[Ir_3(\mu\text{-}PPh_2)_3(CO)_4(tmBuNC)_3]$ (**6.1**) (see Appendix) reacts readily with DMAD to produce a mixture of two clusters (Equation 5.8.1) which exhibit physical and spectroscopic properties very similar to those of **3.5a-b**, discussed in Chapter 3.

$$[Ir_3(\mu\text{-}PPh_2)_3(CO)_4(tmBuNC)_3]\ (\mathbf{6.1}) \ + \ \text{xs DMAD} \ \rightarrow \ \mathbf{6.1a} + \mathbf{6.1b} \qquad (5.8.1)$$

Although not as well characterized as **3.5a-b**, the new alkyne adducts **6.1a-b** are formulated as isomers of stoichiometry $[Ir_3(\mu\text{-}PPh_2)_3(CO)_4(tmBuNC)_3(DMAD)_2]$ on the basis of their ^{1}H NMR spectra. Isomer **6.1a** is fast eluting on an alumina column using conditions employed in the separation of **3.5a-b**. Increasing the THF concentration results in isolation of isomer **6.1b**, the slow eluting band. As discussed in Chapter 3 the fast eluting isomer **3.5a** possesses C_2 symmetry in solution exhibiting two signals in the ^{1}H NMR corresponding to two equivalent axial and one unique equatorial ^{t}BuNC group. The proton NMR spectrum of the fast eluting isomer **6.1a** is, of course, much more complex. However, six signals are observed in the aliphatic region of the spectrum which integrate in relative

ratios of 2 : 6 : 9 : 4 : 12 : 18, indicating two equivalent axial and one unique equatorial isooctyl group consistent with C_2 symmetry. In contrast, the aliphatic region of the proton NMR of the slow eluting isomer **6.1b** consists of nine resonances in relative ratios of 2 : 6 : 9 : 2 : 6 : 9 : 2 : 6 : 9 clearly indicating three inequivalent isooctyl groups. Both isomers **6.1a-b** exhibit only two signals corresponding to the four methoxy group of the coordinated DMAD ligands. Table 5.8.1 compares ^{31}P NMR parameters of the new isomers **6.1a-b** (including the alkyne free parent **6.1**) with those of **3.5a-b**. The spectra of the two sets of isomers are of AX_2 type and extremely similar. Especially remarkable

Cluster	Symmetry	δ_x	δ_a	$^2J\{PaPx\}$
3.5a	C_2	-39.4 (d)	+6.2 (t)	195 Hz
6.1a	C_2	-36.5 (d)	+8.1 (t)	195 Hz
3.5b	C_s	-30.6 (d)	-16.7 (t)	196 Hz
6.1b	C_s	-27.5 (d)	-13.7 (t)	195 Hz
6.1[a]	C_2	+3.8 (d)	+41.1 (t)	144 Hz

a) see Appendix

Table 5.8.1

*^{31}P NMR parameters (CD_2Cl_2) for **3.5a-b**, **6.1a-b** as well as the DMAD free **6.1**.*

is the consistency of coupling constants $^2J\{P_aP_x\}$. Unfortunately, **6.1a-b** do not crystallize readily from solutions but form yellow oils containing residual amounts of DMAD which prevented a full characterization of both isomers. The presence of free alkyne proved especially problematic in obtaining reliable infrared spectra and elemental analyses. However the similar phosphorus NMR parameters (see Table 5.8.1) and the consistency of symmetry encountered in the proton NMR strongly suggest that **6.1a-b** and **3.5a-b** are analogous clusters. Although an isostructural relationship between **3.5a-b** and **6.1a-b** cannot be proven since the characterization of the latter set of isomers is incomplete, the data clearly demonstrate that **6.1** is not inert to DMAD. The lack of reactivity of **5.5** towards DMAD therefore cannot be rationalized on steric grounds but must be a result of the incorporation one rhodium atom into the framework of cluster **5.5,** thus creating a reactivity unique to the heterometallic system.

5.9. Reactivity of $[Ir_2Rh(\mu\text{-}PPh_2)_3(CO)_4(^tBuNC)_3]$ (5.3) and $[Ir_2Rh(\mu\text{-}PPh_2)_3(CO)_4(tmBuNC)_3]$ (5.5) towards iodomethane.

It has recently been shown by our group [48] that oxidative addition reactions on the homometallic $[Ir_3(\mu\text{-}PPh_2)_3(CO)_4(^tBuNC)_3]$ (**1.6**) using iodomethane or benzylbromide proceed at a single, formally 16-electron iridium centre to afford stable cluster cations in which only the R group but not the halide adds to the cluster core as shown in Scheme 5.9.1. Such addition products are unusual in

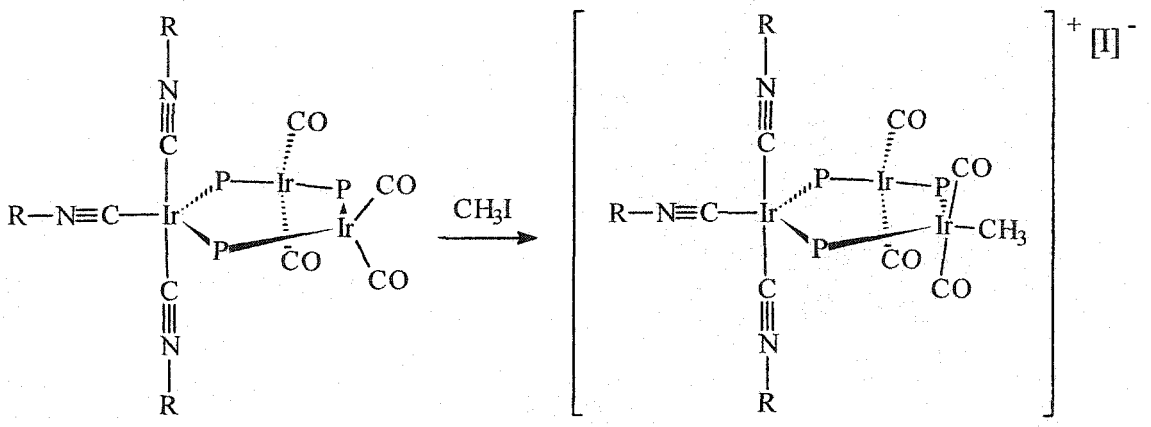

Scheme 5.9.1

*Oxidative addition of iodomethane to $[Ir_3(\mu\text{-}PPh_2)_3(CO)_4(^tBuNC)_3]$ (**1.6**), R=^{t}Bu.*

that they contrast with the expected two-electron, one-centre addition frequently encountered in mononuclear systems and two-electron, two-centre additions commonly found in dinuclear transition metal complexes. The oxidative addition chemistry of the clusters $[Ir_2Rh(\mu\text{-}PPh_2)_3(CO)_4(^tBuNC)_3]$ (**5.3**) and $[Ir_2Rh(\mu\text{-}PPh_2)_3(CO)_4(tmBuNC)_3]$ (**5.5**) was therefore well worth exploring. Since these clusters offer both unsaturated 16-electron rhodium and iridium centres it would be very interesting to determine if oxidative addition could proceed selectively and if so, which of the metal centres would be preferred. Because of the rapid decomposition of **5.3** in solution it was not possible to judge if **5.3** was inert towards iodomethane or if oxidative addition proceeded slower than

decomposition. No traces of the expected addition product could be detected at any time when mixtures of **5.3** and iodomethane were monitored via solution infrared or NMR spectroscopy. $[Ir_2Rh(\mu\text{-}PPh_2)_3(CO)_4(tmBuNC)_3]$ (**5.5**), which is stable in solution for about one day, also shows no reactivity towards iodomethane. Even when using a large excess of iodomethane, ^1H and ^{31}P NMR spectra only indicated decomposition, and no addition products were detected.

5.10. Reactivity of $[Ir_3(\mu\text{-}PPh_2)_3(CO)_4(RNC)_3]$ (R=1,1,3,3-tmBu, 6.1; R=isopr, 6.3; R=cy, 6.5; R=Xy, 6.6) towards iodomethane.

It remains to be answered whether the lack of reactivity of the bimetallic $[Ir_2Rh(\mu\text{-}PPh_2)_3(CO)_4(tmBuNC)_3]$ (**5.5**) towards iodomethane represents a unique feature of the mixed-metal cluster or if instead, it is caused by the bulky isooctyl groups blocking the reactive sites in **5.5**. In order to gain a better understanding of how the steric and electronic parameters of the coordinating isocyanide ligands in clusters of type $[Ir_3(\mu\text{-}PPh_2)_3(CO)_4(RNC)_3]$ affect the outcome of oxidative addition reactions at adjacent metal sites, a series of homometallic tri-iridium isocyanide clusters was prepared, including $[Ir_3(\mu\text{-}PPh_2)_3(CO)_{5-n}(RNC)_{2+n}]$ (n=0: R=isopr, **6.2**; R=Cy, **6.2**; n=1: R=1,1,3,3-tmBu, **6.1**; R=isopr, **6.3**; R=cy, **6.5**; R=Xy, **6.6**). Because these new isocyanide clusters have structural and spectroscopic properties extremely similar to those of the closely related $[Ir_3(\mu\text{-}PPh_2)_3(CO)_{5-n}(^tBuNC)_{2+n}]$ (n=0, **1.5**; n=1, **1.6**) which have already been reported

[28, 44], they will not be discussed in detail. A summary including a better synthetic approach to these clusters, experimental procedures, spectral and analytical data as well as a structural report for **6.1** are described in the Appendix.

The clusters $[Ir_3(\mu\text{-}PPh_2)_3(CO)_4(RNC)_3]$ (R=1,1,3,3-tmBu, **6.1**; R=isopr, **6.3**; R=cy, **6.5** and R=Xy, **6.6**), binding isocyanide ligands with different steric and electronic parameters, were subsequently considered for a study surveying their reactivity towards iodomethane. Addition of excess iodomethane to yellow dichloromethane solutions of the alkyl isocyanide systems **6.1**, **6.3** and **6.5** results in rapid formation of yellow-orange solutions from which the expected addition products $[Ir_3(\mu\text{-}PPh_2)_3(CO)_4(RNC)_3(CH_3)][I]$ (R=1,1,3,3-tmBu, **7.1**; R=isopr, **7.2**; R=cy, **7.3**) were isolated in near quantitative yield. The stoichiometry of clusters **7.1**-**7.3** was confirmed by ^1H NMR spectroscopy, FAB MS, elemental analysis and a crystal structure (for **7.2** only). Because spectroscopic and structural properties of **7.1**-**7.3** are very similar to those described for $[Ir_3(\mu\text{-}PPh_2)_3(CO)_4(^tBuNC)_3(CH_3)][I]$ (**1.7**) [44, 48] they will not be discussed in detail. An account of their IR, NMR, analytical and FAB MS data as well as experimental procedures and structural data (for **7.2** only) is included in the Appendix. The near quantitative isolation of $[Ir_3(\mu\text{-}PPh_2)_3(CO)_4(1,1,3,3\text{-}tmBuNC)_3(CH_3)][I]$ (**7.1**) from solutions of $[Ir_3(\mu\text{-}PPh_2)_3(CO)_4(1,1,3,3\text{-}tmBuNC)_3]$ (**6.1**) and excess

iodomethane after only a few minutes clearly demonstrates that the inert behavior of the bimetallic [$Ir_2Rh(\mu\text{-}PPh_2)_3(CO)_4$(1,1,3,3-tmBuNC)$_3$] (**5.5**) towards iodomethane is not due to the sterically demanding isooctyl groups but must arise from the incorporation of rhodium into the cluster core.

Interestingly the arylisocyanide substituted triiridium cluster [$Ir_3(\mu\text{-}PPh_2)_3(CO)_4(XyNC)_3$] (**6.6**) is inert to iodomethane as well. The proton NMR spectrum of a mixture of **6.6** and iodomethane in benzene remains unchanged for several days. The discussion will comment further on the relevance of this observation.

5.11 Discussion

The chemistry of mixed-metal phosphido-bridged triangular clusters of rhodium and iridium has always been hampered by their inaccessibility in a pure state. The chemistry that was developed for this class of compounds involved almost exclusively cluster mixtures which proved inseparable by means of chromatography or recrystallization. Analysis of the product mixtures involved time consuming 2D NMR experiments and assignments of the spectra obtained often proved impossible. In Section 5.2 a strategy was described for the separation of the mixed-metal clusters based on their different reactivities towards DMAD. The observations that [$Rh_3(\mu\text{-}PPh_2)_3(CO)_5$] (**5.1b**) reacts instantly

with molar quantities of DMAD while the same transformation involving $[Ir_3(\mu\text{-}PPh_2)_3(CO)_6]$ (**2.1**) requires several days for completion led to the assumption that the mixed metal clusters **5.1** and **5.1a** should possess intermediate reactivity. The isolation of **3.3** and unreacted **5.1** from a mixture

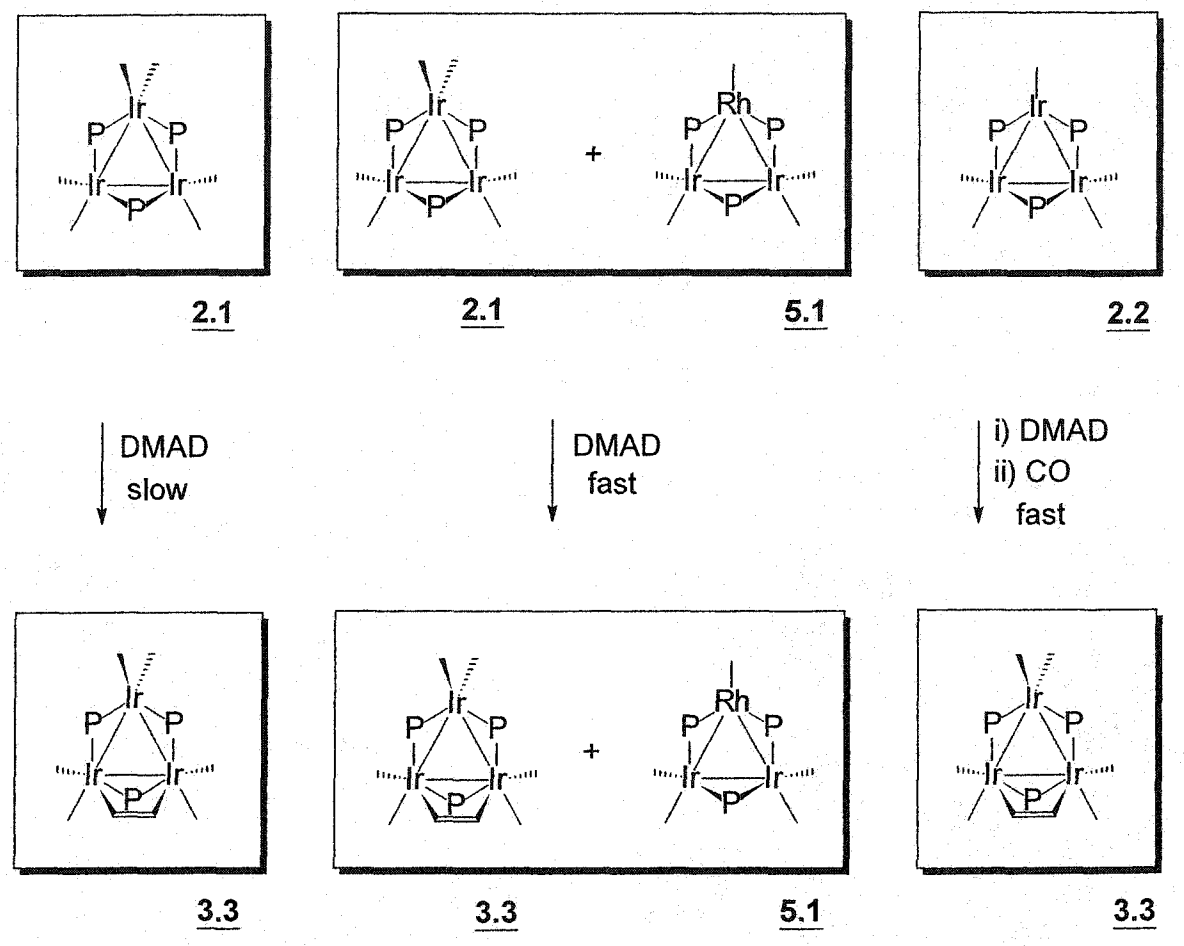

Scheme 5.11.1.

*Reactivity of $[Ir_3(\mu\text{-}PPh_2)_3(CO)_6]$ (**2.1**) towards DMAD when pure (left) and in a cluster mixture (middle) compared to $[Ir_3(\mu\text{-}PPh_2)_3(CO)_5]$ (**2.2**) (right). P=PPh_2, sticks represent CO ligands, COOMe groups of DMAD ligand omitted for clarity.*

containing DMAD and predominantly **2.1** and **5.1** as outlined in Scheme 5.11.1 is in contrast with this prediction. The discovery that **2.2** also reacts instantaneously with molar quantities of DMAD seems to offer an explanation for the successful separation by proposing that the decarbonylation of **2.1** is accelerated by the cluster mixture. $[Ir_3(\mu\text{-}PPh_2)_3(CO)_5]$ (**2.2**) then reacts with DMAD to form **3.2** which adds a CO ligand to form the observed product **3.3**. The decarbonylation of **2.1** is most likely facilitated by $[Ir_2Rh(\mu\text{-}PPh_2)_3(CO)_5]$ (**5.1**) which could form a hexacarbonyl cluster that is present only in small concentrations and thus not detectable by ^{31}P NMR spectroscopy. (^{31}P NMR shows only $[Ir_2Rh(\mu\text{-}PPh_2)_3(CO)_5]$ (**5.1**) and $[Ir_3(\mu\text{-}PPh_2)_3(CO)_6]$ (**2.1**) in the cluster mixture prior to alkyne addition.) The substantial decrease in reactivity of **5.1** towards DMAD addition seems to be a unique feature of the mixed metal cluster and is not readily predicted since both the homometallic iridium and rhodium analogues **2.2** and **5.1b** react immediately with DMAD. Given enough time **5.1**, will, however, react with DMAD to form an adduct that is formulated as $[Ir_2Rh(\mu\text{-}PPh_2)_3(CO)_5(DMAD)]$ (**5.2**). Unfortunately, the instability of **5.2** has prevented a full characterization and the development of further chemistry of this cluster.

A very similar trend appears in the surprising and unpredicted inertness of **5.1** to 1 atm of CO. The bimetallic cluster does not form higher carbonyls in contrast with $[Ir_3(\mu\text{-}PPh_2)_3(CO)_5]$ (**2.2**) and $[Rh_3(\mu\text{-}PPh_2)_3(CO)_5]$ (**5.1b**).

Further investigations to gain more insight into the general chemistry of the bimetallic cluster led to the preparation and characterization of new isocyanide adducts. Although stability problems with these new clusters did not allow for a comprehensive investigation, and especially prevented long reaction times it was established that the bimetallic isocyanide cluster $[Ir_2Rh(\mu\text{-}PPh_2)_3(CO)_4(1,1,3,3\text{-}tmBuNC)_3]$ (**5.5**) is much less susceptible to oxidative addition of either iodomethane or DMAD in comparison to the homometallic and isostructural parent compound $[Ir_3(\mu\text{-}PPh_2)_3(CO)_4(1,1,3,3\text{-}tmBuNC)_3]$ (**6.1**). Only decomposition products result from addition of DMAD or iodomethane to solutions of **5.5**. In contrast $[Ir_3(\mu\text{-}PPh_2)_3(CO)_4(1,1,3,3\text{-}tmBuNC)_3(CH_3)][I]$ (**7.1**) and two isomers of $[Ir_3(\mu\text{-}PPh_2)_3(CO)_4(1,1,3,3\text{-}tmBuNC)_3(DMAD)_2]$ (**6.1a-b**) are readily obtained upon adding iodomethane and DMAD to **6.1** respectively.

There is at present no explanation why the incorporation of one rhodium atom into the cluster framework results in such dramatic reactivity changes. However, the observation that $[Ir_3(\mu\text{-}PPh_2)_3(CO)_4(XyNC)_3]$ (**6.6**) is also reluctant to undergo oxidative addition reactions involving iodomethane or DMAD clearly demonstrates that the reactive 16-electron iridium centres in $[Ir_3(\mu\text{-}PPh_2)_3(CO)_4(RNC)_3]$ are very sensitive to electronic changes caused by the isocyanide ligands on the adjacent iridium site. It might not be accidental that **6.6** exhibits the highest energy carbonyl stretching frequencies observed in the

series $[Ir_3(\mu\text{-}PPh_2)_3(CO)_4(RNC)_3]$ (R=1,1,3,3-tmBuNC, **6.1**; R=isopr, **6.3**; R=cy, **6.5** and R=xy, **6.6**). ν_{CO} vibrations for **6.6** experience an average 5 cm^{-1} shift to higher wavenumbers, while ν_{CN} appears at slightly lower wavenumbers when compared to the aliphatic isocyanide clusters **6.1**, **6.3** and **6.5**. The observation of higher carbonyl stretching frequencies in **6.6** could be interpreted as a result of less efficient π back bonding due to less electron density on the 16-electron iridium centres, which in turn could offer an explanation for the reluctance of this compound to undergo oxidative addition reactions. The same trend is observed for the isostructural clusters $[Ir_2M(\mu\text{-}PPh_2)_3(CO)_4(tmBuNC)_3]$ (M=Ir, **6.1**; M=Rh, **5.5**). The heterometallic **5.5**, which is reluctant to undergo oxidative addition, exhibits carbonyl stretching frequencies that are also shifted to higher energy when compared to **6.1**. Although the shifts in the carbonyl stretching frequencies are small, they are consistent with decreased electron density at the core and this offers at least a qualitative explanation for the observed reactivity changes.

Oxidative additions on the bimetallic isocyanide clusters might be achievable using more severe reagents such as trimethyloxonium tetrafluoroborate or hydrogen chloride gas but the instability and poor solubility of these clusters has made progress difficult.

6. Conclusions and recommendations for future work

The purification of the triangular phosphidobridged iridium cluster [$Ir_3(\mu$-$PPh_2)_3(CO)_6$] (**2.1**) allowed for the determination of its molecular structure. A subsequent comprehensive comparison of structurally characterized phosphido-bridged clusters of group 9 transition metals showed that these clusters could be categorized into five structure groups (Type A-E, Figure 2.3.1 and Table 2.3.1) and that each of these structure types could be associated with a certain valence-electron count, average metal-metal separation and/or certain transition metal of group 9.

The availability of analytically pure [$Ir_3(\mu$-$PPh_2)_3(CO)_6$] (**2.1**) allowed us to carry out truly stoichiometric reactions which led to the synthesis and characterization of a series of novel triangular phosphido-bridged iridium alkyne clusters including [$Ir_3(\mu$-$PPh_2)_3(CO)_5(\kappa^2$-$MeO_2CCC(CO_2Me)C(O)(\mu$-DMAD)] (**3.1**), [$Ir_3(\mu$-$PPh_2)_3(CO)_6(\mu$-DMAD)] (**3.3**), [$Ir_3(\mu$-$PPh_2)_3(CO)_3(\kappa^2$-$MeO_2CCC(CO_2Me)C(O)_2$] (**3.4b**) and [$Ir_3(\mu$-$PPh_2)_3(CO)_5(\mu$-$DMAD)_2$] (**4.1**). The latter clusters, which were structurally characterized possess 50 valence electrons and should thus exhibit a nearly planar $Ir_3(\mu$-$PPh_2)_3$ core with formally non-bonding iridium-iridium distances. This is observed for **3.1**, **3.3** and **3.4b** which exhibit a core geometry of Type-C (Figure 6.1) with iridium-iridium distances averaging 3.134, 3.132 and 3.162 Å respectively. In contrast, there are severe distortions from planarity in the $Ir_3(\mu$-$PPh_2)_3$ core of **4.1**. The orientations of the phosphido bridges in **4.1**

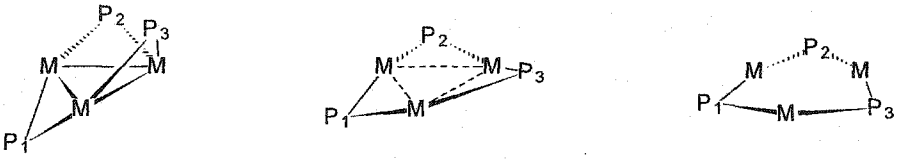

Type-E Hybrid-Structure Type-C

Figure 6.1. *Alternative view of Type-E (left) and Type-C (right) cluster core geometries discussed in Chapter 2, (Figure 2.3.1 and Table 2.3.1) as well as a schematic representation of the cluster core geometry in* ***4.1*** *(middle).*

P_1	48.1(5)	33.32(5)	7.84(1)
P_2	46.3(5)	36.92(5)	6.99(3)
P_3	48.4(5)	43.70(5)	2.67(3)
Average	47.6	37.98	5.83
P_1	2.698(1)	3.0070(3)	2.9320(3)
P_2	2.814(1)	3.1258(4)	3.2295(2)
P_3	2.783(1)	3.0144(3)	3.2414(2)
Average	2.765	3.0490	3.1343

Table 6.1 *Dihedral angles (°) of phosphido bridges with respect to the M_3-plane (top) and metal-metal distances (Å) bridged by $P_{1,2,3}$ bottom for clusters: [$Rh_3(\mu$-$PPh_2)_3(\mu$-$Cl)_2(\mu$-$CO)(CO)_3$] (left column); [$Ir_3(\mu$-$PPh_2)_3(CO)_5(\mu$-DMAD)$_2$] (**4.1**) (middle column) and [$Ir_3(\mu$-$PPh_2)_3(CO)_5(\kappa^2$-$MeO_2CCC(CO_2Me)C(O)(\mu$-DMAD)] (**3.1**) (right column).*

closely mirror those found in a Type-E structure (Figure 6.1). However, in Chapter 2 it was shown that clusters of Type-E structures possess short metal-metal bonds which is in contrast with an average iridium-iridium bond length of 3.049 Å found in **4.1**. Table 6.1 examines metal-metal distances and dihedral angles in **4.1** and two representative examples of a Type-E and Type-C structures: $[Rh_3(\mu\text{-}PPh_2)_3(\mu\text{-}Cl)_2(\mu\text{-}CO)(CO)_3]$ and $[Ir_3(\mu\text{-}PPh_2)_3(CO)_5(\kappa^2\text{-}MeO_2CCC(CO_2Me)C(O)(\mu\text{-}DMAD)]$ (**3.1**), respectively. Since both the average metal-metal bond length and the dihedral angles for **4.1** (Table 6.1) lie in between values for representative examples of clusters with Type-C and E geometry, cluster **4.1** might be understood best as a hybrid showing intermediate geometry with respect to Type-C and-E structures (Figure 6.1). The energies associated with these different geometries are probably very similar and it is not difficult to interconvert between these structures, at least on paper, by a "flip-flop" motion of the phosphido bridges and a simultaneous expansion and contraction of the metal triangle. Although the clusters in Table 6.1 are rigid, many closely related systems are in fact fluxional. For example, $[Co_3(\mu\text{-}Pcy_2)_3(CO)_6]$, which shows D_{3h} symmetry in solution, exhibits a much less symmetrical structure in the solid state, a structure very similar to that of Type-E. The "flip-flop" motion of the phosphido bridges, which is fast on the NMR time scale even at 183 K [34], creates an average signal for the three phosphorus nuclei. It would be very interesting to carry out an extended theoretical study on structures of Type-C and E to learn more about the relevance of inter-metallic motions during their

interconversion.

The isolation of bimetallic **5.1** from a cluster mixture containing primarily [$Ir_2Rh(\mu$-$PPh_2)_3(CO)_5$] (**5.1**) and [$Ir_3(\mu$-$PPh_2)_3(CO)_6$] (**2.1**) was achieved by addition of DMAD which, in the cluster mixture, reacts preferably with **2.1**. In the absence of mixed-metal cluster **5.1** stoichiometric alkyne addition to **2.1** proceeds very slowly. There is at present no clear understanding of the reasons behind the different reactivities of **2.1**. In general the mixed-metal cluster **5.1** was found to be less reactive than the homometallic parent clusters [$Ir_3(\mu$-$PPh_2)_3(CO)_5$] (**2.2**) and [$Rh_3(\mu$-$PPh_2)_3(CO)_5$] (**5.1b**). For example, both **5.1b** and **2.2** react instantly with CO or DMAD to afford higher carbonyls or alkyne adducts, respectively. In contrast, **5.1** is inert towards CO and only reacts slowly with DMAD. Addition of isocyanide to the bimetallic **5.1** afforded the expected [$Ir_2Rh(\mu$-$PPh_2)_3(CO)_4(RNC)_3$] (R=^{t}Bu, **5.3**; R=tmBuNC, **5.5**) which were found to be inert to both iodomethane and DMAD in contrast with their homometallic triiridium analogues. Why the incorporation of one rhodium atom into the cluster frame induces such dramatic reactivity changes in the bimetallic systems is at present not very well understood.

In view of a more general study on the reactivity of triangular phosphido bridged clusters of iridium it would be interesting to examine a variety of different alkynes. This thesis work has focused on dimethylacetylendicarboxylate because

initial attempts involving **2.1** and **1.5**-**1.6** showed inert behaviour of these clusters to a wide variety of less electron deficient alkynes. The very much more reactive **2.2** and **3.1**-**3.2** might however show enhanced reactivity to less activated alkynes. It would be especially interesting to examine terminal alkynes since the clusters have already been shown to accommodate bridging hydrides [44]. No work was carried out with hexafluorobut-2-yne which is also expected to have a rich chemistry with these clusters.

Finally, modifications of the R group on the phosphido bridges have already been shown to result in dramatic effects on the reactivity of the entire cluster in the case of $[Co_3(\mu\text{-}PR_2)_3(CO)_6]$. With R=Ph up to two cluster carbonyls can be substituted by diphenylethylphosphine. However, when R=Cy substitution of cluster carbonyls cannot be induced even using an excess of the less sterically demanding ligand trimethylphosphine and forcing conditions. It would thus be very interesting to examine and compare the reactivity of triangular phosphido bridged iridium clusters with different phosphido groups. So far only one other example has appeared in the literature namely $[Ir_3(\mu\text{-}P^tBu_2)_3(CO)_5]$, but no reactivity of this cluster has been reported [39].

7. Experimental Section

7.1. General Procedure

Unless otherwise stated, all procedures were carried out under an atmosphere of nitrogen using standard Schlenk preparative techniques. Solvents were dried and distilled under nitrogen prior to use: benzene, toluene, diethylether, hexane and pentane from sodium/benzophenone; tetrahydrofuran from potassium; and dichloromethane from calcium hydride.

Crystallographic analyses were carried out by Dr. Bob McDonald, Crystallographer in the Department of Chemistry at the University of Alberta using a Bruker P4/RA/SMART 1000 CCD diffractometer equipped with Mo radiation. Crystals were coated with oil and mounted under a stream of cool nitrogen (-80 °C) for data collection.

Analytical data were supplied by Canadian Microanalytical Services Ltd. Vancouver, B.C. Infrared spectra were recorded on a Bruker IFS25 FT-IR spectrometer as KBr disks. UV Visible spectra were recorded on a Cary 5 UV-VIS-NIR spectrometer using cyclohexane as the solvent.

^{31}P NMR spectra were recorded on a Bruker AMX 360 spectrometer operating at 145.8 MHz. Protons were routinely decoupled by broad band irradiation. Chemical shifts are reported in parts per million relative to external 85 % H_3PO_4.

Positive chemical shifts are downfield of the reference. ^{1}H NMR spectra, unless otherwise specified, were recorded on a Bruker AC300 spectrometer operating at 300 MHz using the solvent residual peak for calibration (+5.23 ppm for *dichloromethane-d_2*).^{13}C NMR spectra, unless otherwise stated, were recorded on a Bruker AMX360 spectrometer operating at 90.6 MHz. The solvent peak was used for calibration (+53.8 ppm for dichloromethane-*d2*)

FAB MS spectra were recorded on a Kratos Concept mass spectrometer operating in positive mode. Samples were dissolved in dichloromethane immediately prior to the experiment and 1 µL of sample solution was transferred by syringe to the probe which contained *meta-nitrobenzyl alcohol* as the matrix.

Alumina refers to Anachemia aluminum oxide activated, neutral, 80~200 mesh. Rhodium(III)chloride hydrate was purchased from Pressure Chemical Co., Pittsburg, PA. Ammonium hexachloroiridate(IV) was obtained from Vancouver Island Precious Metals Ltd. Most solvents and reagents were purchased from Aldrich Chemicals Ltd. including ^{t}BuNC, COD, COE and diphenyl phosphine. 2,5 dimethylphenyl isocyanide was obtained from Fluka Chemicals. Cyclohexyl isocyanide, isopropyl isocyanide and 1,1,3,3-tetramethylbutyl isocyanide were kindly donated by Dr. D. E. Berry of this department. Bis(cyclooctadienyl)-di-μ-chloro-dirhodium [104] and di-μ-chloro-teracarbonyl-dirhodium [105] were prepared according to literature procedures. For the preparation of the

bis(cyclooctene)-μ-chloro-iridium from ammonium hexachloroiridate(VI), the procedure described in reference [106] was slightly modified using a water/isopropanol ratio of 3 :1 to increase the solubility of the iridium salt.

7.2. Synthesis of compounds

$[Ir_3(\mu\text{-}PPh_2)_3(CO)_6]$ (2.1)

A mixture of $[Ir_3(\mu\text{-}PPh_2)_3(CO)_6]$ and $[Ir_3(\mu\text{-}PPh_2)_3(CO)_5]$ was prepared as described previously [44] except using 600 mg $[IrCl(COE)_2]_2$ (0.67 mmol). The solvent was removed in vacuum and the remaining red solid was extracted numerous times with 10 mL of hexane. The combined extracts were evaporated in vacuum and dissolved in a minimal amount of dichloromethane. After filtration through celite, the solution was saturated with carbon monoxide and carefully over layered with hexane to give a black crystalline solid embedded in a red brown precipitate. This mixture was vigorously shaken in an ultrasonic bath for a few seconds to afford a suspension from which small black crystals rapidly settled to the bottom of the vessel leaving a fine brown dust suspended in the supernate solution which was carefully decanted and discharged. The remaining black solid was suspended in hexane and the procedure was repeated twice to afford the desired hexacarbonyl cluster as a black crystalline solid (72 mg, 0.055 mmol) of high purity in 13 % yield. Large black prisms, suitable for crystallographic analysis were obtained by slow diffusion of hexane into a solution containing 35 mg cluster in 0.5 mL of dichloromethane previously

saturated with carbon monoxide, using a 10 mm diffusion tube. Analysis calculated for $Ir_3P_3C_{42}H_{30}O_6$: C, 38.80; H, 2.33 %. Found: C, 38.87; H, 2.31 %. IR (C_6H_6): ν_{CO}: 2068 (w), 2048 (s), 2013 (s), 1988 (s), 1974 (sh), 1943 (s) cm^{-1}. FAB MS (m/z): 1272 (18 %) [M-CO], 1244 (26 %) [M-2CO], 1216 (100 %) [M-3CO], 1188 (13 %) [M-4CO], 1160 (10 %) [M-5CO], 1139 (18 %) [M-phenyl-3CO], 974 (40 %), 896 (40 %), 821 (40 %) amu. ^{31}P NMR (CD_2Cl_2) δ: ambient: 180.6 (s, P_{1-3}); -90 °C: 214.9 (broad, $P_{1,2}$), 133.8 (broad, P_3). ^1H NMR (CD_2Cl_2) δ: 6.9-7.4 (m, P<u>Ph</u>$_2$). ^{13}C NMR (CD_2Cl_2) δ: 182.1 (pseudo quartet, 6 CO), 128.3, 130.1,132.7, 142.1 (m, P<u>Ph</u>$_2$).

$[Ir_3(\mu\text{-}PPh_2)_3(CO)_5]$ (<u>2.2</u>)

A solution of $[Ir_3(\mu\text{-}PPh_2)_3(CO)_6]$ (35 mg, 0.027 mmol) in 20 mL of cyclohexane was purged with dinitrogen for two days during which time the color of the solution gradually brightened from wine red to strawberry red. The solvent was removed in vacuum to give the pentacarbonyl as a bright red solid (32 mg, 0.025 mmol) in 93 % isolated yield. Attempt to crystallize the compound proved unsuccessful partially due to it's high solubility in common organic solvents. IR (cyclohexane): ν_{CO}: 2050 (s), 2017 (s), 1994 (s), 1979 (s), 1964 (s) cm^{-1}. FAB MS (m/z): 1272 (22 %) [M+], 1244 (23 %) [M-CO], 1216 (63 %) [M-2CO], 1139 (23 %) [M-phenyl-2CO], 976 (65 %), 896 (74 %), 821 (100 %) amu. ^{31}P NMR data for the pentacarbonyl cluster have been reported previously. ^1H NMR (C_6D_6) δ: 6.2-7.9 (m, P<u>Ph</u>$_2$).

^{13}C NMR (C_6D_6) δ: 183.3 (t, poorly resolved, CO_{unique},) $^2J\{CP_{cis}\}$ < 10 Hz; 180.2 (d, CO_{axial}) $^2J\{CP_{trans}\}$ = 65 Hz; 186.2 (d, CO_{equat}) $^2J\{CP_{cis}\}$ = 11 Hz.

$[Ir_3(\mu\text{-}PPh_2)_3(CO)_5(\mu\text{-}DMAD)\{\kappa_2\text{-}MeO_2C\underline{C}C(CO_2Me)\underline{C}(O)\}]$ (3.1)

A benzene solution containing $[Ir_3(\mu\text{-}PPh_2)_3(CO)_6]$ (65 mg, 0.05 mmol) was saturated with carbon monoxide. Excess dimethylacetylendicarboxylate (120 µL, 0.98 mmol) was added and the mixture allowed to stand for 2 days in the dark. Removal of the solvent in vacuum and recrystallization from dichloromethane pentane gave the cluster as deep red prisms (42 mg, 0.027 mmol) in 53 % yield. Crystals obtained using this route proved suitable for X-ray analysis only when coated with oil and cooled to -50 °C immediately after removing from the mother liquor, to prevent desolvation.

Analysis calcd. for $Ir_3P_3C_{54}H_{42}O_{14}$: C, 40.93; H, 2.67 %; Found: C, 41.27; H, 2.80 %. IR (KBr): ν_{CH3}: 3052 (w), 2949 (w), ν_{CO}: 2100 (s), 2081 (s), 2059 (s), 2044 (s), 2026 (s), $\nu_{C=O}$: 1716 (s), 1682 (w), $\nu_{C=C}$: 1543 (w), ν_{COC}: 1233 (br) cm^{-1}. FAB MS (m/z): 1585 (100 %) [M+H], 1556 (28 %) [M-CO], 1528 (37 %) [M-2CO], 1500 (52 %) [M-3CO], 1472 (93 %) [M-4CO], 1442 (48 %) [M- alkyne], 1414 (20 %) [M-alkyne-CO], 1386 (63 %) [M- alkyne-2CO], 1358 (22%) [M- alkyne-3CO] amu.

^{31}P NMR (CH_2Cl_2) A_2X, δ: -16.8 (d, P_a), -59.8 (t, P_x) $J^2\{P_aP_x\}$ = 168 Hz.

^1H NMR (CH_2Cl_2), δ: 7.2-8.2 (m, 30H, μ-$P\underline{Ph}_2$), 3.7, 2.6, 2(s, 3H, $\underline{H}_3CO(O)CCCC(O)OC\underline{H}_3$), 2.7 (s, 6H, μ-$\underline{H}_3CO(O)CCCC(O)OC\underline{H}_3$),

^{13}C NMR (CH_2Cl_2) δ: 171.2 (s, $H_3CO(O)\underline{C}CCC(O)OCH_3$), 169.3 (t) $^2J\{CP\}$ = 8 Hz,

168,2 (s, μ-$H_3CO(O)\underline{C}CC\underline{C}(O)OCH_3$), 166.5 (t) $^2J\{CP\}$ = 10 Hz, 164.1 (m, 2CO), 162.7 (s, $H_3CO(O)\underline{C}CCC(O)OCH_3$), 159.9 (t poorly resolved, Ir$C\underline{C}$CO) $^3J\{CP\}$ < 2 Hz, 155.0 (t) $^2J\{CP\}$ = 6 Hz, 153.8 (m, 2CO), 126-139 (m, μ-P$\underline{Ph}_2$), 51.5, 50.5, 2(s, $H_3\underline{C}O(O)CCCC(O)O\underline{C}H_3$), 51.1 (s, μ-$H_3\underline{C}O(O)CCCC(O)O\underline{C}H_3$).

[$Ir_3(\mu$-$PPh_2)_3(\mu$-CO)$(CO)_4(\mu$-DMAD)] (3.2)

[$Ir_3(\mu$-$PPh_2)_3(CO)_5$] (10 mg, 0.008 mmol), prepared as described, was disolved in benzene (1 mL). Addition of dimetylacetylenedicarboxylate (1,0 μL, 0.008 mmol) to the stirred solution resulted in an immediate brightening from dark red to orange red. Stirring was discontinued after five minutes and all volatiles were removed *in vacuo* to give the cluster as a red powder. Attempts to obtain crystalline material via recrystallization all proved unsuccessful.

IR (KBr): ν_{CO}: 2070 (s), 2028 (s), 2000 (s), 1970 (s) 1849 (s), $\nu_{C=O}$: 1706 (s), 1686 (s), 1657 (s) cm^{-1}. FAB MS (m/z): 1386 (100 %) [M-CO], 1358 (98 %) [M-2CO] amu. ^{31}P NMR (C_6D_6) AMX, δ: 142.8 (d, P_a), 80.5 (d of d, P_m), 31.7 (d, P_x), $^2J\{P_aP_m\}$ = 174 Hz, $^2J\{P_mP_x\}$ = 140 Hz, $^2J\{P_aP_x\}$ < 2 Hz. ^1H NMR (C_6D_6) δ: 6.4-8.2 (m, 30H, μ-P$\underline{Ph}_2$), 3.5, 2.8, 2(s, 3H, $\underline{H}_3CO(O)CCCC(O)OC\underline{H}_3$). ^{13}C NMR (C_6D_6) δ: 191.1 (m), 173,1 (broad), 171.7 (m), 170.0 (m, weak), 168.8 (m), 168.0 (s), 164.0 (m), 126-139 (m, μ-P$\underline{Ph}_2$), 115.2 (m, μ-$H_3CO(O)\underline{C}CC\underline{C}(O)OCH_3$).

[$Ir_3(\mu$-$PPh_2)_3(CO)_6(\mu$-DMAD)] (3.3)

[$Ir_3(\mu$-$PPh_2)_3(CO)_5$] was prepared as described above (35 mg, 0.027 mmol).

Dimethylacethylenedicarboxylate (3.4 µL 0.027 mmol) was added to the stirred solution causing an immediate color change from red to orange. After stirring for one minute, carbon monoxide was bubbled vigorously through the solution resulting in formation of a bright yellow solution. After filtration through celite the solvent was removed *in vacuo* and the residue redissolved in a minimal amount of dichloromethane saturated with carbon monoxide and carefully layered with hexane to give the cluster as bright orange crystals (28 mg, 0.019 mmol) in 72 % yield. Analysis calcd. for $Ir_3P_3C_{48}H_{36}O_{10}$: C, 39.96; H, 2.51 %; Found: C, 39.75; H, 2.40 %. IR (KBr): ν_{CO}: 2082 (s), 2056 (s), 2034 (s), 2018 (s), 1977 (s), 1929 (s); $\nu_{C=O}$: 1707 (m), 1682 (m), ν_{COC}: 1234 (br), 1215 (br) cm^{-1}. FAB MS (m/z): 1386 (100 %) [M-2CO], 1358 (68 %) [M-3CO] amu. ^{31}P NMR (CH_2Cl_2) A_2X, δ: +12.2 (d, P_a), -68.0 (t, P_x) $J^2\{P_aP_x\}$ = 164 Hz (broad resonances). ^{13}C NMR (CH_2Cl_2) δ: 188.2 (br, 2CO), 168.0 (s, $2H_3CO(O)\underline{C}CC\underline{C}(O)OCH_3$), 165.4 (br, 2CO), 153,3 (br, 2CO), 127-142 (m, μ-P$\underline{Ph}_2$), 51.2 (s, $2H_3\underline{C}O(O)CCCC(O)O\underline{C}H_3$). ^1H NMR (CH_2Cl_2) δ: 7.2-8.2 (m, 30 H, μ-P$\underline{Ph}_2$), 2.9 (s, broad, 6H, μ-$\underline{H}_3CO(O)CCCC(O)OC\underline{H}_3$).

$[Ir_3(\mu\text{-}PPh_2)_3(CO)_3(t\text{-}BuNC)_2\{\kappa_2\text{-}MeO_2C\underline{C}C(CO_2Me)\underline{C}(O)\}_2]$ (3.4a-b)

Dimethylacetylenedicarboxylate (25 µL 0.20 mmol) was added dropwise to a stirred solution of $[Ir_3(\mu\text{-}PPh_2)_3(CO)_5(t\text{-}BuNC)_2]$ (36 mg, 0.025 mmol) in dichloromethane (3 mL). The mixture was allowed to stand for 2 days after which all volatiles were removed in vacuum to give the dialkyne adduct as a bright

orange solid (40 mg, 0.023 mmol) in two isomeric forms (93 % total yield). Separation of the two isomers was achieved by transferring the remaining solid, dissolved in a minimal amount of benzene, to an alumina column. A yellow green band containing impurities was eluted with benzene and discharged. Next, a bright yellow band containing isomer **3.4a** was eluted with a mixture of benzene-THF (ratio 5:1). Finally, isomer **3.4b** was isolated by increasing the THF concentration in the eluant (ratio of benzene :THF = 3:2). Both isomers were recrystallized from dichloromethane/hexane to give **3.4a** as yellow flakes (11 mg) and **3.4b** as yellow-orange prisms (10 mg). The absence of oxygen was crucial for successful separation especially when THF was present.

3.4a, (fast eluting yellow band, C_2 isomer)

Analysis calcd. for $Ir_3P_3C_{63}H_{60}O_{13}N_2 \cdot CH_2Cl_2$: C, 42.52; H, 3.46; N, 1.55 %. Found: C, 42.62; H, 3.33; N, 1.58 %. IR (KBr): ν_{CH3}: 3052 (w), 2984 (w), 2946 (w), ν_{CN}: 2240 (w), 2218 (s), ν_{CO}: 2018 (sh), 2012 (s), $\nu_{C=O}$: 1714 (s), 1696 (s), $\nu_{C=C}$: 1555 (br), ν_{COC}: 1269 (s), 1223 (s), 1191 (s) cm^{-1}. FAB MS (m/z): 1723 (3 %) [M+H], 1693 (4 %) [M-H-CO], 1663 (17 %) [M-CO-OCH_3], 1638 (4 %) [M-3CO], 1610 (8 %) [M-4CO], 1582 (7 %) [M-5CO], 1551 (6 %) [M-5CO-OCH_3], 1524 (15 %) [M-alkyne-2CO], 1496 (100 %) [M-alkyne-3CO], 1468 (14 %) [M-alkyne-4CO], 1441 (17 %) [M-alkyne-(t-BuNC)-2CO], 1382 (8 %) [M-2alkyne-2CO] 1326 (7 %) [M-2alkyne-4CO] amu. ^1H NMR (CH_2Cl_2) δ: 7.1-8.3 (m, 30 H, μ-P$\underline{Ph}_2$), 4.2, 3.4, 2(s, 6H, $\underline{H}_3CO(O)CCCC(O)OCH_3$), 0.42 (s, 18H, $2CNC(C\underline{H}_3)_3$).

^{31}P NMR (CH_2Cl_2) A_2X, δ: +13.0 (t, P_x), -43.8 (d, P_a) $J^2\{P_aP_x\}$ = 200 Hz. ^{13}C NMR (CH_2Cl_2) δ: 178.0 (m, 2CO), 174.6 (s, $H_3CO(O)\underline{C}CCC(O)OCH_3$), 172.9 (m, 2CO), 160.3 (s, $H_3CO(O)\underline{C}CCC(O)OCH_3$), 156.4, 150.9 (broad, $H_3CO(O)C\underline{CC}C(O)OCH_3$), 146.9 (broad, CO_{equat}), 127-139 (m, μ-P$\underline{Ph}_2$), 99.1 (broad, 2Ir$\underline{C}NC(CH_3)$), 59.4 (s, 2IrCN$\underline{C}(CH_3)_3$), 52.8, 50.6 (s, $H_3\underline{C}O(O)CCCC(O)OCH_3$), 28.3 (s, 2(CNC($\underline{C}H_3)_3$).

3.4b, (slow eluting orange band, C_s isomer)

Analysis calcd. for $Ir_3P_3C_{63}H_{60}O_{13}N_2$: C, 43.92; H, 3.51; N, 1.63 %. Found: C, 44.26; H, 3.78; N, 1.58 %. IR (KBr): ν_{CH3}: 3052 (w), 2985 (w), 2945 (w), ν_{CN}: 2248 (w), 2208 (s), ν_{CO}: 2018 (sh) 2011 (s), 1987 (w), $\nu_{C=O}$: 1714 (s), 1704 (sh) 1693 (sh), $\nu_{C=C}$: 1561 (br), ν_{COC}: 1261 (s), 1224 (s), 1190 (s) cm^{-1}. FAB MS (m/z): 1723 (13 %) [M+H], 1695 (5 %) [M+H-CO], 1666 (6 %) [M-2CO], 1665 (8 %) [M-(t-Bu)], 1663 (8 %) [M-CO-OCH_3], 1639 (7 %) [M-(t-BuNC)], 1638 (7 %) [M-3CO],1637 (7 %) [M-(t-Bu)-CO],1610 (8 %) [M-4CO], 1580 (8 %) [M-alkyne], 1552 (7 %) [M-alkyne-CO], 1524 (13 %) [M-alkyne-2CO], 1496 (100 %) [M-alkyne-3CO], 1468 (20 %) [M-alkyne-4CO], 1441 (20 %) [M-alkyne-(t-BuNC)-2CO], 1326 (13 %) [M-2alkyne-4CO] amu. ^{1}H NMR (CH_2Cl_2) δ 6.8-8.3 (m, 30H, μ-P$\underline{Ph}_2$), 4.0, 3.4, 2(s, 6H, $\underline{H}_3CO(O)CCCC(O)OC\underline{H}_3$), 0.9, 0.0, 2(s, 9H, CNC($C\underline{H}_3)_3$). ^{31}P NMR (CH_2Cl_2) A_2X, δ: +9.7 (t, P_x), -34.7 (d, P_a) $J^2\{P_aP_x\}$ = 200 Hz (Fine splitting of resonances observed). ^{13}C NMR (CH_2Cl_2) δ: 177.7 (m, 2 CO), 173.5 (s, $H_3CO(O)\underline{C}CCC(O)OCH_3$), 171.6 (m, 2CO), 160.3 (s, $H_3CO(O)\underline{C}CCC(O)OCH_3$),

157.9, 148.5, 2(broad, $H_3CO(O)C\underline{C}\underline{C}C(O)OCH_3$), 145.5 (broad, CO_{equat}), 127-142 (m, μ-P$\underline{Ph}_2$), 59.7, 59.5, 2(s, IrCN$\underline{C}(CH_3)_3$), 52.1, 50.7, 2(s, $H_3\underline{C}O(O)CCCC(O)O\underline{C}H_3$) 28.9, 28.3, 2(s, CNC($\underline{C}H_3)_3$) (Isonitrile carbons not observed).

$[Ir_3(PPh_2)_3(CO)_2(t\text{-}BuNC)_3\{\kappa_2\text{-}MeO_2C\underline{C}\underline{C}(CO_2Me)\underline{C}(O)\}_2]$ (3.5a-b)

The synthesis and chromatography employed was as described above for the di-tBuNC system except that $[Ir_3(\mu\text{-}PPh_2)_3(CO)_4(t\text{-}BuNC)_3]$ (100 mg, 0.067 mmol) was used. Recrystallization from dichloromethane/pentane gave isomer **3.5a** as yellow-orange needles (32 mg, 0.017mmol, 26 %) and isomer **3.5.b** as orange prisms (22 mg, 0.012 mmol) in 26 and 18 % isolated yield, respectively.

3.5a (fast eluting yellow band, C_2 isomer)

Analysis calcd. for $Ir_3P_3C_{67}H_{69}O_{12}N_3 \cdot CH_2Cl_2$: C, 43.84; H, 3.84; N, 2.26 %. Found: C, 43.83; H, 3.84; N, 2.28%. IR (KBr): ν_{CH3}: 3051 (w), 2982 (w), 2945 (w), ν_{CN}: 2232 (w), 2204 (s), 2156 (s), ν_{CO}: 2003 (s), $\nu_{C=O}$: 1714 (s), 1695 (s), $\nu_{C=C}$: 1549 (br) ν_{COC}: 1265 (s), 1218 (s), 1191 (br) cm^{-1}. FAB MS (m/z): 1778 (41 %) [M+H], 1749 (30 %) [M-CO], 1721 (47 %) [M-2CO] ,1720 (56 %) [M-^{t}Bu], 1718 (60 %) [M-CO_2CH_3], 1693 (28 %) [M-3CO], 1665 (13 %) [M-4CO], 1607 (28 %) [M-alkyne-CO], 1579 (48 %) [M-alkyne-2CO], 1551 (100 %) [M-alkyne-3CO], 1524 (37 %) [M-alkyne-(t-BuNC)-CO], 1496 (98 %) [M-alkyne-(t-BuNC)-2CO], 1468 (17 %) [M-alkyne-(t-BuNC)-3CO], 1440 (10 %) [M-alkyne-(t-BuNC)-4CO]

amu. ^{1}H NMR (CH_2Cl_2)δ: 7.1-8.4 (m, 30H, μ-P$\underline{Ph}_2$), 4.2, 3.4, 2(s, 6H $\underline{H}_3CO(O)CCCC(O)OCH_3$), 2.0 (s, 9H, $^t\underline{Bu}NC_{equat}$), 0.5 (s, 18H 2 $^t\underline{Bu}NC_{axial}$). ^{31}P NMR ($CH_2Cl_2$) A_2X, δ: +6.2 (t, P_x), -39.4 (d, P_a), $J^2\{P_aP_x\}$ = 195 Hz. ^{13}C NMR (CH_2Cl_2) δ: 178.5 (m, 2CO), 175.1 (s, $H_3CO(O)\underline{C}CCC(O)OCH_3$), 173.0 (m, 2CO), 160.3 (s, $H_3CO(O)\underline{C}CCC(O)OCH_3$), 156.0, 151.7, 2(broad, $H_3CO(O)C\underline{C}\underline{C}C(O)OCH_3$), 127-141 (m, μ-P$\underline{Ph}_2$), 105.1 (very broad, 2^{t}BuN$\underline{C}_{axial}$, 98.5 (broad, ^{t}BuN$\underline{C}_{equat}$), 59.8 (s, $^t\underline{Bu}NC_{equat}$), 58.1 (s, 2$^t\underline{Bu}NC_{axial}$), 51.9, 50.4, 2(s, $H_3\underline{C}O(O)CCCC(O)O\underline{C}H_3$), 31.1 (s, $^t\underline{Bu}NC_{equat}$), 28.4 (s, 2^{t}BuNC$_{axial}$).

3.5b (slow eluting orange band, C_s isomer)

Analysis calcd. for $Ir_3P_3C_{67}H_{69}O_{12}N_3 \cdot CH_2Cl_2$: C, 43.84; H, 3.84; N, 2.26 %. Found: C, 43.78; H, 3.93; N, 2.26 %. IR (KBr): ν_{CH3}: 3048 (w), 2982 (w), 2945 (w), ν_{CN}: 2232 (w), 2198 (s), 2166 (s), ν_{CO}: 2003 (s), 1978 (w), $\nu_{C=O}$: 1722 (s), 1713 (s) 1682 (sh), $\nu_{C=C}$: 1553 (br), ν_{COC}: 1261 (s), 1219 (s), 1188 (s) cm^{-1}. FAB MS (m/z): 1778 (67 %) [M+H], 1749 (17 %) [M-CO], 1721 (27 %) [M-2CO], 1720 (26 %) [M-(t-Bu)], 1718 (22 %) [M-CO-OCH_3], 1693 (18 %) [M-3CO], 1665 (12 %) [M-4CO], 1607 (17 %) [M-alkyne-CO], 1579 (27 %) [M-alkyne-2CO], 1551 (100 %) [M-alkyne-3CO], 1524 (25 %) [M-alkyne-(t-BuNC)-CO], 1496 (97 %) [M-alkyne-(t-BuNC)-2CO], 1468 (17 %) [M-alkyne-(t-BuNC)-3CO], 1440 (14 %) [M-alkyne-(t-BuNC)-4CO] amu.

^{1}H NMR (CH_2Cl_2) δ: 6.9-8.4 (m, 30H, μ-P$\underline{Ph}_2$), 4.1, 3.4, 2(s, 6H, $\underline{H}_3CO(O)CCCC(O)O\underline{C}H_3$), 1.9 (s, 9H, $^t\underline{Bu}NC_{equat}$), 1.0, 0.1, 2(s, 6H, 2$^t\underline{Bu}NC_{axial}$).

^{31}P NMR (CH_2Cl_2) A_2X, δ: -16.7 (t, P_x), -30.6 (d, P_a), $J^2\{P_aP_x\}$ = 196 Hz. ^{13}C NMR (CH_2Cl_2) δ: 178.0 (m, 2CO), 174.2 (s, $H_3CO(O)\underline{C}CCC(O)OCH_3$), 171.7 (m, 2CO), 160.3 (s, $H_3CO(O)\underline{C}CCC(O)OCH_3$), 157.5, 149.6 2(m, $H_3CO(O)C\underline{C}\underline{C}C(O)OCH_3$), 127-143 (m, μ-$P\underline{Ph}_2$), 108.9, 100.0, 2(very broad, $^tBuN\underline{C}_{axial}$), 97,0 (m, $^tBuN\underline{C}_{equat}$), 59.8 (s, $^t\underline{Bu}NC_{equat}$), 58.4, 58.2, 2(s, $^t\underline{Bu}NC_{axial}$), 51.9, 50.5 (s, $H_3\underline{C}O(O)CCCC(O)O\underline{C}H_3$), 31.1 (s, $^t\underline{Bu}NC_{equat}$), 29.1, 28.3 (s) 2(s, $^t\underline{Bu}NC_{axial}$).

$[Ir_3(\mu\text{-}PPh_2)_3(CO)_5(\mu\text{-}DMAD)_2]$ (4.1)

A stirred solution of $[Ir_3(\mu\text{-}PPh_2)_3(CO)_5(\mu\text{-}DMAD)\{\kappa_2\text{-}MeO_2C\underline{C}C(CO_2Me)\underline{C}(O)\}]$ (25 mg, 0.016 mmol) in 5 mL of benzene was irradiated using a photo lamp. Small aliquots were taken hourly to monitor the progress of the reaction via solution IR spectroscopy. After 7 hours the solvent was removed in vacuum to give the photoproduct as a bright yellow solid (22 mg, 0.014 mmol) in 90 % yield. Unfortunately, the cluster is not stable in solution for long periods of time, as noted by darkening from bright yellow to orange and finally red after about one week. Recrystallization from dichloromethane hexane yields a mixture of bright yellow prisms, suitable for X-ray analysis, and dark red flakes. Analysis calculated for $Ir_3P_3C_{53}H_{42}O_{13}$: C, 40.90; H, 2.72 %. Found: C, 41.10; H, 2.79 %. IR (benzene): ν_{CO}: 2090 (s), 2022 (s), 2035 (sh), 2022 (vs), $\nu_{C=O}$: 1690 (br) cm^{-1}. FAB MS (m/z): 1557 (10 %) [M+H], 1528 (38 %) [M-CO], 1500 (50 %) [M-2CO], 1497 (53 %) [M-CO_2Me], 1472 (68 %) [M-3CO],1469 (48 %) [M-CO_2Me-CO],

1441 (58 %) [M-CO_2Me-2CO], 1413 (26 %) [M-CO_2Me-3CO], 1386 (100 %) [M-alkyne-CO], 1358 (70 %) [M-alkyne-2CO] amu. ^{1}H NMR (C_6D_6) δ: 6.3-8.6 (m, 30H, μ-$\underline{Ph_2}$P), 3.31, 3.28, 3.06, 2.80, 4(s, 3H, 2$\underline{Me}O_2CCCCO_2\underline{Me}$). ^{31}P NMR ($C_6D_6$) AMX δ: +80.0 (d, P_a), +52.7 (d of d, P_m), -7.3 (d, P_x) $^2J\{P_xP_m\}$ = 152 Hz, $^2J\{P_aP_m\}$ = 247 Hz, $^2J\{P_aP_x\}$ < 2 Hz.

[Ir_3(μ-PPh_2)$_3$(CO)$_6$(μ-DMAD)$_2$(t-BuNC)] (4.2)

Tert-butylisocyanide (4 μL, 0.035 mmol) was added to a stirred solution of [Ir_3(μ-PPh_2)$_3$(CO)$_5$(μ-DMAD){κ_2-$MeO_2C\underline{C}C(CO_2Me)\underline{C}(O)$}] (30 mg, 0.019 mmol) in 5 mL of dichloromethane. After two days all volatiles were removed in vacuum to give the cluster as a yellow powder (28 mg, 0.017 mmol) in 89 % yield. Purification was achived by transferring the cluster dissolved in a minimal amount of benzene, to an alumina column and eluting a yellow band using a benzene THF mixture (ratio 1:4). The solvent was removed in vacuum to yield the cluster as a bright yellow solid (14 mg). Attempts were made to obtain X-ray quality crystals but all of them proved unsuccessful. Analysis calculated for: $Ir_3P_3C_{59}H_{51}O_{14}N$: C, 42.49; H, 3.08; N, 0.84 %. Found: C, 43.04; H, 2.97; N, 0.96 %. IR (KBr): ν_{CN}: 2205 (s), ν_{CO}: 2069 (s), 2047 (vs), 2020 (s), 2002 (s), $\nu_{C=O}$: 1701 (br), $\nu_{C=O}$: 1560 (w), ν_{C-O-C}: 1228 (br) cm^{-1}. FAB MS (m/z): 1668 (38 %) [M+H], 1639 (20 %) [M-CO], 1611 (34 %) [M-2CO], 1610 (33 %) [M-(t-Bu)], 1583 (37 %) [M-3CO], 1555 (58 %) [M-4CO], 1527 (73 %) [M-5CO], 1525 (61 %) [M-alkyne], 1496 (52 %) [M-OCH_3-5CO], 1469 (37 %) [M-alkyne-2CO], 1441 (100 %) [M-alkyne-3CO], 1413

(32 %) [M-alkyne-4CO], 821 (89 %) amu. ^{1}H NMR (C_6D_6): 7.1-8.0 (m, 30H, μ-$\underline{Ph_2}$P), 3.47, 3.09, 3.06, 3.00, 4(s, 3H 2$\underline{Me}O_2CCCCO_2\underline{Me}$).^{31}P NMR ($C_6D_6$) ABX δ: +151.8 (d of d, P_x), -60.23 (d, P_b), -59.9 (d, P_a), $^{2}J\{P_aP_b\}$ < 2Hz, $^{2}J\{P_bP_x\}$ = Hz, $^{2}J\{P_aP_x\}$ = Hz.

[$Ir_2Rh(\mu$-$PPh_2)_3(CO)_5$] (5.1)

Diethylamine (103 µL, 1.00 mmol) was added drop wise to a stirred suspension of iridiumcarbonylchloride (251 mg, 0.80 mmol) and rhodiumcarbonylchloride (39 mg, 0.10 mmol) in 20 ml of benzene. After 45 minutes most of the material had dissolved forming a pale yellow solution. Addition of diphenylphosphine (174 µL, 1.0 mmol) caused an immediate color change to dark red. After the solution was allowed to stir for an hour, the volume of solvent was reduced under vacuum to about 5 mL and transferred to an alumina column where a dark red band was eluted with benzene. Removal of all volatiles in vacuum and recrystallization of the residual dark red powder from dichloromethane/hexane gave the desired cluster in the supernatant solution. Removal of the solvent in vacuum gave a clean mixture of [$Ir_3(\mu$-$PPh_2)_3(CO)_6$] and [$Ir_2Rh(\mu$-$PPh_2)_3(CO)_5$] (140 mg) in the molar ratio of 1:1.5 respectively (by integration of the ^{31}P NMR signals). The mixture was dissolved in 1 g of benzene-d_6 and dimethylacetylendicarboxylate (9 µL, 0.07 mmol) was added which caused a slight brightening of the dark red solution. After 15 minutes, ^{31}P NMR indicated the consumption of al [$Ir_3(\mu$-$PPh_2)_3(CO)_6$]. The mixture was transferred to an alumina column and a purple

band containing the desired $[Ir_2Rh(\mu\text{-}PPh_2)_3(CO)_5]$ eluted with benzene. Removal of the solvent gave the cluster as a dark purple powder (68 mg 0.06 mmol) in 57 % yield (based on rhodiumcarbonylchloride). Attempts to obtain crystals of the compound by crystallization proved unsuccessful, partially due to the clusters very high solubility in convenient organic solvents. Analysis calculated for $Ir_2RhP_3C_{41}H_{30}O_5 \cdot C_6H_6$: C, 44.76 %; H, 2.88. Found: C, 44.69; H, 3.32 %. IR (Cyclohexane): ν_{CO}: 2047 (s), 2014 (s), 1992 (s), 1975 (vs) cm^{-1}. FAB MS (m/z): 1154 (23 %) [M-CO], 1126 (69 %) [M-2CO], 1098 (13%) [M-3CO), 1070 (50%) [M-4CO), 886 (54 %), 808 (69 %), 731 (100 %) amu. ^1H NMR (C_6D_6) δ: 6.2 - 7.7 (m, 30H, μ-P<u>Ph</u>$_2$). ^{13}C NMR (C_6D_6) δ: 194.1 (d of t, Rh<u>C</u>O) $^1J\{CRh\}$ = 86 Hz, $^2J\{CP\}_{cis}$ = 9 Hz, 184.1 (d, 2CO) $^2J\{CP\}_{cis}$ = 8 Hz, 183.1 (d, 2CO) $^2J\{CP\}_{trans}$ = 67 Hz. ^{31}P NMR (C_6D_6) AM_2X, δ: +259.0 (d of d, P_m), +107.9 (t, P_a) $^1J\{PRh\}$ = 119 Hz, $^2J\{P_aP_m\}$ = 14 Hz.

$[Ir_2Rh(\mu\text{-}PPh_2)_3(CO)_5(\mu\text{-}DMAD)]$ (<u>5.2</u>)

Dimethylacetylenedicarboxylate (2.0 µL, 0.016 mmol) was added to a solution of $[Ir_2Rh(\mu\text{-}PPh_2)_3(CO)_5]$ (20 mg, 0.017 mmol) in 1g of benzene-d_6 and the reaction was monitored by ^{31}P NMR spectroscopy. After 3 hours, conversion was complete and the content of the NMR tube was transferred to an alumina column. First a minor orange-red band containing small amounts of starting material and impurities was eluted with benzene. Finally an orange-red band was eluted using a mixture of THF and benzene (ratio 1:2). The solvent was

evaporated in vacuum to give the desired cluster as a red powder (12 mg, 0.09 mmol) in 53 % yield. Unfortunately the compound is not stable in solution thus ^{13}C NMR data are not available. FAB MS (m/z): 1298 (32 %) [M-CO], 1270 (15 %) [M-2CO], 1242 (18%) [M-3CO), 1214 (24%) [M-4CO), 886 (40 %), 808 (66 %), 731 (100 %) amu. ^{1}H NMR (C_6D_6) δ: 6.3 - 8.3 (m, 30H, μ-P<u>Ph</u>$_2$), 3.4, 2.8, 2(s, 3H, <u>Me</u>O_2CCCCO_2<u>Me</u>). ^{31}P NMR (C_6D_6) AMXY, δ: +128.3 (d, P_a), +104.0 (d of d of d, P_m), +43.7 (d of d, P_x) $^{1}J\{P_mRh\}$ = 112 Hz, $^{2}J\{P_xP_m\}$ = 172 Hz, $^{1}J\{P_xRh\}$ = 87 Hz, $^{2}J\{P_aP_m\}$ = 158 Hz, $^{2}J\{P_aP_x\}$ < 2 Hz).

$[Ir_2Rh(\mu\text{-}PPh_2)_3(CO)_4(t\text{-}BuNC)_3]$ (<u>5.3</u>)

A small excess of *tert*-butylisocyanide (10 µL, 0.1 mmol) was added dropwise to a stirred solution of $[Ir_2Rh(\mu\text{-}PPh_2)_3(CO)_5]$ (25 mg, 0.021 mmol) in 1 mL of benzene which caused an immediate color change from purple to yellow. (When the reaction was carried out with the appropriated 3 equivalents of isocyanide and monitored by ^{31} P NMR spectroscopy, an equilibrium mixture of starting material as well as di- and tri-substituded isocyanide cluster was observed. From the ^{31}P NMR data of the di-substituted intermediate an unambiguous assignment of the NMR signals was possible.) Stirring was discontinued and after one hour a yellow microcrystalline solid started to form. Addition of hexane resulted in rapid precipitation of the compound. The supernatant was carefully decanted and the yellow solid washed with hexane twice and dried in vacuum to give the cluster (21 mg, 0.15 mmol) in 71 % yield. Even in the solid state decomposition occurred

within a few days as noted by a darkening of the initially canary yellow micro crystals to red-brown. Therefore elemental analysis is not available. Solutions of the cluster in dichloromethane or benzene are stable for short periods of time only. Despite its rapid decomposition, the cluster does not react with DMAD, Bzl or MeI. IR (KBr): ν_{CN}: 2207 (w), 2180 (s), 2138 (s), ν_{CO}: 1967 (s), 1942 (s), 1919 (s), 1896 (s) cm^{-1}. FAB MS (m/z): 1378 (70 %) [M-CO], 1350 (58 %) [M-2CO], 1322 (61%) [M-3CO), 1294 (81%) [M-4CO) amu. ^1H NMR (CD_2Cl_2) δ: 7.2 - 8.2 (m, 30H, P<u>Ph</u>$_2$), 1.9 (s, 9H, ^{t}<u>Bu</u>NC)$_{aequat}$), 0.4 (s, 18H, 2^t<u>Bu</u>NC$_{axial}$).
^{31}P NMR is in good agreement with assignements made previously by our group on the basis of 2 D ^{31}P NMR spectra of a mixture of the four observed mixed metal isocyanide clusters [44].

[$Ir_2Rh(\mu$-$PPh_2)_3(CO)_4$(1,1,3,3-tmBuNC)$_3$] (<u>5.5</u>)

The cluster was synthesized as described above except that a four fold excess of 1,1,3,3-tetramethylbutylisocyanide was used (75 % yield). Large yellow prisms, suitable for crystallographic analysis were obtained by carefully over layering a solution containing 15 mg cluster in 0.5 mL of dichloromethane with hexane using a 5 mm NMR tube. Although crystals or solutions of this cluster will decompose as well, this occurs much more slowly. Analysis calculated for $Ir_2RhP_3C_{67}H_{81}O_4N_3$: C, 51.11; H, 5.18; N, 2.67 %; Found: C, 49.16; H, 5.32; N, 2.52 %. IR (KBr): ν_{CN}: 2201 (w), 2171 (s), 2121 (s), ν_{CO}: 1963 (s), 1941 (s), 1916 (s), 1896 (s) cm^{-1}. FAB MS (m/z): 1546 (22 %) [M-CO], 1517 (55 %) [M-(t-Bu)],

1490 (38%) [M-3CO), 1462 (43%) [M-4CO), 731 (100 %) amu.

^{1}H NMR (CD_2Cl_2) δ: 7.2 - 8.2 (m, 30H, μ-P$\underline{Ph}_2$), 2.1 [s, 2H, ($CNC(CH_3)_2C\underline{H}_2C(CH_3)_3)_{aequat}$], 2.0 [s, 6H, ($CNC(C\underline{H}_3)_2CH_2C(CH_3)_3)_{aequat}$], 1.3 [s, 9H, ($CNC(CH_3)_2CH_2C(C\underline{H}_3)_3)_{aequat}$], 0.6 [s, 22H, 2($CNC(CH_3)_2CH_2C(C\underline{H}_3)_3)_{axial}$ and 2($CNC(CH_3)_2C\underline{H}_2C(CH_3)_3)_{axial}$], 0.4 [s, 12H, 2($CNC(C\underline{H}_3)_2CH_2C(CH_3)_3)_{axial}$].

^{31}P NMR (CD_2Cl_2) AMXY δ: P_a: +55.8 (d of d of d, P_a) +20.4 (d of d, P_m) +92.7 (d of d of d, P_x) $^2J\{P_xP_m\}$ = 146 Hz, $^1J\{P_xRh\}$ = 86 Hz, $^1J\{P_aRh\}$ = 102 Hz, $^2J\{P_aP_x\}$ = 167 Hz, $^2J\{P_aP_m\}$ = 137 Hz.

[$Ir_2Rh(\mu$-$PPh_2)_3(CO)_3(\mu$-dppm)] (5.7)

Bis-diphenylphosphinomethane (6 mg, 0.023mmol) was added to a stirred solution of [$Ir_2Rh(\mu$-$PPh_2)_3(CO)_5$] (25 mg, 0.021 mmol) in 2 mL of dichloromethane. The purple color of the solution intensified rapidly and after 1 hour the solvent was removed in vacuum and the residual powder recrystallized from dichloromethane/hexane to give the cluster as a dark crystalline solid (23 mg, 0.015 mmol) in 72 % yield. Analysis calculated for $Ir_2RhP_5C_{64}H_{52}O_3$: C, 50.88; H, 3.47 %; Found: C, 51.55; H, 3.84 %. IR (KBr): ν_{CO}: 1934 (br) cm^{-1}. FAB MS (m/z): 1512 (100 %) [M+H], 1455 (8 %) [M-2CO], 731 (100 %) amu. ^{1}H NMR (C_6D_6) δ: 6.1 - 7.6 (m, 50H, μ-P$\underline{Ph}_2$, dppm), 3.1 (m, 2H, $Ph_2PC\underline{H}_2PPh_2$).

^{31}P NMR (CD_2Cl_2) AM_2X_2Y, δ: +128.1 (t of t, P_a), +255.4 (d of d, P_m) , -13.2 (d, P_x), $^2J\{P_aP_m\}_{cis}$ = 20 Hz, $^2J\{P_aP_x\}_{trans}$ = 168 Hz, $^1J\{RhP_m\}$ = 117 Hz.

Reaction of $[Ir_3(\mu\text{-}PPh_2)_3(CO)_4(1,1,3,3\text{-}tmBuNC)_3]$ (6.1) with DMAD

Dimethylacetylendicarboxylate (50 µL, 0.20 mmol) was added to a solution of $[Ir_3(\mu\text{-}PPh_2)_3(CO)_4(1,1,3,3\text{-}tmBuNC)_3]$ (70 mg, 0.042 mmol) in 5 mL of dichloromethane and the mixture was allowed to stir overnight. The solvent was removed *in vacuo* and the residual oil, dissolved in a minimal amount of benzene, was transferred to an alumina column. Two isomers **6.1a** and **6.1b** were eluted employing the same conditions as described for the separation of isomers **3.4a** and **3.4b**. Recrystallization of **6.1a-b** afforded oils only which proved to be contaminated with residual DMAD as shown by proton NMR and IR spectroscopy. Thus elemental analysis and IR data are not available.

6.1a (fast eluting isomer)

^{1}H NMR (CD_2Cl_2) δ: 7.1-8.4 (m, 30H, μ-PPh_2), 4.3, 3.4, 2(s, 6H, 2MeO_2CCCCO_2Me), 2.2 [s, 2H, $(CNC(CH_3)_2CH_2(CH_3)_3)_{equat}$], 2.1 [s, 6H, $(CNC(CH_3)_2CH_2(CH_3)_3)_{equat}$], 1.3 [s, 9H, $(CNC(CH_3)_2CH_2(CH_3)_3)_{equat}$], 0.9 [s, 4H, $2(CNC(CH_3)_2CH_2(CH_3)_3)_{axial}$], 0.7 [s, 18H, $2(CNC(CH_3)_2CH_2(CH_3)_3)_{axial}$] 0.5 [s, 12H, $2(CNC(CH_3)_2CH_2(CH_3)_3)_{axial}$]. ^{31}P NMR ($CD_2Cl_2$) A_2X δ: -36.5 (d, P_a), +8.1 (t, P_x), $^2J\{P_aP_x\}$ = 195 Hz.

6.1b (slow eluting isomer)

^{1}H NMR (CD_2Cl_2) δ: 6.9-8.5 (m, 30H, μ-PPh_2), 4.1, 3.5, 2(s, 6H, 2MeO_2CCCCO_2Me), 2.2 [s, 2H, $(CNC(CH_3)_2CH_2(CH_3)_3)_{equat}$], 2.1 [s, 6H,

($CNC(C\underline{H}_3)_2CH_2(CH_3)_3)_{equat}$], 1.6 [s, 2H, ($CNC(CH_3)_2C\underline{H}_2(CH_3)_3)_{axial}$], 1.3 [s, 9H, ($CNC(CH_3)_2CH_2(C\underline{H}_3)_3)_{equat}$], 1.1 [s, 6H, ($CNC(C\underline{H}_3)_2CH_2(CH_3)_3)_{axial}$], 0.9 [s, 9H, ($CNC(CH_3)_2CH_2(C\underline{H}_3)_3)_{axial}$],0.6 [s, 9H, ($CNC(CH_3)_2CH_2(C\underline{H}_3)_3)_{axial}$] 0.4 [s, 2H, ($CNC(CH_3)_2C\underline{H}_2(CH_3)_3)_{axial}$], 0.2 [s, 6H, ($CNC(C\underline{H}_3)_2CH_2(CH_3)_3)_{axial}$]. ^{31}P NMR (CD_2Cl_2) A_2X δ: -27.5 (d, P_a), -13.7 (t, P_x), $^2J\{P_aP_x\}$ = 195 Hz.

References

1. Crystallographic characterization of $[Pd_{59}(CO)_{32}(PMe_3)_{21}]$, Tran, N. T., Diss. Abst. Sec. B, 60, **1999**, 182, [DA, 9904206].

2. Chi, Y.; Hwang, D-K., *Comprehensive Organometallic Chemistry II*, Pergamon Press., **1995**, *10*, 85-185.

3. Cotton, F. A.; Wilkinson, G.; Murillo, C. A.; Bochmann, M., *Advanced Inorganic Chemistry*, Wiley, New York **1999**, 652-674.

4. Whittlesey, B. A., *Coord. Chem. Rev.*, **2000**, *206-207*, 395-418.

5. Williams, A. F.; Floriani, C.; Merbach, A. E., *Perspectives in Coordination Chemistry*, Verlag Helvetia Chimica Acta, **1992**, 67-108.

6. Gubin, S. P., *Russ. Chem. Rev.*, **1985**, *54*, 305.

7. Muller, A.; Jostes, R.; Cotton, F. A., *Angew. Chem. Int. Ed. Engl.*, **1980**, *19*, 875.

8. Richmond, M. G., *Coord. Chem. Rev.*, **2001**, *214*, 1-42.

9. Johnson, B. F. G.; Lewis, J.; Kilty, P. A., *J. Chem. Soc. A*, **1968**, 2859.

10. Cook, N.; Smart, L.; Woodward, P., *J. Chem. Soc. Dalton Trans.*, **1977**, 1744.

11. Alonso, E.; Fornies, J.; Fortuno, C.; Martin, A.; Orpen, A. G., *Organometallics*, **2001**, *20*, 850.

12. Lawson, K. E., *Spectrochim. Acta*, **1961**, *17*, 248.

13. Cotton, F. A.; Wilkinson, G., *Advanced Inorganic Chemistry*, Wiley, New York **1988**, 1094-1095.

14. Goates, G. W., *Chem. Rev.*, **2000**, *100*, 1223-1252.

15. Holt, E. M.; Whitmire, K. H; Shriver, D. H., *J. Organometal. Chem.*, **1981**, *213*, 125.

16. Overett, M. J.; Hill, R. O.; Moss, J. R., *Coord. Chem. Rev.*, **2000**, *206-207*, 581-605.

17. Arif, A. M.; Bright, T. A.; Jones, R. A.; Nunn, C. M., *J. Am. Chem. Soc.* **1988**, *110*, 6894.

18. Safarowic, F. J.; Bierdeman, D. J.; Keister, J. B., *J. Am. Chem. Soc.* **1996**, *118*, 11805.

19. Braunstein, P.; Rose, J., *Comprehensive Organometallic Chemistry II*, Pergamon Press., **1995**, *10*, 351-385.

20. Adams, A. D.; Cotton, F. A., *Catalysis by Di- and Polynuclear Metal Cluster Complexes*, Wiley-VHC, New York, **1998**.

21. Hoffmann, R., *Angew. Chem. Int. Ed. Engl.* **1982**, *21*, 711.

22. Alonso, J. A., *Chem. Rev.*, **2000**, *100*, 637-677.

23. Abbet, S.; Sanchez, A.; Heiz, U.; Schneider, W.-D., *J. Catalysis*, **2001**, *198*, 122-127.

24. Johnson, B. F. G.; Lewis, J., *J. Organometal. Chem.*,**1974**, *67*, C75.

25. Jones, R. A.; Wright, T. C.; Atwood, J. L.; Hunter, W. E., Organometallics, **1983**, *3*, 114.

26. Elschembroich, C.; Salzer, A., *Organometallchemie*, Teubner Studienbücher, Stuttgard, **1993**, 267-286.

27. Comstock, M. C.; Willson, S. R.; Shapley, J. R., *Organometallics*, **1994**, *13*, 3805.

28. Berry, D. E.; Browning, J.; Dehghan, K.; Dixon, K. R.; Meanwell, N. J.; Phillips, A. G., *Inorg. Chem.*, **1991**, *30*, 396.

29. Garrou, P. E., *Chem. Rev.*, **1981**, *81*, 229.

30. Dehghan, K., Ph. D. Dissertation, University of Victoria, **1990**.

31. Dixon, K. R.; Rattray, A. D., *Inorg. Chem.*,**1978**, *17*, 1099.

32. Billig, E.; Jamerson, J. D.; Pruett, R. L.; *J. Organometal. Chem.*, **1980**, *192*, C51.

33. Several authors cite the Ph.D. dissertation from Huntsmann, J. R., University of Wisconsin, Madison, WI, **1973**, when referring to structural data for $[Co_3(\mu\text{-}PPh_2)_3(CO)_6]$, which have not yet been published in the literature.

34. Albright, T. A.; Kang, S.-K.; Arif, A. M.; Bard, A. J.; Jones, R. A.,*Inorg. Chem.*, **1988**, *27*, 1246.

35. Jones, R. A.; Stuart, A. L.; Atwood, J. L.; Hunter, W. E., *Organometallics*, **1983**, *2*, 1437.

36. Keller, E.; Vahrenkamp, H., *J. Organometal. Chem.*, **1978**, *155*, C44.

37. Haines, R. J.; Steen, N. D. C. T.; English, R. B., *J. Organometal. Chem.*, **1981**, *209*, C34.

38. Atwood, L. J.; Hunter, W. E.; Jones, R. A., *Inorg. Chem.*,**1983**, *22*, 993.

39. Arif, A. M; Heaton, D. E.; Jones, R. A.; Kidd, K. B.; Wright, T. C.; Whittlesey, B. R.; Atwood, J. L.; Hunter, W. E.; Zhang, H., *Inorg. Chem.*, **1987**, *26*, 4065.

40. Mason, R.; Sotofte, I.; Robinson, S. D.; Uttley, M. F., *J. Organometal. Chem.*, **1972**, *46*, C61.

41. Bellon, R. L.; Benedicenti, C.; Caglio, G.; Manassero, M., *J. Chem, Soc. Chem. Commun.*, **1975**, 946.

42. Harley, D.; Guskey, G. J.; Geoffroy, G. L., *Organometallics*, **1983**, *2*, 53.

43. Haines, R. J.; Steen, N. D. C. T.; English, R. B., *J. Chem. Soc., Dalton Trans.*, **1984**, 515.

44. Asseid, F. M., Ph. D. Dissertation, University of Victoria, **1995**.

45. Haines, R. J.; Steen, N. D. C. T.; English, R. B., *J. Chem. Soc., Dalton Trans.*, *1983*, 2229.

46. Tejel, C.; Ciriano, M. A.; Edwards, A. G.; Lahoz, F. J.; Oro, L. A., *Organometallics*, **2000**, *19*, 4968.

47. Browning, J.; Dixon, K. R.; Meanwell, N. J., *Inorg. Chim. Acta*, **1993**, *213*, 171.

48. Asseid, F. M.; Browning, J.; Dixon, K. R.; Meanwell, N. J., *Organometallics*, **1994**, *13*, 760.

49. Jones, R. A.; Wright, T. C., *Inorg.Chem.*, **1986**, *25*, 4058.

50. Moskovist, M., *Metal Clusters*, Wiley, New York, **1986**.

51. Wade, K., *J. Chem. Soc., Chem Commun.* **1971**, 792.

52. Mingos, D. M. P., *Adv. Organomet. Chem*, **1977**, 15, 1.

53. Chatt, J.; Chini, P., *J. Chem. Soc. A*, **1970**, 1538.

54. Yoshida, T.; Otsuka, S., *J. Am. Chem. Soc.*, **1977**, *99*, 2134.

55. Burrows, A. D.; Mingos, D. M. P., *Coord. Chem. Rev.*, **1996**, *154*, 19.

56. Moseley, K.; Maitlis, P. M., *J. Chem. Soc. Dalton Trans.*, **1974**, 169.

57. Nakamoto, K., *Infrared and Raman Spectra of Inorganic and Coordination Compounds*, Wiley, New York, **1978**, 291.

58. Comstock, M. C.; Shapley, J. R., Organometallics, **1997**, *16*, 4816.

59. Burke, M.; Takats, J., *J. Organomet. Chem.*, **1986**, *302*, C25.

60. Reppe, W., *Liebigs Ann. Chem.*, **1948**, *560*, 1-96.

61. Reppe, W.; v. Kutepow, N., *Angew. Chem. Int. Ed. Engl.*, **1969**, *8*, 727.

62. Wilke, G., *Pure Appl. Chem.*, **1978**, *50*, 677.

63. Heimbach, P.; Jolly, P. W.; Wilke, G., Adv. *Organomet. Chem.*, **1970**, *8*, 29.

64. Wengrovius, J. H.; Sancho. J.; Schrock, R. R., *J. Am. Chem. Soc.*, **1981**, *103*, 3932.

65. Bönnemann, H., *Angew. Chem. Int. Ed. Engl.*, **1978**, 505.

66. Collman, J. P.; Kang, J. W.; Little, W. F.; Sullivan, M. F., *Inorg.Chem.*, **1968**, *7*, 1298.

67. Mori, N.; Ikeda, S.; Odashima, K., *Chem. Commun.*, **2001**, 181.

68. Burt, R.; Cooke, M.; Green, M., *J. Chem. Soc. A*, **1970**, 2981.

69. Mao, T.; Zhang, Z.; Washington, J.; Takats, J.; Jordan, R. B., *Organometallics*, **1999**, *18*, 2331.

70. Jewell, C. F.; Liebeskind, L. S.; Williamson, M., *J. Am. Chem. Soc.*, **1985**, *107*, 6715.

71. Kang, J. W.; McVey, S.; Maitlis, P. M., *Can. J. Chem*, **1968**, *46*, 3189.

72. Herrera, A.; Hoberg, H.; Mynott, R., *J. Organomet. Chem.*, **1981**, 222, 331.

73. Baba, A.; Ohshiro, Y.; Agawa, T., *J. Organomet. Chem.*, **1976**, *110*, 121.

74. Geoffroy, G. L.; Bassner, S. L., *Adv. Organomet. Chem.*, **1988**, *28*, 1.

75. Watkins, Baddley, *J. Chem. Soc. Chem. Commun.*, **1972**, 672.

76. Visser J. P. ; Ramakers-Blom J. E., *J. Organometal. Chem.*, **1972**, *44*, C63.

77. Corrigan, P. A.; Dickson, R. S., *Aust. J. Chem.*, **1979**, *32*, 2147.

78. Padolik, L. L.; Gallucci, J. C.; Wojcicki, A., *J. Am. Chem. Soc.*, **1993**, *115*, 9986.

79. Lindner, E., *Adv. Heterocycl. Chem.*, **1986**, *39*, 237.

80. Campora, J.; Palma, P; Carmona, E., *Coord. Chem. Rev.*, **1999**, *193-195*, 207.

81. Jennings, P. W.; Johnson, L. L., *Chem. Rev.*, **1994**, *94*, 2241.

82. Johnson, K. A.; Gladfelter, W. L., *J. Am. Chem. Soc.*, **1991**, 113, 5097.

83. Johnson, K. A.; Gladfelter, W. L., Organometallics, **1992**, *11*, 2534.

84. Burgess, J.; Kemmitt, R. D. W.; Morton, N.; Mortimer, C. T.; Wilkinson, M. P, *J. Organometal. Chem.*, **1980**, *191*, 477.

85. Huffman, M. A.; Liebeskind, L. S.; Pennington, W. T., *Organometallics*, **1992**, *11*, 255.

86. Casey, C. P.; Carino, R. S; Hayashi, K.; Schladetzky, *J. Am. Chem. Soc.*, **1996**, *118*, 1617.

87. Bellon, P. L.; Benedicenti, C.; Caglio, G.; Manassero, M., *J. Chem. Soc., Chem. Comm.* **1973**, 946.

88. Harley, A. D.; Whittle, R. R.; Geoffroy, G. L., *Organometallics*, **1983**, *2*, 60.

89. Eisenberg, R.; Gaughan, A. P.; Pierpont, Jr.C. G.; Reed, J.; Schultz, A. J., *J. Am. Chem. Soc.*, **1972**, *94*, 6240.

90. Meek, D. W.; Kreter, P. E.; Christoph, G. G., *J. Organomet. Chem.*, **1982**, *231*, C53.

91. Jones, R. A.; Wright, T. C.; Atwood, J. L.; Hunter, W. E., *Organometallis*, **1983**, *2*, 470.

92. Broach, R. W.; Williams, J. M., Inorg. Chem., 1979, 18, 314.

93. Koike, M.; Hamilton, D. H.; Wilson, S. R.; Shapley, J. R., *Organometallics*, **1996**, *15*, 4930.

94. Mirza, H. A.; Vittal, J. J.; Puddephatt, R. J., *Organometallics*, **1994**, *13*, 3063.

95. Finnimore, S. R.; Knox, S. A. R.; Taylor, G. E., *J. Chem. Soc. Dalton Trans.*, **1982**, 1783.

96. Boag, N. M.; Goodfellow, R. J.; Green, M.; Hessner, B.; Howard, J. A. K., *J. Chem. Soc. Dalton Trans.*, **1983**, 2585.

97. Dickson, R. S.; Evans, G. S.; Fallon, G. D., *J. Organomet. Chem.*, **1982**, *236*, C49.

98. Chetcuti, M. J.; Green, K. A., *Organometallics*, **1988**, *7*, 2450.

99. Belt, S. T.; Ryba, D. W.; Ford, P. C., *Inorg. Chem.*, **1990**, *29*, 3634.

100. Noack, K.; Calderazzo, F., J. Organometal. Chem., **1967**, *10*, 101.

101. Dixon, K. R.; Berry, D. E.; Bushnell, G. W.; Moroney, P. M.; Wan, C., *Inorg. Chem.*, **1985**, *24*, 2625.

102. Adams, H.; Bailey, N. A.; Gill, L. J.; Morris, M. J.; Sadler, N. D., *J. Chem. Soc., Dalton Trans.*, **1997**, 3041.

103. Fumagalli, A.; Bianchi, A.; Malatesta, M. C.; Ciani, G.; Moret, M.; Sironi, A., *Inorg.Chem.*, **1998**, *37*, 1324.

104. Giordano, G.; Crabtree, R. H., *Inorg. Synth.*, **1979**, *19*, 218.

105. Cramer, R., *Inorg. Synt.*, **1974**, *15*, 14.

106. Van der Ent, A.; Onderdelinden, A. L., *Inorg. Synt.*, **1973**, *14*, 92.

107. Ziegler, T., "Beating the Heavy Metal Blues with DFT." Departmental Seminar, University of Victoria, **2001**.

108. Ruiz-Morales, Y.; Ziegler, T., *J. Phys. Chem. A*, **1998**, *102*, 3970.

109. Isotopic labeling of the DMAD ligand of **3.3** and subsequent addition of non-labeled alkyne and CO would allow to establish which of the DMAD ligands is involved in the formation of the iridacyclobutenone (by NMR).

Appendix

The main goal of this thesis was to synthesize new diphenylphosphido-bridged iridium alkyne clusters and explore the chemistry of these compounds including the bimetallic $[Ir_2Rh(\mu\text{-}PPh_2)_3(CO)_4(^tBuNC)_3]$ (**5.3**). The instability of this important precursor led to an extensive search for more robust isocyanide clusters of type $[Ir_2Rh(\mu\text{-}PPh_2)_3(CO)_4(RNC)_3]$. Since such bimetallic isocyanide clusters are expected to have similar physical properties (eg. solubility, crystallinity) in comparison to their homometallic triiridium analogs, the search was preceded by synthesizing a series of more readily accessible isocyanide clusters of the type $[Ir_3(\mu\text{-}PPh_2)_3(CO)_{5-n}(RNC)_{2+n}]$ (n=0: R=isopr, **6.2**, R=cy, **6.4**; n=1: R=tmBuNC, **6.1**; R=isopr, **6.3**; R=cy, **6.5**; R=xy, **6.6**) via addition of appropriate amounts of isocyanide to solutions of $[Ir_3(\mu\text{-}PPh_2)_3(CO)_6]$ (**2.1**)

$$[Ir_3(\mu\text{-}PPh_2)_3(CO)_6] + 2RNC \rightarrow [Ir_3(\mu\text{-}PPh_2)_3(CO)_5(RNC)_2] + CO \quad (1)$$

$$[Ir_3(\mu\text{-}PPh_2)_3(CO)_6] + xs\ RNC \rightarrow [Ir_3(\mu\text{-}PPh_2)_3(CO)_4(RNC)_3] + 2CO \quad (1)$$

(Equations 1 and 2). This synthetic pathway led to clean isocyanide clusters and represents an improvement over the strategy previously developed by our group for the synthesis of $[Ir_3(\mu\text{-}PPh_2)_3(CO)_4(^tBuCN)_3]$ (**1.6**) which involved the action of CO and isocyanide on $[Ir_3(\mu\text{-}PPh_2)_3(CO)_3(PPh_3)_2]$ (**1.3**). Because the only by-product in the reactions shown in Equations 1-2 is CO, the isolation of isocyanide

clusters that do not readily crystallize from the reaction mixture became possible. Clusters **6.1**- **6.6** are closely related to $[Ir_3(\mu\text{-}PPh_2)_3(CO)_{5-n}(^tBuNC)_{2+n}]$ (n=0, **1.5**; n=1, **1.6**), prepared previously by our group [28, 44] and exhibit similar spectral properties. ^{31}P NMR parameters for the new isocyanide clusters are summarized in Table A1

cluster	**6.1**	**6.3**	**6.5**	**6.6**[a]	**1.6**[b]
P_a	+3.8	+0.9	+2.0	-7.9	-1.6
P_x	+41.1	+36.6	+37.5	+42.4	+36.4
$^2J\{P_aP_x\}$ [Hz]	144	145	145	152	141

cluster	**6.2**[a]	**6.4**[a]	**1.5**[b]
P_a	-12.8	-12.1	-8.2
P_x	+38.3	+38.4	+38.0
$^2J\{P_aP_x\}$ [Hz]	150	150	144

Table A1 *^{31}P NMR parameters (CD_2Cl_2) for tris-isocyanide adducts **6.1**, **6.3**, **6.5**, **6.6** and **1.6** (top) and bis-isocyanide adducts **6.2**, **6.4** and **1.5** (bottom). a) C_6D_6, b) from reference [44].*

Of the new isocyanide clusters $[Ir_3(\mu\text{-}PPh_2)_3(CO)_4(1,1,3,3\text{-}tmBuNC)_3]$ (**6.1**) proved most stable both in solution and in the solid state and readily crystallized from

dichloromethane or benzene solutions to give well formed yellow prisms (in contrast with **6.2**-**6.6** which could only be obtained as microcrystalline solids or powders). A structural analysis on **6.1** confirmed the coordination of three bulky isooctyl groups to the unique iridium centre. The crystal structure was solved by Dr. Bob McDonald and is shown in an ORTEP diagram in Figure A1 while crystallographic experimental details and selected internuclear distances are given in Tables A2 and A3 respectively. The molecular structure of **6.1** is extremely similar to that of the bimetallic $[Ir_2Rh(\mu\text{-}PPh_2)_3(CO)_4(1,1,3,3\text{-}tmBuNC)_3]$ (**5.5**) discussed in detail in Chapter 5. The iridium triangle exhibits large non-bonding metal-metal distances and the phosphido bridges rest closely within the Ir_3 plane. Thus the core of cluster **6.1** represents a nearly planar six membered Ir_3P_3-ring with the greatest deviation from planarity encountered for P(3) which rests 0.1391(17) Å out of the plane of the iridium atoms.

Oxidative addition reactions of the new isocyanide clusters 6.1, 6.3, and 6.5 with iodomethane

To prove that the lack of reactivity involving oxidative addition of iodomethane to the bimetallic $[Ir_2Rh(\mu\text{-}PPh_2)_3(CO)_4(tmBuNC)_3]$ (**5.5**) cannot be accounted for by the steric bulk of the isooctyl groups, analogous reactions were carried out on the isostructural $[Ir_3(\mu\text{-}PPh_2)_3(CO)_4(tmBuNC)_3]$ (**6.1**). Dichloromethane solutions of **6.1**, **6.3** and **6.5** react readily with excess iodomethane to form the expected addition products as shown in Equation 3. The new clusters were characterized

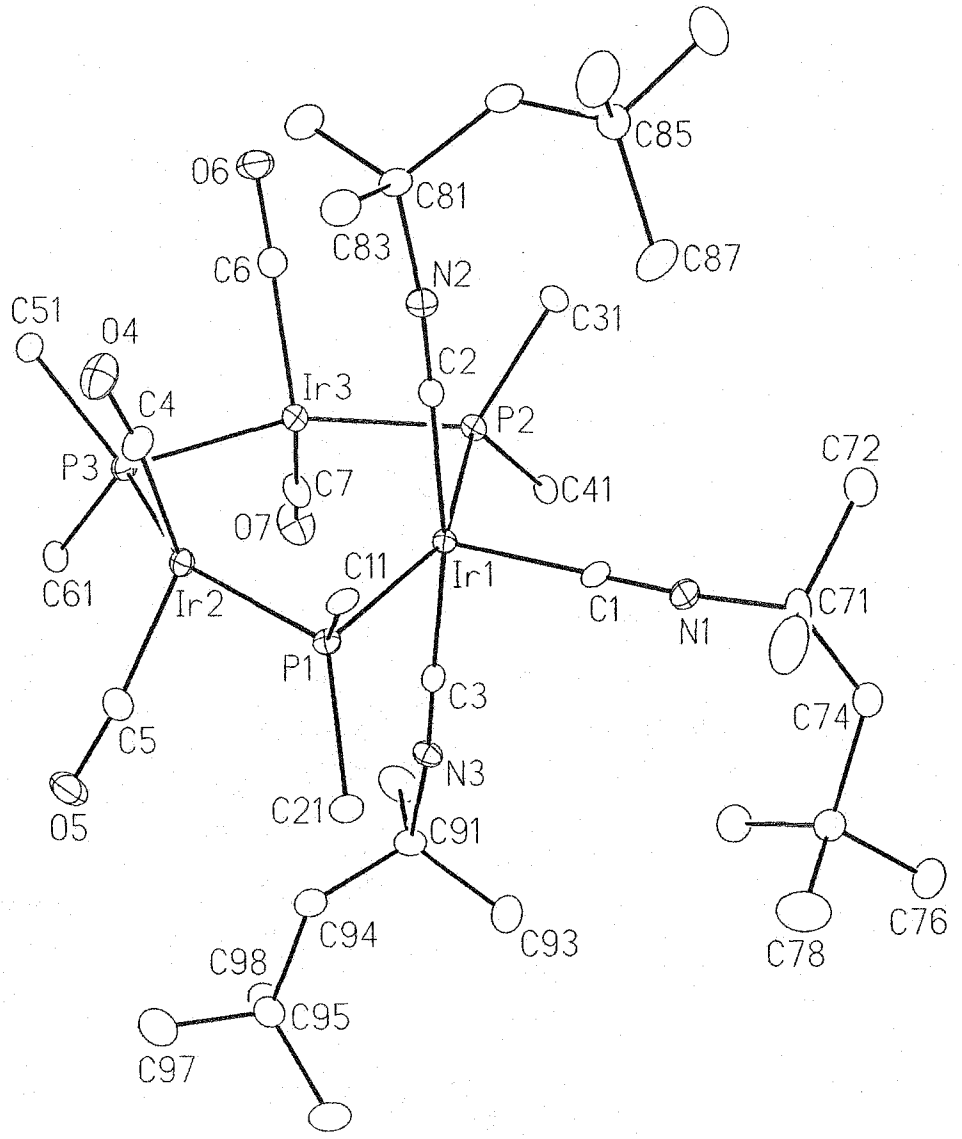

Figure A1 *ORTEP diagram showing the molecular structure of* $[Ir_3(\mu\text{-}PPh_2)_3(CO)_4(1,1,3,3\text{-}tmBuNC)_3]$ (***6.1***)

For clarity only the ipso carbons of the phenyl rings are shown.

A. Crystal Data

formula	$C_{67}H_{81}Ir_3N_3O_4P_3$
formula weight	1661.86
crystal dimensions (mm)	0.36 × 0.16 × 0.12
crystal system	monoclinic
space group	$P2_1$ (No. 4)
unit cell parameters	
a (Å)	12.6852 (5)
b (Å)	22.6542 (10)
c (Å)	12.8399 (5)
β (deg)	117.7709 (11)
V (Å^3)	3264.8 (2)
Z	2
ρ_{calcd} (g cm^{-3})	1.690
μ (mm^{-1})	6.220

B. Data Collection and Refinement Conditions

diffractometer	Bruker P4/RA/SMART 1000 CCD
radiation (λ [Å])	graphite-monochromated Mo Kα (0.71073)
temperature (°C)	−80
total data collected	16219 ($-15 \le h \le 8$, $-28 \le k \le 27$, $-17 \le l \le 16$)
independent reflections	13110
number of observed reflections (*NO*)	12231 [$F_o^2 \ge 2\sigma(F_o^2)$]
R_1 [$F_o^2 \ge 2\sigma(F_o^2)$]	0.0259
wR_2 [$F_o^2 \ge -3\sigma(F_o^2)$]	0.0557

Table A2 *Crystallographic experimental details for*

*$[Ir_3(\mu\text{-}PPh_2)_3(CO)_4(1,1,3,3\text{-}tmBuNC)_3]$ (**6.1**)*

Atoms	Distance	Atoms	Distance
Ir(1)-Ir(2)	3.2147(3)	Ir(1)-C(3)	1.981(6)
Ir(1)-Ir(3)	3.2046(3)	Ir(2)-C(4)	1.881(7)
Ir(2)-Ir(3)	3.3122(3)	Ir(2)-C(5)	1.846(6)
Ir(1)-P(1)	2.3469(13)	Ir(3)-C(6)	1.872(6)
Ir(1)-P(2)	2.3522(12)	Ir(3)-C(7)	1.848(7)
Ir(2)-P(1)	2.2864(13)	N(1)-C(1)	1.147(7)
Ir(2)-P(3)	2.3216(13)	N(2)-C(2)	1.142(8)
Ir(3)-P(2)	2.2934(15)	N(3)-C(3)	1.150(7)
Ir(3)-P(3)	2.3210(14)	O(4)-C(4)	1.146(8)
Ir(1)-C(1)	1.965(5)	O(5)-C(5)	1.169(7)
Ir(1)-C(2)	1.976(6)	O(7)-C(7)	1.173(8)

Atoms	Angles	Atoms	Angles
Ir(2)-Ir(1)-Ir(3)	62.125(6)	P(1)-Ir(1)-C(1)	103.47(15)
Ir(1)-Ir(2)-Ir(3)	58.788(6)	P(1)-Ir(1)-C(2)	88.79(15)
Ir(1)-Ir(3)-Ir(2)	59.087(6)	P(1)-Ir(1)-C(3)	88.75(15)
Ir(1)-P(1)-Ir(2)	87.86(4)	C(2)-Ir(1)-C(3)	170.7(2)
Ir(1)-P(2)-Ir(3)	87.22(5)	C(1)-Ir(1)-C(2)	93.1(2)
Ir(2)-P(3)-Ir(3)	91.03(5)	C(1)-Ir(1)-C(3)	96.2(2)
P(1)-Ir(1)-P(2)	153.02(5)	C(1)-N(1)-C(71)	171.9(6)
P(1)-Ir(2)-P(3)	149.67(5)	C(2)-N(2)-C(81)	172.8(6)
P(2)-Ir(3)-P(3)	150.57(4)	Ir(1)-C(1)-N(1)	179.0(6)

Table A3 *Selected bond distances (Å) and angles (°) for* $[Ir_3(\mu\text{-}PPh_2)_3(CO)_4(1,1,3,3\text{-}tmBuNC)_3]$ ***(6.1)***

Estimated standard deviations are given in parentheses.

by their infrared, NMR and FAB MS spectra, analytical data and a structural analysis (**7.2** only). Spectral and structural parameters for the new adducts are

$$[Ir_3(\mu\text{-}PPh_2)_3(CO)_4(RNC)_3] + CH_3I \rightarrow [Ir_3(\mu\text{-}PPh_2)_3(CO)_4(RNC)_3(CH_3)][I] \quad (3)$$

(R=tmBu, **7.1**; R=isopr, **7.2**; R=cy, **7.3**)

cluster	P_a	P_b	P_x	$^2J\{P_aP_b\}$	$^2J\{P_aP_x\}$	$^2J\{P_bP_x\}$
1.7[a]	-6.4	-8.4	-57.1	157 Hz	139 Hz	130 Hz
7.1	-4.6	-5.8	-54.5	159 Hz	138 Hz	132 Hz
7.2	-5.5	-9.9	-56.2	158 Hz	141 Hz	128 Hz
7.3	-5.4	-9.9	-55.3	158 Hz	142 Hz	127 Hz

Table A4 *Comparison of ^{31}P NMR parameters (CD_2Cl_2) for the new clusters **7.1**- **7.3** with those of **1.7**. a) data from reference 44.*

extremely similar to those of the closely related $[Ir_3(\mu\text{-}PPh_2)_3(CO)_4(^tBuNC)_3(CH_3)][I]$ (**1.7**) discussed in great detail elsewhere [44]. Especially remarkable is the similarity of ^{31}P NMR spectra for the new clusters which are of the ABX-type. Relevant ^{31}P NMR parameters are summerized in Table A4. Because of the cationic nature of the new iodomethane adducts, FAB MS spectroscopy (positive mode) proved especially diagnostic. Molecular ions

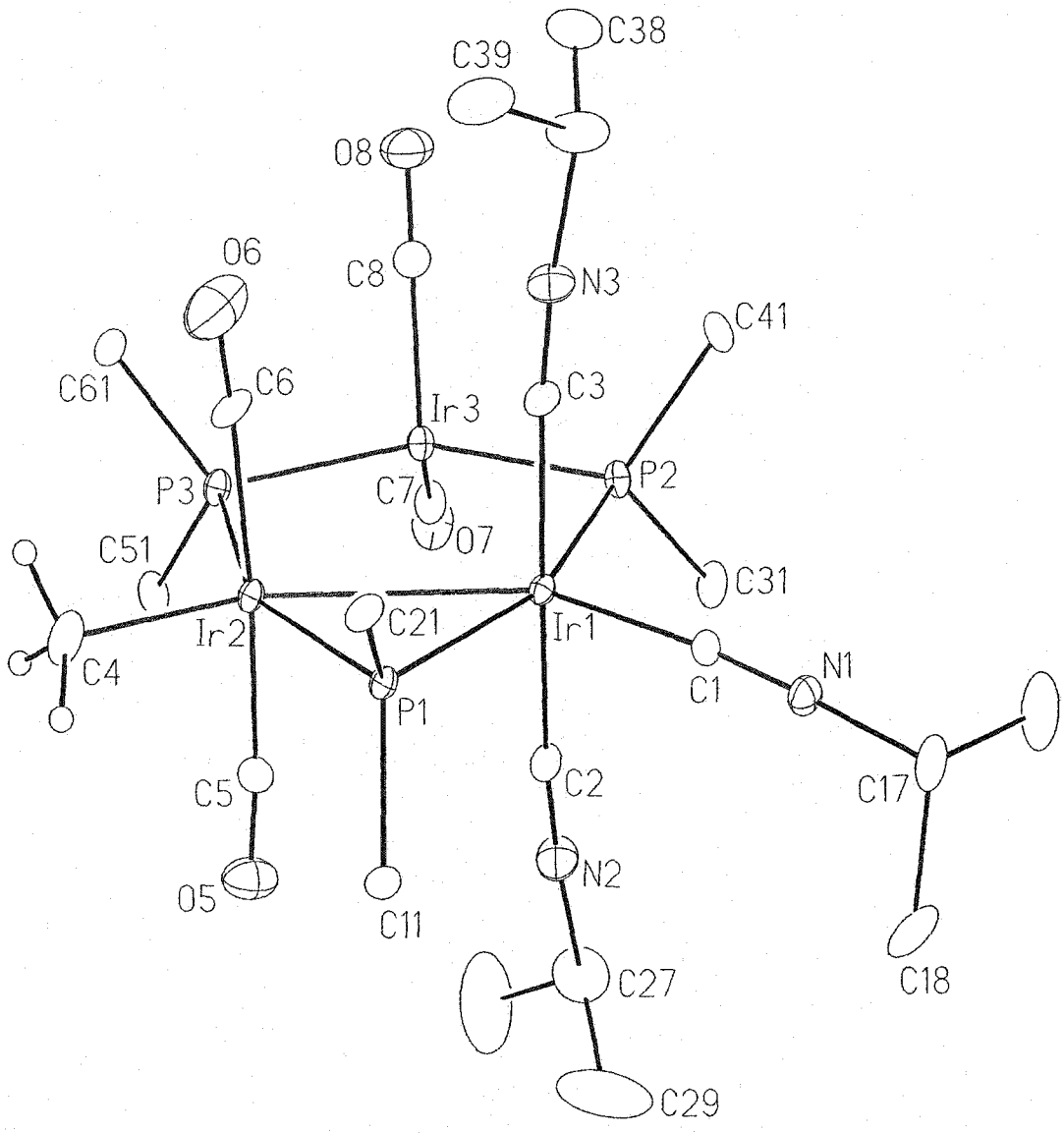

Figure A2 *Molecular structure of* $[Ir_3(\mu\text{-}PPh_2)_3(CO)_4(isoprNC)_3(CH_3)][I]$ (**7.2**) *representing 95 % of the cations in the latice.*

Only the ipso-carbons of the phenyl rings are shown for clarity.

A. Crystal Data

formula	$C_{53.45}H_{54.85}ClI_{1.05}Ir_3N_3O_4P_3$
formula weight	1641.46
crystal dimensions (mm)	0.42 × 0.31 × 0.08
crystal system	monoclinic
space group	$P2_1/n$ (an alternate setting of $P2_1/c$ [No. 14])
unit cell parameters[a]	
a (Å)	13.0405 (7)
b (Å)	34.7771 (18)
c (Å)	13.7802 (7)
β (deg)	112.5069 (10)
V (Å^3)	5773.5 (5)
Z	4
ρ_{calcd} (g cm^{-3})	1.888
μ (mm^{-1})	7.632

B. Data Collection and Refinement Conditions

diffractometer	Bruker PLATFORM/SMART 1000 CCD
radiation (λ [Å])	graphite-monochromated Mo Kα (0.71073)
temperature (°C)	−80
scan type	ω scans (0.2°) (20 s exposures)
data collection	2θ limit (deg) 52.80
total data collected	37170 ($-12 \le h \le 16$, $-43 \le k \le 43$, $-17 \le l \le 17$)
independent reflections	11772
number of observed reflections (NO)	10355 [$F_o^2 \ge 2\sigma(F_o^2)$]
R_1 [$F_o^2 \ge 2\sigma(F_o^2)$]	0.0381
wR_2 [$F_o^2 \ge -3\sigma(F_o^2)$]	0.0994

Table A5 *Crystallographic experimental details for*

*$[Ir_3(\mu\text{-}PPh_2)_3(CO)_4(isoprNC)_3(CH_3)][I]$ (**7.2**)*

Atoms	Distance	Atoms	Distance
Ir(1)-Ir(2)	3.0600(4)	Ir(1)-C(3)	1.980(7)
Ir(1)-Ir(3)	3.2184(4)	Ir(2)-C(4)	1.996(10)
Ir(2)-Ir(3)	3.2844(4)	Ir(2)-C(5)	1.932(8)
Ir(1)-P(1)	2.3550(17)	Ir(2)-C(6)	1.978(8)
Ir(1)-P(2)	2.3659(18)	Ir(3)-C(7)	1.879(8)
Ir(2)-P(1)	2.3288(16)	Ir(3)-C(8)	1.920(9)
Ir(2)-P(3)	2.3694(18)	N(1)-C(1)	1.146(9)
Ir(3)-P(2)	2.2980(18)	N(2)-C(2)	1.137(10)
Ir(3)-P(3)	2.3066(19)	N(3)-C(3)	1.144(9)
Ir(1)-C(1)	1.951(7)	O(5)-C(5)	1.107(10)
Ir(1)-C(2)	1.971(7)	O(6)-C(6)	1.051(11)

Atoms	Angles	Atoms	Angles
Ir(2)-Ir(1)-Ir(3)	63.025(8)	P(1)-Ir(1)-C(1)	102.1(2)
Ir(1)-Ir(2)-Ir(3)	60.844(8)	P(1)-Ir(1)-C(2)	91.7(2)
Ir(1)-Ir(3)-Ir(2)	56.131(8)	P(1)-Ir(1)-C(3)	91.8(2)
Ir(1)-P(1)-Ir(2)	82.01(5)	C(2)-Ir(1)-C(3)	176.0(3)
Ir(1)-P(2)-Ir(3)	87.26(6)	C(5)-Ir(2)-C(6)	174.6(4)
Ir(2)-P(3)-Ir(3)	89.23(6)	C(4)-Ir(2)-C(5)	87.8(4)
P(1)-Ir(1)-P(2)	157.33(6)	C(4)-Ir(2)-C(6)	87.1(4)
P(1)-Ir(2)-P(3)	154.42(6)	P(1)-Ir(2)-C(4)	105.4(3)
P(2)-Ir(3)-P(3)	148.90(6)	P(1)-Ir(2)-C(5)	89.6(2)

Table A6 *Selected bond distances (Å) and angles (°) for* $[Ir_3(\mu\text{-}PPh_2)_3(CO)_4(isoprNC)_3(CH_3)][I]$ (**7.2**)

Estimated standard deviations are given in parentheses.

were detected for clusters **7.1**-**7.3**. In addition to spectral data a crystallographic analyses was preformed on $[Ir_3(\mu\text{-}PPh_2)_3(CO)_4(isoprNC)_3(CH_3)][I]$ (**7.2**) by Dr. Bob McDonald. Figure A2 illustrates the molecular structure of **7.2** which crystallizes with half a molecule of dichloromethane per unit cell. Crystallographic experimental details are given in Table A5. while selected internuclear distances are listed in Table A6. The molecular structure of **7.2** is very similar to that reported for **1.7** [44, 48] differing in one important detail only; 95 % of the molecules in the lattice of **7.2** exhibit the expected arrangement of atoms. However, in the remaining 5 %, iodine coordinates to Ir(2) (see ORTEP for atomic numbering Scheme) instead of the expected methyl group.

Synthesis of new isocyanide clusters 6.1-6.6

$[Ir_3(\mu\text{-}PPh_2)_3(CO)_4(1,1,3,3\text{-}tmBuNC)_3]$ (6.1)

1,1,3,3- tetramethylbutylisocyanide (20 µL, 0.11 mmol) was added dropwise to a stirred solution of $[Ir_3(\mu\text{-}PPh_2)_3(CO)_6]$ (40 mg, 0.031 mmol) in 5 mL of dichloromethane which resulted in immediate formation of a bright yellow solution. After 2 hours all volatiles where removed *in vacuo* and the residual solid recrystallized from dichloromethane-hexane to afford the cluster as bright yellow crystalls (31 mg, 60 % yield). X-Ray quality crystals were obtained using slow

diffusion of hexane in a solution of 25 mg cluster in 0.5 mL dichloromethane using an NMR tube to give bright yellow prisms. Analysis calculated for $Ir_3P_3C_{67}H_{81}O_4N_3$: C, 48.42; H, 4.91; N, 2.53 %; Found: C, 47.88; H, 4.92; N, 2.39 %. IR (KBr) ν_{CN}, 2201 (w), 2174 (s), 2123(s), ν_{CO}, 1955 (s), 1937 (s), 1898 (s) cm^{-1}. FAB MS (m/z): 1638.3 (100%) [M-23] amu (not conclusive). ^{31}P NMR (CD_2Cl_2) A_2X, δ: +3.8 (d, P_a), +41.1 ppm (t, P_x), $^2J\{PP\}$ = 144 Hz. ^1H NMR (CD_2Cl_2) δ: 7.2-8.3 (m, 30 H, μ-P$\underline{Ph}_2$), 2.18 [s, 2H, $(CNC(CH_3)_2C\underline{H}_2(CH_3)_3)_{equat}$], 2.00 [s, 6H, $(CNC(C\underline{H}_3)_2CH_2(CH_3)_3)_{equat}$], 1.35 [s, 9H, $(CNC(CH_3)_2CH_2(C\underline{H}_3)_3)_{equat}$], 0.62 [s, 18H, $2(CNC(CH_3)_2CH_2(C\underline{H}_3)_3)_{axial}$] 0.61 [s,4H, $2(CNC(CH_3)_2C\underline{H}_2(CH_3)_3)_{axial}$], 0.41 [s, 12H, $2(CNC(C\underline{H}_3)_2CH_2(CH_3)_3)_{axial}$]. ^{13}C NMR (CD_2Cl_2) δ: 189.3 (m, 4 CO), 127-143 (m, μ-P$\underline{Ph}_2$), 111.3 (broad, Ir$\underline{C}$NR), 95.3 (broad, Ir$\underline{C}$NR), 62.5, 61.3, 55.2, 52.8, 32.2, 31.9, 31.7, 31.4, 31.1, 28.7, (s, IrCN$\underline{R}$).

$[Ir_3(\mu\text{-}PPh_2)_3(CO)_5(isoprNC)_2]$ (6.2)

Isopropylisocyanide (5.4 µL, 0.059 mmol) was added dropwise to a stirred solution of $[Ir_3(\mu\text{-}PPh_2)_3(CO)_6]$ (26 mg, 0.020 mmol) in 1 mL of benzene-d_6 which caused an immediate color change from dark red to yellow orange accompanied by the release of a gas. NMR spectroscopy *in situ* clearly indicated the formation of the diisocyanide cluster. It proved very difficult to isolate the addition product so elemental analysis, FAB MS and IR data are not available.

^{1}H NMR (C_6D_6) δ: 6.8-8.3 (m, 30 H, μ-P<u>Ph</u>$_2$), 2.63 (heptet, 1H, CNC<u>H</u>$(CH_3)_2$), 0.06 (d, 6H, CNCH$(C\underline{H}_3)_2$), J^3{HH} = 6.6 Hz. ^{31}P NMR (C_6D_6) A_2X, δ: +38.4 (t, P_x), -12.8 (d, P_a), ^2J{PP} = 150 Hz. ^{13}C NMR (C_6D_6) δ: 188.7 (m, 4 CO), 143.5 (broad, CO_{equat}), 127-142 (m, μ-P<u>Ph</u>$_2$), 107.3 (broad, Ir<u>C</u>Nisopr), 48.7 (s, CN<u>C</u>H$(CH_3)_2$), 21.1 (s, CNCH$(\underline{C}H_3)_2$).

$[Ir_3(\mu\text{-}PPh_2)_3(CO)_4(isoprNC)_3]$ (<u>6.3</u>)

A small excess of isopropylisocyanide (10 µL, 0.11 mmol) was added dropwise to a stirred solution of $[Ir_3(\mu\text{-}PPh_2)_3(CO)_6]$ (40 mg, 0.031 mmol) in 5 mL of dichloromethane which caused an immediate color change from dark red to bright yellow. Stirring was continued overnight and the solvent removed *in vacuo* to give the compound as a yellow powder in 90 % yield. Recrystallization from dichloromethane-hexane gave small crystals of high purity but in low yield (10.7 mg, 24% isolated yield). Analysis calculated for $Ir_3P_3C_{52}H_{51}O_4N_3$: C, 43.03; H, 3.54; N, 2.89 %; Found: C,42.71; H, 3.58; N, 2.74 %. IR (KBr) ν_{CN}, 2212 (w), 2183 (s), 2147(s), ν_{CO}, 1958 (s), 1939 (s), 1897 (s), 1885 (sh) cm^{-1}. FAB MS (m/z): 1424 (35 %) [M-CO], 1396 (80 %) [M-2CO], 1368 (63 %) [M-3CO], 1340 (100 %) [M-4CO], 1288, 1262, 1221, 820 amu. ^{31}P NMR (CD_2Cl_2) A_2X, δ: +0.9 (d, P_a), +36.6 ppm (t, P_x), ^2J{PP} = 145 Hz. ^{1}H NMR (CD_2Cl_2) δ: 7.2-8.2 (m, 30 H, μ-P<u>Ph</u>$_2$), 4.65 [heptet, 1H, CNC<u>H</u>$(CH_3)_2)_{equat}$], 2.95 [heptet, 2H, 2(CNC<u>H</u>$(CH_3)_2)_{axial}$], 1.78 [d, 6H, CNCH$(C\underline{H}_3)_2)_{equat}$], 0.33 [d, 12H, CNCH$(C\underline{H}_3)_2)_{axial}$], J^3{HH} = 7 Hz.

^{13}C NMR (C_6D_6, 62.9 MHz) δ: 189.1 (m, 4CO), 127-144 (m, μ-P<u>Ph</u>$_2$), 113.9 (broad, Ir<u>C</u>Nisopr), 97.8 (broad, Ir<u>C</u>Nisopr), 49.0 [s, CN<u>C</u>H(CH$_3$)$_{2equat}$], 48.2 [s, (CN<u>C</u>H(CH$_3$)$_2$)$_{axial}$], 23.4 [s, CNCH(<u>C</u>H$_3$)$_{2equat}$], 21.4 (s, CNCH(<u>C</u>H$_3$)$_{2axial}$].

[Ir$_3$(μ-PPh$_2$)$_3$(CO)$_5$(cyNC)$_2$] (<u>6.4</u>)

Cyclohexylisocyanide (4.6 µL, 0.037 mmol) was added dropwise to a stirred solution of [Ir$_3$(μ-PPh$_2$)$_3$(CO)$_6$] (24 mg, 0.018 mmol) in 1 mL of benzene-d_6 which caused an immediate color change from dark red to orange red. NMR spectroscopy *in situ* clearly indicated the formation of the diisocyanide cluster. Like the isopropylisocyanide case, it proved very difficult to isolate the addition product so elemental analysis, FAB MS and IR data are not available.

^{1}H NMR (C_6D_6) δ: 6.8-8.4 (m, 30 H, μ-P<u>Ph</u>$_2$), 0.3-2.6 (m, 22H, <u>cy</u>NC).

^{31}P NMR (C_6D_6) A_2X, δ: +38.4 (t, P_x), -12.1 (d, P_a), ^{2}J{PP} = 150 Hz.

^{13}C NMR (CD_2Cl_2, 62.9 MHz) δ: 188.3 (m, 4CO), 126-142 (m, μ-P<u>Ph</u>$_2$), 107.0 (broad, Ir<u>C</u>Ncy), 23-57 (IrCN<u>cy</u>).

[Ir$_3$(μ-PPh$_2$)$_3$(CO)$_4$(cyNC)$_3$] (<u>6.5</u>)

Excess cyclohexylisocyanide (18 µL, 0.145 mmol) was added dropwise to a stirred solution of [Ir$_3$(μ-PPh$_2$)$_3$(CO)$_6$] (35 mg, 0.027 mmol) in 5 mL of dichloromethane which caused an immediate color change from dark red to bright yellow. Stirring was continued overnight and the solvent removed *in vacuo*

to give the compound as a yellow powder. Washing twice with 0.5 mL benzene-hexane (ratio 1:3) and drying in vacuum yielded the cluster as a bright yellow solid (27 mg) in 65 % yield. Analysis calculated for $Ir_3P_3C_{61}H_{63}O_4N_3$:C, 46.61; H, 4.00; N, 2.60 %; Found: C,45.95; H, 4.40; N, 3.15 %. IR (KBr) ν_{CN}, 2181 (s), 2147(s), ν_{CO}, 1959 (s), 1939 (s), 1899 (s) cm^{-1}. FAB MS (m/z): 1544 (37 %) [M-CO], 1516 (66 %) [M-2CO], 1488 (52 %) [M-3CO], 1460 (75 %) [M-4CO], 1434 (46 %) [M-CO -CyNC], 1406 (35 %) [M-2CO -CyNC], 1380 (100%) [{M+H} - CyNC - CyH], 1378 (95%) [M-3CO -CyNC], 1301 (55%) amu. ^{31}P NMR (CD_2Cl_2) A_2X, δ: +2.0 (d, P_a), +37.5 ppm (t, P_x), $^2J\{PP\}$ = 145 Hz. ^1H NMR (CD_2Cl_2) δ: 7.2-8.1 (m, 30H, μ-P<u>Ph</u>$_2$), 0.4-4.6 (m, 36H, <u>cy</u>NC). ^{13}C NMR (CD_2Cl_2, 75 MHz) δ: 188.7 (m, 4CO), 127-142 (m, μ-P<u>Ph</u>$_2$), 113.0, 96.0 (broad, Ir<u>C</u>Ncy), 22-55 ppm (IrCN<u>cy</u>).

$[Ir_3(\mu\text{-}PPh_2)_3(CO)_4(XyNC)_3]$ (<u>6.6</u>)

A NMR tube containing crystalline $[Ir_3(\mu\text{-}PPh_2)_3(CO)_6]$ (6.0 mg, 0.005 mmol) was layered with a solution of 1,5-dimethylphenylisocyanide (1.9 mg, 0.015 mmol) in benzene-d_6 (1g) which caused the release of a gas from the crystal surface. The tube was shaken until all starting material had dissolved forming a bright yellow solution. The compound was precipitated using hexane, the supernatant carefully decanted and the remaining yellow powder was washed with hexane twice before dried in vacuum (5 mg, 66 % yield). IR (KBr) ν_{CN}, 2169 (w), 2138 (s),

2110(s), ν_{CO}, 1960 (s), 1942 (s), 1905 (s) cm^{-1}. FAB MS (m/z): 1610 (38 %) [M-CO], 1582 (83 %) [M-2CO], 1554 (64 %) [M-3CO], 1526 (96 %) [M-4CO]amu. ^1H NMR (C_6D_6) δ: 6.3-8.3 (m, 39H, μ-P<u>Ph</u>$_2$, <u>X</u>yNC), 2.20 (s, 6H, <u>X</u>yNC$_{equat}$), 1.56 (s, 12H, <u>X</u>yNC$_{axial}$). ^{31}P NMR (C_6D_6) A_2X, δ: -7.9 (d, P_a), +42.4 (t, P_x), $^2J\{PP\}$ = 152 Hz.

Synthesis of iodomethane adducts 7.1-7.3

[Ir_3(μ-PPh_2)$_3$(CO)$_4$(1,1,3,3-tmBuNC)$_3$(CH_3)][I] (<u>7.1</u>)

Excess iodomethane (20 µL, 0.32 mmol) was added dropwise to a stirred solution of [Ir_3(μ-PPh_2)$_3$(CO)$_4$(1,1,3,3-tmBuNC)$_3$] (35 mg, 0.021 mmol) in 5 mL of dichloromethane. After one hour a bright orange solution had formed. All volatiles where removed *in vacuo* to afford the cluster as yellow-orange solid which was washed with hexane and dried in vacuum (33 mg 87 % yield). The compound was not stable enough in solution to be purified by recrystallization. Analysis calculated for $Ir_3P_3C_{68}H_{84}O_4N_3I$: C, 45.28; H, 4.69; N, 2.33 %; Found: C, 45.54; H, 4.78; N, 2.63 %. IR (KBr) ν_{CN}, 2214 (w), 2184 (s), 2087 (w), ν_{CO}, 2022 (s), 1970 (br), 1919 (br) cm^{-1}. FAB MS (m/z): 1676 (13%) [M^+], 1648 (88%) [M-CO], 1620 (28%) [M-2CO],1604 (48%) [M-C(CH_3)$_4$], 1592 (65%) [M-3CO], 1564 (59%) [M-4CO], 1479 (100%) [M-197] amu. ^{31}P NMR (CD_2Cl_2) ABX, δ: -4.6 (d of d, P_a), -5.8 (d of d, P_b), -54.5 (d of d, P_x), $^2J\{P_aP_b\}$ = 159 Hz, $^2J\{P_aP_x\}$ = 138

Hz, $^2J\{P_bP_x\}$ = 132 Hz. ^1H NMR (CD_2Cl_2) δ: 7.2-8.1 (m, 30H, μ-P<u>Ph</u>$_2$), 2.23 [2H, (CNC(CH_3)$_2$C<u>H</u>$_2$(CH_3)$_3$)$_{equat}$], 2.20 (pseudo t, 3H, IrC<u>H</u>$_3$), $^3J\{HP_a\}$ = $^3J\{HP_b\}$ = 3Hz, 2.11 [6H, (CNC(C<u>H</u>$_3$)$_2$$CH_2$($CH_3$)$_3$)$_{equat}$], 1.37 [9H, (CNC($CH_3$)$_2$$CH_2$(C<u>H</u>$_3$)$_3$)$_{equat}$], 1.04 [4H, 2(CNC($CH_3$)$_2$C<u>H</u>$_2$($CH_3$)$_3$)$_{axial}$], 0.68 (18H, 2(CNC($CH_3$)$_2$$CH_2$(C<u>H</u>$_3$)$_3$)$_{axial}$], 0.61, 0.47 2[6H, 2(CNC(C<u>H</u>$_3$)$_2$$CH_2$($CH_3$)$_3$)$_{axial}$] ^{13}C NMR (CD_2Cl_2, 75.5 MHz) δ: 186.4 (pseudo t, 2CO) $^2J\{CP_a\}$ = $^2J\{CP_b\}$ = 7 Hz, 169.9 (pseudo t, 2CO) $^2J\{CP_a\}$ = $^2J\{CP_b\}$ = 7 Hz, 128 -140 (m, μ-P<u>Ph</u>$_2$), 106.6, 96.6 (broad, Ir<u>C</u>NR), 64.9, 64.3, 54.7, 53.0, 32.3, 31.9, 31.6, 31.4, 31.2, 31.1, 28.5, 27.9 (IrCN<u>R</u>).

[Ir_3(μ-PPh_2)$_3$(CO)$_4$(isoprNC)$_3$(CH_3)][I] (<u>7.2</u>)

Excess iodomethane (200 µL, 3.2 mmol) was added dropwise to a stirred solution of [Ir_3(μ-PPh_2)$_3$(CO)$_4$(isoprNC)$_3$] (20 mg, 0.014 mmol) in 5 mL of dichloromethane. After one hour a bright orange solution had formed. All volatiles where removed *in vacuo* and recrystallization from dichloromethane-hexane gave the cluster as yellow-orange plates (19 mg 83 % yield). X-ray quality crystals were obtained by slow diffusion of hexane in to a solution of 6 mg cluster in 0.3 mL dichloromethane using a narrow diffusion tube.

Analysis calculated for $Ir_3P_3C_{53}H_{54}O_4N_3I\cdot\frac{1}{2}CH_2Cl_2$: C, 39.28; H, 3.39; N, 2.57 %; Found: C, 39.33; H, 3.49; N, 2.50 %. IR (KBr) ν_{CN}, 2232 (w), 2203 (s), 2087 (w), ν_{CO}, 2021 (s), 1970 (br), 1918 (br) cm $^{-1}$. FAB MS (m/z): 1466 (12%) [M^+], 1438 (88%) [M-CO], 1410 (11%) [M-2CO], 1394 (36%) [M-CO - isopropH], 1382

(100%) [M-3CO], 1354 (39%) [M-4CO] amu. ^{31}P NMR (CD_2Cl_2) ABX, δ: -5.5 (d of d, P_a), -9.9 (d of d, P_b), -56.2 (d of d, P_x), $^2J\{P_aP_b\}$ = 158 Hz, $^2J\{P_aP_x\}$ = 141 Hz, $^2J\{P_bP_x\}$ = 128 Hz. ^1H NMR (CD_2Cl_2) δ: 7.3-8.1 (m, 30H, μ-P$\underline{Ph}_2$), 5.32 [heptet, 1H, (CNC$\underline{H}(CH_3)_2)_{equat}$], 3.27 [heptet, 2H, 2(CNC$\underline{H}(CH_3)_2)_{axial}$] $J^3\{HH\}$ = 7 Hz, 2.14 (pseudo t, 3H, IrC$\underline{H}_3$) $^3J\{HP_a\} = {}^3J\{HP_b\}$ = 3Hz, 1.84 [d, 6H, (CNCH(C$\underline{H}_3)_2)_{equat}$] 0.36 [d, 6H, (CNCH(C$\underline{H}_3)_2)_{axial}$], 0.35 [d, 6H, (CNCH(C$\underline{H}_3)_2)_{axial}$] $^3J\{HH\}$ = 7 Hz.

^{13}C NMR (CD_2Cl_2) δ: 186.6 (pseudo t, 2CO) $^2J\{CP_a\} = {}^2J\{CP_b\}$ = 7 Hz, 170.1 (pseudo t, 2CO) $^2J\{CP_a\} = {}^2J\{CP_b\}$ = 9 Hz, 128 -138 (m, μ-P$\underline{Ph}_2$), 52.2 [s (CN$\underline{C}H(CH_3)_2)_{equat}$], 50.1 [s, (CN$\underline{C}H(CH_3)_2)_{axial}$], 23.8, 21.5, 21.1 3[s, CNCH($\underline{C}H_3)_2)_{equat}$], -42.1 (broad, Ir$\underline{C}H_3$). Isonitrile carbons were not resolved.

$[Ir_3(\mu\text{-}PPh_2)_3(CO)_4(cyNC)_3(CH_3)][I]$ (7.3)

Excess iodomethane (80 µL, 1.28 mmol) was added dropwise to a stirred solution of $[Ir_3(\mu\text{-}PPh_2)_3(CO)_4(cyNC)_3]$ (38 mg, 0.024 mmol) in 5 mL of dichloromethane. After one hour a bright orange solution had formed. All volatiles where removed *in vacuo* to afford the cluster as yellow solid which was washed with small aliquots of hexane-benzene (ratio 3:1) and dried in vacuum (22 mg 53 % yield). The compound was not stable enough in solution to be purified by recrystallization. $Ir_3P_3C_{62}H_{66}O_4N_3I$: C, 43.45; H, 3.88; N, 2.45 %; Found: C, 44.65; H, 4.14; N, 2.91 %. IR (KBr) ν_{CN}, 2226 (w), 2199 (s), 2084 (w),

ν_{CO}, 2019 (s), 1968 (s), 1918 (s) cm^{-1}. FAB MS (m/z): 1586 (22%) [M^+], 1558 (88%) [M-CO], 1502 (65%) [M-3CO], 1421 (22%) [M-2CO -CyNC] amu. ^{31}P NMR (CD_2Cl_2) ABX, δ: -5.4 (d of d, P_a), -8.2 (d of d, P_b), -55.3 (d of d, P_x), $^2J\{P_aP_b\}$ = 158 Hz, $^2J\{P_aP_x\}$ = 142 Hz, $^2J\{P_bP_x\}$ = 127 Hz. ^1H NMR (CD_2Cl_2) δ: 7.2-8.0 (m, 30H, μ-P$\underline{Ph}_2$), 2.1 (pseudo t, 3H, IrC$\underline{H}_3$), $^3J\{HP_a\}$ = $^3J\{HP_b\}$ = 3Hz, 0.3-4.9 (m, 36H, $\underline{cy}$NC).